

The impact of salt tectonics on the Mesozoic sedimentation and petroleum systems of the Norwegian Barents Sea

Insights from the Nordkapp and Tiddlybanken
Basins

Luis Alberto Rojo Moraleda

Thesis submitted in fulfilment of
the requirements for the degree of
PHILOSOPHIAE DOCTOR
(PhD)



Faculty of Science and Technology
Department of Energy Resources
2020

University of Stavanger
NO-4036 Stavanger
NORWAY
www.uis.no

©2020 Luis Alberto Rojo Moraleda

ISBN:978-82-7644-947-1
ISSN:1890-1387
PhD: Thesis UiS No. 540

Preface

The present PhD thesis is submitted in fulfilment of the requirements for the degree of *Philosophiae Doctor* (PhD) at the University of Stavanger (UiS), Norway. This research was carried out between February 2016 to December 2019 and was funded by the Ministry of Education of Norway. During this period, I worked as a research fellow at the Department of Energy Resources, Faculty of Science and Technology at UiS. My main supervisor is Professor Nestor Cardozo (UiS) and my co-supervisors are Professor Alejandro Escalona (UiS) and Professor Hemin Koyi (Uppsala University, Sweden). Collaboration was also established with LoCrA and JuLoCrA researchers Dora Marin and Andrés Cedeño at UIS. In addition, industry collaboration was established with Sergio Courtade, Per Salomonsen and Jan Tveiten from the GPM team at Schlumberger, and Emilie O'Neill, Jorn Tore Paulsen, Geir Apeland and Michael Branston from WesternGeco. During my PhD, I helped Professor Nestor Cardozo teaching his master course *Structural Styles* and contributed to some teaching in the bachelor courses: *Basic subsurface interpretation methods* and *Introduction to Geology*.

The PhD has resulted in five publications. Four of these are published in different journals including the *American Association of Petroleum Geologists (AAPG) Bulletin*, *Basin Research*, and *Geosciences*. The last manuscript has been submitted to the *Journal of Structural Geology* and is currently under review. Besides these publications, I have presented my research in several conferences, seminars, and industry forums.

The thesis consists of two chapters. The first chapter is an introduction to the thesis, including the research questions, motivation, objectives, methodology, results, discussion, and conclusions. The second chapter is a compilation of the five papers which are the main body of the thesis.

Acknowledgements

During my PhD, I had the pleasure to work and collaborate with outstanding and inspirational scientists from academia and industry. This work would not have been possible without the motivation, help, and support of my supervisors, industry advisors, colleagues, friends and family.

Foremost, I would like to express my greatest gratitude to my supervisor Professor Nestor Cardozo for his outstanding guidance and continuous support, for his patience, motivation, enthusiasm, and knowledge in structural geology. Thank you for always being available to discuss my work and for the time you took to carefully review the manuscripts and provide constructive feedbacks. I really appreciate the freedom and flexibility you have given me to conduct my research, especially in the last year of my PhD when I moved to Oslo for family reasons. I would also like to express my gratitude to my co-supervisor at UiS, Professor Alejandro Escalona, for his time for discussions and constructive comments. I really appreciate the social environment you created in the department, particularly with barbecues at your place. I would also like to express my gratitude to my co-supervisor Professor Hemin Koyi at Uppsala University. My understanding of salt tectonics increased considerably thanks to the analogue experiments we run together at the Hans Ramberg Tectonic Laboratory (HRTL). Thank you for your constructive reviews and feedbacks and for the numerous discussions, particularly those we had during lunch time at the cafeteria of the Geological Survey of Sweden.

Many thanks to my colleagues Dora, Guro, Bereke, Sayyid, Xiaoan, Andrés and Iván for all the nice discussions, constructive comments about the manuscripts, support and celebrations with delicious food, which made our office D-306 the perfect environment for research.

I would like to thank Snorre Olausen, William Helland-Hansen, Sten-Andreas Grundvåg, Lars Stemmerik and Sverre Ohm for their excellent courses at UNIS, which helped me understand the geology of Svalbard and apply it to my research.

I am also very grateful to the Norwegian Petroleum Directorate (NPD) for providing access to the DISKOS database and WesternGeco Multiclient for permission to use their full azimuth survey (Nordkapp coil) from the Nordkapp Basin. Many thanks to Sergio Courtade, Per Salomonsen and Jan Tveiten from Schlumberger for providing support with the GPM Petrel plug-in. Thanks to Midland Valley and Schlumberger for providing academic licenses of their softwares Move and Petrel-GPM, respectively.

I would like to express my gratitude to my parents, Luis and Francis, and to the rest of my family including, aunts, uncles and grandparents for their continuous support during my career as a geologist. I am also very grateful to my mother in law Flora, whose support and help has been very important in the last year of my PhD.

Finally, but most importantly, I would like to express my sincere love and gratitude to my wife Alla and my daughter Karolina. Your love and support have been an unlimited source of motivation and inspiration throughout these years

Summary

In the Norwegian Barents Sea, Mesozoic and Cenozoic mobilization of Pennsylvanian-lower Permian layered evaporite sequences (LES) resulted in areas with salt tectonics (e.g. Nordkapp, Tromsø and Tiddlybanken basins), which affected the development of Upper Paleozoic and Mesozoic petroleum systems. Over the last three decades, seismic imaging in these salt-bearing basins has been a challenge due to the presence of closely spaced salt diapirs and steep minibasin strata. Consequently, there is limited information and integrated studies, and the dynamics of salt mobilization and its effect on the petroleum systems remain poorly understood. This research applies a wide range of methods to subsurface data in the Nordkapp and Tiddlybanken basins to: (1) provide a tectonostratigraphic evolution of the basins; (2) understand the influence of salt movement on Mesozoic prograding overburdens; and (3) address the thermal effect of salt in the petroleum systems of the Barents Sea. The results are presented in five papers.

Paper I improves the understanding of salt tectonics in the Nordkapp Basin based on interpretation of subsurface data and structural restorations. Our results indicate that a combination of Early Triassic basement-involved extension and sediment progradation resulted in diachronous salt mobilization and sediment infill along the basin. Important processes such as diapirism, minibasins formation, welding, and salt depletion occurred earlier in the central and eastern sub-basins than in the western sub-basin. The paper also highlights the importance of salt rheology and subsalt relief for the nucleation and distribution of salt structures and minibasins.

Paper II aims to understand the controls on suprasalt structural style in confined salt-bearing basins based on analogue experiments. The paper compares the structural styles resulting from basement involved extension and progradational loading. Moreover, it highlights the impact

of subsalt relief on suprasalt deformation by comparing different subsalt basin configurations. Finally, the models are upscaled and compared to seismic sections through the Nordkapp Basin to illustrate the influence of these processes on the evolution and structural style of the basin.

Paper III combines subsurface data, 3D structural restorations and forward stratigraphic modelling in the Tiddlybanken Basin to understand the influence of salt tectonics on Mesozoic prograding overburdens. The paper illustrates how salt mobilization causes drastic vertical and lateral changes in relative sea level, which in turn induce lateral variations in clinoform geometry and progradation rates. These variations result in complex spatial and temporal stacking patterns in salt minibasins. Moreover, this study emphasises the importance of forward stratigraphic modelling in the study of tectonically active areas such as salt bearing basins, since the isolated use of conventional methodologies might lead to potential pitfalls with negative consequences for exploration models.

Paper IV combines subsurface data and minibasin/prospect-scale restorations to describe near-diapir deformation and minibasin subsidence in the Nordkapp Basin. Diapir growth resulted in different scales of drape folding such as megaflaps, minibasin-scale folding, and composite halokinetic sequences, which could work as structural traps. Salt growth also produced sediment erosion and reworking of the Triassic overburden, which explains the deposition of peridiapiric wedges at diapir flanks. This paper also illustrates the role of minibasin subsidence on the temporal and spatial distribution of Triassic depositional environments, where salt withdrawal caused the retrogradation of Triassic fluviodeltaic systems and favoured local embayments with deposition of source rocks.

Paper V combines structural restorations from paper I and thermal modelling to show the impact of salt tectonics on the thermal evolution and petroleum system of confined salt-bearing basins such as the Nordkapp Basin, commonly characterized by narrow minibasins and

closely-spaced diapirs. The results indicate that thermal anomalies associated to closely-spaced diapirs mutually interfere and induce a combined anomaly that reduces the overall temperature in the basin. The presence of isolated diapirs also reduce the temperature in adjacent minibasins. However, this effect is laterally limited and depends on the shape and width of the diapir. Finally, the paper emphasises the importance of integrating structural restorations and thermal modelling in confined salt-bearing basins since the thermal effect of evolving salt structures can unlock new exploration concepts such as deep hydrocarbon kitchens and reservoirs.

This PhD thesis has implications for the understanding of salt tectonics, minibasin infill, and the petroleum system of confined salt-bearing basins in the Norwegian Barents Sea. Furthermore, the results contribute to the understanding of these processes in similar basins worldwide.

Table of Contents

Preface	iii
Acknowledgements.....	iv
Summary.....	vi
List of Papers	xi
Chapter 1 – Introduction	xiii
1 Introduction.....	1
1.1 Problem 1. Tectonostratigraphic evolution of the Nordkapp Basin	3
1.2 Problem 2. The influence of salt tectonics on the Mesozoic prograding sediments	5
1.3 Problem 3. The thermal influence of salt on the petroleum systems.....	7
1.4 Research objectives.....	7
2 Study area and geological setting.....	9
2.1 Late Paleozoic	9
2.2 Mesozoic.....	11
2.3 Cenozoic	12
3 State of the art	13
3.1 Salt tectonics in confined salt-bearing basins	13
3.2 Importance of base salt on salt-bearing basins	15
3.3 Clinoform progradation across salt-bearing basins	17
3.4 Near-diapir deformation and reservoir distribution.....	18
3.5 The thermal effect of salt on the petroleum system	21
4 Data	25
5 Methods.....	27
5.1 Seismic interpretation	27
5.2 Velocity modelling.....	27
5.3 2D/3D structural restorations	28
5.4 Forward stratigraphic modelling	29
5.5 Sandbox models	29

5.6	Thermal modelling.....	30
6	Summary of papers	31
6.1	Paper I: Structural style and evolution of the Nordkapp Basin, Norwegian Barents Sea	31
6.2	Paper II: Controls on suprasalt deformation in confined salt-bearing basins: insights from analogue modelling.....	33
6.3	Paper III: The influence of halokinesis on prograding clinoforms: insights from the Tiddlybanken Basin, Norwegian Barents Sea	35
6.4	Paper IV: Controls on minibasin infill in the Nordkapp Basin: evidence of complex Triassic syn-sedimentary deposition influenced by salt tectonics	37
6.5	Paper V: The impact of salt tectonics on the thermal evolution and petroleum system of confined rift basins: insights from Basin Modelling of the Nordkapp Basin, Norwegian Barents Sea	39
7	Discussion	43
7.1	Global implications for the understanding of salt-bearing rift basins	43
7.2	Global implications for the understanding of minibasin infill by prograding overburdens	45
7.3	Regional implications for the Triassic paleogeography and petroleum system	47
7.4	Limitations	48
8	Future work.....	51
9	Conclusions.....	53
10	References.....	55
	Chapter 2 – Compilation of Papers	71
	Paper I	73
	Paper II.....	115
	Paper III.....	153
	Paper IV	181
	Paper V.....	217
	Appendix.....	243
	Conference abstracts	244

List of Papers

Paper I: Structural style and evolution of the Nordkapp Basin, Norwegian Barents Sea.

Luis Alberto Rojo, Nestor Cardozo, Alejandro Escalona, and Hemin Koyi.

2019, AAPG Bulletin, v.103, no. 9, pp. 2177-2217,
DOI:10.1306/01301918028

Paper II: Controls on suprasalt deformation in confined salt-bearing basins: insights from analogue modelling.

Luis Alberto Rojo, Hemin Koyi, Nestor Cardozo, and Alejandro Escalona

Submitted to the Journal of Structural Geology

Paper III: The influence of halokinesis on prograding clinoforms: Insights from the Tiddlybanken Basin, Norwegian Barents Sea

Luis Alberto Rojo, Dora Marin, Nestor Cardozo, Alejandro Escalona, and Hemin Koyi

2019, Basin Research, DOI: 10.1111/bre.12411

Paper IV: Controls on minibasin infill in the Nordkapp Basin: Evidence of complex Triassic synsedimentary deposition influenced by salt tectonics

Luis Alberto Rojo and Alejandro Escalona

2018, AAPG Bulletin, v. 102, no. 7, pp. 1239-1272,
DOI: 10.1111/bre.12411

Paper V: The impact of salt tectonics on the thermal evolution and petroleum systems of confined rift basins: Insights from basin modelling of the Nordkapp Basin, Norwegian Barents Sea

Andrés Cedeño, Luis Alberto Rojo, Nestor Cardozo, Luis Centeno, and
Alejandro Escalona

2019, Geosciences, v.9, DOI: 10.3390/geosciences9070316

Chapter 1 – Introduction

Introduction

Intentionally left blank

1 Introduction

Pennsylvanian to lower Permian layered evaporite sequences (LES) from the Gipsdalen Group are widespread across the Norwegian Barents Sea (Stemmerik, 2000; Henriksen et al., 2011b; Rowan and Lindsø, 2017), including the onshore territories of Spitsbergen (Sorento et al., 2019). Late Paleozoic multiphase rift events accompanied by an arid climate led to the isolation of grabens and half grabens (e.g. Tromsø, Nordkapp, and Tidlybanken basins; Fig. 1A), which resulted in the deposition of synrift to early postrift halite-rich sequences (Jensen and Sørensen, 1992; Stemmerik, 2000; Worsley, 2008). Graben shoulders and surrounding platforms (e.g. Finnmark and Bjarmeland platforms) were, on the other hand, characterized by deposition of carbonate and gypsum-rich evaporite sequences with relatively minor halite content (Stemmerik, 2000; Nordaunet-Olsen, 2015; Sorento et al., 2019). The occurrence of LES played an important role in the tectonostratigraphic evolution of the Barents Sea. Thin LES commonly act as detachment levels of listric faults in extensional systems (e.g. Hammerfest Basin) and thrusts in compressional systems (e.g. Spitsbergen; Henriksen et al., 2011b), whereas the Mesozoic and Cenozoic mobilization of thick halite-rich LES in confined grabens (e.g. Nordkapp Basin) resulted in areas dominated by salt tectonics (Jensen and Sørensen, 1992; Koyi et al., 1995b; Nilsen et al., 1995; Rowan and Lindsø, 2017).

The Norwegian Barents Sea is known to host various petroleum systems (Ohm et al., 2008; Henriksen et al., 2011b). Discoveries such as the Snøhvit and Goliat fields in the Hammerfest Basin prove the existence of Triassic and Jurassic source rocks (Mohammedyasin et al., 2016; Mulrooney et al., 2017), while the Alta and Ghotia discoveries in the Loppa High prove the presence of upper Permian source rocks. Furthermore, outcrops in Svalbard and shallow wells in the Finnmark platform prove the existence of a gas-prone Carboniferous source rock.

Introduction

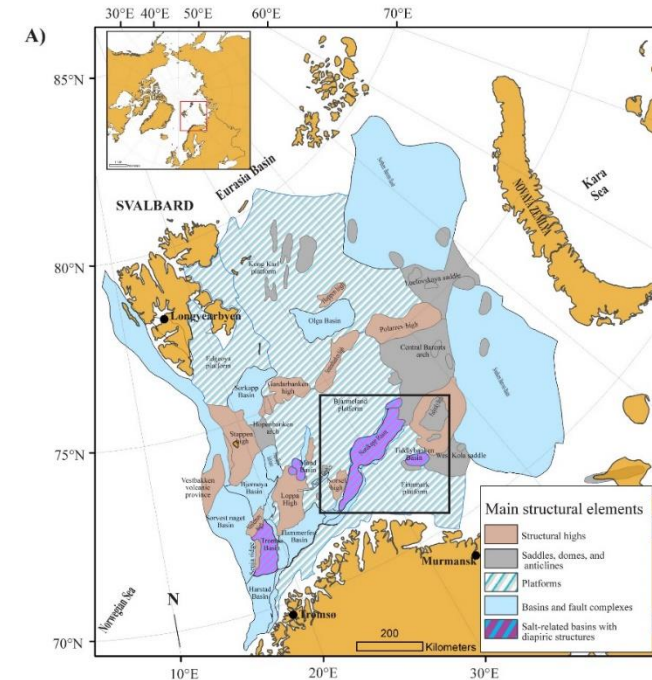
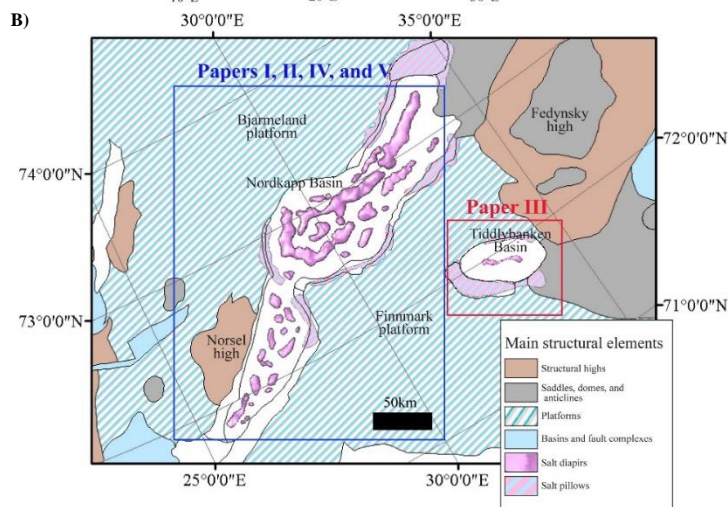


Figure 1. Main structural elements of the Barents Sea. The Tromsø, Nordkapp, and Tiddlybanken basins are salt-bearing basins with abundant diapiric structures. B) Structural elements of the Nordkapp and Tiddlybanken basins. The blue square highlights the location of the Nordkapp Basin, which is the subject of papers I, II, IV, and V. The red square highlights the location of the Tiddlybanken Basin, which is the subject of paper III.



(Bugge et al., 1995; Worsley, 2008). Based on these arguments, equivalent age petroleum systems could be present in salt-bearing basins, where salt mobilization influenced the distribution of reservoirs and source rocks, the style and timing of structural and stratigraphic traps, and the maturation and migration of hydrocarbons (Jackson and Hudec, 2017; Rowan and Lindsø, 2017). Nevertheless, salt-bearing basins such as the Nordkapp and Tiddlybanken basins are frontier areas of exploration. Seismic imaging and interpretation in these basins are challenging due to the presence of closely-spaced salt diapirs and high-dipping minibasin strata (Jones and Davison, 2014; Rojo et al., 2016). Consequently, there is limited information, few integrated studies, and poor understanding of the following three main problems:

1.1 Problem 1. Tectonostratigraphic evolution of the Nordkapp Basin

The Nordkapp Basin is a NE-SW Upper Paleozoic salt-bearing rift basin. It is one of the best examples of salt tectonics in the southwestern Barents Sea (Gabrielsen et al., 1992; Jensen and Sørensen, 1992). The basin is subdivided into three sub-basins or rift segments: a NE-SW western sub-basin; a E-W central sub-basin; and a NE-SW eastern sub-basin (Rowan and Lindsø, 2017; Fig. 1B). Most of the publications describing the tectonostratigraphic evolution of the Nordkapp Basin date back to the 1990s. These studies are based on observations from 2D seismic reflection data across the western and central sub-basins (Dengo and Røssland, 1992; Gabrielsen et al., 1992; Jensen and Sørensen, 1992), combined with observations from analogue models (Koyi et al., 1993b; Koyi et al., 1995a; Koyi et al., 1995b; Nilsen et al., 1995). Most authors in the 1990s agreed that Early Triassic basement-involved extension triggered salt mobilization, resulting in the formation of closely-spaced diapirs and thick Triassic minibasins (Jensen and Sørensen, 1992; Koyi et al., 1995a; Koyi et al., 1995b; Nilsen et al., 1995; Fig. 2A). These studies were contradicted by Dengo and Røssland (1992) who proposed

Introduction

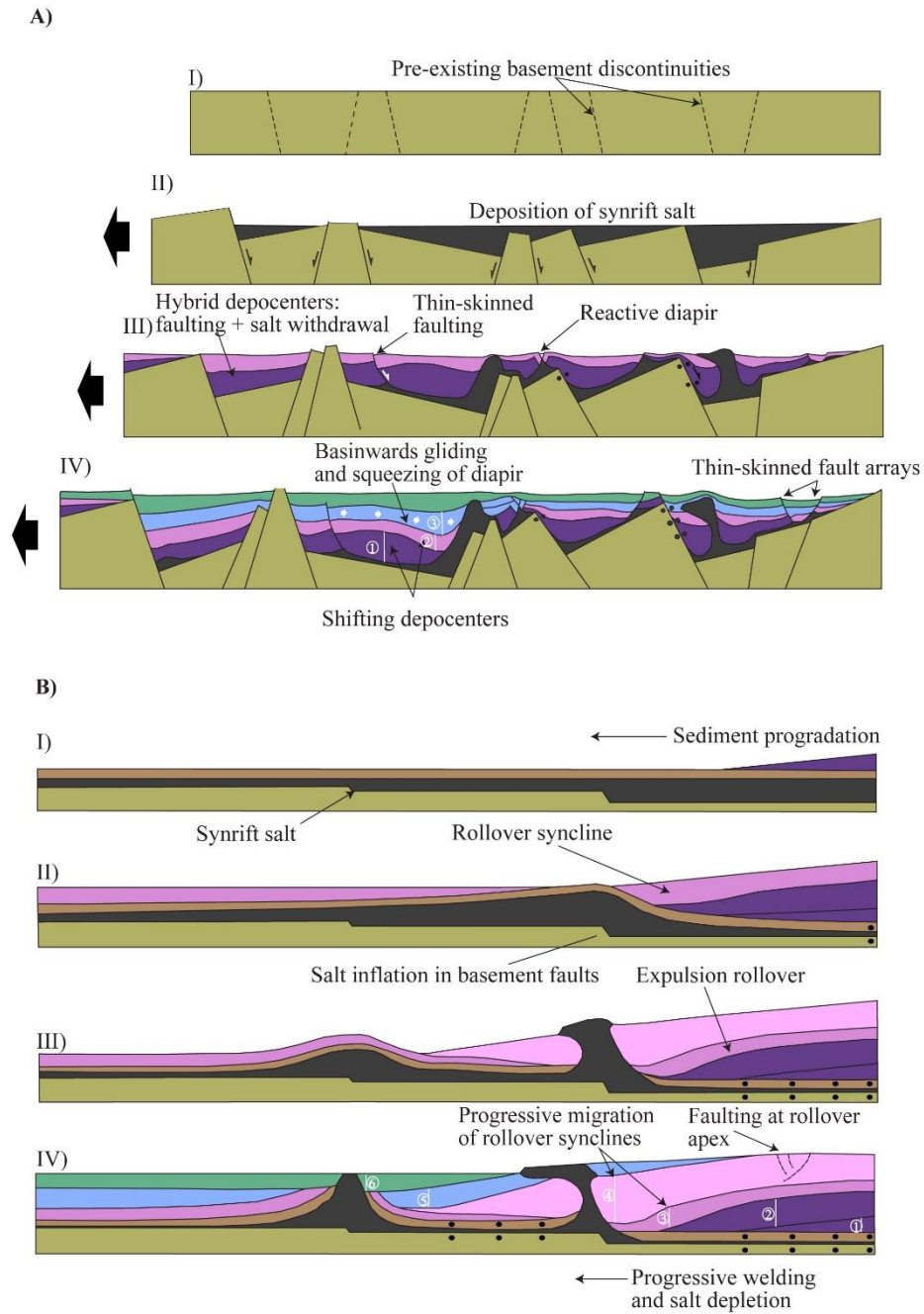


Figure 2. Possible models explaining the structural styles of the Nordkapp Basin. A) Basement-involved extension (modified from Jackson and Hudec, 2017). B) Progradational loading (modified from Ge et al., 1997).

progradational loading and salt mobilization in response to Early Triassic northwest-progradation of Triassic clinoforms (Fig. 2B). With the recent opening for exploration of the eastern sub-basin, Rowan and Lindsø (2017) document examples of Triassic salt tectonics driven by sediment progradation with no evidence of extension. Previous publications describe the tectonostratigraphic evolution of the Nordkapp Basin based on observations from one or two sub-basins. Important factors controlling the suprasalt structural style such as base salt relief and salt lithological variation have been barely addressed. Moreover, there is limited information and integrated regional studies combining isochore maps and structural restorations in the three sub-basins. Therefore, the evolution and along-strike variability of salt mobilization, depocenter distribution, welding and salt depletion remain poorly understood.

1.2 Problem 2. The influence of salt tectonics on the Mesozoic prograding sediments

Along its geological history, the Barents Shelf has experienced two periods of clinoform progradation: the Triassic (Fig. 3A) and the Cretaceous (Fig. 3B), with the Jurassic as a transitional period between these two (Worsley, 2008; Henriksen et al., 2011b). During the Triassic, prograding shelf-edge and coastal/deltaic clinoforms sourced from the Urals and Fennoscandia prograded towards the northwestern part of the shelf (Riis et al., 2008; Glørstad-Clark et al., 2010; Klausen et al., 2015; Eide et al., 2017; Klausen et al., 2018; Fig. 3A). During the Cretaceous, on the other hand, the clinoforms were sourced from the northern part of the shelf and prograded towards the southeast and southwest (Grundvåg et al., 2017; Marin et al., 2017; Fig. 3B). Based on seismic observations and paleogeographic maps in the Triassic and Cretaceous (Glørstad-Clark et al., 2010; Marin et al., 2017), both clinoforms systems bypassed salt-bearing basins with ongoing salt mobilization such as the Nordkapp and Tiddlybanken basins.

Introduction

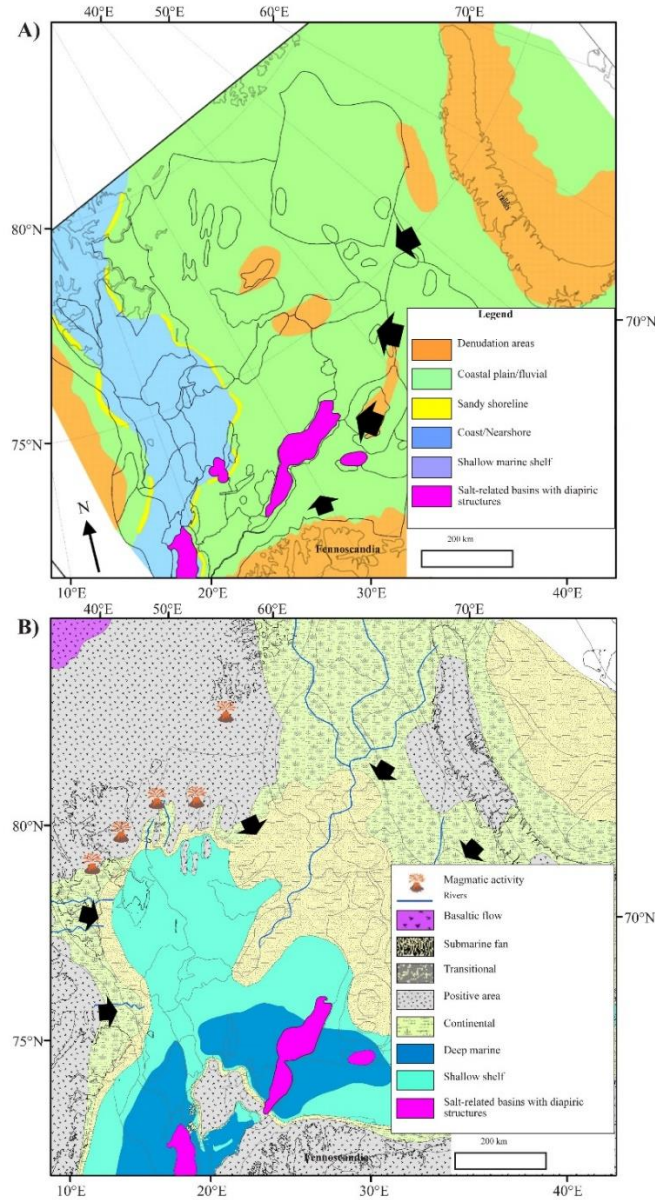


Figure 3. A) Paleogeography during the Late Triassic in the Barents Shelf. Shelf-edge clinoforms prograded towards the NW of the Barents Sea and across salt-related basins (e.g. Tiddlybanken and Nordkapp basins) with ongoing halokinesis (modified from Henriksen et al., 2011). B) Paleogeography during the Early Cretaceous (modified after LoCrA 2018). Shelf-edge clinoforms prograded towards the southern part of the Barents Sea and across salt-related basins with ongoing halokinesis. Black arrows in maps A and B indicate the progradation direction

(Koyi et al., 1993b; Koyi et al., 1995b; Rowan and Lindsø, 2017). Previous studies analyse the Triassic and Cretaceous clinoforms in tectonically stable areas (e.g. Finnmark and Bjarmeland platforms) (Glørstad-Clark et al., 2010; Klausen et al., 2015; Eide et al., 2017; Grundvåg et al., 2017; Marin et al., 2017; Klausen et al., 2018). However, none of these studies look at the clinoforms in salt-bearing basins where salt tectonics could have potentially affected clinoform progradation and depositional environments within salt minibasins.

1.3 Problem 3. The thermal influence of salt on the petroleum systems.

The Norwegian Barents Sea is known for hosting various petroleum systems sourced from Upper Paleozoic and Mesozoic organic-rich intervals (Ohm et al., 2008; Henriksen et al., 2011b). These organic-rich intervals are deeply buried in the Nordkapp Basin due to the large accommodation space created by Mesozoic and Cenozoic halokinesis (Koyi et al., 1995b; Nilsen et al., 1995). Consequently, it is reasonable to expect these source rocks to be overmatured today, especially those from the Upper Paleozoic. However, studies by Mello et al. (1995) and McBride et al. (1998) in offshore Brazil and the Gulf of Mexico indicate that salt plays an important role in retarding or accelerating the maturation of source rocks. Despite, the large number and variety of salt structures present in the Barents Sea, there are no studies analysing the thermal effect of salt movement on the petroleum systems. In important salt-bearing basins such as the Nordkapp Basin, this thermal effect remains unknown.

1.4 Research objectives

This PhD thesis covers the Tiddlybanken and the Nordkapp basins, with $\frac{3}{4}$ of the research concentrated on the last one. The work follows a multidisciplinary approach combining observations from 2D/3D seismic reflection and well data, 2D/3D structural restorations, analogue

(sandbox) models, forward stratigraphic modelling, and thermal modelling to accomplish the following objectives:

- 1) Provide a regional tectonostratigraphic evolution of the Nordkapp Basin with emphasis on the timing of salt mobilization, triggering mechanisms, depocenter distribution, welding, and the impact of pre-salt relief on the suprasalt structural style.
- 2) Understand the influence of salt mobilization on prograding clinoforms and the implications for reservoir partitioning in salt minibasins
- 3) Evaluate the thermal effect of salt diapirs on the petroleum system of the Nordkapp Basin.

This study consists of five publications targeting the three fundamental problems above in the Nordkapp and Tiddlybanken basins. **Paper 1** utilises 2D/3D seismic reflection data, borehole data and 2D structural restorations to provide a tectonostratigraphic evolution of the Nordkapp Basin. **Paper 2** combines sandbox experiments and seismic examples from the Nordkapp Basin to understand the relative contribution of thick-skinned extension and sediment loading in the structural style of confined salt-bearing basins, and evaluate the impact of subsalt relief on suprasalt deformation. **Paper 3** uses 2D seismic reflection data in the Tiddlybanken Basin, 3D structural restorations, and forward stratigraphic modelling to understand the impact of halokinesis on prograding clinoforms and reservoir partitioning in minibasins. **Paper 4** utilizes 3D seismic reflection data and well data in the Nordkapp Basin to better understand deformation processes, reservoir and source rock distribution, and trapping mechanisms in areas adjacent to salt diapirs. Finally, **Paper 5** combines 2D structural restorations of the Nordkapp Basin with thermal modelling to evaluate the impact of salt tectonics on the thermal evolution and petroleum system of the basin.

2 Study area and geological setting

The Barents Sea is an epicontinental shelf on the offshore territories of the Norwegian and Russian Arctic. It consists of a complex distribution of platforms, structural highs, and basins (Henriksen et al., 2011b; Fig. 1A).

The study area covers the Nordkapp and Tiddlybanken basins (Fig. 1B). The Nordkapp Basin is a Upper Paleozoic salt-bearing basin consisting of three subbasins: a NE-SW western sub-basin, a E-W central sub-basin; and a NE-SW eastern sub-basin (Gabrielsen et al., 1992; Jensen and Sørensen, 1992). The Tiddlybanken Basin is an Upper Paleozoic NW-SE salt-bearing basin located southeast of the Nordkapp Basin (Rowan and Lindsø, 2017). The tectonostratigraphic evolution of these basins is the result of a series of tectonic events and climatic variations affecting the Barents Sea from the Mississippian to the present (Worsley, 2008; Henriksen et al., 2011b; Fig. 4).

2.1 Late Paleozoic

The formation of the Nordkapp and Tiddlybanken basins is the result of pre-Mississippian-Pennsylvanian multiphase extension on a previous NE-SW and NW-SE Caledonian structural grain (Dengo and Røssland, 1992; Faleide et al., 2008; Gernigon et al., 2014; Gernigon et al., 2018). Pre-Mississippian NE-SW extension formed the central sub-basin of the Nordkapp Basin and the Tiddlybanken Basin whereas Pennsylvanian NW-SE extension formed the western and eastern sub-basins of the Nordkapp Basin (Gernigon et al., 2014; Rowan and Lindsø, 2017; Gernigon et al., 2018). Based on outcrops from Svalbard and drilling in the Finnmark platform (Bugge et al., 1995; Worsley, 2008), pre-salt strata might consist of synrift alluvial-fluvial systems interlayered with coal (Billefjorden Gp.; Fig. 4C). During the Pennsylvanian-

Study area and geological setting

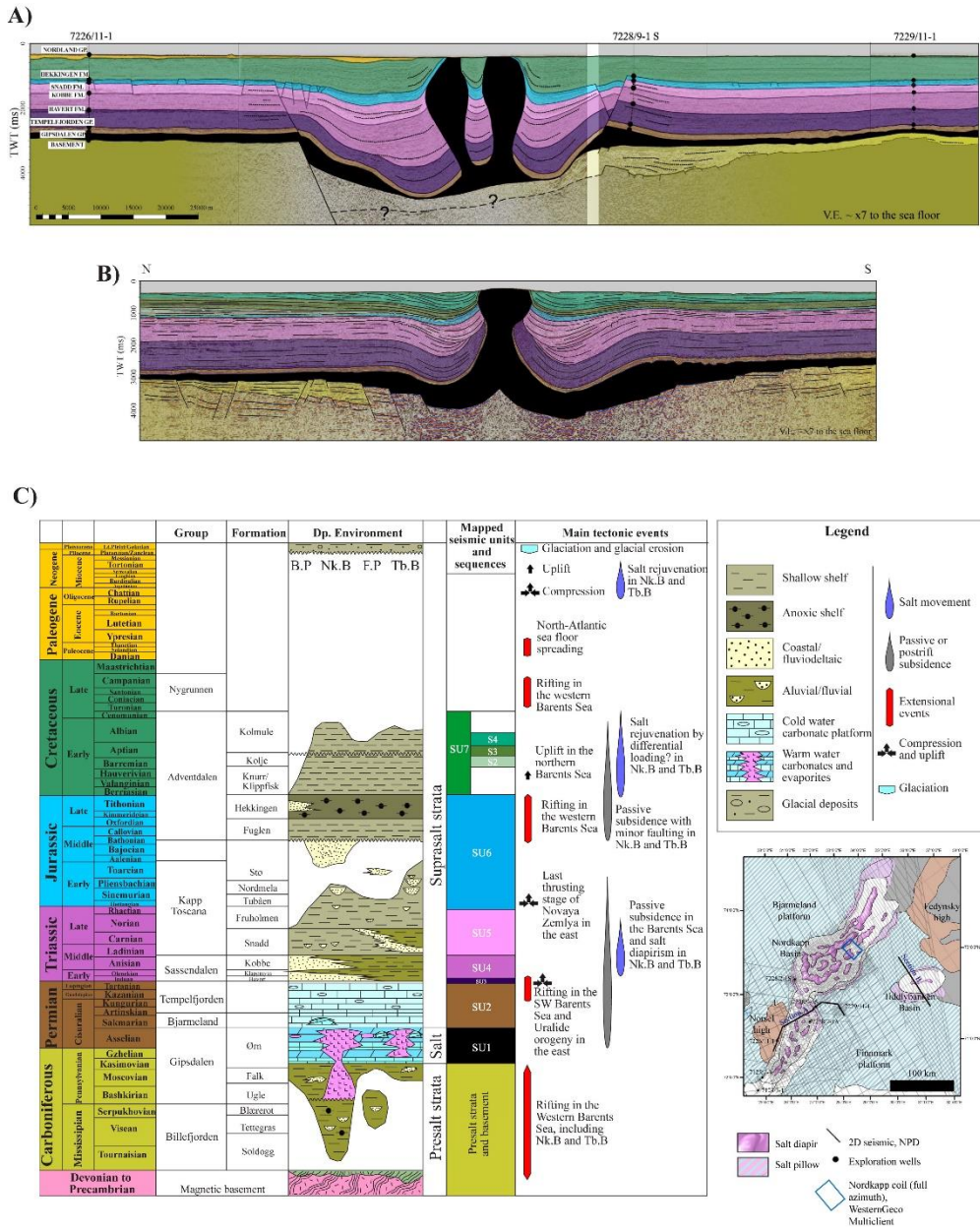


Figure 4. A) Regional seismic line across the Nordkapp Basin. B) Regional seismic line across the Tiddlybanken Basin. C) Lithostratigraphic chart illustrating the main stratigraphic units, depositional environments, and tectonic events (modified after Larsen et al. 2002 and Gernigon et al. 2018). B.P.=Bjarmeland platform; Nk.B.=Nordkapp Basin; F.P.=Finnmark platform; Tb. B.= Tiddlybanken Basin. Inset shows the location of seismic lines A and B.

early Permian, the last phases of extension together with the drifting of Pangea towards arid latitudes, favoured basin isolation and precipitation of synrift to early postrift halite-rich LES evaporite sequences in the Nordkapp Basin, and mostly postrift halite-rich LES in the Tiddlybanken Basin (Gipsdalen Gp.; Stemmerik et al., 1999; Stemmerik, 2000; Rowan and Lindsø, 2017; Fig. 4). Crustal extension ceased during the Permian, and these basins were affected by a period of passive subsidence afterwards (Gudlaugsson et al., 1998; Henriksen et al., 2011b; Fig. 4A and B). Movement of Pangea towards colder latitudes resulted in the deposition of cool-water carbonates (Bjarmeland Gp.) and cold-water carbonates with spiculites (Tempelfjorden Gp.) (Stemmerik et al., 1999; Worsley, 2008; Fig. 4C).

2.2 Mesozoic

The Early Triassic in the Nordkapp Basin was marked by the onset of salt mobilization triggered either by Early Triassic thick-skinned extension (Koyi et al., 1993b; Koyi et al., 1995b; Nilsen et al., 1995) or sediment loading by Triassic clinofolds (Dengo and Røssland, 1992; Rowan and Lindsø, 2017; Fig. 4A). Salt mobilization in the Tiddlybanken Basin occurred later in response to an Early Triassic-Middle Triassic contractional event associated with the development of the Uralides (Rowan and Lindsø, 2017; Fig. 4B). The minibasin infill in both basins consists of NE-SW striking transgressive-regressive fluviodeltaic sediments sourced from the Uralides and Fennoscandia (Sanssendalen Gp.; Riis et al., 2008; Glørstad-Clark et al., 2010; Klausen et al., 2015; Eide et al., 2017; Klausen et al., 2018; Fig. 4C).

During the Late Triassic-Jurassic, salt diapirism and minibasin subsidence decreased dramatically, leading to the burial of salt diapirs in the Nordkapp and Tiddlybanken basins (Jensen and Sørensen, 1992; Nilsen et al., 1995; Rowan and Lindsø, 2017; Fig. 4A and B). A decrease of accommodation space in the entire Barents Shelf favoured the reworking of previous Triassic deposits, which resulted in the deposition

of fluviodeltaic deposits with complex drainage patterns (Kapp Toscana Gp. (Henriksen et al., 2011b; Anell et al., 2014; Fig. 4C).

The Late Jurassic-Early Cretaceous was a period of passive subsidence in the Nordkapp and Tiddlybanken basins (Fig. 4A and B). Minor faulting occurred in association with the opening of the North Atlantic in the western Barents Sea (Faleide et al., 2008). Late Jurassic regional flooding resulted in the deposition of Upper Jurassic organic-rich shales (Adventdalen Gp.; Henriksen et al., 2011b; Fig. 4C). This episode was followed by Early Cretaceous uplift and erosion of the northern part of the Barents Shelf (Grantz et al., 2011; Corfu et al., 2013). Consequently, organic-rich shales in the Nordkapp and Tiddlybanken basins were overlaid by Lower Cretaceous shoreline and shelf deposits, which prograded towards the southern part of the shelf (Grundvåg et al., 2017; Marin et al., 2017; Fig. 4C).

2.3 Cenozoic

During the Late Cretaceous-Cenozoic, the Nordkapp and Tiddlybanken basins were affected by several compressional events probably due to plate reconfigurations associated with the opening of the North Atlantic (Faleide et al., 1993; Faleide et al., 2008). Salt structures were rejuvenated by contractional diapirism (Jensen and Sørensen, 1992; Koyi et al., 1993b; Koyi et al., 1995b; Nilsen et al., 1995; Rowan and Lindsø, 2017; Figs. 4A and B). Upper Cretaceous-Cenozoic sediments are not present in either basin due to successive events of Cenozoic uplift and erosion, which removed ca. 1.5 km of Cenozoic and Cretaceous strata (Ohm et al., 2008; Henriksen et al., 2011a; Baig et al., 2016).

3 State of the art

3.1 Salt tectonics in confined salt-bearing basins

Confined salt-bearing basins consist of an interaction of narrow (< 80 km wide) grabens and half grabens where syn-rift evaporites are limited by fault blocks (Fig. 2A, step II; Warren, 2010). Grabens and half grabens display along-strike variations in geometry, tilting and differential subsidence, subdividing the basin into rift segments or sub-basins of different initial salt thickness (Jensen and Sørensen, 1992; Stewart and Clark, 1999; Withjack and Callaway, 2000). The structural style of salt-bearing rift basins consists of narrow and thick minibasins surrounded by closely-spaced salt diapirs (Koyi et al., 1993a; Koyi et al., 1993b; Koyi et al., 1995b). Other structures such as salt pillows, rollers, and suprasalt complexes are common at the basin boundaries (Gabrielsen et al., 1992; Jackson and Lewis, 2016).

Most works explain the structural style of confined salt-bearing basins as the result of basement-involved extension (Koyi et al., 1993a; Jackson and Vendeville, 1994; Koyi et al., 1995b; Nilsen et al., 1995). During this process, subsalt faulting creates depressions that become preferential areas of sediment loading and salt evacuation (Fig. 2A, step III-IV). Simultaneously, overburden extension contributes to the generation of reactive diapirs that later may evolve into passive diapirs (Fig. 2A, step III-IV; Koyi et al., 1993a). Extension can additionally result in tilting of fault blocks and subsequent basinward gliding of suprasalt strata, causing extension at basin boundaries and contraction of salt structures at the basin axis (Fig. 2A, step III-IV; Nilsen et al., 1995; Stewart et al., 1997). Salt rheology and thickness strongly control the coupling between subsalt faults and overburden (Withjack and Callaway, 2000; Jackson and Lewis, 2016; Jackson and Stewart, 2017; Jackson et al., 2019). Salt pillows, rollers, and soft-linked fault complexes commonly form at basin boundaries where halite-rich sequences are thin and interlayered with

other non-mobile lithologies (e.g. carbonates, gypsum; (Jackson and Lewis, 2016). Salt diapirs and deep minibasins, on the other hand, are generally located at the basin axis, where halite-rich evaporite sequences are thicker (Jackson et al., 2019). In areas with carbonate-dominated facies (e.g. platforms, structural highs), basement-involved extension results in the formation of hard-linked faults (Jackson and Lewis, 2016).

Fewer studies describe the structural style of salt-bearing rift basins as the result of progradational loading (Moragas et al., 2017; Rowan and Lindsø, 2017). In this scenario, a sedimentary wedge induces differential loading into the underlying salt, which results in salt expulsion and formation of a salt plateau (Fig. 2B, step I-II). Continuous wedge progradation and salt expulsion cause the formation of salt welds overlaid by expulsion rollovers, which get younger in the progradation direction (Fig. 2B, steps II-IV; Ge et al., 1997). It is important to mention that this process do not require extension to form salt diapirs. Subsalt faults facing sediment progradation can act as barriers of salt flow, favouring salt inflation, salt diapirs and roof erosion (Fig. 2B, step II-IV; Ge et al., 1997). Extension is neither required to form suprasalt fault complexes since these can form in response to local arching as expulsion rollovers sink into the underlying salt (Fig. 2B, step IV; Rowan and Lindsø, 2017).

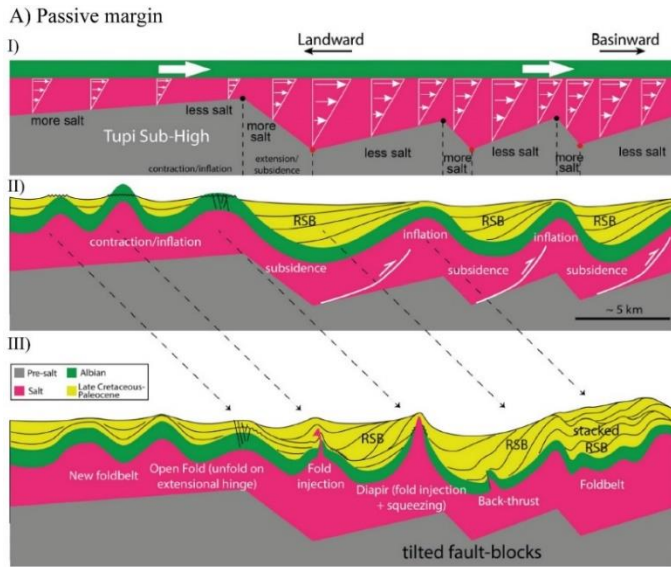
Many salt-bearing rift basins such as the Sverdrup Basin (Jackson and Harrison, 2006), the North-Sea (Coward and Stewart, 1995), and the Nordkapp Basin (Koyi et al., 1995b; Nilsen et al., 1995), experienced along its geological history a change in tectonic regime from extension to contraction. Consequently, salt diapirs formed during extension were squeezed during contraction, which caused their vertical growth (Hudec and Jackson, 2007; Jackson and Hudec, 2017).

3.2 Importance of base salt on salt-bearing basins

The impact of pre-salt basin configuration on the suprasalt deformation of salt-bearing basins has been described by previous works in foreland basins (e.g. Paradox Basin; Trudgill, 2011), rift basins (e.g. North Sea; Koyi and Petersen, 1993; Ge et al., 2017), and passive margins (e.g. Gulf of Mexico and offshore Angola; Koyi, 1996; Ge et al., 1997; Jackson and Hudec, 2005).

Most studies investigate this effect in passive margins, where downdip salt flow by gravity gliding and spreading occurs over a relatively unconfined and wide basin (> 100 km; Rowan et al., 2004; Brun and Fort, 2011; Morley et al., 2011; Peel, 2014a). Here, base salt relief causes perturbations in the downdip salt flow and controls the distribution of extensional and contractional salt structures and ramp synclines above subsalt structural highs and lows, respectively (Fig. 5A; Jackson and Hudec, 2005; Dooley et al., 2018; Pichel et al., 2018; M. Pichel et al., 2019; Pichel et al., 2019).

Fewer publications, however, study the impact of pre-salt basin configuration on the evolution of salt-bearing rift basins (Koyi et al., 1993a; Stewart et al., 1997; Ge et al., 2017). As opposed to passive margins, salt-bearing rift basins consist of subsalt rift segments and accommodation zones (Fig. 5B; Rosendahl et al., 1986; Scott and Rosendahl, 1989; Morley et al., 1990). Rift segments generally host evaporites of significant thickness (> 1.5 km) delimited by subsalt faults with large throw, length, and spacing. Accommodation zones, on the other hand, consist of smaller normal faults with thin evaporites deposited in their hanging walls. These lateral variations in pre-salt



B) Salt-influenced rift basin

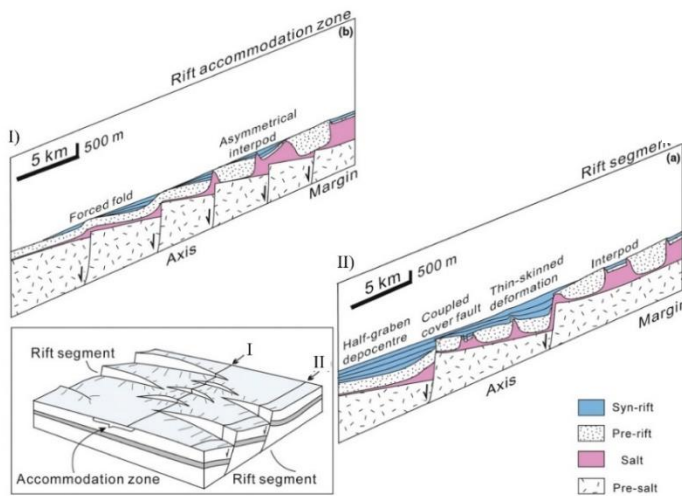


Figure 5. A) Kinematic model showing the structural style caused by downdip salt flow and overburden translation over the Tupi High and closely-spaced pre-salt tilted blocks (offshore Brazil; modified from Pichel et al., 2019). B) Sketch showing the impact of pre-salt configuration on the suprasalt structural style of the North Sea (modified from Ge et al. 2017). The suprasalt structural style in rift segments consists of deep minibasins surrounded by salt diapirs, whereas salt deformation in accommodation zones is characterized by smaller salt structures and shallower

relief and salt thickness result in different structural styles. Thick minibasins surrounded by salt diapirs commonly develop in rift segments with high initial salt thickness and large fault throws (Fig. 5B, step II), whereas salt pillows and rollers affect suprasalt strata above accommodation zones (Fig. 5B, step II; Ge et al., 2017). Most studies describe the impact of pre-rift configuration during polyphase extension and subsequent halokinesis (Jackson and Lewis, 2016; Ge et al., 2017). Few studies though describe the impact of pre-salt basin configuration on the evolution of salt-bearing rift basins triggered by sediment progradation (Moragas et al., 2017; Rowan and Lindsø, 2017). Consequently, there is a lack of understanding in how along-strike changes in graben configuration control the timing of salt mobilization, nucleation of salt structures and minibasins.

3.3 *Clinoform progradation across salt-bearing basins*

Clinoforms have been studied in passive margins (Steckler et al., 1999; Anderson, 2005; Anderson et al., 2016), foreland basins (Steel et al., 2002; Pellegrini et al., 2017), back-arc basins (Salazar et al., 2016; Salazar et al., 2018), and epicontinental seas (Glørstad-Clark et al., 2010; Eide et al., 2017; Klausen et al., 2018). These studies use trajectory and geometrical analysis of clinoforms to decipher the evolution and infill of sedimentary basins. As such, they are crucial to understand the distribution of reservoirs, seals, and source rocks from the shoreline to the basin floor (Dreyer et al., 2005; Helland-Hansen and Hampson, 2009; Houseknecht et al., 2009). Clinoform progradation across salt-bearing basins is a bi-directional process between salt and sediments. On the one hand, prograding overburdens induce differential loading of the underlying salt resulting in salt mobilization and diapirism (Koyi, 1996; Ge et al., 1997; Gaullier and Vendeville, 2005; Vendeville, 2005). On the other hand, minibasin subsidence and diapir uplift generate spatial and temporal variations in paleobathymetry, which result in a complex

distribution of depositional environments (Matthews et al., 2007; Banham and Mountney, 2013; Carter et al., 2016). Most publications on clinoform progradation on salt-bearing passive margins (Koyi, 1996; Jackson et al., 2015), foreland basins (Trudgill, 2011), and rift basins (Moragas et al., 2017; Rowan and Lindsø, 2017) focus on the impact of differential loading by prograding overburdens on the suprasalt structural style. Few studies though analyse the influence of salt movement on prograding clinoforms where lateral variations in bathymetry might influence clinoform trajectory and geometry (Cohen and Hardy, 1996).

3.4 *Near-diapir deformation and reservoir distribution*

Near-diapir deformation studies of strata flanking salt diapirs are essential in hydrocarbon exploration since they can be used to predict hydrocarbon traps against salt, including trap geometry and reservoir distribution (Hearon IV et al., 2014; Rowan et al., 2016). Most of these studies are based on outcrop observations since near-diapir areas in seismic sections are noisy due to the verticality of salt structures and the complexity of salt-sediment deformation (Giles and Lawton, 2002; Rowan et al., 2003; Aschoff and Giles, 2005; Giles and Rowan, 2012; Kernén et al., 2012). However, new advances in seismic acquisition and processing (e.g. full azimuth seismic data) have allowed the application of outcrop-based concepts to subsurface data (Hearon IV et al., 2014).

The growth of salt structures commonly results in drape folding of adjacent syn-kinematic strata at three different scales (Giles and Rowan, 2012; Rowan et al., 2016): (1) Minibasin-scale folding (Fig. 6A), which consists of packages of growth strata with wide (> 1 km) areas of folding and thinning. Turtle structures, broad synclines, and expulsion rollovers are examples of this category, (2) Megaflaps (Fig 6B), which consist of deep minibasin strata that have been upturned and even overturned along several kilometres, and (3) Composite halokinetic sequences (CHS; Fig. 6C), which involve packages of growth strata upturned and truncated by

angular unconformities produced by local (< 1 km) drape folding and upturn of ephemeral and thin diapir roofs.

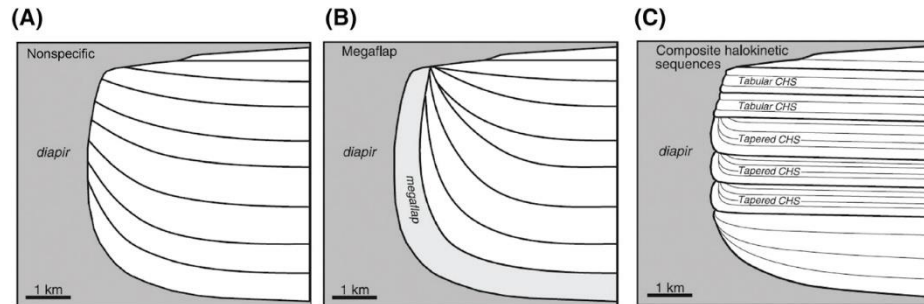


Figure 6. A) Minibasin-scale deformation where drape folding occurs in wide zones (> 1 km). B) Megaflap where deep minibasin strata is upturned along several km. C) Composite halokinetic sequences where drape folding occurs in narrow zones (< 1km). Modified from Rowan et al. (2016).

Giles and Lawton (2002); Giles and Rowan (2012) define two halokinetic sequences (HS) end-members: (1) Hook HS, characterized by narrow zones of folding (< 200 m) and high angle truncations (> 70°) beneath the top unconformity (Fig. 7A, step I). This end member is formed when the diapir growth rate R exceeds the sediment accumulation rate A , (2) Wedge HS, characterized by broad zones of drape folding (200 – 1000 m), and low angle truncations (< 30°) beneath the top unconformity (Fig. 7B, step I). These form when the sediment accumulation rate A exceeds the diapir growth rate R . The vertical stack of hooks and wedges lead to the formation of third order depositional cycles (1-10 m.y) called tabular composite halokinetic sequences (CHS) and tapered composite halokinetic sequences (Fig. 7A and B, Step V).

The study of halokinetic deformation have implications for understanding reservoir distribution in fluvial (Matthews et al., 2007; Banham and Mountney, 2013), shallow marine (Aschoff and Giles, 2005; Kernén et al., 2012), and deep water systems (Hearon IV et al., 2014; Carter et al., 2016). Low diapir growth rates and high sedimentation rates in tapered CHS can favour the deposition of thick sands near salt diapirs, which can end up trapped against these structures

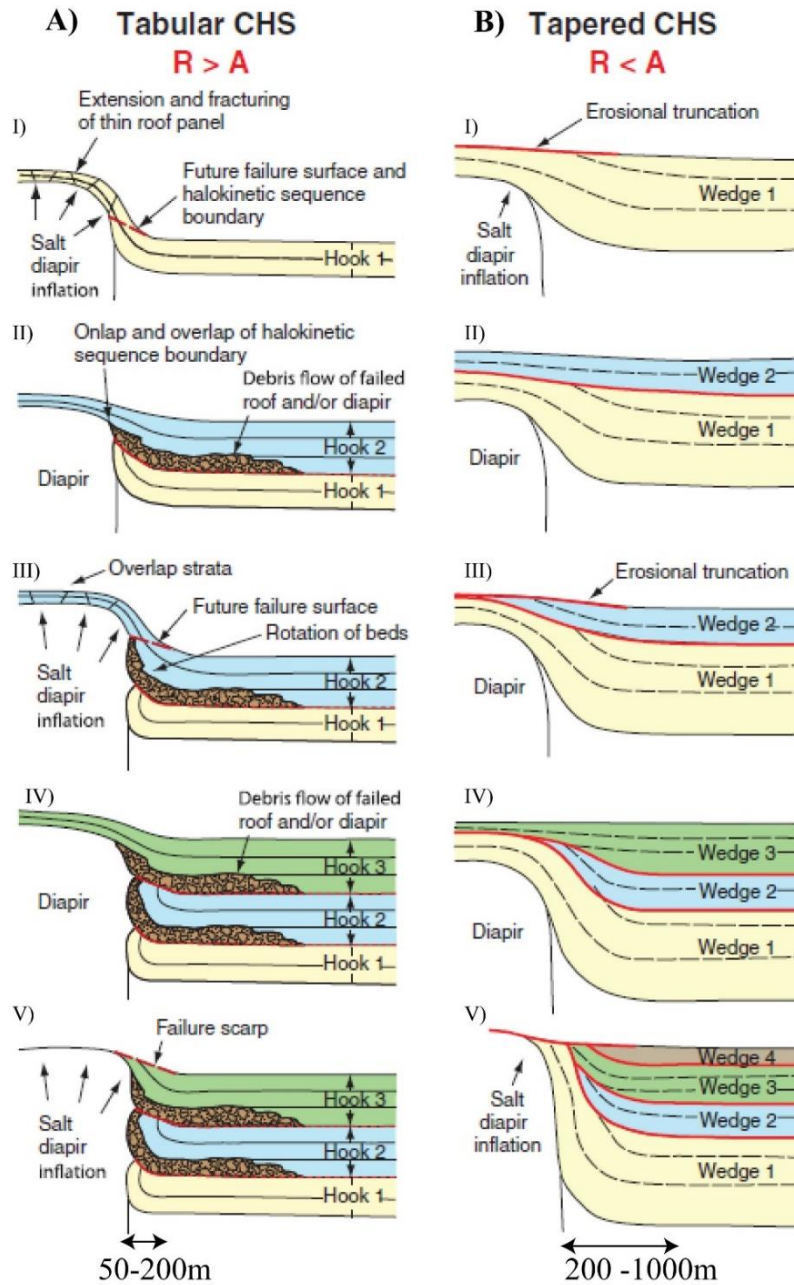


Figure 7. Genetic models showing the development of tabular (A) and tapered (B) composite halokinetic sequences (CHS). A = sediment accumulation rate, R = diapir growth rate. Modified from Giles and Rowan (2012).

after continued diapir growth (Giles and Rowan, 2012; Carter et al., 2016). Halokinetic deformation also affects reservoir development. For example, fluvial channels or turbidites deposited in tabular CHS should not have structurally controlled facies transitions until a distance of 100-200 m from the diapir. On the other hand, sands deposited in tapered CHS can have structurally controlled facies over a wider area (1000 m), meaning that sands might decrease reservoir quality or even shale out in these wide areas (Giles and Rowan, 2012). It is important to mention that salt diapirs can locally act as local sources of sediment reworking, triggering the formation of mass transport complexes (Giles and Lawton, 2002), which can be potential reservoirs. Furthermore, diapir-related bathymetric highs favour the growth of carbonate platforms (Giles and Lawton, 2002; Rowan et al., 2003), which can become potential reservoirs at diapir flanks.

3.5 The thermal effect of salt on the petroleum system

Rock salt has a thermal conductivity three times higher than porous sediments. Therefore, the evolution of salt structures within salt-bearing basins can produce spatial and temporal fluctuations in the thermal regime by focusing or defocusing heat (Mello et al., 1995; McBride et al., 1998; Jackson and Hudec, 2017). Salt structures covered by thick overburden create a dipole-shaped thermal anomaly (Fig. 8C): (1) a negative thermal anomaly towards the base, which reduces the temperature of strata below the structure; and (2) a positive anomaly towards the top, which increases the temperature of strata above the structure (Mello et al., 1995). When salt structures pierce the overburden and become passive diapirs (Barton, 1933), this dipole thermal anomaly becomes a negative monopole (Fig. 8D), and the diapirs act as conduits of heat out of the basin (Mello et al., 1995; Jackson and Hudec, 2017). The negative thermal anomaly reduces the temperature of adjacent minibasins, and its ratio of influence is dependent on the size and shape

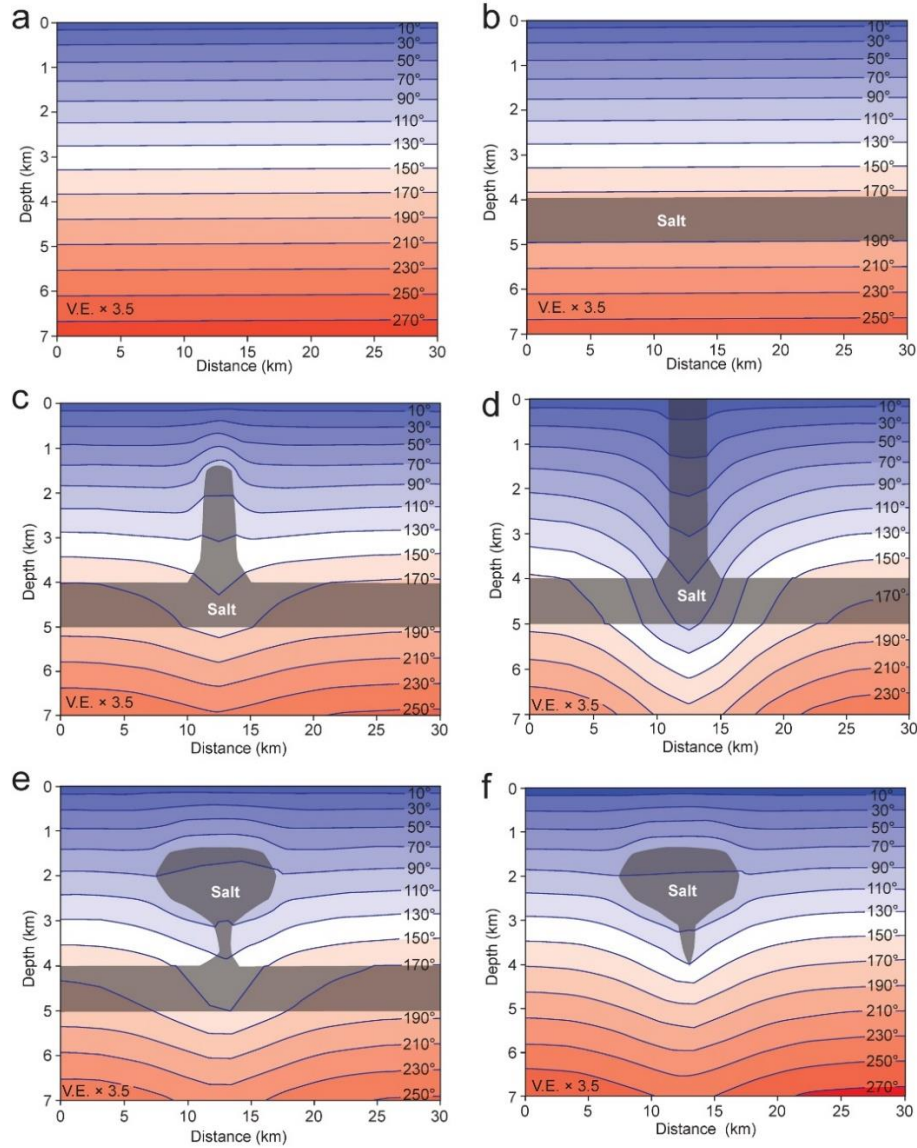


Figure 8. A) Temperature versus depth of a basin without salt. B) By introducing a salt layer of 1 km, the temperature in the subsalt strata decreases by 20°C. C) Dipole thermal anomaly associated with a salt diapir not reaching the surface. D) Monopole negative thermal anomaly induced by a diapir reaching the surface. E) Thermal anomaly resulting from a mushroom-shaped salt diapir connected to the salt source layer. D) Thermal anomaly induced by a mushroom-shaped salt diapir not connected to the source (modified from Jackson and Hudec, 2017).

of the diapir (Yu et al., 1992; Mello et al., 1995). The intrusion and horizontal growth of allochthonous salt sheets can additionally reduce the temperature of subsalt strata (McBride et al., 1998). Numerical models by Mello et al. (1995) indicate that an intrusion of a 1 km thick salt sheet can potentially reduce the temperature of subsalt strata by 20°C (Fig. 8B). The thermal effect of salt structures has strong implications in the petroleum system of salt-bearing basins since it can retard or accelerate temperature-controlled processes such as reservoir diagenesis and kerogen maturation (McBride et al., 1998).

State of the art

Intentionally left blank

4 Data

This PhD thesis uses 2D and 3D seismic reflection data provided by the Norwegian Petroleum Directorate (NPD) via the Diskos database (Fig. 9A). These data cover an area of 150.000 km² that includes part of the Bjarmeland platform, Norsel High, central and western sub-basins of the Nordkapp Basin and part of the Finnmark platform. Seismic quality in the central sub-basin of the Nordkapp Basin is poor due to the presence of closely-spaced salt structures. In order to provide a better interpretation of this area, I also use a full azimuth 3D cube (Nordkapp coil) provided by WesternGeco Multiclient where the salt-sediment interface is well imaged (Fig. 9A). NPD also provided the 2D seismic survey NPD BA-11 which covers the new areas recently opened for exploration such as the eastern sub-basin of the Nordkapp Basin and the Tiddlybanken Basin (Fig. 9A).

This study uses seven exploration wells located in the Nordkapp Basin (7228/2-1S, 7228/9-1S and 7228/7-1A), Finnmark platform (7229/11-1), Norsel High (7226/11-1), and Bjarmeland platform (7125/1-1 and 7124/3-1; Fig. 9A). The closest distance between wells is 24 km. Borehole data comprise a conventional suit of wireline logs (e.g. gamma ray, caliper, neutron, density, sonic, and resistivity), core images, check shots, and well tops (Fig. 9B). Borehole data were used to provide age constraints and correlate the main seismic units across the basin, correlate seismic facies with depositional environments interpreted from core and wireline logs, and construct a velocity model for time to depth conversion of the seismic profiles.

Data

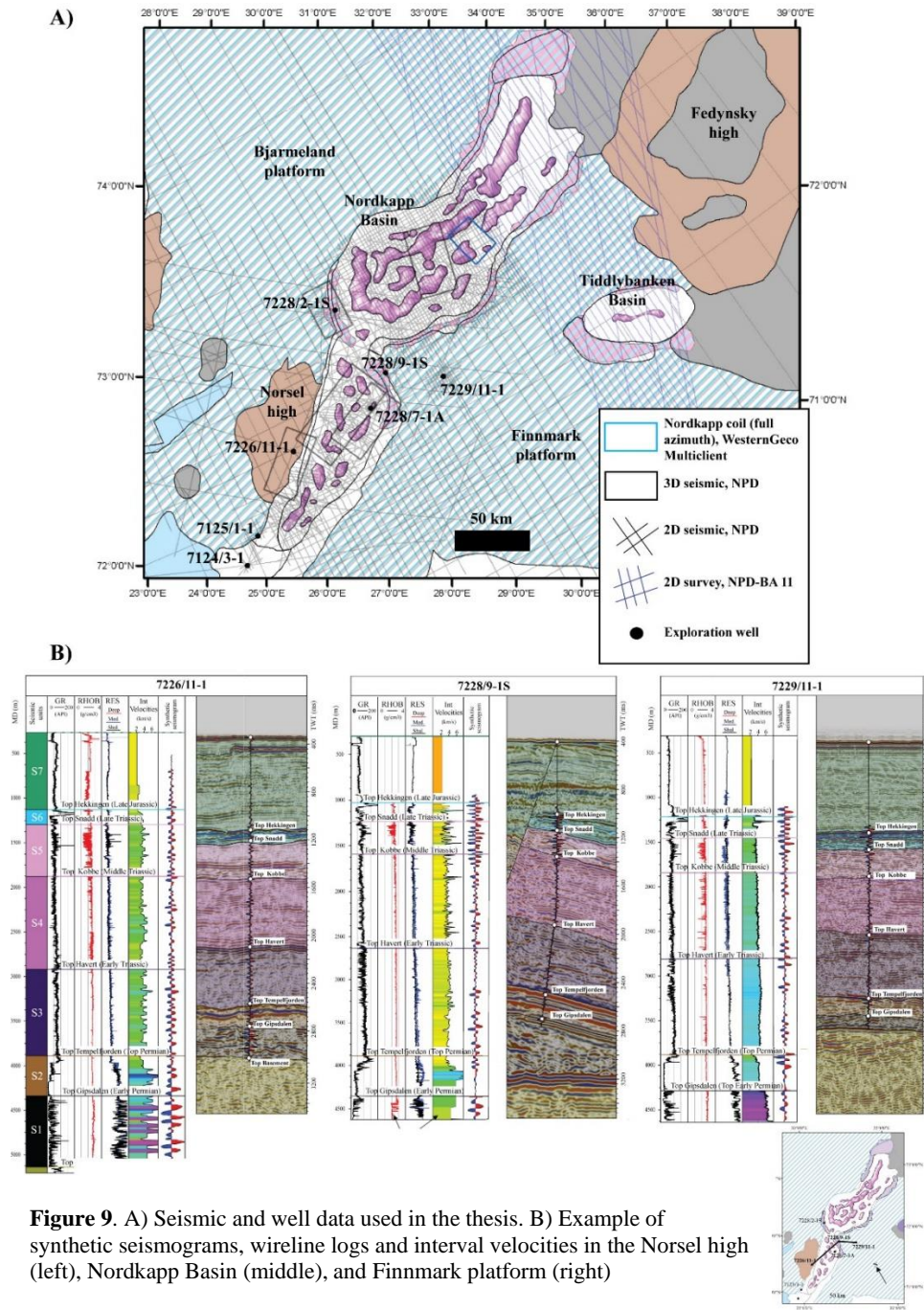


Figure 9. A) Seismic and well data used in the thesis. B) Example of synthetic seismograms, wireline logs and interval velocities in the Norsel high (left), Nordkapp Basin (middle), and Finnmark platform (right)

5 Methods

5.1 Seismic interpretation

Eight key horizons and seven seismic units were interpreted to map regionally the Nordkapp and Tiddlybanken basins (Fig. 4C). These horizons were identified based on reflection amplitude, stratal terminations, regional continuity of seismic reflectors, and previous studies (e.g. (Glørstad-Clark et al., 2010; Henriksen et al., 2011b; Marin et al., 2017). The ages of the seismic units were obtained from borehole data, which were tied to the seismic using synthetic seismograms (Fig. 9B). The regional seismic horizons are: Base Gipsdalen Gp. (Pennsylvanian), Top Gipsdalen Gp. (lower Permian), Top Tempelfjorden Gp. (upper Permian), Top Havert Fm. (Lower Triassic), Top Kobbe Fm. (Middle Triassic), Top Snadd Fm. (Upper Triassic), Top Hekkingen Fm. (Upper Jurassic), and the sea floor (Fig. 9B). Papers III and IV use in addition a subdivision of the Triassic and Lower Cretaceous that follows the stratigraphic framework of Glørstad-Clark et al. (2010), Klausen et al. (2015), Grundvåg et al. (2017) and Marin et al. (2017). In papers I, III, and IV, seismic facies were calibrated with core data and well logs to determine lateral variations in salt rheology and in depositional environments within minibasins.

5.2 Velocity modelling

The velocity model is based on wells 7228/2-1S, 7228/9-1S, 7228/7-1A, 7229/11-1, 7226/11-1, 7125/1-1 and 7124/3-1, and it is used to depth convert 2D seismic profiles and surfaces across the Nordkapp and Tiddlybanken basins. The model includes the sea floor, Top Hekkingen Fm, Top Snadd Fm, Top Havert Fm, Top Tempelfjorden Gp., Top Gipsdalen Gp., and Base Gipsdalen Gp. as the main velocity transitions. An initial interval velocity was assigned to each horizon followed by the calculation of the K factor, which describes the change of interval

velocities with depth in each interval. For consistency, depth conversion results were compared to other velocity models and depth-converted regional profiles from Clark et al. (2014), Gernigon et al. (2014) and Gernigon et al. (2018).

5.3 2D/3D structural restorations

2D/3D structural restorations were implemented in order to: (1) illustrate the 2D progressive evolution of salt structures and minibasins in the Nordkapp Basin (paper I), (2) understand the 4D salt flow resulting from different triggering mechanisms and subsalt basin configurations (paper II), (3) illustrate salt-related surface deformation and subsequent changes in relative sea level through time (papers II and III), (4) study prospect/minibasin-scale processes such as near-diapir deformation and minibasin subsidence (paper IV), and (5) study the thermal effect of salt structures through time (paper V). The restorations used flexural slip and simple shear algorithms to remove salt-related deformation (Rowan, 1996; Rowan and Ratliff, 2012). 2D/3D flexural slip was used to reconstruct horizons/surfaces affected by minibasin-scale deformation, which is associated with progressive folding and limb rotation of deep minibasin strata during the early stages of salt mobilization. Vertical simple shear, on the other hand, was used to reconstruct deformation caused by passive diapirism. Length loss associated with this mechanism is insignificant in comparison to the length of the regional profiles. Sediments were decompacted using the method of Sclater and Christie (1980) since this method fits well the porosity and depth curves from borehole data in the Barents Sea (Klausen and Helland-Hansen, 2018). For the isostatic compensation of loads, the restorations incorporated flexural isostasy with an elastic thickness of 20 km, which is supported by basin modelling studies from Gac et al. (2016). Paper II is the only study that does not consider decompaction and flexural isostasy since the restorations were performed on sandbox experiments where these processes are negligible.

5.4 Forward stratigraphic modelling

Forward stratigraphic modelling is used in paper III to analyse the dynamics of prograding sediments influenced by salt-related uplift and/or subsidence. For this purpose, we used the Geological Process Modelling (GPM) Petrel plug-in (Schlumberger), which is a simulation and visualization package that models erosion, transport and sedimentation based on physical equations (Tetzlaff et al., 2014). Clinoform progradation was modelled using the diffusion and steady flow equations. The diffusion equation describes the rate at which sediments move downslope proportionally to the slope gradient (Tetzlaff and Harbaugh, 1989; Flemings and Grotzinger, 1996). Consequently, the topography or bathymetry becomes smoother through time. The steady flow equation simulates erosion, transport, and sedimentation (Tetzlaff et al., 2007). The algorithm calculates the transport capacity from the flow depth and velocity for each simulation cell. Erosion occurs when the flow contains less sediment than it can transport, whereas deposition takes place when the sediment carried by the flow exceeds the flow's transport capacity. Sedimentary simulations were coupled with tectonics, whose input such as initial paleo-bathymetry and uplift/subsidence rates maps came from the 3D structural restorations.

5.5 Sandbox models

Sandbox models were used in paper II to illustrate the differences in suprasalt structural style resulting from different triggering mechanisms (basement-involved extension versus progradational loading) and subsalt basin configurations. The models follow classical techniques applied in brittle-ductile analogue modelling of salt tectonics. The modelling materials include: (1) a transparent silicone polydimethylsiloxane (PDMS) with a density of 987 kg/m^3 and a viscosity of $5 \times 10^4 \text{ Pa s}$ at 20°C , which was used to reproduce the ductile behaviour of salt (Weijermars et al., 1993); and (2) dry sand with a grain size of $250 \mu\text{m}$, density 1500 kg/m^3 , and internal friction angle of 30° , which was used

to reproduce the brittle, frictional behaviour of the overburden (Krantz, 1991; Weijermars et al., 1993). The analogue models were upscaled following scaling principles by Hubbert (1937), and compared to seismic profiles through the Nordkapp Basin.

5.6 Thermal modelling

Thermal modelling was used to study the effect of salt tectonics on the thermal evolution and petroleum system of the Nordkapp Basin. The thermal modelling was performed for several stages throughout the evolution of the basin (structural restorations from paper I), using the PetroMod software (Schlumberger). The lower and upper boundary conditions for each restoration step were the heat flow and the sediment-water interface temperature (SWIT). The evolution of basal heat flow through time was calculated from the present thermal gradient from nearby wells, the history of rifting and associated stretch factor β (Clark et al., 2014), and inverse modelling using a modified McKenzie model. The water-sediment surface temperature (SWIT) was reconstructed from the paleo-latitude of the basin and water depths through time.

6 Summary of papers

6.1 *Paper I: Structural style and evolution of the Nordkapp Basin, Norwegian Barents Sea*

This paper provides the first regional tectonostratigraphic evolution of the Nordkapp Basin, based on observations from 2D and 3D seismic data, borehole data, isochrone maps, and structural restorations (Fig. 10A). The paper emphasizes: (1) triggering mechanisms of salt movement, (2) along-strike differences in the timing of salt diapirism, welding and salt depletion, and (3) geological controls that explain the different structural styles of the basin.

Our results indicate that along-strike differences in structural style in the Triassic result from the combination of two triggering mechanisms: thick-skinned extension and sediment loading. Diapirism and minibasin nucleation were strongly influenced by the reactivation of subsalt structures which: (1) created preferential areas of sediment loading, (2) caused faulting and stretching of the overburden, and (3) acted as salt flow barriers favouring salt inflation and diapirism above these structures. Rheological variations within the salt layer played also an important role, with salt diapirs located in halite-rich areas (e.g. basin axes), while salt pillows developed at basin shoulders where the halite thickness was less and the carbonate and anhydrite content was larger.

Isochrone maps and restored profiles indicate that salt mobilization and diapirism occurred earlier in the eastern and central sub-basins due to earlier arrival of the lowest Triassic prograding sediments sourced from the Uralides (Fig. 10B, step I). The western sub-basin, however, experienced the main salt mobilization and diapirism during the Early-Middle Triassic (Fig. 10B, step II). Differences in timing of salt welding and depletion are also observed along the basin, with the underlying salt

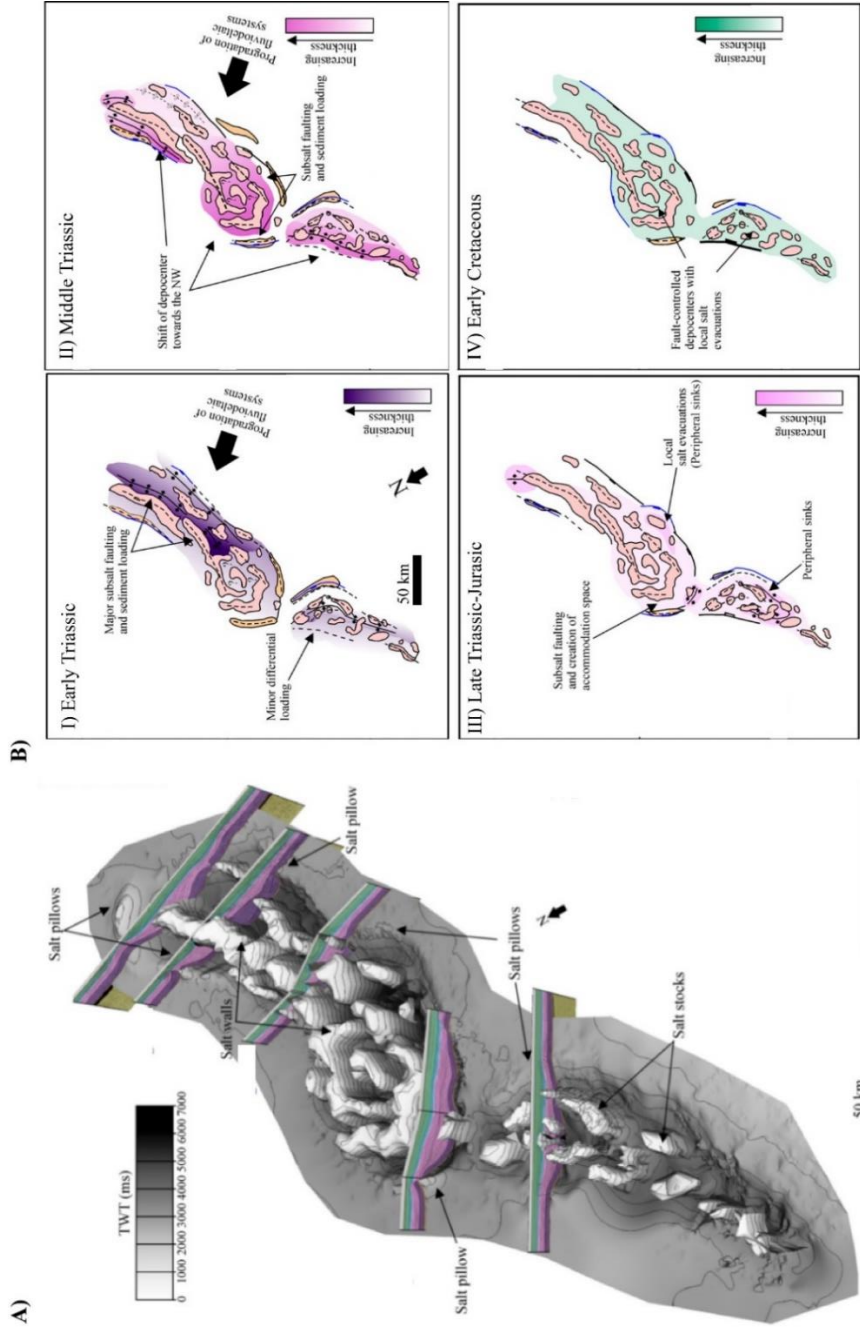


Figure 10. A) Two-way travel-time (TWT) map of the top salt illustrating the distribution of salt structures and location of key seismic transects analysed in this study. B) Basin infill evolution of the Nordkapp Basin based on observations from time-thickness maps

in the eastern and central sub-basins depleted by the Middle Triassic, whereas in the western sub-basin salt depletion occurred by the end of the Early Cretaceous (Fig. 10B, step IV). Even though in the eastern and central sub-basins the salt was depleted by the Middle Triassic, the diapirs continued growing until the end of the Mesozoic by evacuation of the remaining salt adjacent to them, thin-skinned gliding, and subsequent shortening.

6.2 *Paper II: Controls on suprasalt deformation in confined salt-bearing basins: insights from analogue modelling*

Paper II uses three sandbox experiments to understand the factors contributing to the variation of structural styles in confined salt-bearing basins (CSBB) such as the Nordkapp Basin. The first two experiments reproduce the effect of sediment progradation into a salt layer deposited in a symmetric (Fig. 11C, lower figure) or an asymmetric graben (Fig. 11B, lower figure), whereas the third experiment reproduces the effect of basement-involved extension in a symmetric graben (Fig. 11A, lower figure). These three experiments evaluate (1) the impact of the two triggering mechanisms above on suprasalt deformation, and (2) the influence of subsalt relief on salt flow and its contribution to the nucleation and timing of salt structures and minibasins along CSBB.

Salt tectonics driven by sediment progradation (experiments 1 and 2) display a structural style consisting of younger depocenters and salt structures in the progradation direction (Fig. 11B and C, lower figures). Basement involved extension (experiment 3), on the other hand, consists of vertical stacked depocenters near basin boundary faults. Salt diapirs and pillows are located above both basin boundary faults and display an opposite timing of growth with the older diapirs located in the distal basin boundary (Fig. 11A, lower figure). Experiments 1 and 2 indicate that basin configuration plays an important role in the

Summary of papers

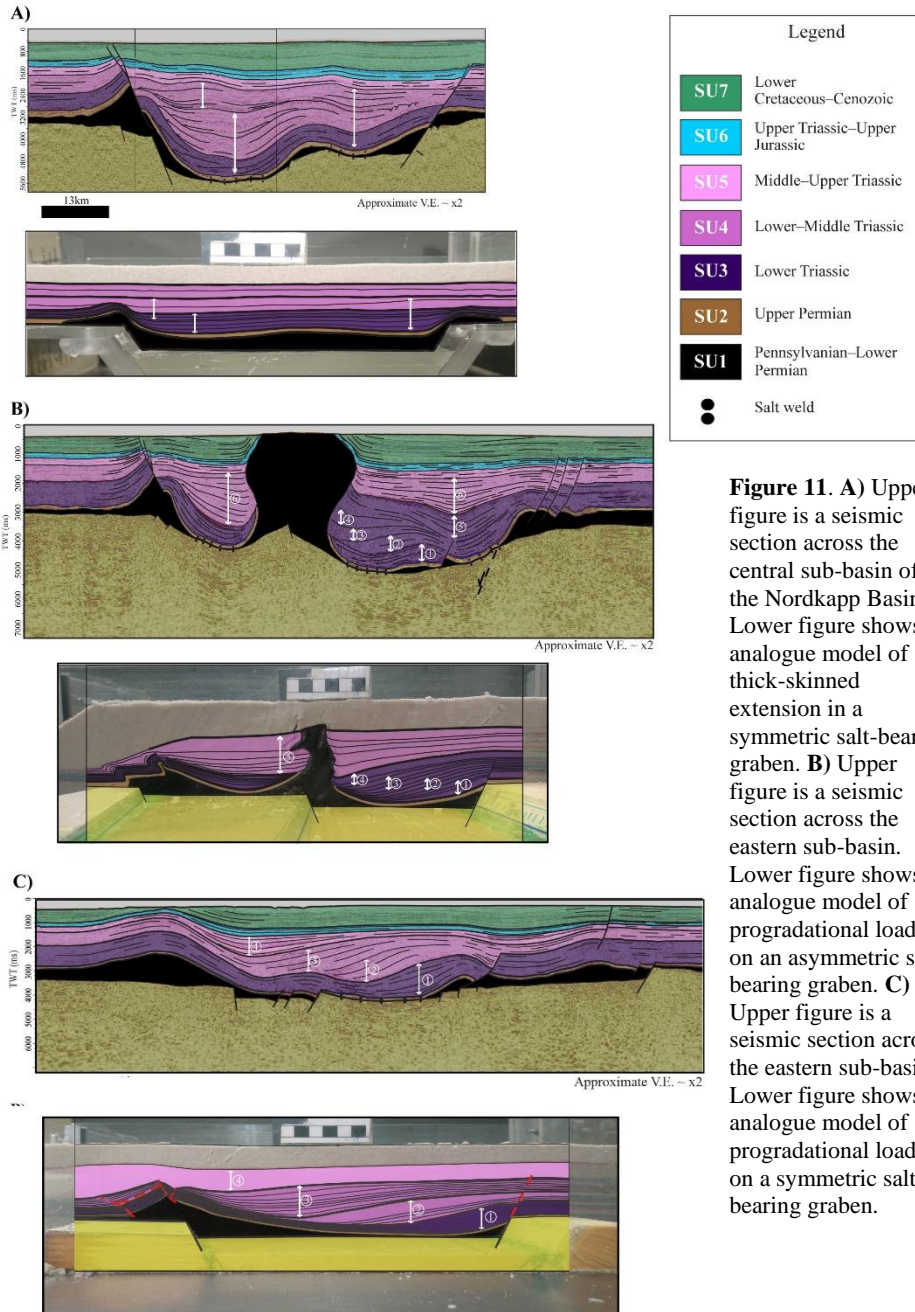


Figure 11. A) Upper figure is a seismic section across the central sub-basin of the Nordkapp Basin. Lower figure shows an analogue model of thick-skinned extension in a symmetric salt-bearing graben. B) Upper figure is a seismic section across the eastern sub-basin. Lower figure shows an analogue model of progradational loading on an asymmetric salt-bearing graben. C) Upper figure is a seismic section across the eastern sub-basin. Lower figure shows an analogue model of progradational loading on a symmetric salt-bearing graben.

structural style in the following ways: (1) Subsalt faults facing sediment progradation and perpendicular to the progradation act as barriers to salt flow, favouring salt inflation and the formation of salt diapirs above these structures (Fig 11B, lower figure), (2) Faults oblique to the progradation front cause the partitioning of salt flow into a component perpendicular to the progradation which favours salt flow along strike, and a component parallel to the progradation which results in minor inflations and subsequent formation of salt pillows, (3) Fault intersections facing the progradation direction favour salt accumulation and diapirism, and (4) Along-strike narrowing of the basin, either by the presence of intrabasinal faults or by non-parallel basin bounding faults, results in earlier timing of salt withdrawal and diapirism due to the reduced space salt has to flow and accommodate sediment loading.

Finally, the paper compares the final stage of the analogue models to seismic sections across the eastern and central sub-basins of the Nordkapp Basin, where the relative contribution of the studied triggers and variations in subsalt relief resulted in similar structural styles (Fig. 11)

6.3 *Paper III: The influence of halokinesis on prograding clinoforms: insights from the Tiddlybanken Basin, Norwegian Barents Sea*

Paper III combines observations from 2D seismic reflection data, borehole data, 3D structural restorations, and forward stratigraphic modelling to evaluate the impact of salt movement on the Lower Cretaceous clinoforms prograding across the Tiddlybanken Basin (Norwegian Barents Sea). The results from this integrated approach indicate that salt mobilization influenced clinoform progradation by: (1) creating lateral variations in progradation rates (Fig. 12B and E), which controlled the location of the coastline and shelf break along the salt-

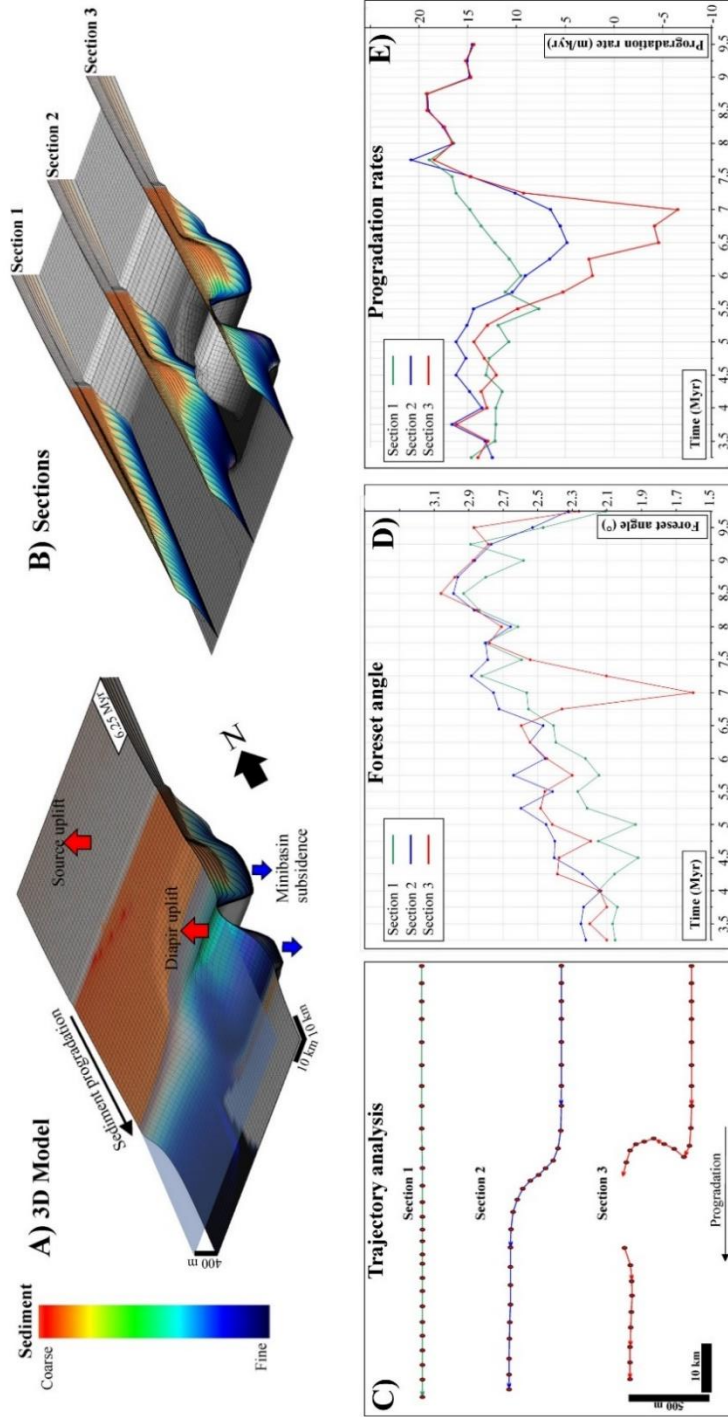


Figure 12. A) Synthetic GPM model illustrating the effects of salt tectonics on prograding clinoforms. B) Location of the sections 1, 2, and 3. Section 1 is located on a stable platform without influence of salt tectonics. Section 2 covers the edge of a salt withdrawal minibasin without salt diapirs. Section 3 crosses a salt wall and two minibasins. Note that salt tectonics induce lateral variations in clinoform trajectory, geometry and stacking patterns of depositional environments. C) Comparison between different trajectories observed in sections 1, 2, 3. D) Foreset angles along sections 1, 2, 3. E) Progradation rates along sections 1, 2, 3.

bearing basin (Fig. 12A), (2) inducing spatial and temporal variations in clinoform trajectory, which controlled stacking patterns and reservoir distribution in salt minibasins (Fig. 12B and C), and (3) increasing foreset angles, which affected the clinoform profile and trigger slope-readjustment processes (Fig. 12B and D).

Finally, the paper highlights the importance of using forward stratigraphic models to analyse clinoforms in tectonically active areas. Processes such as progressive tilting and post-depositional rotation of clinoforms could lead to wrong interpretation of foreset angles and trajectories, which can negatively affect reservoir prediction.

6.4 *Paper IV: Controls on minibasin infill in the Nordkapp Basin: evidence of complex Triassic syn-sedimentary deposition influenced by salt tectonics*

Paper IV combines observations from 3D seismic data, borehole data, and prospect/minibasin-scale restorations in a small area of the western sub-basin of the Nordkapp Basin with the purpose of: (1) evaluating the processes that control diapir growth and minibasin subsidence, (2) identifying and describing near-diapir deformation processes, and (3) understanding how diapir growth and minibasin subsidence affect the distribution of Triassic reservoirs and source rocks around salt structures.

In terms of salt tectonics, the area of study was affected by: (1) late Permian-Early Triassic minor salt mobilization, (2) Early-Middle Triassic transition from reactive to passive diapirism, (3) Middle Triassic-Jurassic passive diapirism, (4) Late Jurassic-Early Cretaceous active diapirism, and (5) Cenozoic contraction and diapir rejuvenation (Fig. 13). Rapid horizontal and vertical changes in depositional environments in well 7228/7/1A, together with high variability in seismic response and strata terminations indicate complex Triassic syn-sedimentation induced by salt tectonics (Fig. 13). During the Early-

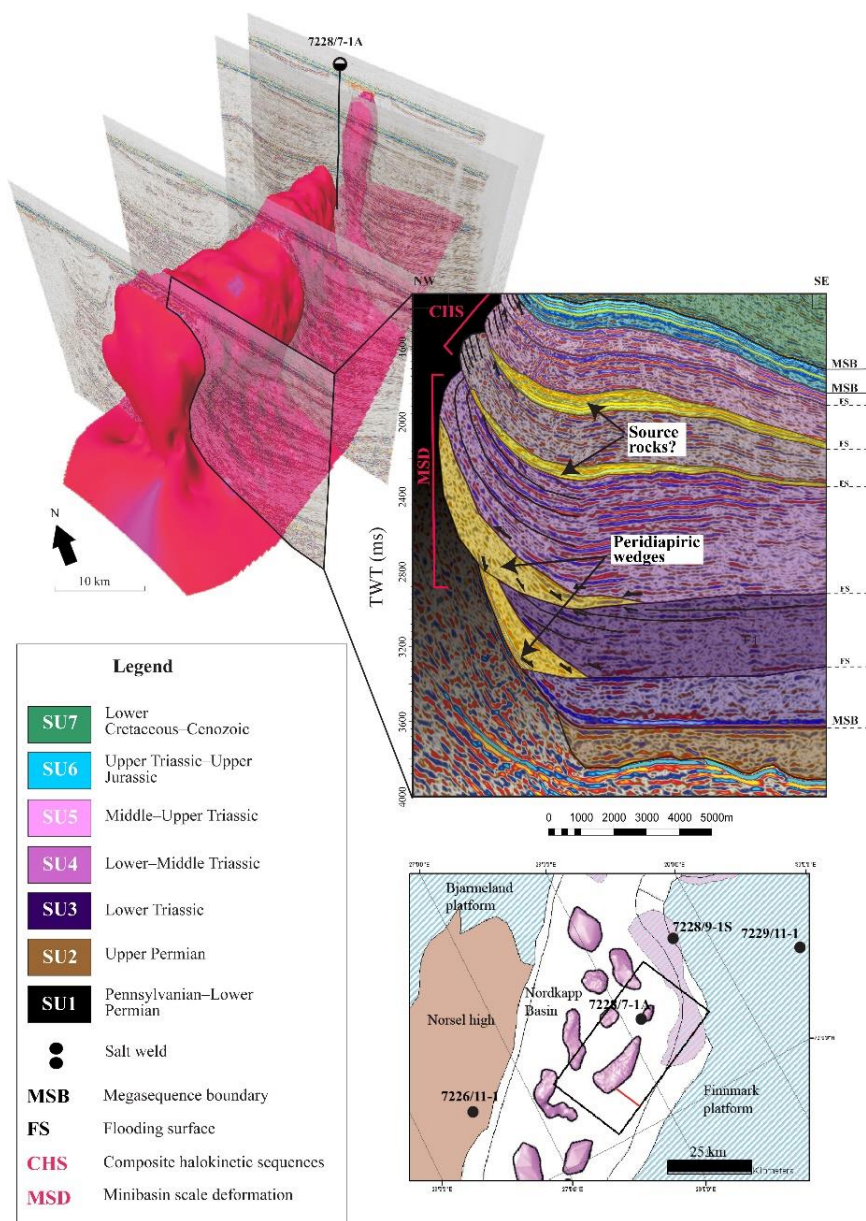


Figure 13. In the western sub-basin of the Nordkapp Basin, the Lower Triassic and Middle Triassic was characterized by minibasin scale deformation (MSD) resulting in wide areas of wide folding (>1 km). Composite Halokinetic Sequences (CHS) formed during the Middle-Late Triassic, and they were characterized by localized areas of drape folding (< 1km). Note also the complex minibasin infill with peridiapiric wedges near salt diapirs and possible intervals of source rocks (local high amplitudes) in salt minibasins.

Middle Triassic, the transition from a roller to a passive diapir generated wide areas of diapir-related deformation (> 2 km) causing minibasin-scale drape folding of adjacent sediments (Fig. 6A and 13). Since the Barents Sea was a shallow shelf, salt-related uplift formed topographic highs which acted as local sources of sediments and sediment reworking, resulting in the deposition of peri-diapiric wedges at diapir flanks (Fig. 13). The interpretation of these wedges is uncertain. Based on the presence of fan-shape depocenters, they are interpreted as debris flows or fan deltas locally sourced from the uplifted roof of salt diapirs. However, the deposition of carbonate platforms above the salt diapirs remains a possibility. During the Middle-Triassic -Jurassic, salt diapirs acted as topographic highs, whereas ongoing sedimentation occurred in the surrounding minibasins. Passive growth resulted in local drape folding (<1 km) of adjacent strata, forming composite halokinetic sequences (CHS; Fig. 6C and 13). Minibasin subsidence, on the other hand, controlled the spatial and temporal distribution of fluviodeltaic systems. Areas of large subsidence resulted in the local embayment of minibasins, which favoured the deposition of organic-rich source intervals (Fig. 13). As salt-related subsidence decreased due to welding, new progradation of fluviodeltaic sediments covered previous embayments and may have deposited potential reservoirs adjacent to the salt structures.

6.5 *Paper V: The impact of salt tectonics on the thermal evolution and petroleum system of confined rift basins: insights from Basin Modelling of the Nordkapp Basin, Norwegian Barents Sea*

Paper V, in which I am the second author, combines structural restorations from paper I with thermal modelling (Fig. 14), with the objective of understanding the impact of salt movement on the thermal evolution and petroleum system of the Nordkapp Basin.

The paper tests two contrasting scenarios in the Nordkapp Basin: (1) closely-spaced diapirs in the central sub-basin, and (2) an isolated and wide salt diapir in the eastern sub-basin. Thermal modelling in the first case indicates that the negative thermal anomalies produced by each diapir mutually interfere, and form a combined thermal anomaly that reduces the temperature in the minibasins by up to 50° C with respect to the adjacent basin shoulders (Fig. 14B). In the eastern sub-basin, however, the presence of a wide and isolated diapir induces a strong but laterally limited negative thermal anomaly, with the strata adjacent to the salt diapir cooled down by up to 70° C. Based on these observations, deep Paleozoic source rocks (e.g. Permian and Carboniferous) could be still generating hydrocarbons in areas adjacent to salt diapirs and at basin boundaries (Fig. 14C). At the basin axis, however, Middle Triassic source rocks (Top Kobbe-Lower Snadd) seem to be the most important source rock as observed in the Pandora discovery (7228/7-1A). Upper Jurassic source rocks, on the other hand, remain immature with localized areas entering the early oil window after the Cenozoic sedimentation (Fig. 14C).

These findings open the possibility for new exploration concepts such as deeper hydrocarbon kitchens, deeper reservoirs, and entrapment in near-diapir structural and stratigraphic traps (Fig. 14C).

Summary of papers

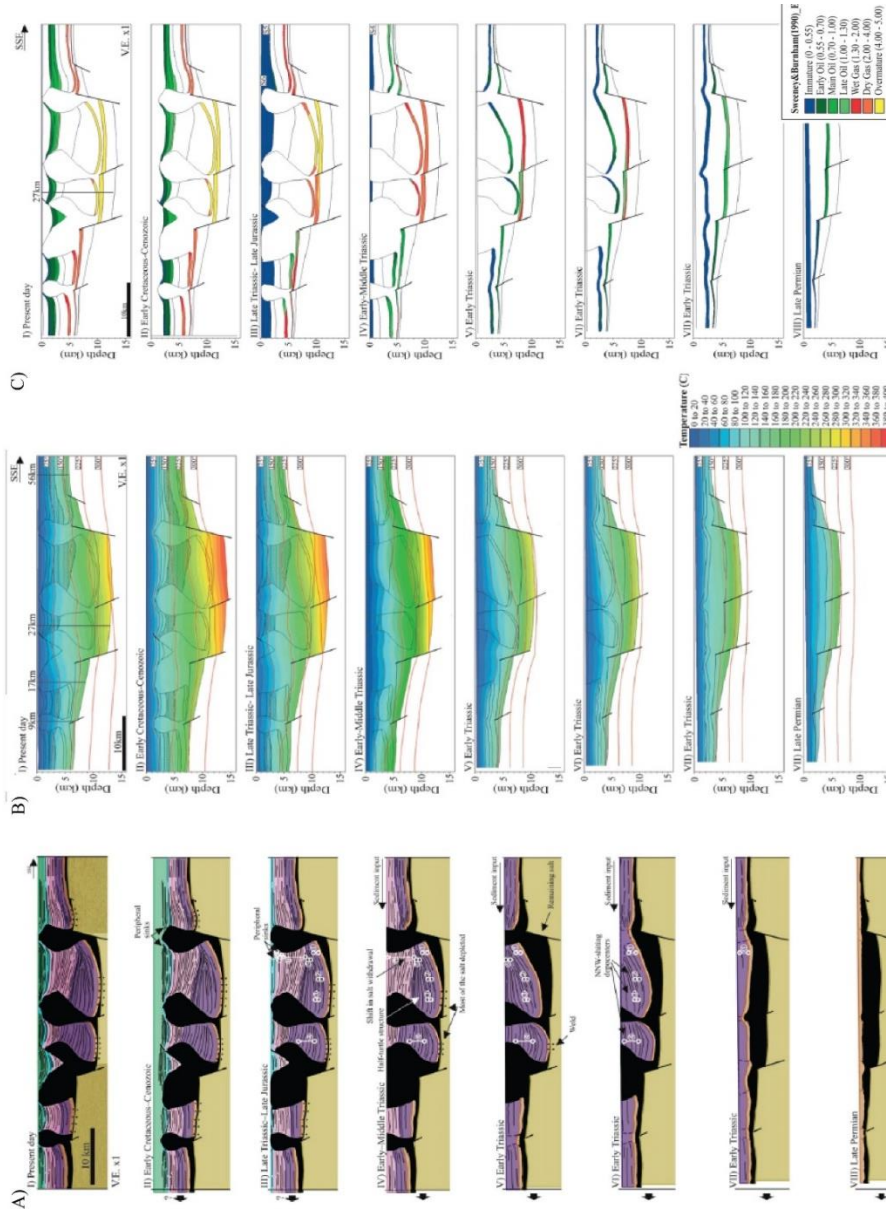


Figure 13. A) Structural restoration of a section across the central sub-basin of the Nordkapp Basin. B) Thermal evolution of the section. Notice how the closely-spaced diapirs decrease the temperature in the basin. C) Source rock maturation through time in the section.

Summary of papers

Intentionally left blank

7 Discussion

This section highlights the main findings and contributions of this study to the existing knowledge of salt tectonics in the Barents Sea and similar tectonic settings worldwide.

7.1 *Global implications for the understanding of salt-bearing rift basins*

Traditionally, salt tectonics in salt-bearing rift basins has been described as the result of basement involved extension (Koyi et al., 1993a; Stewart et al., 1997; Jackson and Lewis, 2016). Few studies have considered the coexistence of two processes such as basement involved extension and sediment progradation (Moragas et al., 2017). Papers I and II in the Nordkapp Basin demonstrate that the relative contribution of these two triggering mechanisms and subsalt relief had important implications for the following:

Along-strike variations in structural style

Seismic sections across the Nordkapp Basin show important differences in structural style along the basin (Fig. 10A). Papers I and II explain this variability in terms of the relative contribution of basement-involved extension versus sediment loading. For example, a higher contribution of progradational loading in the eastern sub-basin with respect to basement-involved extension generated younger diapirs and minibasins in the progradation direction (Fig. 11B and C). On the other hand, in areas where the contribution of basement-involved extension is higher such as in the central sub-basin, salt diapirs and pillows grew at both basin boundaries, they show opposite timing (distal diapirs are older), and minibasins display vertically stacked depocenters (Fig. 11A). Paper II additionally shows that each triggering mechanism results in different surface deformation, which has implications for understanding the spatial and temporal variation of sediment infill.

Timing of salt mobilization

Paper I shows that the combination of both triggering mechanisms resulted in along-strike differences in the timing of salt mobilization, welding, and depletion along the Nordkapp Basin (Fig. 10). Even though Early Triassic basement involved extension affected most of the basin, the central and eastern sub-basins underwent earlier sediment loading and subsequent salt mobilization due to their closer proximity to the sediment source, the Urals (Fig. 10B, step I). This produced earlier welding and salt depletion in these sub-basins, where most of the salt was evacuated by the end of the Middle Triassic (Fig. 10B, step III). Salt mobilization in the western sub-basin started by the end of the Early Triassic and continued until the end of the Early Cretaceous (Fig. 10B, step II-IV).

Nucleation of salt structures and minibasins

Analogue experiments from paper II together with seismic profiles across the Nordkapp Basin indicate that the presence of subsalt faults strongly controlled the distribution of salt structures in the basin (Figs. 10A, 11B). Subsalt faults perpendicular to the progradation direction and dipping oppositely to it, acted as flow barriers favouring the inflation and nucleation of salt walls above these structures (Figs. 10A, 11B).

Salt-related deformation rates

Paper II in addition demonstrates that lateral changes in subsalt relief not only contribute to the nucleation of salt structures and minibasins (Ge et al., 1997; Rowan and Lindsø, 2017), but also play an important role in the timing of diapirism and salt-related deformation rates. Increase in basin confinement by the presence of intrabasinal faults facing sediment progradation or by along-strike graben narrowing, results in an earlier timing of salt withdrawal and diapirism due to the reduced space salt has to flow and accommodate sediment loading. Since salt finds its way out through passive diapirism, salt-related deformation rates increase

considerably resulting in the formation of deep minibasins surrounded by salt diapirs. The role of basin confinement in the Nordkapp Basin is clear; the highest deformation rates occurred in narrow grabens (< 30 km) and in half grabens with intrabasinal faults facing sediment progradation (Fig. 11B and C).

Initial salt thickness estimates

Deciphering the mechanisms triggering salt movement in basins such as the Nordkapp Basin is difficult. The presence of prograding depocenters could indicate sediment progradation (Ge et al., 1997; Rowan and Lindsø, 2017). However, it is hard to tell whether subsalt faults were active during salt mobilization since most of the deformation associated with them can be accommodated by the salt (Koyi et al., 1995b; Nilsen et al., 1995; Withjack and Callaway, 2000). In Paper I, structural restorations provide clues about the triggering mechanisms of salt movement by looking at the restored initial salt thickness. Restorations assuming only sediment loading result in an unrealistic initial salt thickness > 6 km, while those including both sediment progradation and basement involved extension result in a more reasonable initial salt thickness of ~3 km. This tells us that the structural style of the basin results from the combination of these two processes.

7.2 *Global implications for the understanding of minibasin infill by prograding overburdens*

Salt-sediment interaction is a complex bi-directional process in which salt and sediments influence each other. Sandbox experiments in paper II illustrate how prograding overburdens induce differential loading and trigger salt mobilization, which results in the formation of salt diapirs and minibasins (Fig. 11B and C). This has been shown in many studies using analogue experiments (Koyi, 1996; Ge et al., 1997), numerical modelling (Albertz and Ings, 2012), and seismic interpretation (Trudgill, 2011; Rowan and Lindsø, 2017). The sandbox experiments also illustrate

that salt-related uplift and subsidence generate lateral variations in accommodation space along the basin. Paper III indicates that these variations result in lateral variations of clinoform trajectories, foreset angles, and progradation rates, which in turn have implications for reservoir partitioning (Fig. 12). In paper III, forward stratigraphic models and seismic sections show that clinoforms prograding across actively subsiding minibasins increase their foreset angle due to increasing water depth caused by salt withdrawal (Fig. 12B and D). Consequently, this process can affect clinoform equilibrium and trigger slope-readjustment processes such as slope erosion and sediment bypass via gravity flows and submarine fan-apron deposition.

Along-strike variations in clinoform trajectory result in a wide variability of stacking patterns and depositional environments (Fig. 12B and C). Ascending trajectories favour the vertical seaward stacking of shelf and fluviodeltaic depositional environments (Fig. 12B, section 2). Minibasin subsidence can also lead to important processes such as channel steering and lobe stacking as described in analogue experiments by Kopp and Kim (2015) and Liang et al. (2016). Paper III also illustrates that high minibasin subsidence can result in aggradation or even back-stepped stacking of shelf/fluviodeltaic deposits (Fig. 12B, section 3). This process is identified in the Nordkapp Basin (Paper IV) where minibasin subsidence during the Middle-Late Triassic favoured the marine embayment of minibasins and local deposition of source rocks (Fig. 13). Finally, forward stratigraphic models in paper III also illustrate erosion and sediment reworking above growing salt diapirs, which result in the deposition of peri-diapiric wedges as in the Nordkapp Basin (paper IV) and Tiddlybanken Basin (paper III; Fig. 13). In addition, diapir-induced force regressions can be an important process for delivering sediments to the slope and basin floor as documented in outcrops of the Lusitanian Basin (Pena dos Reis et al., 2017; Pimentel and Pena Dos Reis, 2018).

7.3 Regional implications for the Triassic paleogeography and petroleum system

The Triassic in the Norwegian Barents Sea has been generally interpreted as a tectonically quiet period, when transgressive-regressive fluviodeltaic systems sourced from the Urals and Fennoscandia prograded towards the northwestern part of the shelf (Riis et al., 2008; Glørstad-Clark et al., 2010; Klausen et al., 2015; Eide et al., 2017; Klausen et al., 2018). Paper I demonstrates that the Nordkapp Basin underwent a more complex tectonostratigraphic evolution characterized by the presence of subsalt and suprasalt faulting, shifting salt withdrawal depocenters, and extensive areas of salt diapirism (Fig. 10).

Sandbox experiments from paper II illustrate that important factors such as the type of triggering mechanism and subsalt relief, generate a wide variation of suprasalt structural styles, which in turn result in complex surface deformation. In the Nordkapp Basin, salt-related lateral variations in relative sea level played an important role in controlling the spatial and temporal distribution of the Triassic sequences defined by Glørstad-Clark et al. (2010). Papers III and IV show that salt-induced uplift could have induced sediment reworking and deposition of reservoirs above salt pillows or at diapir flanks. Salt withdrawal, on the other hand, might have caused the vertical stacking of fluviodeltaic deposits in salt minibasins, meaning that Triassic and Jurassic reservoirs could be thicker in the Nordkapp Basin than in the Finnmark and Bjarmeland platforms. Papers III and IV also illustrate that rapid salt withdrawal might result in the embayment of minibasins, providing good conditions for deposition of local source rocks. Moreover, Triassic to Jurassic fluviodeltaic reservoirs could be present in a wide number of traps, including megaflaps and halokinetic sequences near salt diapirs (paper IV, Fig. 13), half turtle structures caused by minibasin inversion (paper I), and suprasalt fault complexes at basin boundaries (paper I).

Finally, the study of spatial and temporal thermal fluctuations induced by salt mobilization is essential for the evaluation of the petroleum system in confined salt-bearing basins such as the Nordkapp Basin. Paper V indicates that thermal anomalies produced by closely-spaced diapirs mutually interfere and induce a combined anomaly that reduces the temperature in minibasins by up to 50° C with respect to the adjacent Finnmark and Bjarmeland platforms. Based on these results, Paleozoic source rocks (e.g. Carboniferous and Permian) could be still generating hydrocarbon in areas near salt diapirs and at basin boundaries. Diapir-induced negative thermal anomalies could have also prevented reservoir diagenesis, which enhances the prospectivity of Middle and Early Triassic reservoirs at large (> 3 km) depths. It is worth to mention that diapir-induced negative thermal anomalies might have also negative consequences in the petroleum system. Shallower Middle Triassic source rocks proven in well 7228/7-1A and presently laying in the oil window, could be still immature or in the early oil window in the near past due to the thermal effect of the diapirs. Based on these arguments, the thermal effect of salt can result in positive and negative consequences for the petroleum system, which deserves further and more detailed studies in the Nordkapp Basin.

7.4 Limitations

Although this study has significant implications for the understanding of salt tectonics in confined rift basins, it is important to highlight the main limitations. Understanding these limitations is essential for future research since it can promote the development of new methods in seismic acquisition and processing, as well as improve modelling tools to better understand salt-sediment interaction and hydrocarbon prospectivity.

Seismic data

The occurrence of closely-spaced salt structures in confined salt-bearing basins such as the Nordkapp Basin, makes seismic imaging and

interpretation of salt structures and minibasins challenging. This is a common problem in salt-bearing basins due to the steeply dipping diapir flanks and the complex ray paths of the seismic waves travelling through the salt (Jones and Davison, 2014; Rojo et al., 2016). Poor imaging of salt structures can lead to incorrect interpretation of their geometry and flanking minibasin strata (Giles and Rowan, 2012), which in turn increases the uncertainty in describing their progressive evolution from 2D and 3D structural restorations. Moreover, incorrect mapping of salt structures has a large impact in thermal modelling and petroleum system evaluation since diapir-induced thermal anomalies are strongly dependent on the shape of the diapirs (Mello et al., 1995). Thus, special techniques such as full azimuth seismic data (e.g. Nordkapp coil from WesternGeco Multiclient) are essential to study and evaluate the potential of confined-salt bearing basins.

Well data

The central and eastern sub-basins of the Nordkapp Basin and Tiddlybanken Basin are frontier areas with no exploration wells through their minibasins. Consequently, interval velocities of deep sediments in minibasins are unknown, increasing the uncertainty in depth conversion, structural restorations, and basin modelling. The lack of exploration wells also makes difficult the correlation between gamma-ray logs and seismic facies. Several seismic facies in paper IV have no well control, and the interpretation of depositional environments is based on seismic reflectivity and internal architectures.

Forward stratigraphic modelling

Forward stratigraphic modelling in paper III carries important limitations. Even though the modelling results clearly show the impact of salt tectonics on the geometry and trajectory of clinofolds, the GPM software does not reproduce the effect of differential sediment loading on the salt. In order to reproduce this effect, a time-dependent tectonic function was created where subsidence values were increased locally

Discussion

when the clinoforms reach the salt layer. This function was tuned up until the modelled clinoform geometries coincided with the ones observed on seismic profiles.

8 Future work

Towards a bidirectional understanding of salt tectonics and sedimentation

Future research can be oriented towards analysing bidirectional salt-sediment interaction. This can be studied via analogue and numerical models. In analogue models, a water current transporting sand of different grain sizes could form distributary channels and deposit deltaic lobes on top of a mobile substratum (e.g. silicone PDMS). This way, the syn-kinematic deposition of deltaic lobes and variations in stacking patterns induced by silicone mobilization underneath could be analysed. In forward stratigraphic models, the effect of sediment loading into a mobile substrate can be included explicitly as shown in numerical models by Albertz and Ings (2012), Peel (2014b) and Pichel et al. (2019).

The sandbox models from Paper II indicate that variables such as the type of triggering mechanism and subsalt basin configuration not only produce variations in structural style, but also result in different surface deformation. In natural examples, these salt-related surface deformations result in lateral fluctuations in relative sea level. Therefore, important variables in salt tectonics such as type of triggering mechanism, subsalt configuration, salt rheology and thickness, could be additionally taken into account in future sandbox experiments and numerical models to better understand the influence of these factors on sedimentation and reservoir distribution.

Hydrocarbon exploration in the Nordkapp Basin

Although this PhD provides a regional understanding of salt tectonics and basin infill of the Nordkapp Basin, large uncertainty remains in the interpretation due to the presence of closely-spaced salt structures that make seismic imaging difficult. Based on results from the Nordkapp coil (full azimuth 3D survey), the central and eastern sub-basins might host

Future work

significant amounts of hydrocarbons trapped in structural (e.g. truncations against salt) and stratigraphic traps (e.g. pinch-outs, halokinetic sequences) adjacent to salt structures. Therefore, future research in hydrocarbon exploration should primary focus on illuminating these areas properly via wide azimuth and full azimuth seismic acquisition since most of the prospects will be located near salt structures. Secondly, regional thickness maps in Paper I display large subsidence during the earliest Triassic (Havert Fm.) and Early-Middle Triassic (Klappmyss and Kobbe Fms) in the underexplored central and eastern subbasins. This large accommodation could have resulted in the generation of restricted subbasins and deposition of Lower Triassic (Klappmyss Fm.) and Middle Triassic (Kobbe Fm.) source rocks. Therefore, the presence of potential and thicker Triassic source rocks in the two basins remains a possibility and deserves further research. Finally, future studies in basin evolution and thermal modelling should intend to integrate 3D structural restorations with 3D thermal modelling. This will offer a more precise understanding of the basin in terms of salt mobilization, paleobathymetry, source rock maturity, and migration pathways through time.

9 Conclusions

Based on a multidisciplinary approach consisting on the interpretation of seismic and well data in the Nordkapp and Tiddlybanken basins, structural restorations, basin modelling, forward stratigraphic modelling, and sandbox experiments, this thesis significantly contributes to the knowledge of confined salt-bearing basins in the Barents Sea and similar tectonic settings worldwide. Our main findings are:

- 1) Confined salt-bearing basins such as the Nordkapp Basin might also display a mixed-mode triggering behaviour consisting of basement-involved extension and progradational loading. Areas where sediment loading has a higher contribution are characterized by the formation of younger minibasins and salt structures in the progradation direction. Areas dominated by thick-skinned extension, on the other hand, are characterized by deep minibasins surrounded by salt diapirs at both basin boundaries, and older distal diapirs. Based on these arguments, each salt-flow triggering process create along-strike differences in structural style and surface deformation, which play an important role in reservoir and source rock distribution and in the timing of structural and stratigraphic traps. Mixed-mode salt-flow triggers is a useful concept to understand the tectonostratigraphic evolution of confined salt-bearing basins as well as its implication for the petroleum system.
- 2) Lateral changes in subsalt relief strongly influence the suprasalt structural style of confined salt-bearing basins in the following ways: (1) subsalt faults facing perpendicularly the progradation front contribute to salt inflation and formation of salt diapirs whereas thin-skinned faults form above subsalt faults dipping in the progradation direction; (2) subsalt faults facing obliquely the progradation front induce partitioning of the salt flow and favour salt flow along the graben; and (3) along strike differences in basin confinement either by graben narrowing or by the presence of intrabasinal faults induce

Conclusions

along strike variations in the timing of salt mobilization and deformation rates, which in turn result in different surface deformation and lateral changes in relative level.

- 3) Changes in relative sea level by salt tectonics cause lateral variations in progradation rates, foreset angle and trajectory of prograding clinoforms. Firstly, an increase in foreset angles due to an increase in water depth by minibasin subsidence can affect clinoform equilibrium and subsequently, trigger slope-readjustment processes such as slope erosion and sediment bypass via gravity flows and submarine fan-apron deposition. Secondly, ascending trajectories caused by salt withdrawal could lead to channel steering and lobe stacking, resulting in relatively thicker shallow marine and fluviodeltaic reservoirs stored in salt minibasins. In addition, minibasin subsidence might also result in the local flooding of minibasins, favouring the deposition of source rocks. Finally, diapir uplift might contribute to sediment reworking and the deposition of potential reservoirs near salt diapirs and on top of salt pillows.
- 4) Salt mobilization affected the petroleum systems of the Barents Sea. Minibasin subsidence led to the deposition of thicker Triassic and Jurassic reservoirs in salt minibasins. However, rapid minibasin subsidence could also result in local embayments and deposition of Triassic source rocks. Diapir growth, on the other hand, produced erosion/reworking of Triassic overburdens, which may have led to the deposition of potential reservoirs near salt structures. These reservoirs could have been trapped in megaflaps, minibasin-scale drape folding, and halokinetic sequences caused by diapir growth. Finally, the negative thermal anomalies induced by salt diapirs may have retarded rock source maturation and reservoir diagenesis, increasing the chances for deep hydrocarbon kitchens and reservoirs, and near-diapir traps.

10 References

- Albertz, M., and S. J. Ings, 2012, Some consequences of mechanical stratification in basin-scale numerical models of passive-margin salt tectonics: Geological Society, London, Special Publications, v. 363, p. 303-330, doi: 10.1144/sp363.14.
- Anderson, J. B., 2005, Diachronous development of late Quaternary shelf-margin deltas in the northwestern Gulf of Mexico: implications for sequence stratigraphy and deep-water reservoir occurrence, *in* L. Giosan, and J. P. Bhattacharya, eds., *River Deltas—Concepts, Models, and Examples*, v. 83, SEPM Special Publication, p. 257-276, doi: 10.2110/pec.05.83.0257.
- Anderson, J. B., D. J. Wallace, A. R. Simms, A. B. Rodriguez, R. W. R. Weight, and Z. P. Taha, 2016, Recycling sediments between source and sink during a eustatic cycle: Systems of late Quaternary northwestern Gulf of Mexico Basin: *Earth-Science Reviews*, v. 153, p. 111-138, doi: 10.1016/j.earscirev.2015.10.014.
- Anell, I., A. Braathen, and S. Olaussen, 2014, The Triassic--Early Jurassic of the northern Barents Shelf: a regional understanding of the Longyearbyen CO 2 reservoir: *Norwegian Journal of Geology*, v. 94, p. 83-98,
- Aschoff, J. L., and K. A. Giles, 2005, Salt diapir-influenced, shallow-marine sediment dispersal patterns: Insights from outcrop analogs: *AAPG Bulletin*, v. 89, p. 447-469, doi: 10.1306/10260404016.
- Baig, I., J. I. Faleide, J. Jahren, and N. H. Mondol, 2016, Cenozoic exhumation on the southwestern Barents Shelf: Estimates and uncertainties constrained from compaction and thermal maturity analyses: *Marine and Petroleum Geology*, v. 73, p. 105-130, doi: 10.1016/j.marpetgeo.2016.02.024.

References

- Banham, S. G., and N. P. Mountney, 2013, Controls on fluvial sedimentary architecture and sediment-fill state in salt-walled mini-basins: Triassic Moenkopi Formation, Salt Anticline Region, SE Utah, USA: *Basin Research*, v. 25, p. 709-737, doi: 10.1111/bre.12022.
- Barton, D. C., 1933, Mechanics of formation of salt domes with special reference to Gulf Coast salt domes of Texas and Louisiana: *AAPG Bulletin*, v. 17, p. 1025-1083,
- Brun, J.-P., and X. Fort, 2011, Salt tectonics at passive margins: Geology versus models: *Marine and Petroleum Geology*, v. 28, p. 1123-1145, <https://doi.org/10.1016/j.marpetgeo.2011.03.004>.
- Bugge, T., G. Mangerud, G. Elvebakk, A. Mork, I. Nilsson, S. Fanavoll, and J. Vigran, 1995, Upper Paleozoic succession on the Finnmark platform, Barents Sea: *Norwegian Journal of Geology*, v. 75, p. 3-30,
- Carter, R. C., M. R. Gani, T. Roesler, and A. K. Sarwar, 2016, Submarine channel evolution linked to rising salt domes, Gulf of Mexico, USA: *Sedimentary Geology*, v. 342, p. 237-253, doi: 10.1016/j.sedgeo.2016.06.021.
- Clark, S. A., E. Glorstad-Clark, J. I. Faleide, D. Schmid, E. H. Hartz, and W. Fjeldskaar, 2014, Southwest Barents Sea rift basin evolution: comparing results from backstripping and time-forward modelling: *Basin Research*, v. 26, p. 550-566, doi: 10.1111/bre.12039.
- Cohen, H. A., and S. Hardy, 1996, Numerical modelling of stratal architectures resulting from differential loading of a mobile substrate: *Geological Society, London, Special Publications*, v. 100, p. 265-273, doi: 10.1144/gsl.Sp.1996.100.01.17.
- Corfu, F., S. Polteau, S. Planke, J. I. Faleide, H. Svensen, A. Zayoncheck, and N. Stolbov, 2013, U–Pb geochronology of Cretaceous magmatism on Svalbard and Franz Josef Land, Barents

References

- Sea Large Igneous Province: *Geological Magazine*, v. 150, p. 1127-1135, doi: 10.1017/S0016756813000162.
- Coward, M., and S. Stewart, 1995, Salt-influenced structures in the Mesozoic-Tertiary cover of the southern North Sea, UK
- Dengo, C., and K. Røssland, 1992, Extensional tectonic history of the western Barents Sea, *in* R. M. Larsen, H. Brekke, B. T. Larsen, and E. Talleraas, eds., *Structural and Tectonic Modelling and Its Application to Petroleum Geology: Norwegian Petroleum Society (NPF), Special Publications*, v. 1, p. 91-108,
- Dooley, T. P., M. R. Hudec, L. M. Pichel, and M. P. A. Jackson, 2018, The impact of base-salt relief on salt flow and suprasalt deformation patterns at the autochthonous, paraautochthonous and allochthonous level: insights from physical models: *Geological Society, London, Special Publications*, v. 476, p. SP476.13, 10.1144/sp476.13.
- Dreyer, T., M. Whitaker, J. Dexter, H. Flesche, and E. Larsen, 2005, From spit system to tide-dominated delta: integrated reservoir model of the Upper Jurassic Sognefjord Formation on the Troll West Field: *Geological Society, London, Petroleum Geology Conference series*, p. 423-448.
- Eide, C. H., T. G. Klausen, D. Katkov, A. A. Suslova, and W. Helland-Hansen, 2017, Linking an Early Triassic delta to antecedent topography: Source-to-sink study of the southwestern Barents Sea margin: *GSA Bulletin*, v. 130, p. 263-283, doi: 10.1130/B31639.1.
- Faleide, J. I., E. Vågnes, and S. T. Gudlaugsson, 1993, Late Mesozoic-Cenozoic evolution of the south-western Barents Sea in a regional rift-shear tectonic setting: *Marine and Petroleum Geology*, v. 10, p. 186-214, doi: 10.1016/0264-8172(93)90104-Z.
- Faleide, J. I., F. Tsikalas, A. J. Breivik, R. Mjelde, O. Ritzmann, O. Engen, J. Wilson, and O. Eldholm, 2008, Structure and evolution of

References

- the continental margin off Norway and the Barents Sea: Episodes, v. 31, p. 82-91,
- Flemings, P. B., and J. P. Grotzinger, 1996, STRATA: Freeware for analyzing classic stratigraphic problems: GSA Today, v. 6, p. 1-7,
- Gabrielsen, R., O. Kløvjan, A. Rasmussen, and T. Stølan, 1992, Interaction between halokinesis and faulting: structuring of the margins of the Nordkapp Basin, Barents Sea region, *in* B. Larsen, H. Brekke, B. Larsen, and E. Talleraas, eds., Structural and tectonic modelling and its implication to petroleum geology: Norwegian Petroleum Society (NPF), Special Publications, v. 1, p. 121-131,
- Gac, S., P. Klitzke, A. Minakov, J. I. Faleide, and M. Scheck-Wenderoth, 2016, Lithospheric strength and elastic thickness of the Barents Sea and Kara Sea region: Tectonophysics, v. 691, p. 120-132, doi: 10.1016/j.tecto.2016.04.028.
- Gaullier, V., and B. C. Vendeville, 2005, Salt tectonics driven by sediment progradation: Part II—Radial spreading of sedimentary lobes prograding above salt: AAPG Bulletin, v. 89, p. 1081-1089, 10.1306/03310503064.
- Ge, H., M. P. Jackson, and B. C. Vendeville, 1997, Kinematics and dynamics of salt tectonics driven by progradation: AAPG Bulletin, v. 81, p. 398-423,
- Ge, Z., R. L. Gawthorpe, A. Rotevatn, and M. B. Thomas, 2017, Impact of normal faulting and pre-rift salt tectonics on the structural style of salt-influenced rifts: the Late Jurassic Norwegian Central Graben, North Sea: Basin Research, v. 29, p. 674-698, 10.1111/bre.12219.
- Gernigon, L., M. Brönnner, D. Roberts, O. Olesen, A. Nasuti, and T. Yamasaki, 2014, Crustal and basin evolution of the southwestern Barents Sea: from Caledonian orogeny to continental breakup: Tectonics, v. 33, p. 347-373, doi: 10.1002/2013TC003439.

References

- Gernigon, L., M. Brönnner, M.-A. Dumais, S. Gradmann, A. Grønlie, A. Nasuti, and D. Roberts, 2018, Basement inheritance and salt structures in the SE Barents Sea: Insights from new potential field data: *Journal of Geodynamics*, v. 119, p. 82-106, doi: 10.1016/j.jog.2018.03.008.
- Giles, K. A., and T. F. Lawton, 2002, Halokinetic sequence stratigraphy adjacent to the El Papalote diapir, northeastern Mexico: *AAPG Bulletin*, v. 86, p. 823-840,
- Giles, K. A., and M. G. Rowan, 2012, Concepts in halokinetic-sequence deformation and stratigraphy, *in* G. I. Alsop, S. G. Archer, A. J. Hartley, N. T. Grant, and R. Hodgkinson, eds., *Salt Tectonics, Sediments and Prospectivity: Geological Society, London, Special Publications*, v. 363, p. 7-31, doi: 10.1144/SP363.2.
- Glørstad-Clark, E., J. I. Faleide, B. A. Lundschieen, and J. P. Nystuen, 2010, Triassic seismic sequence stratigraphy and paleogeography of the western Barents Sea area: *Marine and Petroleum Geology*, v. 27, p. 1448-1475, doi: 10.1016/j.marpetgeo.2010.02.008.
- Grantz, A., P. E. Hart, and V. A. Childers, 2011, Geology and tectonic development of the Amerasia and Canada Basins, Arctic Ocean, *in* A. M. Spencer, A. F. Embry, D. L. Gautier, A. V. Stoupakova, and K. Sørensen, eds., *Arctic Petroleum Geology: Geological Society, London, Memoirs*, v. 35, p. 771-799, doi: 10.1144/M35.50.
- Grundvåg, S. A., D. Marin, B. Kairanov, K. K. Śliwińska, H. Nøhr-Hansen, M. E. Jelby, A. Escalona, and S. Olausen, 2017, The Lower Cretaceous succession of the northwestern Barents Shelf: Onshore and offshore correlations: *Marine and Petroleum Geology*, v. 86, p. 834-857, doi: 10.1016/j.marpetgeo.2017.06.036.
- Gudlaugsson, S., J. Faleide, S. Johansen, and A. Breivik, 1998, Late Palaeozoic structural development of the south-western Barents Sea: *Marine and Petroleum Geology*, v. 15, p. 73-102, doi:10.1016/S0264-8172(97)00048-2.

References

- Hearon IV, T. E., M. G. Rowan, K. A. Giles, and W. H. Hart, 2014, Halokinetic deformation adjacent to the deepwater Auger diapir, Garden Banks 470, northern Gulf of Mexico: Testing the applicability of an outcrop-based model using subsurface data: *Interpretation*, v. 2, p. SM57-SM76, doi: 10.1190/INT-2014-0053.1.
- Helland-Hansen, W., and G. J. Hampson, 2009, Trajectory analysis: concepts and applications: *Basin Research*, v. 21, p. 454-483, doi: 10.1111/j.1365-2117.2009.00425.x.
- Henriksen, E., H. Bjørnseth, T. Hals, T. Heide, T. Kiryukhina, O. Kløvjan, G. Larssen, A. Ryseth, K. Rønning, and K. Sollid, 2011a, Uplift and erosion of the greater Barents Sea: impact on prospectivity and petroleum systems, *in* A. M. Spencer, A. F. Embry, D. L. Gautier, A. V. Stoupakova, and K. Sørensen, eds., *Arctic Petroleum Geology: Geological Society, London, Memoirs*, v. 35, p. 271-281, doi: 10.1144/M35.17.
- Henriksen, E., A. Ryseth, G. Larssen, T. Heide, K. Rønning, K. Sollid, and A. Stoupakova, 2011b, Tectonostratigraphy of the greater Barents Sea: implications for petroleum systems, *in* A. M. Spencer, A. F. Embry, D. L. Gautier, A. V. Stoupakova, and K. Sørensen, eds., *Arctic Petroleum Geology: Geological Society, London, Memoirs*, v. 35, p. 163-195, doi: 10.1144/M35.10.
- Houseknecht, D. W., K. J. Bird, and C. J. Schenk, 2009, Seismic analysis of clinoform depositional sequences and shelf-margin trajectories in Lower Cretaceous (Albian) strata, Alaska North Slope: *Basin Research*, v. 21, p. 644-654, doi: 10.1111/j.1365-2117.2008.00392.x.
- Hubbert, M. K., 1937, Theory of scale models as applied to the study of geologic structures: *GSA Bulletin*, v. 48, p. 1459-1520, 10.1130/gsab-48-1459.

References

- Hudec, M. R., and M. P. Jackson, 2007, Terra infirma: Understanding salt tectonics: *Earth-Science Reviews*, v. 82, p. 1-28, doi: 10.1016/j.earscirev.2007.01.001.
- Jackson, C. A.-L., G. M. Elliott, E. Royce-Rogers, R. L. Gawthorpe, and T. E. Aas, 2019, Salt thickness and composition influence rift structural style, northern North Sea, offshore Norway: *Basin Research*, v. 31, p. 514-538, 10.1111/bre.12332.
- Jackson, C. A. L., M. P. A. Jackson, and M. R. Hudec, 2015, Understanding the kinematics of salt-bearing passive margins: A critical test of competing hypotheses for the origin of the Albian Gap, Santos Basin, offshore Brazil: *GSA Bulletin*, v. 127, p. 1730-1751, doi: 10.1130/B31290.1.
- Jackson, C. A. L., and M. M. Lewis, 2016, Structural style and evolution of a salt-influenced rift basin margin; the impact of variations in salt composition and the role of polyphase extension: *Basin Research*, v. 28, p. 81-102, doi: 10.1111/bre.12099.
- Jackson, C. A. L., and S. A. Stewart, 2017, Chapter 8 - Composition, Tectonics, and Hydrocarbon Significance of Zechstein Supergroup Salt on the United Kingdom and Norwegian Continental Shelves: A Review, in J. I. Soto, J. F. Flinch, and G. Tari, eds., *Permo-Triassic Salt Provinces of Europe, North Africa and the Atlantic Margins*, Elsevier, p. 175-201, <https://doi.org/10.1016/B978-0-12-809417-4.00009-4>.
- Jackson, M., and B. Vendeville, 1994, Regional extension as a geologic trigger for diapirism: *Geological Society of America bulletin*, v. 106, p. 57-73,
- Jackson, M., and J. Harrison, 2006, An allochthonous salt canopy on Axel Heiberg Island, Sverdrup Basin, Arctic Canada: *Geology*, v. 34, p. 1045-1048, doi: 10.1130/G22798A.1.

References

- Jackson, M. P., and M. R. Hudec, 2017, *Salt Tectonics: Principles and Practice*, Cambridge University Press, 498 p.
- Jackson, M. P. A., and M. R. Hudec, 2005, Stratigraphic record of translation down ramps in a passive-margin salt detachment: *Journal of Structural Geology*, v. 27, p. 889-911, <https://doi.org/10.1016/j.jsg.2005.01.010>.
- Jensen, L. N., and K. Sørensen, 1992, Tectonic framework and halokinesis of the Nordkapp Basin, Barents Sea, in R. M. Larsen, H. Brekke, B. T. Larsen, and E. Talleraas, eds., *Structural and Tectonic Modelling and its Application to Petroleum Geology: Norwegian Petroleum Society (NPF), Special Publications*, v. 1, p. 109-120,
- Jones, I. F., and I. Davison, 2014, Seismic imaging in and around salt bodies: *Interpretation*, v. 2, p. SL1-SL20,
- Kernen, R. A., K. A. Giles, M. G. Rowan, T. F. Lawton, and T. E. Hearon, 2012, Depositional and halokinetic-sequence stratigraphy of the Neoproterozoic Wonoka Formation adjacent to Patawarta allochthonous salt sheet, Central Flinders Ranges, South Australia, in G. I. Alsop, S. G. Archer, A. J. Hartley, N. T. Grant, and R. Hodgkinson, eds., *Salt Tectonics, Sediments and Prospectivity: Geological Society, London, Special Publications*, v. 363, p. 81-105, doi: 10.1144/SP363.5.
- Klausen, T., T. J. Aas, E. C. Haug, A. Behzad, O. Snorre, and C. Domenico, 2018, Clinoform development and topset evolution in a mud-rich delta – the Middle Triassic Kobbe Formation, Norwegian Barents Sea: *Sedimentology*, v. 65, p. 1132-1169, doi:10.1111/sed.12417.
- Klausen, T., and W. Helland-Hansen, 2018, Methods For Restoring and Describing Ancient Clinoform Surfaces: *Journal of Sedimentary Research*, v. 88, p. 241-259, doi: 10.2110/jsr.2018.8.

References

- Klausen, T. G., A. E. Ryseth, W. Helland-Hansen, R. Gawthorpe, and I. Laursen, 2015, Regional development and sequence stratigraphy of the Middle to Late Triassic Snadd Formation, Norwegian Barents Sea: *Marine and Petroleum Geology*, v. 62, p. 102-122, doi: 10.1016/j.marpetgeo.2015.02.004.
- Kopp, J., and W. Kim, 2015, The effect of lateral tectonic tilting on fluviodeltaic surficial and stratal asymmetries: experiment and theory: *Basin Research*, v. 27, p. 517-530, doi: 10.1111/bre.12086.
- Koyi, H., M. K. Jenyon, and K. Petersen, 1993a, The effect of basement faulting on diapirism: *Journal of Petroleum Geology*, v. 16, p. 285-312, DOI: 10.1111/j.1747-5457.1993.tb00339.x.
- Koyi, H., and K. Petersen, 1993, Influence of basement faults on the development of salt structures in the Danish Basin: *Marine and Petroleum Geology*, v. 10, p. 82-94, DOI: [http://dx.doi.org/10.1016/0264-8172\(93\)90015-K](http://dx.doi.org/10.1016/0264-8172(93)90015-K).
- Koyi, H., C. J. Talbot, and B. O. Tørudbakken, 1993b, Salt diapirs of the southwest Nordkapp Basin: analogue modelling: *Tectonophysics*, v. 228, p. 167-187, doi: 10.1016/0040-1951(93)90339-L.
- Koyi, H., C. J. Talbot, and B. Torudbakken, 1995a, Analogue models of salt diapirs and seismic interpretation in the Nordkapp Basin, Norway: *Petroleum geoscience*, v. 1, p. 185-192, doi: 10.1144/petgeo.1.2.185.
- Koyi, H., C. J. Talbot, and B. O. Tørudbakken, 1995b, Salt tectonics in the Northeastern Nordkapp basin, Southwestern Barents sea, *in* M. P. A. Jackson, D. G. Roberts, and S. Snelson, eds., *Salt Tectonics: A Global Perspective*, AAPG Memoir 65, p. 437-447,
- Koyi, H., 1996, Salt flow by aggrading and prograding overburdens, *in* G. I. Alsop, D. J. Blundell, and I. Davison, eds., *Salt tectonics*,

References

- Geological Society, London, Special Publications, v. 100, p. 243-258, doi: 10.1144/gsl.sp.1996.100.01.15.
- Krantz, R. W., 1991, Measurements of friction coefficients and cohesion for faulting and fault reactivation in laboratory models using sand and sand mixtures: *Tectonophysics*, v. 188, p. 203-207, [https://doi.org/10.1016/0040-1951\(91\)90323-K](https://doi.org/10.1016/0040-1951(91)90323-K).
- Liang, M., W. Kim, and P. Passalacqua, 2016, How much subsidence is enough to change the morphology of river deltas?: *Geophysical Research Letters*, v. 43, p. 10,266-10,276, doi: 10.1002/2016gl070519.
- M. Pichel, L., E. Finch, and R. L. Gawthorpe, 2019, The Impact of Pre-Salt Rift Topography on Salt Tectonics: A Discrete-Element Modeling Approach: *Tectonics*, v. 38, p. 1466-1488, 10.1029/2018tc005174.
- Marin, D., A. Escalona, H. Nøhr-Hansen, K. Śliwińska Kasia, and A. Mordasova, 2017, Sequence stratigraphy and lateral variability of Lower Cretaceous clinoforms in the SW Barents Sea: *AAPG Bulletin*, v. 101, p. 1487-1517, doi: 10.1306/10241616010.
- Matthews, W. J., G. J. Hampson, B. D. Trudgill, and J. R. Underhill, 2007, Controls on fluvio-lacustrine reservoir distribution and architecture in passive salt-diapir provinces: Insights from outcrop analogs: *AAPG Bulletin*, v. 91, p. 1367-1403,
- McBride, B. C., P. Weimer, and M. G. Rowan, 1998, The effect of allochthonous salt on the petroleum systems of northern Green Canyon and Ewing Bank (offshore Louisiana), northern Gulf of Mexico: *AAPG Bulletin*, v. 82, p. 1083-1112,
- Mello, U. T., G. D. Karner, and R. N. Anderson, 1995, Role of salt in restraining the maturation of subsalt source rocks: *Marine and Petroleum Geology*, v. 12, p. 697-716, doi: 10.1016/0264-8172(95)93596-V.

References

- Mohammedyasin, S. M., S. J. Lippard, K. O. Omosanya, S. E. Johansen, and D. Harishidayat, 2016, Deep-seated faults and hydrocarbon leakage in the Snøhvit Gas Field, Hammerfest Basin, Southwestern Barents Sea: *Marine and Petroleum Geology*, v. 77, p. 160-178, <https://doi.org/10.1016/j.marpetgeo.2016.06.011>.
- Moragas, M., J. Vergés, T. Nalpas, E. Saura, J. D. Martín-Martín, G. Messager, and D. W. Hunt, 2017, The impact of syn- and post-extension prograding sedimentation on the development of salt-related rift basins and their inversion: Clues from analogue modelling: *Marine and Petroleum Geology*, v. 88, p. 985-1003, <https://doi.org/10.1016/j.marpetgeo.2017.10.001>.
- Morley, C., R. Nelson, T. Patton, and S. Munn, 1990, Transfer zones in the East African rift system and their relevance to hydrocarbon exploration in rifts (1): *AAPG Bulletin*, v. 74, p. 1234-1253.
- Morley, C. K., R. King, R. Hillis, M. Tingay, and G. Backe, 2011, Deepwater fold and thrust belt classification, tectonics, structure and hydrocarbon prospectivity: A review: *Earth-Science Reviews*, v. 104, p. 41-91, <https://doi.org/10.1016/j.earscirev.2010.09.010>.
- Mulrooney, M. J., J. Leutscher, and A. Braathen, 2017, A 3D structural analysis of the Goliat field, Barents Sea, Norway: *Marine and Petroleum Geology*, v. 86, p. 192-212, <https://doi.org/10.1016/j.marpetgeo.2017.05.038>.
- Nilsen, K. T., B. C. Vendeville, and J.-T. Johansen, 1995, Influence of regional tectonics on halokinesis in the Nordkapp Basin, Barents Sea, *in* M. P. A. Jackson, D. G. Roberts, and S. Snelson, eds., *Salt tectonics: a global perspective*: AAPG Memoir 65, p. 413-436.
- Nordaunet-Olsen, E., 2015, Controls on Upper Paleozoic carbonate build-up development in the South Central Norwegian Barents Sea: Master thesis, University of Stavanger, Norway, 154 p.

References

- Ohm, S. E., D. A. Karlsen, and T. Austin, 2008, Geochemically driven exploration models in uplifted areas: Examples from the Norwegian Barents Sea: *AAPG Bulletin*, v. 92, p. 1191-1223, doi: 10.1306/06180808028.
- Peel, F. J., 2014a, The engines of gravity-driven movement on passive margins: Quantifying the relative contribution of spreading vs. gravity sliding mechanisms: *Tectonophysics*, v. 633, p. 126-142, <https://doi.org/10.1016/j.tecto.2014.06.023>.
- Peel, F. J., 2014b, How do salt withdrawal minibasins form? Insights from forward modelling, and implications for hydrocarbon migration: *Tectonophysics*, v. 630, p. 222-235, <https://doi.org/10.1016/j.tecto.2014.05.027>.
- Pellegrini, C., V. Maselli, F. Gamberi, A. Asioli, K. Bohacs, T. M. Drexler, and F. Trincardi, 2017, How to make a 350-m-thick lowstand systems tract in 17,000 years: The Late Pleistocene Po River (Italy) lowstand wedge: *Geology*, v. 45, p. 327-330, doi: 10.1130/G38848.1.
- Pena dos Reis, R., N. Pimentel, R. Fainstein, M. Reis, and B. Rasmussen, 2017, Chapter 14 - Influence of Salt Diapirism on the Basin Architecture and Hydrocarbon Prospects of the Western Iberian Margin, in J. I. Soto, J. F. Flinch, and G. Tari, eds., *Permo-Triassic Salt Provinces of Europe, North Africa and the Atlantic Margins*, Elsevier, p. 313-329, doi: 10.1016/B978-0-12-809417-4.00015-X.
- Pichel, L. M., F. Peel, C. A. L. Jackson, and M. Huuse, 2018, Geometry and kinematics of salt-detached ramp syncline basins: *Journal of Structural Geology*, v. 115, p. 208-230, <https://doi.org/10.1016/j.jsg.2018.07.016>.
- Pichel, L. M., C. A.-L. Jackson, F. Peel, and T. P. Dooley, 2019, Base-salt relief controls salt-tectonic structural style, São Paulo Plateau, Santos Basin, Brazil: *Basin Research*, v. 010.1111/bre.12375.

References

- Pimentel, N., and R. Pena Dos Reis, 2018, Salt tectonics at the Lusitanian Basin, Field-Trip Guide, Global Analogues for the Atlantic Margin, AAPG European Regional Conference, Lisbon (Portugal)
- Riis, F., B. A. Lundschieen, T. Høy, A. Mørk, and M. B. E. Mørk, 2008, Evolution of the Triassic shelf in the northern Barents Sea region: *Polar Research*, v. 27, p. 318-338, doi: 10.1111/j.1751-8369.2008.00086.x.
- Rojo, L. A., A. Escalona, and L. Schulte, 2016, The use of seismic attributes to enhance imaging of salt structures in the Barents Sea: *First Break*, v. 34, p. 41-49, doi: 10.3997/1365-2397.2016014
- Rosendahl, B. R., D. J. Reynolds, P. M. Lorber, C. F. Burgess, J. McGill, D. Scott, J. J. Lambiase, and S. J. Derksen, 1986, Structural expressions of rifting: lessons from Lake Tanganyika, Africa: *Geological Society, London, Special Publications*, v. 25, p. 29-43, 10.1144/gsl.Sp.1986.025.01.04.
- Rowan, M. G., 1996, Benefits and limitations of section restoration in areas of extensional salt tectonics: an example from offshore Louisiana: *Geological Society, London, Special Publications*, v. 99, p. 147-161,
- Rowan, M. G., T. F. Lawton, K. A. Giles, and R. A. Ratliff, 2003, Near-salt deformation in La Popa basin, Mexico, and the northern Gulf of Mexico: A general model for passive diapirism: *AAPG Bulletin*, v. 87, p. 733-756,
- Rowan, M. G., F. J. Peel, and B. C. Vendeville, 2004, Gravity-driven fold belts on passive margins
- Rowan, M. G., and R. A. Ratliff, 2012, Cross-section restoration of salt-related deformation: Best practices and potential pitfalls: *Journal of Structural Geology*, v. 41, p. 24-37, doi: 10.1016/j.jsg.2011.12.012.

References

- Rowan, M. G., K. A. Giles, T. E. Hearon IV, and J. C. Fiduk, 2016, Megaflaps adjacent to salt diapirs: AAPG Bulletin, v. 100, p. 1723-1747, doi: 10.1306/05241616009.
- Rowan, M. G., and S. Lindsø, 2017, Chapter 12 - Salt Tectonics of the Norwegian Barents Sea and Northeast Greenland Shelf A2 - Soto, Juan I, in J. I. Soto, J. F. Flinch, and G. Tari, eds., Permo-Triassic Salt Provinces of Europe, North Africa and the Atlantic Margins, Elsevier, p. 265-286, doi: 10.1016/B978-0-12-809417-4.00013-6.
- Salazar, M., L. Moscardelli, and L. Wood, 2016, Utilising clinoform architecture to understand the drivers of basin margin evolution: a case study in the Taranaki Basin, New Zealand: Basin Research, v. 28, p. 840-865, doi: 10.1111/bre.12138.
- Salazar, M., L. Moscardelli, and L. Wood, 2018, Two-dimensional stratigraphic forward modeling, reconstructing high-relief clinoforms in the northern Taranaki Basin: AAPG Bulletin, v. 102, p. 2409-2446, doi: 10.1306/04241817235.
- Sclater, J. G., and P. A. F. Christie, 1980, Continental stretching: An explanation of the Post-Mid-Cretaceous subsidence of the central North Sea Basin: Journal of Geophysical Research: Solid Earth, v. 85, p. 3711-3739, doi:10.1029/JB085iB07p03711.
- Scott, D. L., and B. R. Rosendahl, 1989, North Viking graben: an east African perspective: AAPG Bulletin, v. 73, p. 155-165,
- Sorento, T., S. Olaussen, and L. Stemmerik, 2019, Controls on deposition of shallow marine carbonates and evaporites – lower Permian Gipshuken Formation, central Spitsbergen, Arctic Norway: Sedimentology, v. 010.1111/sed.12640.
- Steckler, M. S., G. S. Mountain, K. G. Miller, and N. Christie-Blick, 1999, Reconstruction of Tertiary progradation and clinoform development on the New Jersey passive margin by 2-D

References

- backstripping: *Marine Geology*, v. 154, p. 399-420, doi: 10.1016/S0025-3227(98)00126-1
- Steel, R., T. Olsen, J. Armentrout, and N. Rosen, 2002, Clinofolds, clinofold trajectories and deepwater sands: Sequence-stratigraphic models for exploration and production: Evolving methodology, emerging models and application histories: Gulf Coast Section SEPM 22nd Research Conference, Houston, Texas, p. 367-381.
- Stemmerik, L., G. Elvebakk, and D. Worsley, 1999, Upper Palaeozoic carbonate reservoirs on the Norwegian arctic shelf; delineation of reservoir models with application to the Loppa High: *Petroleum Geoscience*, v. 5, p. 173-187, doi: 10.1144/petgeo.5.2.173.
- Stemmerik, L., 2000, Late Palaeozoic evolution of the North Atlantic margin of Pangea: Palaeogeography, Palaeoclimatology, Palaeoecology, v. 161, p. 95-126, doi: 10.1016/S0031-0182(00)00119-X.
- Stewart, S., A. Ruffell, and M. Harvey, 1997, Relationship between basement-linked and gravity-driven fault systems in the UKCS salt basins: *Marine and Petroleum Geology*, v. 14, p. 581-604, doi: 10.1016/S0264-8172(97)00008-1.
- Stewart, S. A., and J. A. Clark, 1999, Impact of salt on the structure of the Central North Sea hydrocarbon fairways: Geological Society, London, Petroleum Geology Conference series, v. 5, p. 179-200, 10.1144/0050179.
- Tetzlaff, D., J. Tveiten, P. Salomonsen, and A. Christ, 2014, Geologic Process Modelling. Conference Paper. IX Conference of Hydrocarbon Exploration and Development, Mendoza, Argentina.
- Tetzlaff, D. M., and J. W. Harbaugh, 1989, Simulating clastic sedimentation: New York, Van Nostrand Reinhold Series on Computer Methods in Geosciences, 202 p., doi: 10.1007/978-1-4757-0692-5.

References

- Tetzlaff, D. M., M.-T. Schafmeister, J. Harff, W. W. Hay, and D. M. Tetzlaff, 2007, Interaction among sedimentation, compaction, and groundwater flow in coastal settings, *Coastline Changes: Interrelation of Climate and Geological Processes*, v. 426, Geological Society of America, p. 0, 10.1130/2007.2426(05).
- Trudgill, B. D., 2011, Evolution of salt structures in the northern Paradox Basin: controls on evaporite deposition, salt wall growth and supra-salt stratigraphic architecture: *Basin Research*, v. 23, p. 208-238, doi: 10.1111/j.1365-2117.2010.00478.x.
- Vendeville, B. C., 2005, Salt tectonics driven by sediment progradation: Part I—Mechanics and kinematics: *AAPG Bulletin*, v. 89, p. 1071-1079, 10.1306/03310503063.
- Warren, J. K., 2010, Evaporites through time: Tectonic, climatic and eustatic controls in marine and nonmarine deposits: *Earth-Science Reviews*, v. 98, p. 217-268, doi: 10.1016/j.earscirev.2009.11.004.
- Weijermars, R., M. P. A. Jackson, and B. Vendeville, 1993, Rheological and tectonic modeling of salt provinces: *Tectonophysics*, v. 217, p. 143-174, [https://doi.org/10.1016/0040-1951\(93\)90208-2](https://doi.org/10.1016/0040-1951(93)90208-2).
- Withjack, M. O., and S. Callaway, 2000, Active normal faulting beneath a salt layer: an experimental study of deformation patterns in the cover sequence: *AAPG bulletin*, v. 84, p. 627-651,
- Worsley, D., 2008, The post-Caledonian development of Svalbard and the western Barents Sea: *Polar Research*, v. 27, p. 298-317, doi: 10.1111/j.1751-8369.2008.00085.x.
- Yu, Z., I. Lerche, and A. Lowrie, 1992, Thermal impact of salt: Simulation of thermal anomalies in the Gulf of Mexico: *Pure and Applied Geophysics*, v. 138, p. 181-192,

Chapter 2 – Compilation of Papers

Intentionally left blank

Paper I

Structural style and evolution of the Nordkapp Basin, Norwegian Barents Sea

Luis Alberto Rojo¹, Nestor Cardozo¹, Alejandro Escalona¹, and Hemin Koyi²

¹Department of Energy Resources, University of Stavanger, 4036 Stavanger, Norway

²Hans Ramberg Tectonic Laboratory, Department of Earth Sciences, Uppsala University, Sweden

AAPG Bulletin, v.103, No. 9, pp. 2177-2217
DOI: :10.1306/01301918028

This paper is not in Brage due to copyright

Paper I

Intentionally left blank

Paper II

Controls on suprasalt deformation in confined salt-bearing basins: insights from analogue modelling

Luis Alberto Rojo¹, Hemin Koyi², Nestor Cardozo¹ and
Alejandro Escalona¹

¹Department of Energy Resources, University of Stavanger, 4036
Stavanger, Norway

²Hans Ramberg Tectonic Laboratory, Department of Earth Sciences,
Uppsala University, Sweden

Submitted to the Journal of Structural Geology

Controls on suprasalt deformation in confined salt-bearing basins: insights from analogue modelling

Luis Alberto Rojo¹, Hemin Koyi², Nestor Cardozo¹ and Alejandro Escalona¹

¹Department of Energy Resources, University of Stavanger, 4036 Stavanger, Norway

²Hans Ramberg Tectonic Laboratory, Department of Earth Sciences, Uppsala University, Sweden

ABSTRACT

In confined salt-bearing basins (CSBB), narrow (<100 km wide) full and half grabens delimit sub-basins of different initial salt thickness. These sub-basins contain close-spaced diapirs surrounded by thick (6-7 km) and narrow minibasins. CSBB exhibit shorter salt-related deformation periods (10 Myr) than those of unconfined salt-bearing basins (100 Myr). Most studies explain CSBB as the result of thick-skinned extension, while few consider other elements such as sediment loading and subsalt basin configuration. In this study, we use sandbox models of sediment loading and thick-skinned extension, as well as different basin configurations, to evaluate the impact of these factors on the suprasalt structural style and the distribution and timing of salt structures in CSBB. Sediment loading models display prograding depocenters and younger salt structures in the progradation direction. Thick-skinned extension models display stacked depocenters near basin boundary faults and opposite timing of diapir growth. Along strike changes in basin configuration and subsalt faults facing sediment progradation impact salt flow and salt structures as follows: (1) Perpendicular faults contribute to the formation of salt diapirs, (2) Oblique faults favour salt flow along strike, (3) Fault intersections cause salt inflation and salt diapirs, and (4) Basin confinement by graben narrowing or intrabasinal faults strongly controls the timing and rate of salt mobilization. Finally, sections through the sandbox models show close resemblance and are directly comparable to seismic sections through the Nordkapp Basin (Norwegian Barents Sea) where the relative contribution of the studied triggers together with changes in subsalt basin configuration produced a similar variation of structural styles along the basin.

INTRODUCTION

In extensional systems, large accumulations of layered evaporite sequences (LES) occur in two different scenarios (Warren, 2010): (1) Confined salt-bearing basins (e.g. full and half grabens) where synrift evaporites are delimited by fault blocks (Fig. 1B), and (2) Unconfined salt-bearing basins (e.g. passive margins) where the base salt relief is less than in confined basins and evaporites are unconfined and deposited in a sag basin formed by thermal subsidence (Fig. 1A).

In passive margins, salt typically moves by the combination of two thin-skinned, gravity driven processes: gliding and spreading (Rowan et al., 2004; Morley et al., 2011; Peel, 2014). The combination of these processes generates an up-dip extensional domain dominated by synthetic growth faults, salt rollers and rollover systems (Lundin, 1992; Rouby et al., 2002; Brun and Fort, 2011), and a downdip contractional domain characterized by folds, thrusts, and compressional diapirs (Brun and Fort, 2004; Rowan et al., 2004; Morley et al., 2011) (Fig. 1A). However, base salt relief such as subsalt faults and ramps plays an important role on suprasalt deformation, controlling the distribution of extensional and contractional salt structures as well as ramp syncline basins (Jackson and Hudec, 2005; Pichel et al., 2018). Unconfined basins commonly display salt-related deformation over a period of 100 My, and some of them are active today (Brun and Fort, 2011) (e.g. Fig. 1A).

Confined salt-bearing basins (CSBB) on the other hand, consist of narrow (<100 km wide) full and half grabens in the basement where syn-rift evaporites are limited by fault blocks (Fig. 1B). Grabens often exhibit tilting, differential subsidence, and changes in geometry along strike, subdividing the basin into sub-basins or rift segments with large variation in initial salt thickness (Stewart and Clark, 1999). The structural style commonly consists of vertical and closely spaced salt diapirs surrounded by narrow and deep (up to 6-7 km thick) minibasins, which display a complex history of salt withdrawal, including prograding depocenters and inverted minibasins (Rojo et al., 2019A; Fig. 1B). Subsalt relief plays an essential role, promoting diversions of salt flow and controlling the distribution of salt diapirs, which are often encountered above major subsalt faults (Koyi et al., 1993A; Ge et al., 1997). Unlike unconfined basins, confined basins exhibit faster salt-related deformation occurring during a relatively short time period, which in some cases is restricted to less than 10 My (Fig. 1B, Rojo et al., 2019A).

Deciphering the tectonostratigraphic evolution of CSBB is challenging. Firstly, the presence of closely spaced diapirs makes the imaging and interpretation of minibasins and subsalt strata challenging (Jones and Davison, 2014; Rojo et al., 2016). Full azimuth seismic data become essential. Secondly, given the deep minibasins and the fast deformation rates, finding the initial triggering mechanism of salt mobilization is not straightforward (Rojo et al., 2019A). Reactivation of subsalt faults by thick-skinned extension may trigger salt mobilization (Fig. 1B). During this process, fault-related subsidence creates preferential areas of sediment loading, which result in salt evacuation (Koyi et al., 1993A; Jackson and Vendeville, 1994; Stewart et al., 1997). Up-dip salt flow from the hanging wall blocks together with stretching of the overburden favour the formation of salt diapirs above subsalt faults (Burliga et al., 2006). This explains the fast deformation rates and the presence of narrow and deep minibasins (Jackson and Lewis, 2016). However, it is often difficult to decipher whether or not subsalt faults were active during salt mobilization and estimate their displacement, since most of the deformation is accommodated by the salt (Rojo et al., 2019A).

Paper II

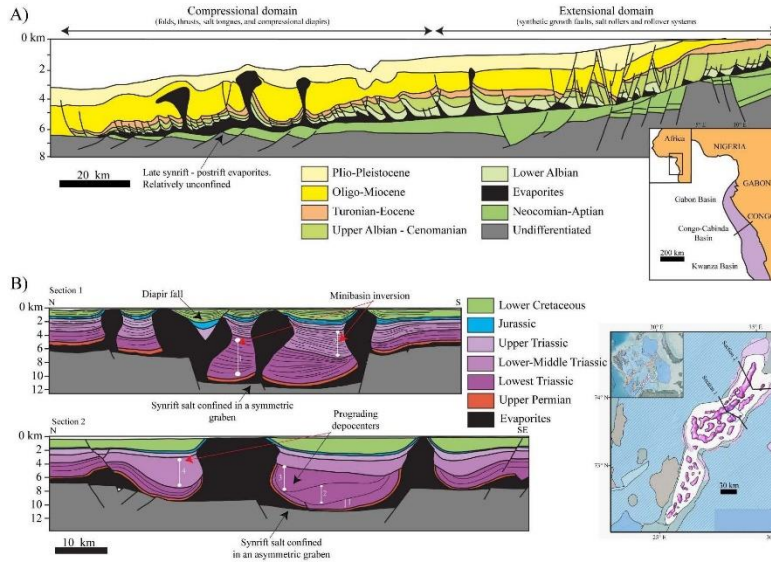


Figure 1. A) The Congo-Cabinda Basin is an example of an unconfined salt-bearing basin in offshore Congo. Unconfined basins display deformation periods over 100 My (modified from Roubay et al. 2001). **B)** The Norddippe Basin is an example of a confined salt-bearing basin in the Norwegian Barents Sea. These basins can display deformation periods below 10 My, which is 10 times shorter than in passive margins. In confined basins, it is often difficult to interpret the initial trigger of salt mobilization: thick-skinned extension or sediment loading (modified from Rojo et al., 2019 and Rowan and Lindsay 2017).

Another triggering mechanism of salt mobilization in confined basins is sediment loading by progradation (Ge et al., 1997; Trudgill, 2011; Warsitzka et al., 2013; Rowan and Lindsø, 2017). This process does not require extension. Instead, overburden thickness variations cause differential loading which trigger formation of minibasins and salt diapirs. In this scenario, even static subsalt configuration plays an important role in controlling salt flow since elevated fault blocks can act as flow barriers, favouring salt inflation and the formation of salt diapirs (Koyi, 1996; Ge et al., 1997; Cotton and Koyi, 2000; Trudgill, 2011; Rowan and Lindsø, 2017). Rojo et al. (2019A) illustrate that the choice of these two triggering mechanisms or their combination have significant influence on any attempt to estimate initial salt thickness in the basin. Therefore, identifying the right triggering mechanism(s) is essential because initial salt thickness variations have strong implications for reconstructing the tectonostratigraphic and thermal evolution of the basin (Mello et al., 1995; McBride et al., 1998; Cedeño et al., 2019; Rojo et al., 2019A).

Analogue models provide a dynamic venue of investigation. Most works in analogue modelling of CSBB describe the impact of basement faulting on salt mobilization (Koyi et al., 1993A and B; Jackson and Vendeville, 1994; Nilsen et al., 1995). Few studies though describe the impact of sediment loading on confined basins (Warsitzka et al., 2013; Moragas et al., 2017), with most studies focusing on the impact of sediment loading on unconfined basins (Koyi, 1996; Ge et al., 1997; Gaullier and Vendeville, 2005; Vendeville, 2005). In this manuscript, we present results of three sandbox models that incorporate the effects of sediment loading, subsalt geometry, and thick-skinned extension on CSBB. The main objectives are: (1) to describe the structural styles of CSBB driven by sediment loading; (2) to understand the impact of subsalt relief on salt flow, and (3) to compare sediment loading versus thick-skinned extension models in terms of structural style and timing of salt mobilization. Finally, we extrapolate the results of the models to a confined salt-bearing basin: The Nordkapp Basin in the Norwegian Barents Sea. This study provides insight into the triggering mechanisms of salt mobilization in the Nordkapp Basin, as well as other basins alike.

MODELLING METHODOLOGY

Modelling materials and scaling

This study uses classical techniques applied in previous brittle-ductile analogue modelling experiments at the Hans Ramberg Tectonic Laboratory (Uppsala University, Sweden; Koyi, 1998; Koyi, 1991; Koyi et al., 2008; Table 1). A transparent silicone polymer, polydimethylsiloxane (PDMS) with a density of 987 kg/m³ and viscosity of 5×10^4 Pa s at 20°C, was used in the experiments to reproduce the ductile behaviour of salt (Weijermars et al., 1993). The brittle sedimentary overburden was modelled using dry sand of grain size 250 µm, density 1500 kg/m³, and Mohr-Coulomb behaviour with an internal friction angle of 30° (Krantz, 1991; Weijermars et al., 1993; Maillot and Koyi, 2006; Table 1).

We use the geometric and dynamic scaling principles of Hubbert (1937), which have been applied to the analogue modelling of salt tectonics (Ramberg, 1981; Vendeville et al., 1987; Koyi, 1988; Weijermars et al., 1993). Geometric scaling to the size of CSBB in nature (e.g.

Figure 1B) was achieved by a length ratio of 3.85×10^{-6} , where 1 cm in the model is equivalent to 2.6 km in nature (Table 1). With a dry sand density of 1500 kg/m^3 and a sediment density of 2500 kg/m^3 , a density ratio of 0.60 was calculated for the overburden. Similarly, with a silicone density of 987 kg/m^3 and a salt density of 2200 kg/m^3 , a density ratio of 0.45 was calculated for the source layer. Dynamic scaling was achieved by an acceleration ratio of 1.0 since gravity in the model and nature is equal, a stress ratio of 1.73×10^{-6} (using the source density ratio), and a viscosity ratio between 10^{-15} - 10^{-14} since salt viscosity ranges between 10^{18} - 10^{19} Pa s (Ge et al., 1997; Table 1). The time ratio varies considerably depending on salt viscosity. In order to recreate deformation rates similar to those observed in a CSBB (e.g. the Nordkapp Basin; Rojo et al., 2019A), we assume a salt viscosity of $9.70 \times 10^{18} \text{ Pa s}$. This gives a viscosity ratio of 5.15×10^{-15} , a strain rate ratio of 3.35×10^8 , and a time ratio of 2.98×10^{-9} , where 1 h in the model is equivalent to 38.25 kyr in nature (Table 1).

MODEL	NATURE	RATIO
Density overburden $\rho_m = 1400 - 1700 \text{ kg/m}^3$ (e.g. $\rho_m = 1500 \text{ kg/m}^3$)	$\rho_n = 2400 - 2500 \text{ kg/m}^3$ (e.g. $\rho_n = 2500 \text{ kg/m}^3$)	$\rho_r = \frac{\rho_m}{\rho_n} = 0.6$
Density source $\rho_m = 987 \text{ kg/m}^3$	$\rho_n = 2200 \text{ kg/m}^3$	$\rho_r = \frac{\rho_m}{\rho_n} = 0.45$
Acceleration $g_m = 9.81 \text{ m/s}^2$	$g_n = 9.81 \text{ m/s}^2$	$g_r = \frac{g_m}{g_n} = 1$
Length $l_m = 1 \text{ cm}$	$l_n = 2.60 \text{ km}$	$l_r = \frac{l_m}{l_n} = 3.85 \times 10^{-6}$
Stress		$\sigma_r = \rho_r * g_r * l_r = 1.73 \times 10^{-6}$
Viscosity $\eta_m = 5 \times 10^4 \text{ Pa} \cdot \text{s}$	$\eta_n = (10^{18} - 10^{19} \text{ Pa} \cdot \text{s})$ (e.g. $\eta_n = 9.70 \times 10^{18}$)	$\eta_r = \frac{\eta_m}{\eta_n} = 5.15 \times 10^{-15}$
Strain rate		$\epsilon_r = \frac{\sigma_r}{\eta_r} = 3.35 \times 10^8$
Time $t_m = 1 \text{ h}$	$t_n = 38.25 \text{ kyr}$	$t_r = \frac{t_m}{t_n} = \frac{1}{\epsilon_r} = 2.98 \times 10^{-9}$

Table 1. Scaling relations used in this study. A salt viscosity of $9.70 \times 10^{18} \text{ Pa s}$ was assumed to match the deformation rates observed in the Nordkapp Basin.

Model design and procedures

Three analogue models were performed in this study. In two models progradational sediment loading was simulated, and in the third model the effect of thick-skinned extension was simulated (Fig. 2).

The experiments simulating sediment loading were performed with two different basin configurations: a symmetric (Fig. 2A) and an asymmetric graben (Fig. 2B). The symmetric graben was delimited by a proximal fault dipping 60° in the progradation direction, and a distal fault dipping 60° in the opposite direction (Fig. 2A, step V). The graben had a constant depth of 1.5 cm and along-strike length of 30 cm. The distal fault was parallel to the proximal fault for about half of its length, but then it changed strike such that the graben narrowed from 21.5 cm to 18.5 cm along strike. In the second model, the asymmetric graben consisted of the same bounding fault geometries and dimensions, but in this case, an intrabasinal fault dipping 60° against the progradation direction divided the model in two sub-basins: a proximal 1.5 cm deep sub-basin, and a distal 0.5 cm deep distal sub-basin (Fig. 2B, step V).

These grabens were filled with PDMS, which simulated evaporites, and covered part of the adjacent platforms. A 0.3 cm thick overburden layer of sand was then added on top of the PDMS to simulate pre-kinematic sedimentation. Syn-kinematic sedimentation in the models was simulated by alternating progradational and aggradational sand wedges. An initial 0.4 cm thick progradational sand wedge was added at the proximal part of the graben to trigger differential loading and subsequent movement of the PDMS (Fig. 2A and B, step IV). During the model evolution, subsequent 0.4 cm thick progradational sand wedges were deposited in time intervals of 48-56 h. These sedimentary wedges were successively deposited 3 cm towards the distal part of the model, with the main purpose to reproduce progradation of shelf-edge clinofolds at rates ranging between 0.1 – 100 m/kyr (Patrino and Helland-Hansen, 2018; Fig. 2A and B, steps I-III). Between the time periods of 48-56 h, the depocenters resulting from PDMS withdrawal were filled by 0.1 cm of aggradational sand wedges. This scenario of alternating prograding and aggrading sedimentary wedges is supported by salt-sediment interaction studies from Rojo et al. (2019B), where salt-withdrawal reduces progradation rates and favors the aggradation of clinofolds, while welding and decreasing salt withdrawal decreases accommodation space and favors the progradation of clinofolds across the basin.

The third experiment consisted of a 30 cm long, 21.5 cm wide, and 1.5 cm deep symmetric graben made of three heavy plexiglass blocks: two footwalls and one hanging wall (Fig. 2C, step V). The distal footwall was fixed during the experiment whereas the proximal footwall was attached to a moveable wall motored by an electrical engine. Similar to the two previous experiments, the initial graben was filled by PDMS which also covered the basin shoulders. The PDMS was then covered by a 0.3 cm overburden layer of sand representing prekinematic sedimentation (Fig. 2C, step IV). Outward movement of the moveable wall resulted in extension and subsidence of the hanging wall block. Successive pulses of extension with a velocity of (20 mm/h) were applied during 3 min in time intervals of approximately 12 h during the first 48 h. The accommodation space generated by hanging wall subsidence and silicone withdrawal was then filled by aggradational sand layers (Fig. 2C, step III). After 48 h, no extension was applied, and the model was driven by the differential loading of aggradational

sand layers above the underlying PDMS (Fig. 2C, steps I-II). It is important to mention that the experiments were not set to a specific duration. Instead, the experiments were terminated once the PDMS layer was welded and depleted, which in turn, was governed by the deformation rates of the PDMS in each experiment (Fig. 2).

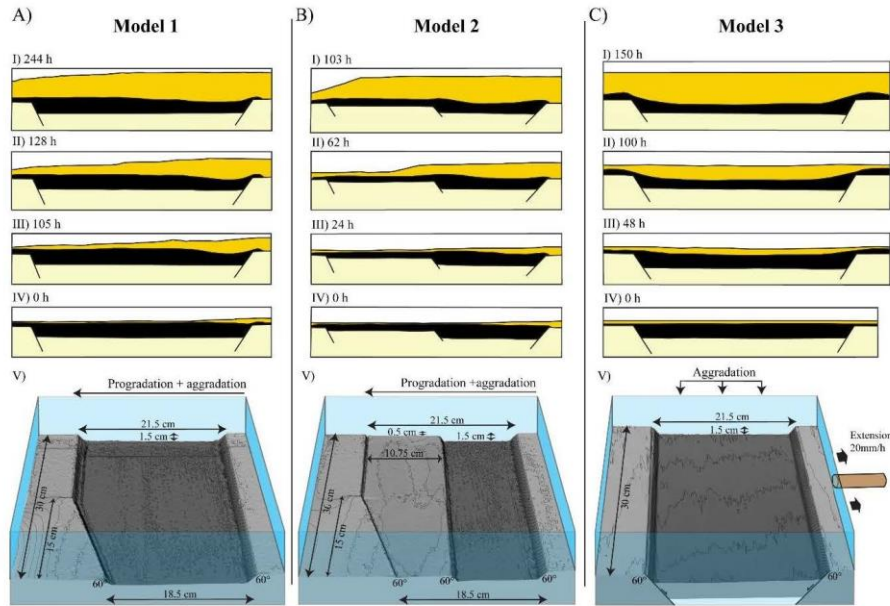


Figure 2. Evolution (steps I-IV) and basement geometry (step V) of the **A)** progradation + aggradation symmetric graben, **B)** progradation + aggradation asymmetric graben, and **C)** basement extension + aggradation models. Steps I-IV illustrate the models' evolution viewed from the left glass plate. Notice minor salt movement and lack of salt structures due to the boundary effect of the glass plate.

3D models from 2D sections and top surface scans

We follow the methodology of Vidal-Royo et al. (2008), by reconstructing 3D geometries from the models 2D side sections and top surfaces (Fig. 3). During the runs, top view photos and elevation maps (1 x 1 mm) were acquired using a laser scanner in time intervals of 4-8 h, depending on deformation rates. These elevation maps are very useful since they represent the evolution of the top surface topography through time. Once the model was terminated, 2D sections at a spacing of 1.5 cm and oriented perpendicular to the graben were cut and photographed. Top view photos of the 2D sections were also taken in order to determine the x and y locations of the sections. All of this information was imported into the program Move and georeferenced to their corresponding x, y and z coordinates. Horizons and structural elements (e.g. faults and diapirs) were interpreted on each section, and then they were interpolated between sections to produce triangulated surfaces. This procedure allowed recreating the 3D structural framework of each experiment (Fig. 3).

3D structural restoration of the reconstructed models was performed to illustrate the 4D evolution of the PDMS structures and their related surface deformation (Fig. 3). As opposed to the structural restoration of seismic profiles, the restoration of the analogue models required no depth conversion and it did not incorporate decompaction since compaction of the sand is negligible for the thickness of the experiments. Another advantage of restoring the analogue models is that the undeformed state or regional datum of each layer is given by the scanned surface elevation. Therefore, unfolding the layers to these surface datums, recreated the subsurface PDMS configuration through time. In order to avoid length losses, 3D flexural-slip was used to unfold the layers.

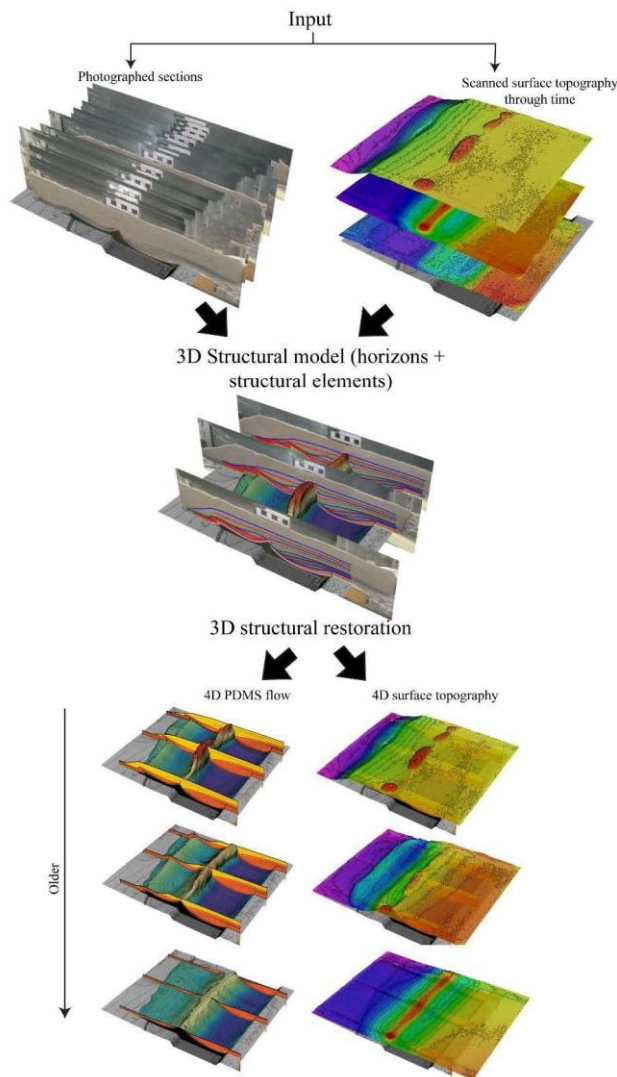


Figure 3. Workflow used to reconstruct 3D structural models from 2D sections and top surface scans of the experiments. These 3D models were then restored, having as constraint the scanned top surface topography through time.

RESULTS

Model 1. Progradation across a symmetric salt-related graben

Model 1 investigates the structural styles resulting from sediment progradation across a symmetric salt-filled graben which displays a change in strike on its distal fault. Bounding faults in the graben were inactive and acted as basement steps during the experiment which was run for a period of 244 h (~ 10 days).

Structural style

No diapiric structures occur in the proximal part of model 1. Instead, diapiric structures are localized above the distal basin boundary fault (Fig. 4, inset). These structures follow the strike of the underlying basin boundary fault and are of the following types: (1) a NE-SW striking pillow which characterizes the distal part of the narrow graben (Fig. 4A); (2) a predominant 2-cm wide and 7 cm tall diapir with a basinward overhang at the location where the distal fault changes trend (i.e., intersection between the narrow and wide grabens; Fig. 4B); and (3) a transition between a pillow and a passive diapir at the distal part of the wider graben (Fig. 4C). Due to salt flow, the overburden layers are faulted, where they are cut by a thin-skinned normal fault in the proximal part and by a thrust in the distal part (Fig. 4).

The overburden layers consist of 5 sequences: a prekinematic sequence S1, a synkinematic sequence S2 deposited during the first 50 h, a second synkinematic sequence S3 deposited between 50-124 h, a third synkinematic sequence S4 deposited between 124-172 h, and a fourth synkinematic sequence S5 deposited between 172-244 h (Fig. 4). In sections of the final stage, the synkinematic units exhibit a characteristic sigmoidal shape and internally display a progressive shift of depocenters in the progradation direction, with the thickest depocenter in S4 (Fig. 4). The sequences S3 and S4 thin above the pillow and are slightly offset by a thrust fault at the distal part of the model. In areas adjacent to the diapir, S1, S2, and S3 are strongly tilted to overturned, whereas S4 thins towards the diapir (Figs. 4B-C). These sequences are truncated and overlain by S5 which displays diapiric contacts. Welding of the buoyant layer occurs at approximately half of the graben length beyond which it is absent towards the distal part.

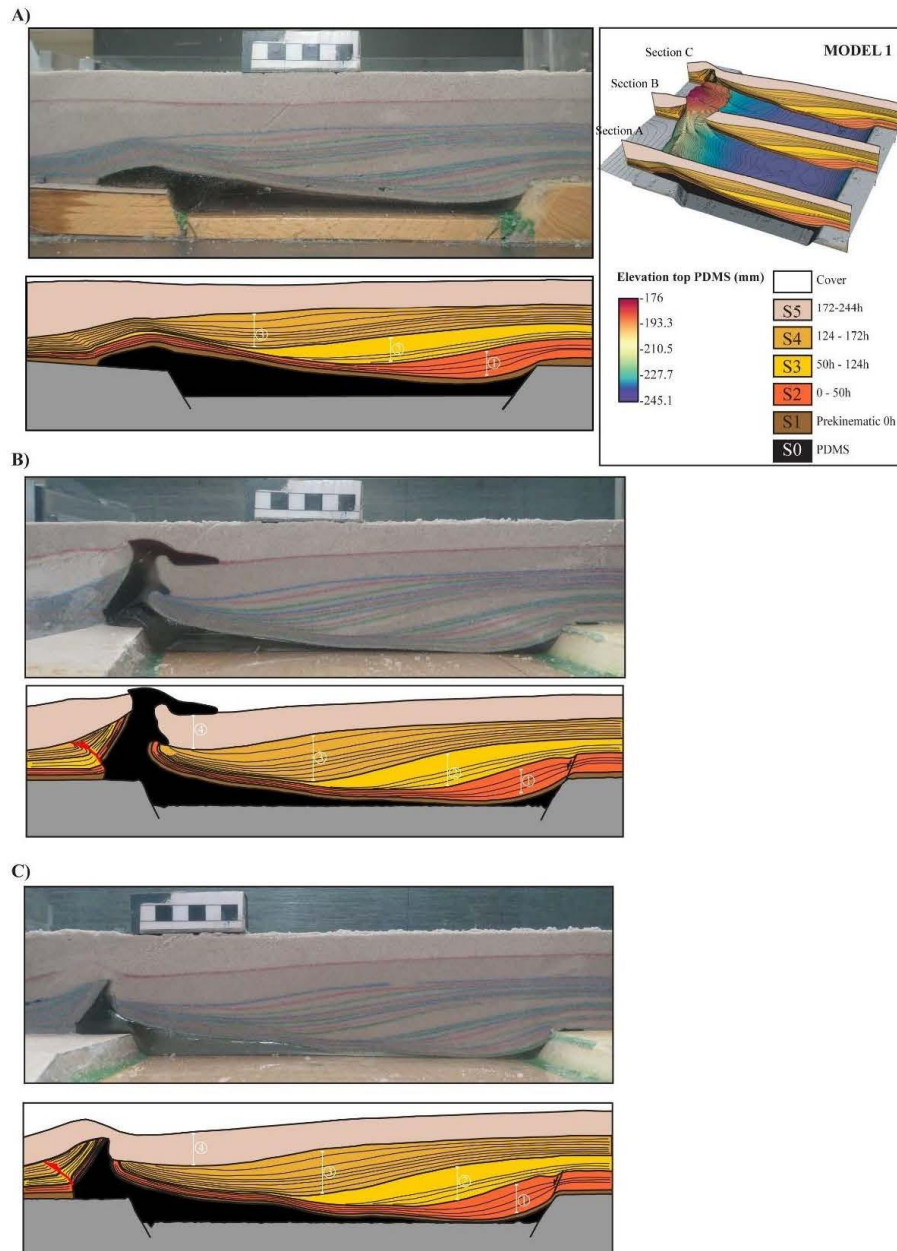


Figure 4. Uninterpreted and interpreted sections across the narrow symmetric graben (A), intersection between grabens (B), and wide symmetric graben (C) of model 1. Note that PDMS structures are located above the distal basement fault. Lines with numbers highlight the prograding switch in PDMS withdrawal as observed in S2 to S5. Inset on the right displays the PDMS top surface and the location of the three sections at the final stage.

4D Evolution

Model 1 started with the deposition of prekinematic sequence S1 which resulted in a flat topography with no signs of movement of the buoyant layer (Fig. 5A-B; step V). During the first 52 h, progradational and aggradational wedges were deposited in the proximal part of the graben, causing withdrawal and expulsion of the buoyant layer towards the distal part. It is important to note that the withdrawal front of the buoyant layer (Fig. 5A; step IV, red dashed line) was not linear along strike but showed more effective withdrawal in the narrow graben. Expulsion of the buoyant layer towards the distal part prompted the inflation of a plateau which occupied approximately 2/3 of the model (Fig. 5A; step IV). On the top surface, withdrawal of the buoyant layer in the proximal part produced an elongated rollover syncline with the deepest point in the narrow graben (Fig. 5B; step IV), whereas the accumulation and ramping of the buoyant layer at the distal basement fault created a plateau on the top surface whose trend followed the underlying graben configuration (Fig. 5A-B; step IV).

During the time interval 67 to 114 h, progradation and aggradation of S3 caused withdrawal of the buoyant layer in the centre of the graben and subsequent expulsion towards the distal part of the model (Fig. 5A; step III). Similar to the previous step, the withdrawal front (Fig. 5A; step III, red dashed line) was not linear and displayed more efficient withdrawal in the narrow graben. Expulsion of the buoyant layer resulted in a higher and narrower plateau which covered half of the model (Fig. 5A; step III). Progressive progradation of the sedimentary wedge caused the formation of a new rollover syncline whose deepest point was located in the narrow graben (Fig. 5B; step III). The growth of the plateau was also manifested on the top followed the underlying basin configuration (Figs. 5A-B; step III). Elevation contours indicate that the plateau was higher at the location where the distal fault changes trend.

During the time interval 114 to 189 h, deposition of S4 resulted in evacuation of a large amount of the buoyant material in the distal part where three diapirs formed above the distal basin boundary fault: a stock in the narrow graben; a large diapir with a basinward overhang at the intersection between the two grabens; and an elongated diapir in the wider graben (Fig. 5A, step II). Movement of the buoyant material resulted in a shift of withdrawal towards the distal part and formation of a new rollover syncline whose deepest point was now located in the wide graben (Fig. 5B, step II). The growth of passive diapirs also created topographic highs on the surface of the model. Due to the slow deformation rates observed after 189 h, the model was stopped by covering it with a 1.5-cm thick layer of sand (S5; Fig. 5A, step I). However, this did not stop the buoyant layer flowing towards the distal fault of the wide graben which kept the central diapir growing and forming a broad overhang. As a result, a new rollover syncline whose deepest point was located in the wide graben was formed (Fig. 5B, step I). The other diapirs, however, stopped growing due to the thick overburden and the limited supply of the buoyant material. After 244 h, the model was terminated by covering it with an additional 2-cm thick sand layer.

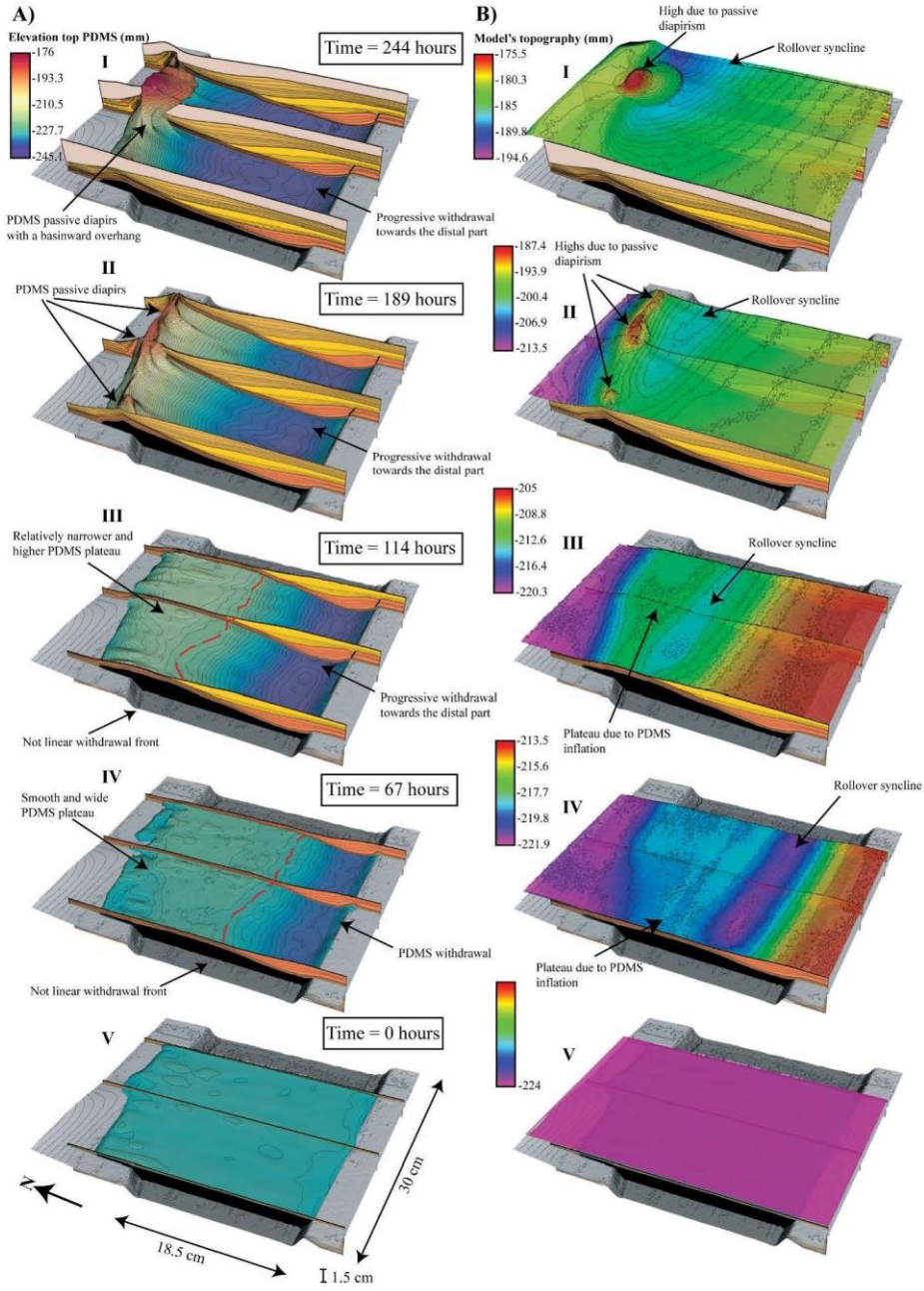


Figure 5. A) Evolution of the PDMS top surface in model 1 together with the three sections of Figure 4. B) Evolution of model 1 top surface topography. Figure 5 illustrates the evolution of model 1 based on 3D structural restoration.

Model 2. Progradation across an asymmetric salt-related graben

Model 2 investigates the structural style resulting from sediment progradation across a salt-filled asymmetric graben. The model was run for a period of 103 h (~ 4 days) and faults delimiting the asymmetric graben remained inactive during the experiment.

Structural style

Model 2 displays structures mainly above the intrabasinal fault where pillows and reactive diapirs develop in half of the model (Fig. 6 inset, and A), while taller passive diapirs dominate in the other half of the model (Fig. 6 inset, B, C). Pillows and associated thrust faults are observed in the distal part, following the underlying basin boundary fault (Fig. 6).

The model infill comprises three sequences: a prekinematic sequence S1, a synkinematic sequence S2 deposited in the first 50 h, and a synkinematic sequence S3 deposited between 50 and 124 h. In the proximal part of the graben, S1 and S2 are offset by a thin-skinned normal fault which coincides with the location of the underlying “sub-salt” fault (Figs. 6A-C). In the central part, S1 is upturned and truncated by sequences S2 and S3, where S2 thins in areas adjacent to the diapirs (Figs. 6A-C). The upper part of S2 and S3 are affected by a thin-skinned fault in first half of the model (Fig. 6A) and exhibit diapiric contacts with the central diapir in the second half of the model (Figs. 6B-C). Toward the distal part, S1 and S2 are thrust and overturned. In addition, S2 thins above the pillow underneath (Fig. 6). The model displays two main depocenters: a depocenter in the proximal sub-basin which consists of S2, and a depocenter in the distal sub-basin consisting of S3. It is important to note that the depocenters in S2 (0-50 h) and S3 (50-124 h) are thicker than those of the same sequences in model 1, indicating faster deformation rates in model 2.

4D Evolution

The experiment started with the deposition of constant thickness S1, which did not trigger mobilization of the buoyant layer (Fig. 7A, step V) and hence no changes in the model surface topography (Fig. 7B, step V). During the first 14 h, prograding and aggrading layers of S2 induced differential loading and withdrawal of the buoyant material at the proximal basin (Figs. 6 and 7A, step IV). In contrast to model 1, model 2 displayed a linear withdrawal front, resulting in the formation of an elongated rollover syncline parallel to the strike of the graben (Fig. 7B, step IV). Rapid subsidence due to withdrawal of the buoyant layer additionally contributed to the formation of a thin-skinned fault above the proximal fault, which internally offset S2 (Figs. 7A-B, step IV). Withdrawal and subsequent expulsion in the progradation direction also resulted in inflation of the buoyant material above the intrabasinal fault (Fig. 7A, step IV). This inflation was manifested at the model surface where a narrow and elongated plateau was formed (Figs. 7A-B, step IV).

During the time interval 14 to 51 h, continued progradation and aggradation of sand layers produced withdrawal of the buoyant material in both proximal and distal sub-basins (Fig. 7A, step III). Larger withdrawal in the proximal sub-basin than in the distal sub-basin resulted in the formation of a new rollover syncline, which was displaced in the progradation direction with respect to the previous one (Figure 7B, step III). Above the intrabasinal fault, the plateau

became narrower and higher, forming a pillow (Fig. 7A, step III). The growth of this pillow resulted in an elongated high topography on the model surface (Fig. 7B, step III).

During the time interval 51 to 84 h, successive progradation and aggradation of S3 caused withdrawal of the buoyant material in the distal sub-basin (Fig. 7A, step II), which resulted in an elongated rollover syncline (Fig. 7B, step II). Withdrawal in the proximal sub-basin was, on the other hand, relatively minor due to depletion of the of the buoyant material and the formation of a weld. Continuous supply of the buoyant material from both sub-basins favoured the formation of elongated diapir above the intrabasinal fault, whereas expulsion of the buoyant material from the distal minibasin prompted the inflation of pillows and the development of thrust faults above the distal basin boundary fault (Fig. 7A, step II). Uplift due to passive diapirism resulted in the formation of topographic highs on the model surface (Fig. 7B, step II). Similar to model 1, pillow growth and associated thrusting above the distal basin boundary fault also produced a topographic high on the model surface, with the highest topographic point above the change in strike of this fault (Fig. 7B, step II).

Between 84 and 103 h, continuous progradation of S3 sediments filled the distal minibasin causing its welding (Fig. 7A, step I). Consequently, distal pillows reduce their growth and were buried by S3 deposits. The passive elongate diapir branched into two passive diapirs which continued their growth by evacuation of the remaining buoyant material in the proximal and distal minibasins (Figs. 7A-B, step I). After 103 h, the model was terminated due to depletion of the buoyant layer and its welding. It is important to note that for the same triggering mechanism, mainly sediment progradation, deformation rates were faster in model 2 (asymmetric graben) than in model 1 (symmetric graben). This is also supported by the higher thickness of S2 and S3 in model 2 (Figs. 4 to 7).

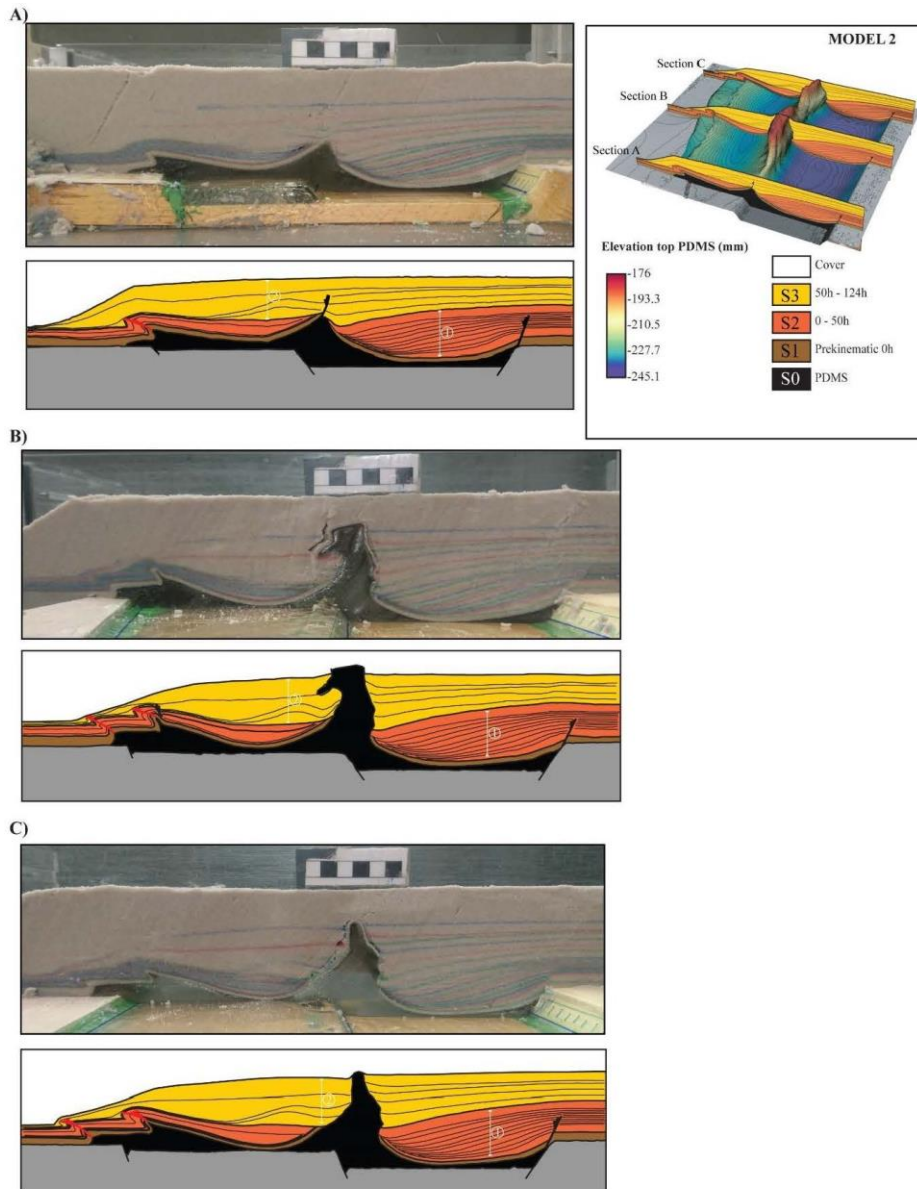


Figure 6. Uninterpreted and interpreted sections across the narrow asymmetric graben (A), intersection between grabens (B), and wide asymmetric graben (C) of model 2. Note that PDMS structures are located above the intrabasinal and distal faults and get younger in the progradation direction. Lines with numbers highlight the prograding depocenters in S2 and S3. Note that this configuration shows larger depocenters in S2 and S3 suggesting higher deformation rates than in model 1. Inset on the right displays the PDMS top surface and the location of the three sections at the final stage.

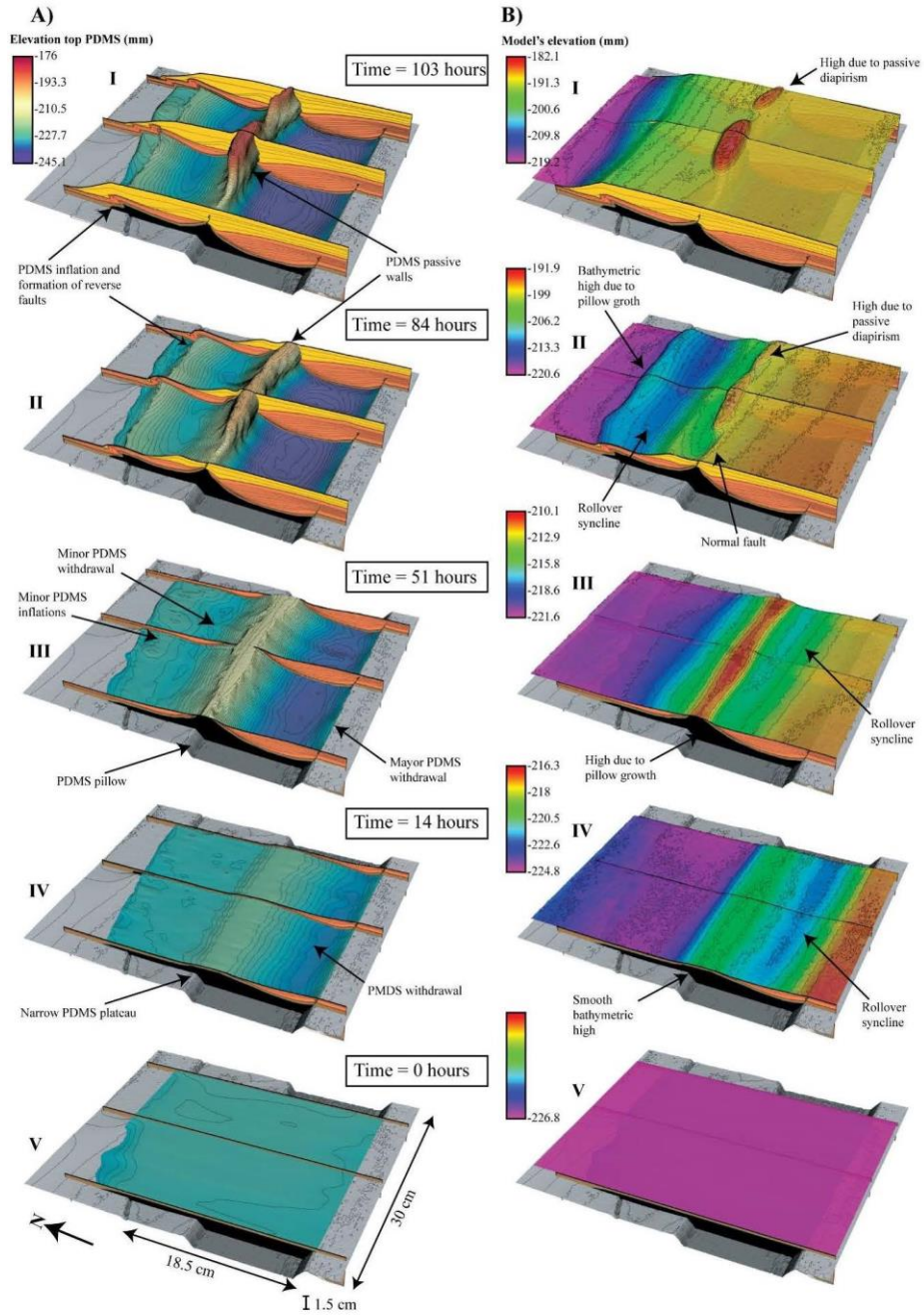


Figure 7. Evolution of model 2 based on 3D structural restoration **A)** Evolution of the PDMS top surface in model 2 together with the three sections of Figure 6. **B)** Evolution of model 2 top surface topography.

Model 3. Thick-skinned extension and sediment aggradation

Model 3 explores the structural style resulting from thick-skinned extension of a salt-bearing symmetric graben. Four successive pulses of extension with a strain rate of 20 mm/h were applied during 3 min in time intervals of approximately 12 h during the first 50 h of model evolution. The model was deformed for a total time period of 150 h (~ 6 days).

Structural style

Unlike models 1 and 2 (Figs. 4 and 6), model 3 displays diapiric structures above both the proximal and distal graben bounding faults (Fig. 8, inset map). The proximal basin shows a pillow, a stock and an elongated diapir, whereas the distal basin displays a pillow and a wall-like diapir with a basinward overhang (Figs. 8A to C). These structures are smaller, both in height and width, than those observed in models 1 and 2.

The model infill consists of a prekinematic sequence S1, a first synkinematic sequence S2 deposited in the first 50 h, a second synkinematic sequence S3 deposited between 50 and 124 h, and a third synkinematic sequence S4 deposited between 124 and 172 h. In contrast to models 1 and 2, synkinematic sequences do not display a wedge shape because the basin infill was only aggradation. S2 shows two depocenters, each of them situated near the proximal and distal graben bounding faults (Fig. 8). These depocenters are separated by a 4-5 cm wide plateau of the buoyant material at approximately the graben axis. S2 thins towards diapirs and pillows at basin boundaries, and above the central plateau. Near the diapirs, S2 show internal angular unconformities. S1 and the lower part of S2 are truncated by the uppermost part of S2 in the distal basin, while in the proximal basin, S1 and S2 are truncated by S3 (Figs. 8B and C). S3 displays a tabular shape increasing in thickness towards the distal part of the model, where it forms a depocenter (Figs. 8B and C). Near the diapirs, S3 displays diapiric contacts whereas it thins above pillows. Finally, S4 displays a general tabular architecture and overlies most of the pillow structures, except for localized areas above the basin boundaries where it displays diapiric contacts.

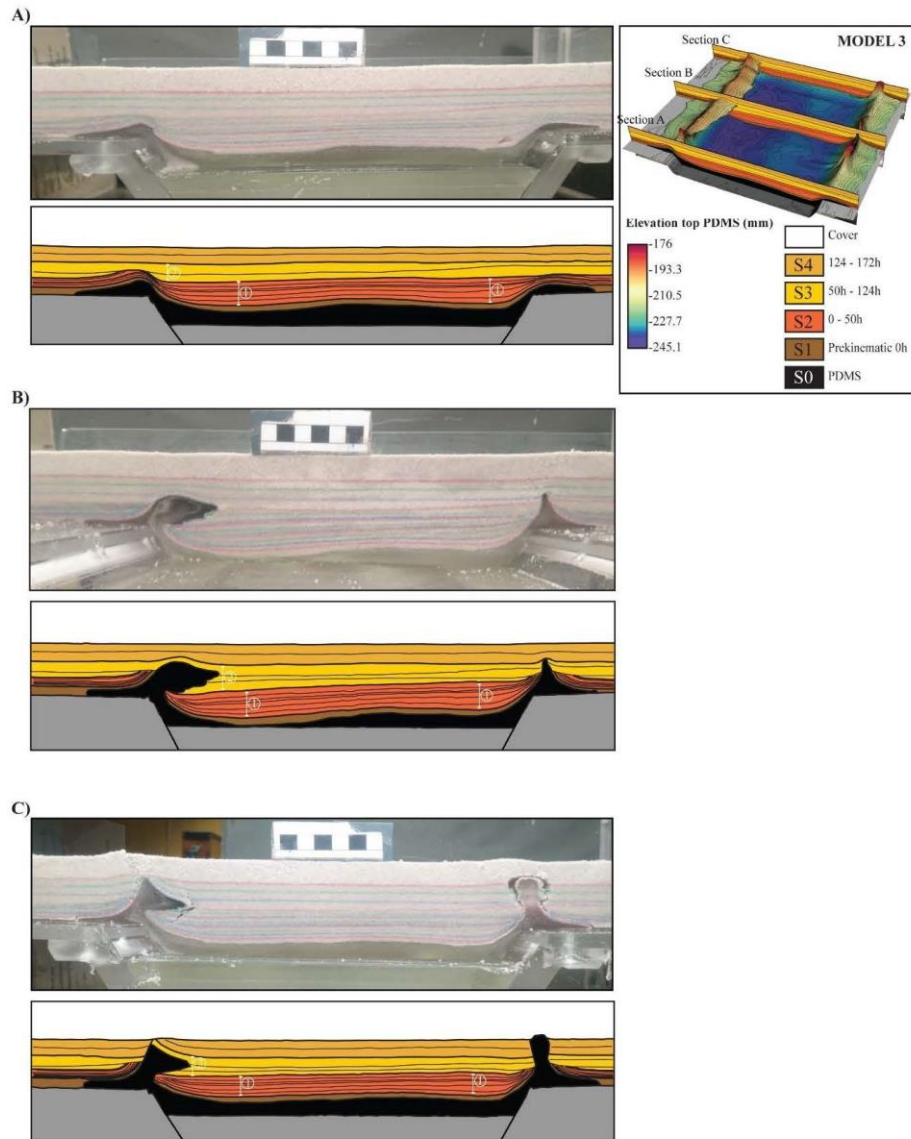


Figure 8. Uninterpreted and interpreted sections across the left part (A), middle part (B), and right part (C) of the symmetric graben in model 3. Note that PDMS structures are located above both basin boundary faults and show different timing than in previous models, with earlier diapir growth at the distal part of the model. Lines with numbers highlight the depocenters in S2 and S3. Note that thick-skinned extension caused higher deformation rates than those in model 1. Inset on the right displays the PDMS top surface and the location of the three sections at the final stage.

4D Evolution

The experiment started with the deposition of the prekinematic unit S1 (Fig. 9A, step V), which did not induce mobilization of the buoyant layer and therefore, no changes in the surface topography were recorded (Fig. 9B, step V). During the first 15 h of model evolution, thick-skinned extension and differential loading by the S2 aggrading overburden triggered mobilization of the buoyant layer, with the main withdrawal areas adjacent to the basin boundary faults (Fig. 9A, step IV). Thick-skinned extension and withdrawal resulted in a tectonically induced depocenter on the top surface above the underlying graben (Fig. 9B, step IV).

During the time interval 15 to 62 h, thick-skinned extension (only until 48 h) and continuous loading by the S2 aggrading overburden enhanced withdrawal of the buoyant material at both proximal and distal basin boundaries (Fig. 9A, step III). Evacuation of the buoyant material in the distal part resulted in the growth of a passive wall-like diapir above the distal basin boundary fault, whereas a salt pillow developed above the proximal basin boundary fault (Fig. 9A, step III). It is important to note that models 1 and 2 displayed younger diapiric structures in the progradation direction (Figs. 5 and 7). In model 3 instead, passive diapirism occurred first at the distal basin boundary, and it was followed by the formation of a pillow at the proximal basin boundary (Fig. 9). In the distal part, the growth of the passive diapir resulted in an elongated topographic high on the model surface, whereas a smooth and subtle topographic high occurred above the proximal fault due to the growth of a pillow (Fig. 9B, step III).

During the time interval 62 to 124 h, differential loading by S3 contributed to continuous withdrawal at both basin boundaries, although it was larger in the distal part. These two areas of evacuation of the buoyant material were separated by an elongated plateau of remaining buoyant layer located approximately at the graben axis (Fig. 9A, step II). Evacuation of the buoyant material towards the footwalls resulted in the formation of a “salt glacier” at the distal basin boundary and the generation of passive diapirs at the proximal basin boundary (Fig. 9A, step II). Growth of these structures led to the formation of topographic highs whereas large withdrawal underneath resulted in a depression (Fig. 9B, step II).

During the time interval 124 to 150 h, most of the diapiric structures at the distal basin boundary stopped growing due depletion of the buoyant material and formation of welds and were covered by S4. Passive diapirs in the proximal part, however, continued growing due to the evacuation of remaining of the buoyant material (Fig. 9A, step I). These structures formed local highs on the model surface whereas subtle subsidence occurred above the graben (Fig. 9B, step I).

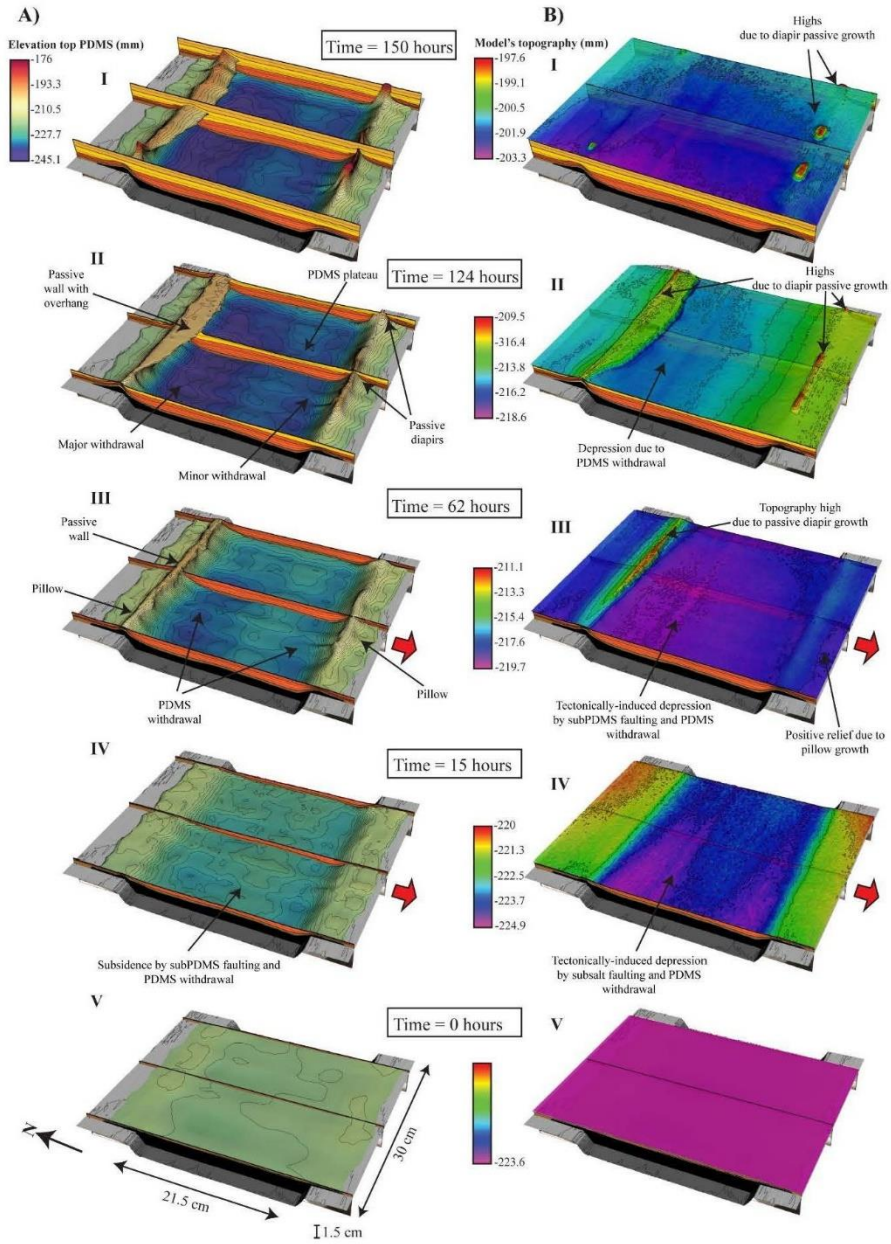


Figure 9. A) Evolution of the PDMS top surface in model 3 together with the three sections of Figure 8. B) Evolution of model 3 top surface topography.

CSBB: NATURE VS ANALOGUE MODELS

A natural example of a confined salt-bearing basin is the Nordkapp Basin in the Norwegian Barents Sea (inset Fig. 1B). The Nordkapp Basin consists of a series of NE-SW and NNW-SSE rift segments or sub-basins composed of an alternation of full and half grabens (Fig. 10; Gabrielsen et al., 1992; Jensen and Sørensen, 1992). Most of the mobilization and evacuation of salt in the basin occurred from the Early to Middle Triassic, leading to the formation of thick (> 5 km) Lower-Middle Triassic minibasins displacing the underlying salt into the adjacent salt structures (stocks and walls; Fig. 10). Salt mobilization also took place during the Late Triassic, Jurassic and Early Cretaceous (Koyi et al., 1993B; Koyi et al., 1995b; Rojo et al., 2019A). Finally, pre-existing salt structures were reactivated by contractional diapirism during the Cenozoic (Koyi et al., 1995B; Nilsen et al., 1995; Rowan and Lindso, 2017; Rojo et al., 2019). Based on results of analogue modelling and seismic interpretation, most workers propose basement-involved extension to explain the Triassic onset of salt mobilization and high deformation rates of the basin (Jensen and Sørensen, 1992; Koyi et al., 1993B; Koyi et al., 1995A; Koyi et al., 1995B; Nilsen et al., 1995; Rojo and Escalona, 2018). However, Dengo and Røssland (1992) and Rowan and Lindso (2017) propose progradational loading in response to Early Triassic NW progradation of fluviodeltaic sediments from the Urals, as the trigger of salt mobilization. The purpose of this section is to compare the results of the sandbox models with seismic sections across the central and eastern sub-basins of the Nordkapp Basin (Fig. 10) to better understand the influence of basement involved extension and/or progradational loading in the suprasalt structural style of the basin.

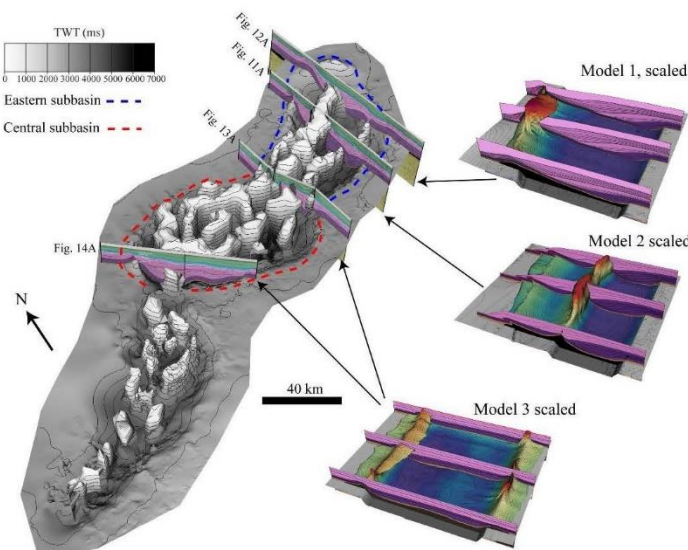


Figure 10. Left) 3D visualization of the top salt surface in the Nordkapp Basin together with the location of seismic sections in Figures 11A, 12A, 13A and 14A. Right) Sandbox models scaled with the length and time ratios of Table 1. The central sub-basin of the Nordkapp Basin (red dashed line) is a symmetric graben that narrows towards the east. This sub-basin is compared to model 3. The eastern sub-basin (blue dashed line) consist of an asymmetric graben similar to the one reproduced by model 2. This graben changes towards the east to a wider basin as the one reproduced by model 1.

Eastern Nordkapp sub-basin

The western part of the eastern sub-basin consists of a 40-50 km wide, NE-SW asymmetric graben delimited by proximal (NNE-dipping) and distal (SSW-dipping) basin boundary faults, and a SSE-dipping intrabasinal fault (Figs. 10 and 11A). A salt wall occurs above the intrabasinal fault whereas pillows are located above the basin boundary faults (Fig. 11). Two large minibasins flank the central salt wall. The southern minibasin consists of Lowest Triassic strata (SU2, equivalent to < 50 h in model 2) which forms diapiric contacts with the wall indicating the diapiric initiation stage. Internally, SU2 depocenters (and salt withdrawal) are shifted in the northwards direction (Fig. 11). The northern minibasin comprises Lower-Middle Triassic stacked sedimentary wedges (SU3; equivalent to 50-172 h interval in model 2) displaying diapiric contacts with the central wall and onlapping the Lowest Triassic strata above the distal pillow (Fig. 11).

Towards the east, displacement along the proximal basin boundary fault and the intrabasinal fault decrease (Figs. 10 and 12A). This part of the basin is similar to model 1 (Fig. 12). Both the basin and model 1 display prograding depocenters with the largest sediment growth recorded in SU2 and SU3, indicating that the largest salt mobilization and evacuation mainly occurred during the Lower to Middle Triassic (equivalent to 50-172 h in model 1). Sediment progradation and salt evacuation and expulsion towards the north resulted in the formation of a distal salt pillow as salt ramped up against a basement fault acting as a step (Fig 12).

Similar to models 1 and 2, the eastern sub-basin displays earlier diapirism and faster deformation in the asymmetric graben (Fig. 11) where salt withdrawal, salt diapirs, and welding had already occurred by the Early Triassic (SU2; approx. 2 My after the onset of salt mobilization). It is important to mention that the basin and the models also have some differences such as: (1) no thrusting in the distal part (Figs. 11A and 12A), which is observed in models 1 and 2 (Figs. 11B and 12B), (2) minibasin inversions (depocenters 5 and 6 in Figure 11A), which do not match the progressive depocenters migration of model 2 (Fig. 11B), and (3) salt withdrawal occurs at the basin axis, leaving a significant amount of salt in the proximal part (Figs. 11A and 12A). This contradicts withdrawal of the source layer (PDMS) at the proximal basin boundary in models 1 and 2 (Figs. 11B and 12B). These differences will be further addressed in the discussion section.

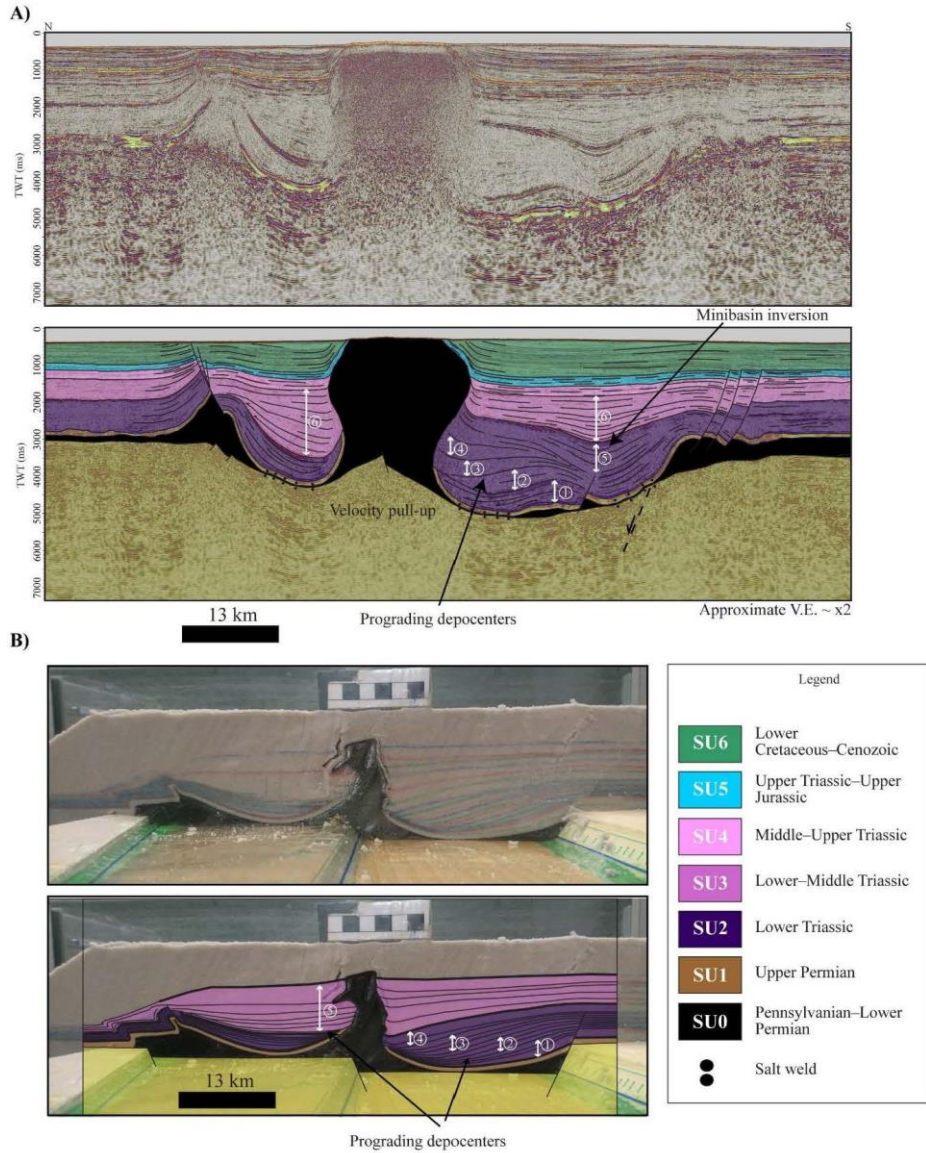


Figure 11. **A)** Uninterpreted and interpreted seismic section across the asymmetric graben of the eastern sub-basin. See location in Figure 10. **B)** Uninterpreted and interpreted section across model 2. Note that the model is scaled to nature following the model ratios of Table 1. Both seismic and model shows prograding depocenters and younger salt structures in the progradation direction, indicating a structural style mainly dominated by progradational loading. Seismic section A also shows minor evidence of thick-skinned extension such as minibasin inversion, initial loading of the basin axis, and salt pillows at both basin boundaries. These are all features observed in model 3.

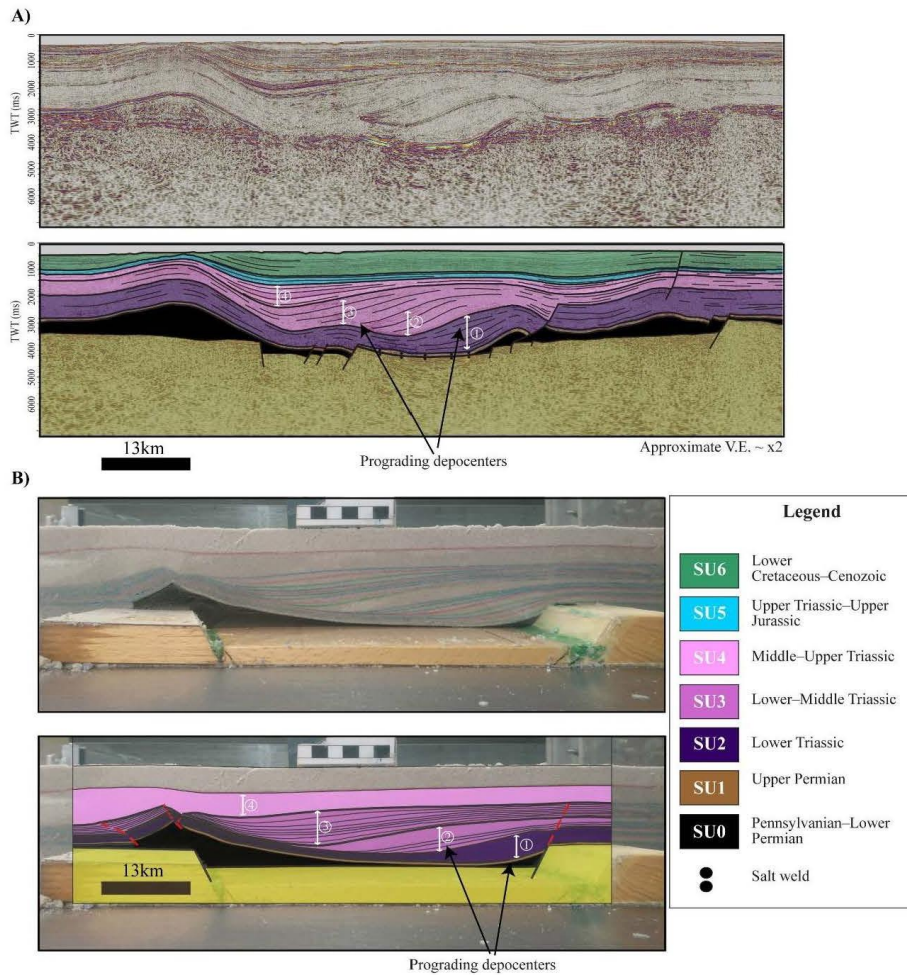


Figure 12. A) Uninterpreted and interpreted seismic section across the symmetric graben of the eastern sub-basin. See location in Figure 10. B) Uninterpreted and interpreted section across model 1. Note that the model is scaled to nature following the model ratios of Table 1. Both seismic and model display prograding depocenters and the formation of a pillow on top of the distal basin boundary fault, indicating a structural style resulting from progradational loading. Initial sediment loading at the basin axis is not observed in model 1 but in model 3, and it suggests a minor influence of subsalt fault activity during the Early Triassic.

Central sub-basin

The central sub-basin is a 30 km wide symmetric salt-related graben in the east that widens to 80-100 km to the west (Figs. 10). The graben is delimited to the north by a SE-dipping normal fault that changes dip direction to the SW as it approaches the eastern sub-basin. The southern basin boundary fault also changes dip direction from NE to NW close to the eastern sub-basin,

The largest Triassic thickness variations are located in the narrower (30 km wide) graben (Fig. 13A). This graben resembles section C of model 3 (Figs. 8C and 13) where salt structures are encountered at both basin boundaries. In contrast the eastern sub-basin (Figs. 11A and 12A), in this part of the central sub-basin, Early Triassic salt withdrawal and welding occurred first on the distal part, forming an E-W trending salt wall above the distal basin boundary fault (Fig. 13). The remaining salt at the proximal part was evacuated during the Early-Middle Triassic (SU2-SU3, equivalent to 50-124 h in model 3), causing minibasin inversion and forming a younger salt diapir at the proximal basin boundary (Fig. 13A). In model 3, this proximal diapir started first as a pillow during the deposition of SU2, and it became a passive diapir due to the loading of SU3 (Fig. 13B).

The 80 km wide graben on the western part of the central sub-basin resembles section A of model 3 (Figs. 8A and 14). Both model and nature examples contain salt pillows and sediment depocenters at both basin boundaries near the subsalt faults (Fig. 14). The distal pillow is more inflated due to an earlier and larger salt evacuation, and proximal and distal depocenters are separated by a salt-cored intrabasinal high where the Lower to Middle Triassic strata thin (SU2-SU3, equivalent to 50-124 h in model 3). Note that important characteristics of the central sub-basin such as salt structures at both basin boundaries and older salt structures at the distal part are only observed in model 3.

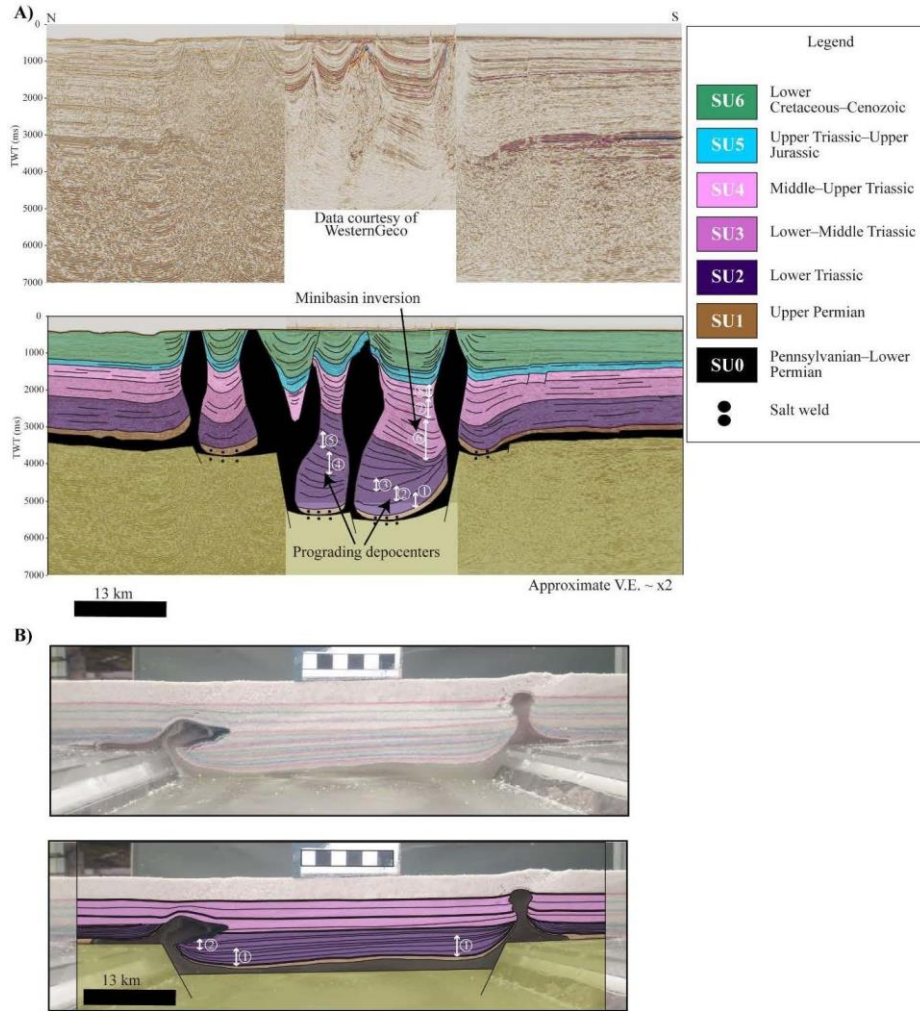


Figure 13. **A)** Uninterpreted and interpreted seismic section across the symmetric graben of the central sub-basin. See location in Figure 10. **B)** Uninterpreted and interpreted section across model 3. Note that the model is scaled to nature following the model ratios of Table 1. Both seismic and model show the first loading of salt at the distal basin boundary during S2, leaving a significant amount of salt at the proximal basin boundary. This remaining salt was evacuated during S3 and contributed to the growth of a younger diapir at the proximal basin boundary. Thus, the timing of salt diapirs is opposite to the timing of salt diapirs in models 1 and 2 and in the eastern sub-basin (Figs. 11 and 12). This indicates that thick-skinned extension played an important role in the central sub-basin.

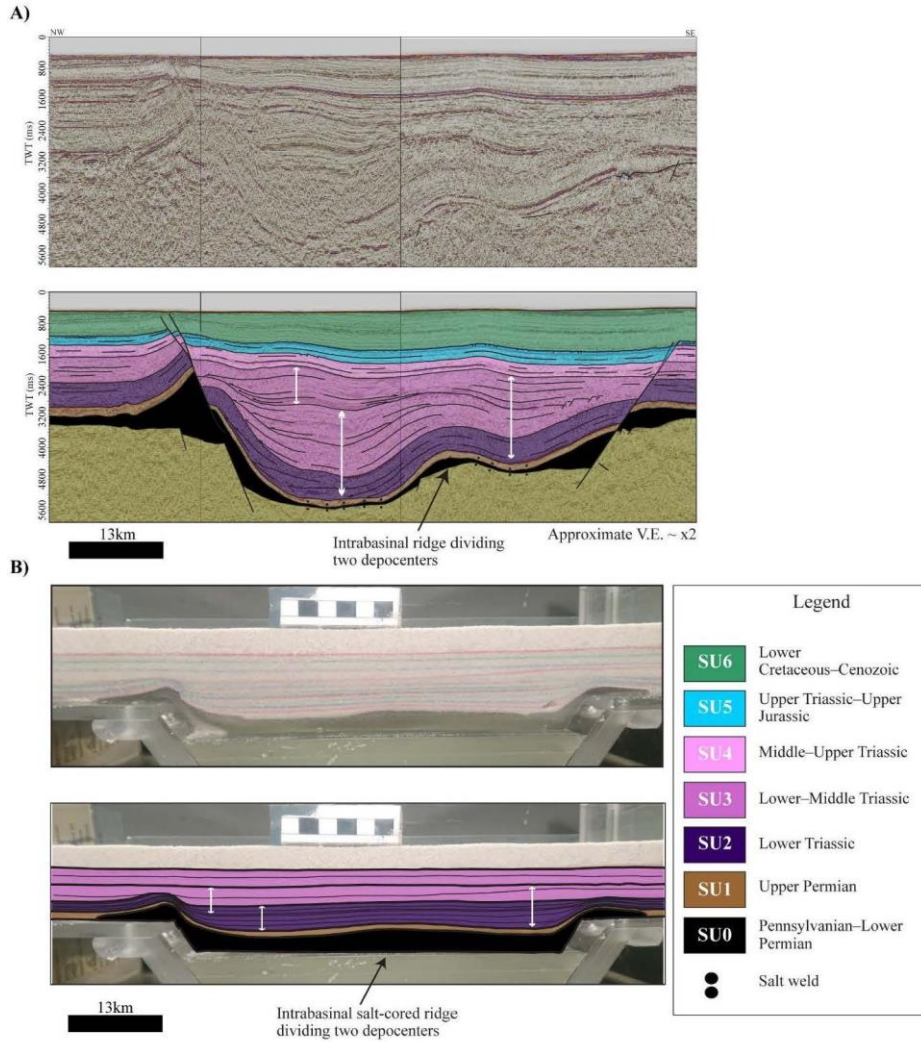


Figure 14. **A)** Uninterpreted and interpreted seismic section across the westernmost central sub-basin. See location in Figure 10. **B)** Uninterpreted and interpreted section across model 3. Note that the model is scaled to nature following the model ratios of Table 1. Both seismic and model 3 show salt pillows, and near-vertically stacked depocenters close to the subsalt faults. These features indicate that thick-skinned extension played an important role in the central sub-basin.

DISCUSSION

The impact of subsalt basin configuration in the structural evolution of CSBB

The influence of subsalt relief has been documented in passive margins where it causes variations in the direction of salt flow due to lateral and vertical buttressing effects (Dooley et al., 2018; Pichel et al., 2018; Pichel et al., 2019A, B). This results in complex 4D suprasalt deformation as downdip salt flow and overburden translation occur above abrupt variations in subsalt relief. In this tectonic setting, downdip salt flow occurs over a wide basin (> 100 km) and over a long period of 100 My (Brun and Fort, 2011).

CSBB involve a complex interaction of narrow symmetric and asymmetric grabens, which display lateral changes in width and orientation as well as sub-salt fault displacement (Koyi et al., 1993A; Stewart et al., 1997; Stewart and Clark, 1999; Withjack and Callaway, 2000; Ge et al., 2017). Syn-rift salt deposition occurs within these fault blocks which often undergo differential subsidence, leading to differences in salt thickness across neighbouring sub-basins (Jensen and Sørensen, 1992). Based on the model results presented here, subsalt basin configuration affects salt flow in CSBB in the following ways:

- 1) Nucleation of salt structures is enhanced by subsalt basin configuration. The sandbox models focused on studying three scenarios: (1) Effect of subsalt faults inline with sediment progradation, (2) Impact of subsalt faults facing sediment progradation, and (3) Influence of the change in strike of subsalt faults (Figs. 4 to 9).

Model results show that no salt (i.e. PSDM) structures develop above subsalt faults dipping in the progradation direction in models 1 and 2 where the basement fault was static and only provided a step. In model 3 where the basement fault is active during deposition of overburden layers, however, pillows and diapirs form due to overburden extension and salt supply from the hanging walls (Figs. 5, 7, and 9). The lack of salt structures above faults dipping in the progradation direction in models 1 and 2 is attributed to the deposition of a progressively thicker overburden by the vertical stacking of prograding wedges, which hinders the growth of pillows and diapirs above these inactive faults which only provide a step (Figs. 4 to 7). Since these basement steps dip in the direction of sediment progradation, they are likely to assist salt flow away from the step by the accumulating sediments rather than salt flow towards it. Furthermore, faults dipping in the progradation direction favour the formation of thin-skinned normal faults due to differential loading and subsidence. These overburden faults dip towards the progradation direction and their hanging-wall sediments drive the ductile layer away from the fault steps (Figs. 4 and 6). In our models, where static and active basement faults were studied, it was possible to see the effect of these kinds of faults. In nature, it is therefore important to carefully examine these faults since they could be the result of either sediment progradation or thick-skinned extension, which would have a significant impact on salt diapirism. For example, in the Nordkapp Basin in the western part of the central sub-basin (Fig. 14A), it is difficult to interpret whether the proximal fault is a thin-skinned fault resulting from Early-Middle Triassic progradational loading, or a thick-skinned fault formed by thick-skinned extension.

Similar to Koyi, (1996), Ge et al. (1997), Trudgill (2011) and Rowan and Lindso (2017), sub-salt faults facing sediment progradation play an important role in the nucleation of salt structures in models 1 and 2 since these faults act as barriers to salt flow, favouring the inflation and growth of pillows, which eventually may grow into a diapir. This effect can be observed in the Nordkapp Basin where salt structures are generally observed above these faults (Figs. 11 to 14). Model results also show that strike variation of faults facing sediment progradation also control the nucleation and type of salt structures. Progradational loading in model 1 formed a pillow above the fault step facing sediment progradation obliquely (Fig. 4A) whereas a diapir was located above the fault step facing sediment progradation orthogonally (Fig. 4C), with the highest relief at the intersection between these two fault segments (Figs. 4B and 5). These different structures can be explained by alterations of the salt flow due to sub-salt faults, with diapirs formed where the salt flow is perpendicular to the fault (Fig. 5B, step II). In the case of oblique faults, the salt flow is partitioned into two components: (1) one parallel to the progradation direction which favours the formation of pillows above the fault (Fig. 5B, step II), and (2) another oblique to the progradation direction which results in salt flow along the strike and towards the wider graben. (Fig. 5B, step II).

- 2) The role of basin confinement in the timing and rate of salt-related deformation. Based on results of models 1 and 2, variations in basin confinement due to: (1) narrowing grabens along strike; and (2) the presence of intrabasinal faults, strongly affect the timing of salt withdrawal and diapirism as well as salt-related deformation rates along the basin. A narrowing graben causes perturbations in the withdrawal front, with salt withdrawal occurring earlier in the narrower areas (Fig. 5A, steps IV-V). Similar characteristics can be observed in the Nordkapp Basin, where the earliest salt mobilization and thickest depocenter occurred during the Earliest Triassic in the narrowest part of the central sub-basin (Figs. 10 and 13A). Increasing confinement by the presence of intrabasinal faults produces also earlier diapirism and higher deformation rates in model 2 than in model 1 (Figs. 5 and 7). This effect is also identified in the eastern sub-basin where the western asymmetric graben with an intrabasinal fault (Fig. 11A) displays earlier timing of salt diapirism and higher deformation rates than the eastern symmetric graben (Fig. 12A). All of these effects relate to the available space salt has to flow and accommodate sediment loading. In the case of wide grabens, salt deformation and flow induced by sediment loading can be accommodated over a wide area, forming a smooth plateau (Fig. 5A, steps III-IV). However, in narrower grabens, salt has limited space to flow within, resulting in rapid inflation and formation of salt diapirs above subsalt faults (Fig. 7A, steps III-IV). It is important to mention that once a passive diapir is formed, salt deformation rates increase dramatically since salt finds its way out, causing the rapid depletion of the source layer. Note that in the eastern sub-basin, most of the salt is evacuated by the end of the Middle Triassic in the western narrow asymmetric graben (Fig. 11), whereas salt deformation continues until the Late Triassic and Jurassic in the wider symmetric graben (Fig. 12). Thus, basin confinement is an important factor that explains the

shorter periods of salt-related deformation observed in CSBB such as the Nordkapp Basin.

- 3) Lateral variations in surface topography/bathymetry. Based on the modelling results, important factors such as the type of triggering mechanism and lateral variation in subsalt basin configuration control the nucleation of salt structures and minibasins, which result in different surface deformation. Salt bearing-basins triggered by basement-involved extension are characterized by a tectonically induced depression which is often bounded at both basin boundaries by salt walls, which act as topographic/bathymetric highs favouring sediment reworking (Fig. 9B). Because of these structural highs at both basin boundaries, the main sediment entrance is expected to occur along the basin axis as it has been shown in the Central High Atlas (Morocco) by Moragas et al. (2017). In salt-bearing basins triggered by sediment progradation, the resulting topographic deformation will highly depend on the subsalt basin configuration along strike (Figs. 5 and 7). Wide grabens as in model 1 will display long periods of lateral salt-migration deformation with smooth variations in surface topography since salt flows within a large area to accommodate the loading induced by the progradational wedges (Fig. 5B). Symmetric grabens can change laterally into asymmetric grabens where the presence of faults facing sediment progradation will cause rapid inflation and early formation of salt diapirs. These diapirs can act as topography/bathymetric highs controlling sediment pathways and providing local areas of reworking (Fig. 7B). Early formation of salt diapirs can additionally result in acceleration of minibasin subsidence since salt is extruded by passive diapirism. Therefore, as observed in the models, progressive migration of depocenters bounded by salt diapirs together with differences in subsidence and uplift rates along strike will play an important role on the spatial and temporal distribution of depositional environments (Rojo et al., 2019B)

Relative contribution of thick-skinned extension and progradational loading: implications for the tectonostratigraphic evolution of CSBB

The onset of salt mobilization in CSBB is commonly interpreted to be the result of either thick-skinned extension or sediment loading. The first case is the most assumed process in the North Sea (e.g. Koyi and Petersen, 1993; Coward and Stewart, 1995; Stewart et al., 1997; Jackson and Lewis, 2016; Ge et al., 2017) and Barents Sea (Koyi et al., 1995a; Koyi et al., 1995b; Rojo and Escalona, 2018). However, a regional study by Rojo et al. (2019) in the Nordkapp Basin demonstrates that neither of these two triggers alone explains the different structural styles of the Nordkapp Basin. Comparison to the sandbox models suggests that both mechanisms must have operated in the Nordkapp Basin. For example, a higher contribution of thick-skinned extension with respect to progradational loading can be interpreted in the central sub-basin since in model 3 salt pillows and diapirs are present at both basin boundaries and younger salt structures are observed towards the proximal part (Figs. 13 and 14). A minor influence of progradational loading can be observed in SU2, which shows depocenters progressively shifted in the direction of sediment progradation (Fig. 13A). The eastern sub-basin, on the other hand, displays a larger contribution of progradational loading similar to models 1 and 2, with

prograding rollover synclines in SU2 and SU3 units and younger salt structures in the progradation direction (Figs. 11 and 12). A minor influence of thick-skinned extension is supported by the presence of salt pillows and suprasalt fault complexes at both basin boundaries, which were likely formed by subsalt faulting during the Lower Triassic (SU2). It is also important to note that preferential loading occurred along the basin axis, leaving a considerable amount of salt at the proximal boundary (Figs. 11 and 12). Subsalt faulting also favours loading along the basin axis as observed in model 3.

There are differences between the sandbox models and the Nordkapp Basin though, such as the presence of distal thrust faults in the models (Figs. 11B and 12B). The lack of these structures in the Nordkapp Basin could be attributed to: (1) a mixed influence of thick skinned extension and progradational loading, (2) oblique sediment progradation; (3) differences between the homogeneous model materials (sand and PSDM) versus the heterogeneous stratigraphy in nature (e.g. siliciclastic and carbonate sediments, and evaporites); or (4) salt thickness and basin dimensions.

The Nordkapp Basin is not the only example of the combination of thick-skinned extension and salt mobilization due to sediment loading. Moragas et al. (2017) suggest basement-involved extension and progradational loading to explain the Mesozoic structural style of the Central High Atlas diapiric basin (Morocco). Stewart and Clark (1999) also identify sediment loading and basement-involved extension in different areas of the Central North Sea. Based on results of the sandbox models, the relative contribution of each salt-flow triggering process will create differences in structural style and surface deformation, which will play an important role in reservoir and source rock distribution and in the timing of structural and stratigraphic traps. Therefore, assuming mixed-mode salt-flow triggers in natural examples is preferred in order to understand the tectonostratigraphic evolution of salt-bearing basins as well as its implication for the petroleum system.

CONCLUSIONS

Based on the comparison between results of sandbox models and seismic sections through the Nordkapp Basin (Norwegian Barents Sea), we conclude that the suprasalt structural style of confined-salt-bearing basins is influenced by the following factors:

- 1) Triggering mechanisms: CSBB triggered by sediment progradation display characteristic prograding depocenters and younger salt structures in the progradation direction. On the other hand, CSBB triggered by thick-skinned extension, display vertically stacked depocenters near active subsalt faults and salt diapirs at both basin boundaries. Younger salt diapirs occur in the proximal part of the basin, which is opposite to the timing of the salt diapirs formed by sediment progradation. Natural examples likely display a mixed-mode triggering behaviour. Analysing the relative contribution of each process is key to understand the tectonostratigraphic evolution of a basin and its petroleum system.
- 2) Lateral changes in basin configuration along strike have a great impact on salt flow and the distribution of salt structures in the following ways: (1) Subsalt faults facing

perpendicularly the progradation front contribute to salt inflation and formation of salt diapirs whereas thin-skinned faults form above subsalt faults inline with the progradation, (2) Subsalt faults facing obliquely the progradation front favor salt flow along the graben, (3) Salt flow converges at fault intersections which results in salt inflation and formation of salt diapirs, and (4) Salt mobilization and deformation rates along the basin are strongly controlled by basin confinement either by graben narrowing or by the presence of intrabasinal faults.

REFERENCES

- Brun, J.-P., and X. Fort, 2004, Compressional salt tectonics (Angolan margin): *Tectonophysics*, v. 382, p. 129-150, <https://doi.org/10.1016/j.tecto.2003.11.014>.
- Brun, J.-P., and X. Fort, 2011, Salt tectonics at passive margins: Geology versus models: *Marine and Petroleum Geology*, v. 28, p. 1123-1145, <https://doi.org/10.1016/j.marpetgeo.2011.03.004>.
- Cedeño, A., L. A. Rojo, N. Cardozo, L. Centeno, and A. Escalona, 2019, The Impact of Salt Tectonics on the Thermal Evolution and the Petroleum System of Confined Rift Basins: Insights from Basin Modeling of the Nordkapp Basin, Norwegian Barents Sea: *Geosciences*, v. 9, p. 316.
- Coward, M., and S. Stewart, 1995, Salt-influenced structures in the Mesozoic-Tertiary cover of the southern North Sea, UK
- Dengo, C., and K. Røssland, 1992, Extensional tectonic history of the western Barents Sea, *in* R. M. Larsen, H. Brekke, B. T. Larsen, and E. Talleraas, eds., *Structural and Tectonic Modelling and Its Application to Petroleum Geology: Norwegian Petroleum Society (NPF), Special Publications*, v. 1, p. 91-108.
- Dooley, T. P., M. R. Hudec, L. M. Pichel, and M. P. A. Jackson, 2018, The impact of base-salt relief on salt flow and suprasalt deformation patterns at the autochthonous, paraautochthonous and allochthonous level: insights from physical models: *Geological Society, London, Special Publications*, v. 476, p. SP476.13, 10.1144/sp476.13.
- Gabrielsen, R., O. Kløvjan, A. Rasmussen, and T. Stølan, 1992, Interaction between halokinesis and faulting: structuring of the margins of the Nordkapp Basin, Barents Sea region, *in* B. Larsen, H. Brekke, B. Larsen, and E. Talleraas, eds., *Structural and tectonic modelling and its implication to petroleum geology: Norwegian Petroleum Society (NPF), Special Publications*, v. 1, p. 121-131.
- Gaullier, V., and B. C. Vendeville, 2005, Salt tectonics driven by sediment progradation: Part II—Radial spreading of sedimentary lobes prograding above salt: *AAPG Bulletin*, v. 89, p. 1081-1089, 10.1306/03310503064.
- Ge, H., M. P. Jackson, and B. C. Vendeville, 1997, Kinematics and dynamics of salt tectonics driven by progradation: *AAPG Bulletin*, v. 81, p. 398-423.
- Ge, Z., R. L. Gawthorpe, A. Rotevatn, and M. B. Thomas, 2017, Impact of normal faulting and pre-rift salt tectonics on the structural style of salt-influenced rifts: the Late

- Jurassic Norwegian Central Graben, North Sea: Basin Research, v. 29, p. 674-698, 10.1111/bre.12219.
- Hubbert, M. K., 1937, Theory of scale models as applied to the study of geologic structures: GSA Bulletin, v. 48, p. 1459-1520, 10.1130/gsab-48-1459.
- Jackson, C. A. L., and M. M. Lewis, 2016, Structural style and evolution of a salt-influenced rift basin margin; the impact of variations in salt composition and the role of polyphase extension: Basin Research, v. 28, p. 81-102, doi: 10.1111/bre.12099.
- Jackson, M., and B. Vendeville, 1994, Regional extension as a geologic trigger for diapirism: Geological Society of America bulletin, v. 106, p. 57-73,
- Jackson, M. P. A., and M. R. Hudec, 2005, Stratigraphic record of translation down ramps in a passive-margin salt detachment: Journal of Structural Geology, v. 27, p. 889-911, <https://doi.org/10.1016/j.jsg.2005.01.010>.
- Jensen, L. N., and K. Sørensen, 1992, Tectonic framework and halokinesis of the Nordkapp Basin, Barents Sea, in R. M. Larsen, H. Brekke, B. T. Larsen, and E. Talleraas, eds., Structural and Tectonic Modelling and its Application to Petroleum Geology: Norwegian Petroleum Society (NPF), Special Publications, v. 1, p. 109-120,
- Jones, I. F., and I. Davison, 2014, Seismic imaging in and around salt bodies: Interpretation, v. 2, p. SL1-SL20,
- Koyi, H., M. K. Jenyon, and K. Petersen, 1993A, The effect of basement faulting on diapirism: Journal of Petroleum Geology, v. 16, p. 285-312, DOI: 10.1111/j.1747-5457.1993.tb00339.x.
- Koyi, H., and K. Petersen, 1993B, Influence of basement faults on the development of salt structures in the Danish Basin: Marine and Petroleum Geology, v. 10, p. 82-94, DOI:10.1016/0264-8172(93)90015-K.
- Koyi, H., C. J. Talbot, and B. O. Torudbakken, 1993b, Salt diapirs of the southwest Nordkapp Basin: analogue modelling: Tectonophysics, v. 228, p. 167-187, doi: 10.1016/0040-1951(93)90339-L.
- Koyi, H., C. J. Talbot, and B. O. Torudbakken, 1995a, Analogue models of salt diapirs and seismic interpretation in the Nordkapp Basin, Norway: Petroleum geoscience, v. 1, p. 185-192, doi: 10.1144/petgeo.1.2.185.
- Koyi, H., C. J. Talbot, and B. O. Torudbakken, 1995b, Salt tectonics in the Northeastern Nordkapp basin, Southwestern Barents sea, in M. P. A. Jackson, D. G. Roberts, and S. Snelson, eds., Salt Tectonics: A Global Perspective, AAPG Memoir 65, p. 437-447,
- Koyi, H., 1996, Salt flow by aggrading and prograding overburdens, in G. I. Alsop, D. J. Blundell, and I. Davison, eds., Salt tectonics, Geological Society, London, Special Publications, v. 100, p. 243-258, doi: 10.1144/gsl.sp.1996.100.01.15.
- Koyi, H., 1998. The shaping of salt diapirs. Journal of Structural Geology 20 (4), 321-338.
- Koyi, H., 2001. Modeling the influence of sinking anhydrite blocks on salt diapirs targeted for hazardous waste disposal. Geology 29 (5), 387-390.
- Koyi, H., Ghasemi, A., Hessami, K., and Dietl, C., 2008. The mechanical relationship between strike-slip faults and salt diapirs in the Zagros fold-thrust belt. Journal of the Geological Society 165 (6), 1031-1044

- Krantz, R. W., 1991, Measurements of friction coefficients and cohesion for faulting and fault reactivation in laboratory models using sand and sand mixtures: *Tectonophysics*, v. 188, p. 203-207, [https://doi.org/10.1016/0040-1951\(91\)90323-K](https://doi.org/10.1016/0040-1951(91)90323-K).
- Lundin, E. R., 1992, Thin-skinned extensional tectonics on a salt detachment, northern Kwanza Basin, Angola: *Marine and Petroleum Geology*, v. 9, p. 405-411, [https://doi.org/10.1016/0264-8172\(92\)90051-F](https://doi.org/10.1016/0264-8172(92)90051-F).
- Maillet, B., and Koyi, H., 2006. Thrust dip and thrust refraction in fault-bend folds: analogue models and theoretical predictions. *Journal of Structural Geology* 28 (1), 36-49
- McBride, B. C., P. Weimer, and M. G. Rowan, 1998, The effect of allochthonous salt on the petroleum systems of northern Green Canyon and Ewing Bank (offshore Louisiana), northern Gulf of Mexico: *AAPG Bulletin*, v. 82, p. 1083-1112,
- Mello, U. T., G. D. Karner, and R. N. Anderson, 1995, Role of salt in restraining the maturation of subsalt source rocks: *Marine and Petroleum Geology*, v. 12, p. 697-716, doi: 10.1016/0264-8172(95)93596-V.
- Moragas, M., J. Vergés, T. Nalpas, E. Saura, J. D. Martín-Martín, G. Messenger, and D. W. Hunt, 2017, The impact of syn- and post-extension prograding sedimentation on the development of salt-related rift basins and their inversion: Clues from analogue modelling: *Marine and Petroleum Geology*, v. 88, p. 985-1003, <https://doi.org/10.1016/j.marpetgeo.2017.10.001>.
- Morley, C. K., R. King, R. Hillis, M. Tingay, and G. Backe, 2011, Deepwater fold and thrust belt classification, tectonics, structure and hydrocarbon prospectivity: A review: *Earth-Science Reviews*, v. 104, p. 41-91, <https://doi.org/10.1016/j.earscirev.2010.09.010>.
- Nalpas, T., and J. P. Brun, 1993, Salt flow and diapirism related to extension at crustal scale: *Tectonophysics*, v. 228, p. 349-362, [https://doi.org/10.1016/0040-1951\(93\)90348-N](https://doi.org/10.1016/0040-1951(93)90348-N).
- Nilsen, K. T., B. C. Vendeville, and J.-T. Johansen, 1995, Influence of regional tectonics on halokinesis in the Nordkapp Basin, Barents Sea, in M. P. A. Jackson, D. G. Roberts, and S. Snelson, eds., *Salt tectonics: a global perspective*: AAPG Memoir 65, p. 413-436,
- Patruno, S., and W. Helland-Hansen, 2018, Clinoforms and clinoform systems: Review and dynamic classification scheme for shorelines, subaqueous deltas, shelf edges and continental margins: *Earth-Science Reviews*, v. 185, p. 202-233, doi: 10.1016/j.earscirev.2018.05.016.
- Peel, F. J., 2014, The engines of gravity-driven movement on passive margins: Quantifying the relative contribution of spreading vs. gravity sliding mechanisms: *Tectonophysics*, v. 633, p. 126-142, <https://doi.org/10.1016/j.tecto.2014.06.023>.
- Pichel, L. M., F. Peel, C. A. L. Jackson, and M. Huuse, 2018, Geometry and kinematics of salt-detached ramp syncline basins: *Journal of Structural Geology*, v. 115, p. 208-230, <https://doi.org/10.1016/j.jsg.2018.07.016>.
- Pichel, L. M., E. Finch, and R. L. Gawthorpe, 2019A, The Impact of Pre-Salt Rift Topography on Salt Tectonics: A Discrete-Element Modeling Approach: *Tectonics*, v. 38, p. 1466-1488, 10.1029/2018tc005174.

- Pichel, L. M., C. A.-L. Jackson, F. Peel, and T. P. Dooley, 2019B, Base-salt relief controls salt-tectonic structural style, São Paulo Plateau, Santos Basin, Brazil: *Basin Research*, v. 010.1111/bre.12375.
- Ramberg, H., 1981, Gravity, deformation and the earth's crust: in theory, experiments and geological application, Academic press.
- Rojo, L. A., A. Escalona, and L. Schulte, 2016, The use of seismic attributes to enhance imaging of salt structures in the Barents Sea: *First Break*, v. 34, p. 41-49, doi: 10.3997/1365-2397.2016014
- Rojo, L. A., and A. Escalona, 2018, Controls on minibasin infill in the Nordkapp Basin: Evidence of complex Triassic synsedimentary deposition influenced by salt tectonics: *AAPG Bulletin*, v. 102, p. 1239-1272, doi: 10.1306/0926171524316523.
- Rojo, L. A., N. Cardozo, A. Escalona, and H. Koyi, 2019, Structural style and evolution of the Nordkapp Basin, Norwegian Barents Sea, in press: *AAPG Bulletin* doi: 10.1306/01301918028.
- Rouby, D., S. Raillard, F. Guillocheau, R. Bouroullec, and T. Nalpas, 2002, Kinematics of a growth fault/raft system on the West African margin using 3-D restoration: *Journal of Structural Geology*, v. 24, p. 783-796, [https://doi.org/10.1016/S0191-8141\(01\)00108-0](https://doi.org/10.1016/S0191-8141(01)00108-0).
- Rowan, M. G., F. J. Peel, and B. C. Vendeville, 2004, Gravity-driven fold belts on passive margins
- Rowan, M. G., and S. Lindsø, 2017, Chapter 12 - Salt Tectonics of the Norwegian Barents Sea and Northeast Greenland Shelf A2 - Soto, Juan I, in J. I. Soto, J. F. Flinch, and G. Tari, eds., *Permo-Triassic Salt Provinces of Europe, North Africa and the Atlantic Margins*, Elsevier, p. 265-286, doi: 10.1016/B978-0-12-809417-4.00013-6.
- Stewart, S., A. Ruffell, and M. Harvey, 1997, Relationship between basement-linked and gravity-driven fault systems in the UKCS salt basins: *Marine and Petroleum Geology*, v. 14, p. 581-604, doi: 10.1016/S0264-8172(97)00008-1.
- Stewart, S. A., and J. A. Clark, 1999, Impact of salt on the structure of the Central North Sea hydrocarbon fairways: Geological Society, London, *Petroleum Geology Conference series*, v. 5, p. 179-200, 10.1144/0050179.
- Trudgill, B. D., 2011, Evolution of salt structures in the northern Paradox Basin: controls on evaporite deposition, salt wall growth and supra-salt stratigraphic architecture: *Basin Research*, v. 23, p. 208-238, doi: 10.1111/j.1365-2117.2010.00478.x.
- Vendeville, B., P. R. Cobbold, P. Davy, P. Choukroune, and J. P. Brun, 1987, Physical models of extensional tectonics at various scales: Geological Society, London, *Special Publications*, v. 28, p. 95-107, 10.1144/gsl.Sp.1987.028.01.08.
- Vendeville, B. C., 2005, Salt tectonics driven by sediment progradation: Part I—Mechanics and kinematics: *AAPG Bulletin*, v. 89, p. 1071-1079, 10.1306/03310503063.
- Vidal-Royo, O., O. Ferrer, H. Koyi, B. C. Vendeville, J. A. Muños, and E. Roca, 2008, 3D reconstruction of analogue modelling experiments from 2D datasets: *Bolletino di Geofisica teorica ed applicata*, v. 49, p. 524-528,
- Warren, J. K., 2010, Evaporites through time: Tectonic, climatic and eustatic controls in marine and nonmarine deposits: *Earth-Science Reviews*, v. 98, p. 217-268, doi: 10.1016/j.earscirev.2009.11.004.

Paper II

- Warsitzka, M., J. Kley, and N. Kukowski, 2013, Salt diapirism driven by differential loading—Some insights from analogue modelling: *Tectonophysics*, v. 591, p. 83-97, doi: 10.1016/j.tecto.2011.11.018.
- Weijermars, R., M. P. A. Jackson, and B. Vendeville, 1993, Rheological and tectonic modeling of salt provinces: *Tectonophysics*, v. 217, p. 143-174, [https://doi.org/10.1016/0040-1951\(93\)90208-2](https://doi.org/10.1016/0040-1951(93)90208-2).
- Withjack, M. O., and S. Callaway, 2000, Active normal faulting beneath a salt layer: an experimental study of deformation patterns in the cover sequence: *AAPG bulletin*, v. 84, p. 627-651,

Intentionally left blank

Paper III

The influence of halokinesis on prograding clinoforms: Insights from the Tiddlybanken Basin, Norwegian Barents Sea


Luis Alberto Rojo¹, Dora Marin¹, Nestor Cardozo¹,
Alejandro Escalona¹, and Hemin Koyi²

¹Department of Energy Resources, University of Stavanger, 4036
Stavanger, Norway

²Hans Ramberg Tectonic Laboratory, Department of Earth Sciences,
Uppsala University, Sweden

2019, Basin Research, DOI: 10.1111/bre.12411

The influence of halokinesis on prograding clinoforms: Insights from the Tiddlybanken Basin, Norwegian Barents Sea

Luis Alberto Rojo¹  | Dora Marín¹ | Nestor Cardozo¹ | Alejandro Escalona¹ | Hemin Koyi²

¹Department of Energy Resources, University of Stavanger, Stavanger, Norway

²Department of Earth Sciences, Hans Ramberg Tectonic Laboratory, Uppsala University, Uppsala, Sweden

Correspondence

Luis Alberto Rojo, Department of Energy Resources, University of Stavanger, 4036 Stavanger, Norway.
Email: luis.a.moraleda@uis.no

Funding information

Ministry of education and Research, Norway.

Abstract

Although the trajectory and geometry of clinoforms in different types of basins have been described in many studies, few studies discuss the influence of halokinesis on clinoforms in salt-related basins. In this study, we analyse the Lower Cretaceous clinoforms in the Tiddlybanken Basin, Norwegian Barents Sea to evaluate the impact of salt mobilization on the geometry and trajectory of clinoforms as well as its implications on sediment partitioning. To accomplish this objective, we use a multidisciplinary approach consisting of seismic and well-interpretation, 3D structural restoration, and forward stratigraphic modelling. The results show that salt mobilization affects prograding clinoforms by: (a) causing lateral variations in progradation rates, resulting in complex palaeogeography, (b) increasing slope angles, which affect the equilibrium of the clinoform profile and can trigger slope-readjustment processes and (c) producing lateral and temporal variations in accommodation space, leading to different clinoform trajectories, stacking patterns and reservoir distribution along the basin. Forward stratigraphic modelling shows that in salt-related basins and other tectonically active basins, the isolated use of conventional methods for clinoform analysis might lead to potential interpretation pitfalls such as misinterpretation of trajectories and overestimation of foreset angles, which can have negative consequences for exploration models.

1 | INTRODUCTION

Clinofoms represent accretionary strata that are characterized by topset, foreset and bottomset geometries, marking the transition from shallow to deeper waters. They are commonly used to interpret the changes in sedimentary environments and relative sea level in frontier basins, since they represent 'frozen' palaeobathymetric profiles (Patrino, Hampson, Jackson, & Whipp, 2015; Patrino & Helland-Hansen, 2018; Pirmez, Pratson, & Steckler, 1998; Sangree & Widmier, 1978; Steel et al., 2008; Steel, Olsen, Armentrout, & Rosen,

2002). Depending on their scale and sedimentary environments, clinoforms can be classified into the following types (Figure 1a; Helland-Hansen & Hampson, 2009; Patrino & Helland-Hansen, 2018): (a) Shoreline or deltaic clinoforms, which are generally produced by the progradation of deltas, barrier-islands, shorelines and strandplains. These clinoforms are normally up to a few tens of meters in height (low relief) and are typically formed over periods of 0.1–1 Myr; (b) Shelf-edge clinoforms, which display heights of hundreds of meters (high relief) and are accreted in periods of 0.1–20 Myr as result of shelf-margin progradation; and (c) Continental

This is an open access article under the terms of the Creative Commons Attribution License, which permits use, distribution and reproduction in any medium, provided the original work is properly cited.

© 2019 The Authors. *Basin Research* published by International Association of Sedimentologists and European Association of Geoscientists and Engineers and John Wiley & Sons Ltd.

margin clinoforms, forming sets thousands of meters high, which represent the transition from continent to ocean, and are accreted in periods of 5–100 Myr.

During the last several decades, both academia and industry have carried out detailed studies of clinoform successions to decipher the evolution and infill of sedimentary basins, since this analysis is crucial to the understanding of the distribution of reservoirs, seals and source rocks from the shoreline to the basin floor (Dreyer, Whitaker, Dexter, Flesche, & Larsen, 2005; Helland-Hansen & Hampson, 2009; Houseknecht, Bird, & Schenk, 2009; Rønnevik, Beskow, & Jacobsen, 1982; Ulmishek, 2003). Different techniques have been adopted to analyse the distribution of coarse-grained sediments within clinoforms:

1. Sequence stratigraphy, which is based on the analysis of stacking patterns, geometric relationships and stratal terminations, to identify key surfaces formed as result of relative sea level fluctuations (Catuneanu et al., 2011; Mitchum, Vail, & Sangree, 1977). These key surfaces representing breaks in sedimentation divide the sedimentary succession into genetic units with chronostratigraphic significance.
2. Trajectory analysis, which is based on the study of vertical and lateral migration of clinoforms and associated sedimentary environments resulting from the interplay between sediment input, bathymetry, eustatic sea level fluctuations and tectonics (Bullimore, Henriksen, Liestøl, & Helland-Hansen, 2005; Helland-Hansen & Gjelberg, 1994; Helland-Hansen & Hampson, 2009). This method has been commonly used for outcrops and seismic reflection profiles to understand the changes in palaeoenvironmental conditions and associated lithological distribution within shoreline clinoforms (Hernández-Molina et al., 2000; Marin, Escalona, Nøhr-Hansen, Śliwińska Kasia, & Mordasova, 2017; Patruno et al., 2015), shelf-edge clinoforms (Glørstad-Clark, Faleide, Lundschieen, & Nystuen, 2010; Johannessen & Steel, 2005; Marin et al., 2017; Poyatos-Moré et al., 2016; Steel et al., 2002) and continental margin clinoforms (Salazar, Moscardelli, & Wood, 2016, 2018). Trajectory analysis of shelf-edge clinoforms is based on the description of the rollover point migration (i.e. shelf-edge), which can be classified into ascending, flat or descending trajectory (Helland-Hansen & Hampson, 2009). Flat and descending shelf-edge trajectories are formed as result of a stable or falling relative sea level, respectively, and commonly display oblique progradational seismic patterns (Figure 1c,d). These trajectories indicate less storage potential on the shelf due to marine and subaerial erosion, and subsequent sediment bypass to the slope and basin floor (Carvajal & Steel, 2006; Johannessen & Steel, 2005). On the other hand, ascending shelf-edge trajectories are formed under a long-term rise in relative sea level, and generally show sigmoidal progradational seismic patterns (Figure 1b). Due to the

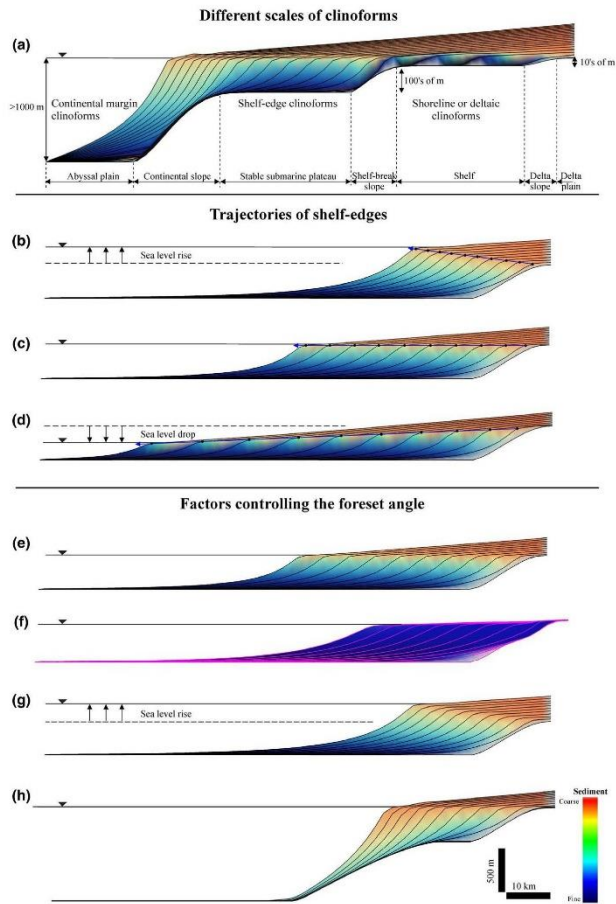
Highlights

- Salt mobilization causes drastic vertical and lateral changes in relative sea level, which in turn induce lateral variations in clinoform trajectory, foreset angle, relief and progradation rates.
- Salt withdrawal and uplift produces complex spatial and temporal stacking patterns of depositional environments resulting in different palaeogeographies through time.
- The use of forward stratigraphic models is essential in tectonically active areas, since the insolated use of conventional methodologies in clinoform analysis might conduct to interpretation pitfalls such as wrong interpretation of trajectories and overestimation of foreset angles
- This study has implications in understanding sediment partitioning of salt-bearing basins filled by prograding overburdens.

continuous rise in relative sea level, these trajectories favour higher sediment storage on the shelf than in the slope and basin floor (Helland-Hansen & Hampson, 2009). However, in the case of narrow shelves with anomalously high sediment supply, or lack of wave-remobilization of sediment at the shoreline, shoreline or deltaic clinoforms can reach the shelf-edge forming shelf-edge deltas, delivering significant amount of sediment to the slope and basin floor even during the periods of relative sea level rise (Carvajal, Steel, & Petter, 2009; Carvajal & Steel, 2006; Dixon, Steel, & Olariu, 2012; Jones, Hodgson, & Flint, 2015)

3. Geometric analysis of clinoforms involves studies such as the measurement of foreset angles (Mitchum et al., 1977; Patruno et al., 2015; Pirmez et al., 1998). A relationship between foreset angles and lithology has been suggested based on the observations of modern deltas, outcrops and analogue models (Anderson, Chidsey, Ryer, Adams, & McClure, 2004; Nemeč, 2009; Orton & Reading, 1993; Patruno et al., 2015; Pirmez et al., 1998). These studies conclude that sandy clinoforms tend to have steeper foreset angles than fine-grained clinoforms (Figure 1e,f; Adams & Schlager, 2000; Anderson et al., 2004; Orton & Reading, 1993; Pirmez et al., 1998). However, other factors can also affect the foreset angles, including: (a) basin physiography and tectonics, where the foreset angles tend to increase during progradation into deeper waters (Figure 1h; Klausen et al., 2018; Orton & Reading, 1993; Pirmez et al., 1998; Porębski & Steel, 2003; Ross, Halliwell, May, Watts, & Syvitski, 1994; Steckler, Mountain, Miller, & Christie-Blick, 1999); (b) sediment input; where the foreset angles tend to increase in areas with low sediment

FIGURE 1 (a) Cross-section parallel to depositional dip, displaying the different scales of clinoforms (based on Helland-Hansen & Hampson, 2009). (b) Ascending trajectory of the shelf-edge formed during relative sea level rise. (c) Flat trajectory of the shelf-edge resulting from a constant relative sea level. (d) Falling trajectory of the shelf-edge due to a drop in relative sea level. (e and f) Variation of foreset angle as function of grain size. Sand-prone clinoforms (e) tend to have higher foreset angles ($>2^\circ$) than mud-prone clinoforms (f, $<2^\circ$). (g) Clinoforms deposited during sea level rise display higher foreset angles than those deposited under constant sea level (c). (h) Clinoforms prograding into deeper waters increase their foreset angle (after Ross et al., 1994, and Pirmez et al., 1998). Figures produced using the GPM Petrel plugin (Schlumberger)



input and decrease in areas with high sediment input (Coleman & Wright, 1975; O'Grady, Syvitski, Pratson, & Sarg, 2000); (c) relative sea level, where periods of relative sea level rising lead to steepening foreset angles (Figure 1g; Pirmez et al., 1998; Ross et al., 1994); and (d) turbidity currents, which tend to decrease the foreset angles (Kostic, Parker, & Marr, 2002; Pratson et al., 2007).

Previous studies have mostly analysed the geometry and trajectory of clinoforms in passive margins (Anderson, 2005; Anderson et al., 2016; Steckler et al., 1999), foreland basins (Pellegrini et al., 2017; Steel et al., 2002), back-arc basins (Salazar, Moscardelli, & Wood, 2016, 2018) and

epicontinental seas (Eide, Klausen, Katkov, Suslova, & Helland-Hansen, 2017; Glørstad-Clark et al., 2010; Klausen et al., 2018; Klausen, Ryseth, Helland-Hansen, Gawthorpe, & Laursen, 2015; Marin et al., 2017; Riis, Lundschieen, Høy, Mørk, & Mørk, 2008). However, the literature also provides few examples of shelf-edge clinoforms prograding through basins with ongoing halokinesis such as salt-related passive margins (e.g. Gulf of Mexico and Santos Basin; (Ge, Jackson, & Vendeville, 1997; Jackson, Jackson, & Hudec, 2015; Koyi, 1996), salt-related foreland basins (e.g. Paradox Basin; Trudgill, 2011) and salt-related rift basins (e.g. Nordkapp Basin; Koyi, Talbot, & Tørudbakken, 1995; Rojo & Escalona, 2018; Rowan & Lindsø, 2017). Contrary to other

basins without the presence of salt, salt-bearing basins show a complex feedback between the salt and the sediments. On one hand, prograding overburdens cause differential loading on the underlying salt and trigger halokinesis (Ge et al., 1997; Koyi, 1996; Trudgill, 2011). On the other hand, salt movement generates spatial and temporal variations in palaeobathymetry. These variations consisting of uplift (e.g. salt diapirs) and subsidence (e.g. minibasins) influence the progradation of clinoforms and the spatial and temporal distribution of sedimentary environments (Banham & Mountney, 2013; Rojo & Escalona, 2018). Among these two salt–sediment interaction processes, the effect of prograding overburdens is well-understood by both analogue and numerical models (Albertz & Ings, 2012; Ge et al., 1997; Koyi, 1996; Warsitzka, Kley, & Kukowski, 2013) and has been studied in many salt-bearing basins (Ge et al., 1997; Jackson et al., 2015; Koyi, 1996; Trudgill, 2011), whereas

few studies discuss the influence of salt movement on prograding clinoforms (Cohen & Hardy, 1996) or other similar geometries such as sand dunes (Kopriva & Kim, 2015; Piliouras, Kim, Kocurek, Mohrig, & Kopp, 2014).

The study area includes part of the Norwegian Barents Shelf, which displays a complex distribution of rift basins (some of which are salt-bearing), structural highs and platforms (Figure 2a; Faleide, Vågnes, & Gudlaugsson, 1993; Worsley, 2008). Along its geological history, the Barents Shelf has experienced two main episodes of clinoform progradation; (a) during the Triassic (Figure 2b) and (b) during the Cretaceous (Figure 2c), where clinoforms prograded across the entire shelf. Most previous studies have analysed Triassic (Eide et al., 2017; Glørstad-Clark et al., 2010; Klausen et al., 2018, 2015; Riis et al., 2008) and Cretaceous clinoforms (Grundvåg et al., 2017; Marin et al., 2017) in tectonically stable areas (e.g. Bjørnøland and Finnmark platforms). However, few studies (e.g. Heiberg,

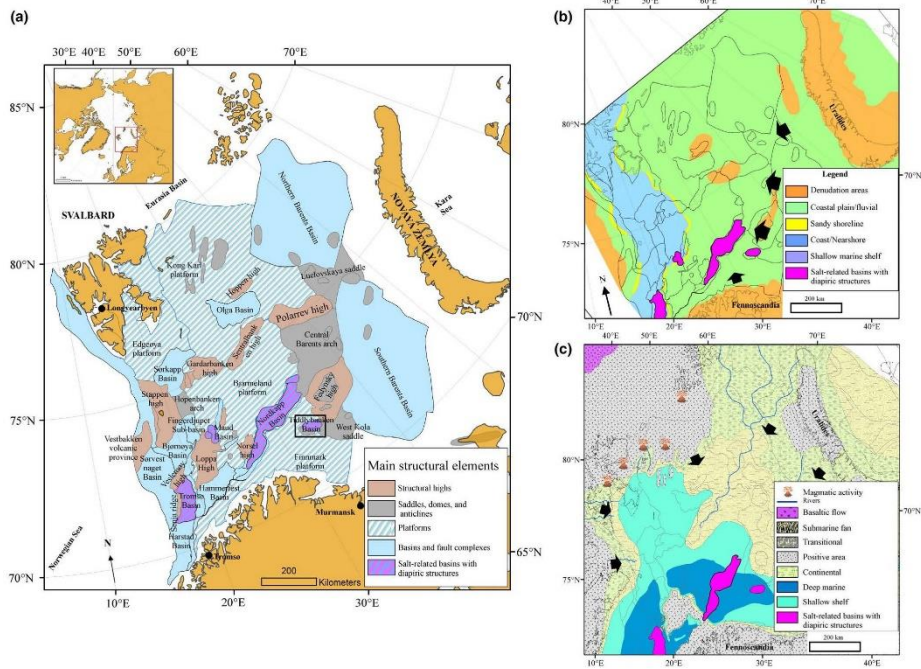


FIGURE 2 (a) Main structural elements of the Barents Sea. The Tromsø, Nordkapp and Tyddlibanken basins are salt-related basins with abundant diapiric structures. Inset map shows the location of the Barents Sea in the Arctic region (after Rojo et al., 2019). (b) Palaeogeography during the Late Triassic in the Barents Shelf. Shelf-edge clinoforms prograded towards the NW of the Barents Sea and across salt-related basins (e.g. Tyddlibanken and Nordkapp basins) with ongoing halokinesis (modified from Henriksen, Bjørnseth, et al., 2011). (c) Palaeogeography during the Early Cretaceous (modified after LoCrA (2018)). Shelf-edge clinoforms prograded towards the southern part of the Barents Sea and across salt-related basins with ongoing halokinesis. Black arrows in maps B and C indicate the progradation direction

2018) have been carried out in salt-related basins (e.g. Nordkapp or Tiddlybanken Basins) where salt tectonics may have influenced clinoform progradation and sedimentary environments. Therefore, this study combines seismic interpretation, 3D structural restoration, and forward stratigraphic modelling of the Tiddlybanken Basin to accomplish the following objectives: (a) decipher the impact of salt movement on the geometry and trajectory of Lower Cretaceous clinoforms and (b) understand the implications of clinoform geometry and trajectory variations on sediment partitioning in the basin. The study area provides an excellent opportunity to understand how salt movement triggers the formation of complex basin physiography. This results in local changes in clinoforms geometry and trajectory, whose analysis is crucial for understanding the infill and evolution of the basin, as well as predicting potential reservoirs.

2 | GEOLOGICAL SETTING

The Tiddlybanken Basin is a 50 km-wide, NW–SE elongated salt basin between the Finnmark platform and the Fedynsky High (Figure 2a). A 30-km long, NW–SE trending salt wall is present at the basin axis, whereas an E–W salt-cored anticline, known as the Signalhorn dome, defines the southwestern basin boundary (Figure 3a; Mattingsdal, Høy, Simonstad, & Brekke, 2015). The Tiddlybanken Basin is considered a frontier basin without exploration wells, since for decades it was part of a politically disputed area between Norway and Russia until the border agreement was established in 2011 (Gernigon et al., 2018; Rowan & Lindsø, 2017). The geological history of this basin has been strongly influenced by tectonic events and climate variations that affected the entire Barents Sea (Gernigon et al., 2018, 2014; Henriksen, Ryseth, et al., 2011; Worsley, 2008).

2.1 | Tectonostratigraphy

2.1.1 | Late palaeozoic

The Tiddlybanken Basin formed during the Late Devonian–Mississippian, as the result of extension and reactivation of the major Timanian–Caledonian structures (NW–SE magnetic trends) and basement-related structures of the Norwegian Barents Shelf (Gernigon et al., 2018, 2014; Rowan & Lindsø, 2017). Based on outcrop observations in Spitsbergen (Worsley, 2008) and shallow wells in the Finnmark platform (Bugge et al., 1995), it is interpreted that pre-salt strata may consist of Mississippian–Pennsylvanian, synrift alluvial to fluvial deposits interbedded with coal (Billefjorden Gp.; Figure 3a,b).

During the Pennsylvanian–early Permian, extensional faulting ceased and the basin underwent a period of post-rift subsidence, evolving as a sag basin until the end of the Palaeozoic (Gernigon et al., 2018; Rowan & Lindsø, 2017). The northward movement of Pangea towards arid

latitudes allowed the deposition of warm-water carbonates and platform evaporites at basin shoulders and platforms (e.g. Finnmark platform), whereas thick, late synrift-early post-rift halite-rich evaporite sequences precipitated in the basin axis (Gipsdalen Gp.; Figure 3a, b; Gernigon et al., 2018; Henriksen, Ryseth, et al., 2011; Rowan & Lindsø, 2017; Stemmerik, Elvebakk, & Worsley, 1999; Stemmerik & Worsley, 2005). During the late Permian, continuous northward movement of Pangea towards colder latitudes accompanied by ongoing passive subsidence favoured the deposition of cool and cold water carbonates with spiculites (Figure 3a, b; Henriksen, Ryseth, et al., 2011; Stemmerik et al., 1999; Stemmerik & Worsley, 2005). During the Early Middle Triassic, contraction associated with the development of the Uralides to the east triggered salt mobilization in the Tiddlybanken Basin (Rowan & Lindsø, 2017). Resulting accommodation from salt withdrawal was then filled by NE–SW striking transgressive–regressive fluviodeltaic sediments sourced from the Uralides and Fennoscandia (Sanssendalen Gp.; Figures 2b, and 3a,b; Gjørstad-Clark et al., 2010; Klausen et al., 2015, 2018; Lundschieen, Høy, & Mørk, 2014).

During the Late Triassic–Jurassic, minibasin subsidence and diapir uplift decreased dramatically causing the burial of the NW–SE salt wall at the basin axis (Figure 3a,b; Rowan & Lindsø, 2017). This decrease in accommodation was experienced in most of the Barents Sea and resulted in the deposition of condensed, shallow marine–fluviodeltaic deposits with complex drainage systems (Kapp Toscana Gp.; Figure 3a,b; Anell, Braathen, & Olaussen, 2014; Henriksen, Ryseth, et al., 2011).

The Late Jurassic–Early Cretaceous period was marked by passive subsidence with minor faulting possibly associated with the opening of the North Atlantic in the western Barents Sea (Figure 3a,b; Faleide et al., 2008, 1993). Late Jurassic regional flooding resulted in the deposition of fine siliciclastics and organic shales in most of the Barents Sea (Adventalen Gp.; Figure 3a,b; Henriksen, Ryseth, et al., 2011). Uplift in the northern part of the Barents Sea during the Barremian (Early Cretaceous) induced a new regression of the shoreline and shelf deposits towards the south (Adventalen Gp.; Figure 2c; Grundvåg et al., 2017; Marin et al., 2017). This episode was followed by Aptian–Albian sea level rise and subsequent basin infill with shelf deposits (Figure 3a,b). Thinning of the Lower Cretaceous strata towards the salt wall in the Tiddlybanken Basin indicates that diapir growth was likely rejuvenated due to the differential loading induced by these prograding Lower Cretaceous sediments towards the south of the shelf (Figures 2c, and 3a,b; Gernigon et al., 2018; Heiberg, 2018).

2.1.2 | Cenozoic

During the Late Cretaceous–Cenozoic, the basin underwent several contractional events caused by plate reorganizations

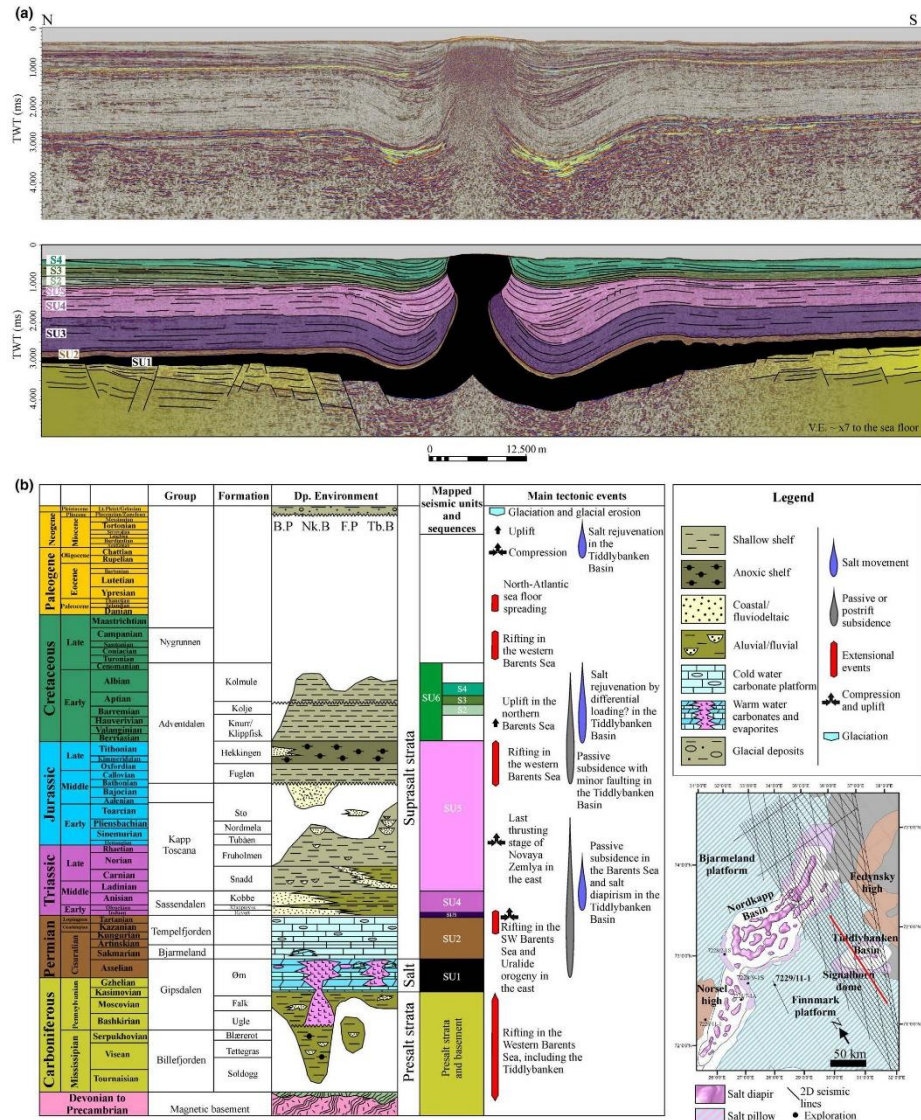


FIGURE 3 (a) N-S regional seismic line through the Tiddlybanken Basin showing the seismic units and sequences mapped in this study (See Figure 3d for colour indexing). (b) Lithostratigraphic chart illustrating the main stratigraphic units, depositional environments and tectonics events affecting the Barents Sea and the Tiddlybanken Basin (modified after Larsen et al. 2002). B.P = Bjarmeland platform; Nk. B = Nordkapp Basin; F.P = Finnmark platform; Tb.B = Tiddlybanken Basin. Inset map shows the location of the seismic line

associated with the opening of the North Atlantic (Faleide et al., 2008, 1993). Consequently, the salt wall was squeezed and rejuvenated by contraction (Figure 3a,b; Gernigon et al., 2018; Rowan & Lindsø, 2017). Finally, successive events of Cenozoic uplift and erosion, including the Pleistocene glacial erosion, removed ca. 1.5 km of Cenozoic and Cretaceous strata in the Tiddlybanken Basin (Figure 3a,b; Baig, Faleide, Jahren, & Mondol, 2016; Henriksen, Bjørnseth, et al., 2011; Ohm, Karlsen, & Austin, 2008).

3 | DATASET

We use one exploration well and 2D full-stack reflection data provided by the Norwegian Petroleum Directorate (NPD; Figure 3, inset map). The 2D reflection seismic survey covers an area of 54,150 km², including part of the Bjarmeland platform, eastern Nordkapp Basin, Finnmark platform and most of the Tiddlybanken Basin. The 2D seismic lines have a spacing of 4.5 km and maximum two-way travel time (TWT) of 9,216 ms. The Cretaceous interval shows frequencies ranging between 30 and 60 Hz, which allows detailed analysis of Lower Cretaceous clinoforms in terms of scale, geometry and trajectory.

Since the Tiddlybanken Basin is a frontier area, the closest exploration well-available (7229/11-1) in the dataset is located in the Finnmark platform ca. 100 km west of the study area (Figure 3, inset map). Well data consist of a conventional suite of wireline logs (e.g. gamma ray, caliper, neutron, density, sonic and resistivity), check-shots and well tops, which were integrated to: (a) provide age constraints and correlate the main seismic units and sequences across the basin, (b) assign a lithology to the clinoforms and (c) construct a 3D velocity model for time-to-depth conversion of the surfaces resulting from seismic interpretation.

4 | METHODOLOGY

4.1 | Stratigraphic framework

Based on reflection amplitude, strata terminations and continuity of seismic events, eight key horizons were identified for the regional interpretation of the Tiddlybanken Basin and nearby platforms (Figure 3a,b). The ages of these horizons are determined from well data, which were tied to the seismic using a synthetic seismogram. The interpretation of these horizons resulted in the following units: Pennsylvanian–lower Permian (SU1), upper Permian (SU2), lowest Triassic (SU3), Lower–Middle Triassic (SU4), Middle Triassic to Upper Jurassic (SU5) and Lower Cretaceous (SU6). In order to better understand the impact of salt tectonics on the Lower Cretaceous clinoforms, SU6 was further subdivided into three sequences bounded by flooding surfaces. These

sequences are: S2 (Barremian–Aptian), S3 (Aptian) and S4 (Aptian–Albian; Marin et al., 2017; Figure 3a,b). In complex areas influenced by salt tectonics, workflows proposed by Rojo, Escalona, and Schulte (2016) were used to map salt structures in 3D and highlight strata terminations within adjacent salt minibasins.

4.2 | Structural restoration

We use the velocity model of Rojo, Cardozo, Escalona, and Koyi (2019) to depth-convert the surfaces from the seismic interpretation. More information regarding interval velocities, K factors (change of interval velocities with depth) and densities of the different intervals is given by Clark et al., 2014; Gernigon et al., 2018; Rojo et al., 2019. The 3D structural restoration of the Tiddlybanken Basin was performed to: (a) show the progressive evolution of salt structures and palaeobathymetries through time; (b) remove salt-related deformation and compaction effects before measuring the angles and trajectories of the Lower Cretaceous clinoforms; and (c) provide uplift and subsidence maps (mm/yr) for S4 sequence, which are the tectonic input for the forward stratigraphic modelling. During the restoration process, regional levels were defined on the Finnmark platform, which does not show major salt-related deformation. The eroded and missing Cretaceous and Cenozoic strata were reconstructed based on previous publications (Baig et al., 2016; Henriksen, Bjørnseth, et al., 2011; Ohm et al., 2008). The reconstructed Cenozoic folding above salt diapirs was then unfolded using 3D flexural-slip to remove the shortening during this period. The Lower Cretaceous sequence boundaries S2 to S4 were restored as well with 3D flexural-slip to remove the salt-related deformation and avoid length losses in upturned strata close to salt diapirs (Rowan, 1996; Rowan & Ratliff, 2012). Sediments were decompacted using the method of Sclater and Christie (1980) since it fits well the porosity versus depth curves observed on borehole data in the Barents Sea (Klausen & Helland-Hansen, 2018). For the isostatic compensation of loads, we use flexural isostasy since there are large thickness variations along the basin and wedge-shape geometries characterizing the Lower Cretaceous sequences. An elastic thickness of 20 km was assumed based on Gac, Klitzke, Minakov, Faleide, and Scheck-Wenderoth (2016).

4.3 | Forward stratigraphic modelling

We use forward stratigraphic modelling to analyse the morphodynamics of prograding sediments influenced by salt-related subsidence and/or uplift. Specifically, we use the Geological Process Modelling (GPM) Petrel plugin (Schlumberger), which is a sedimentary simulation and visualization package that models the erosion, transport and deposition of clastic sediments based on physical equations

(Flemings & Grotzinger, 1996; Tetzlaff & Harbaugh, 1989). To start the sedimentation model, it is necessary to input the undeformed and backstripped surface resulting from the 3D restoration, which represents the predepositional palaeobathymetry of the sequence of interest, one of a series of parameters associated with the time zero in the model (Table 1). Other parameters include information about the location of the source and type of sediment, as well as the areas and rates of uplift and subsidence (mm/yr). It is important to note that GPM does not reproduce the effect of differential loading on salt. To reproduce this effect, we created a time-dependent tectonic function in which values of subsidence and uplift are increased locally when clinoforms reach the salt-related basin (Table 1). This tectonic function was adjusted until the simulated clinoforms geometries resembled those on the seismic profiles. Clinoform progradation was modelled using the diffusion and steady flow equations (Table 1). The diffusion equation defines the rate at which sediments move downslope proportionally to the slope gradient (Flemings & Grotzinger, 1996). Consequently, the topography or bathymetry becomes smoother over time. The steady flow equation simulates erosion, transport and deposition of sediments (Tetzlaff and Schafmeister, 2007, their equations 5 and 6). At each single point of the simulation grid, the algorithm calculates the transport capacity from the flow depth and velocity.

Erosion occurs when the flow contains less sediment than it can transport. Conversely, deposition takes place when the sediment carried by the flow exceeds the flow's transport capacity. Values of sediment input (mm/yr) and water velocities (m/s) were adjusted to generate shelf-edge clinoforms similar to those in the seismic profiles, with realistic accretion times (0.1–20 Myr) and progradation rates (1–100 m/kyr), as described by Patruino and Helland-Hansen (2018).

5 | THE INFLUENCE OF SALT TECTONICS ON PROGRADING CLINOFORMS: THEORETICAL CONSIDERATIONS

The purpose of this section is to illustrate the potential influence of salt tectonics on prograding clinoforms based on a synthetic GPM model coupled with tectonics (Table 1, model 1 and Figure 4a). The model presented here represents a submarine platform 100 km-wide, 170 km-long and below sea level (maximum water depth = 400 m). It consists of a stable platform to the west and a salt wall bounded by two salt minibasins to the east. Diffusion and steady flow simulate constant sediment input during a period of 10 Myr. Each reproduced shelf-edge clinoform represents a time interval of

TABLE 1 Input parameters used in the synthetic model (Figure 4) and the case study in the Tiddlybanken Basin (Figure 13). The models were run using the GPM Petrel plugin. Sediment source abbreviations in the last column are: crsd: coarse sandstone, fsd: fine sandstone, slt: silt, and cly: clay

INPUT PARAMETERS				
	Paleobathymetry	Subsidence and uplift map	Tectonic function	Sedimentary processes
MODEL 1 (Synthetic model)				<p>Sediment diffusion</p> $\frac{\partial h}{\partial t} = K \frac{\partial^2 h}{\partial x^2}$ <p>Diffusion coefficient (K): 10 m²/yr</p> <p>Steady flow</p> <p>Sediment source: 25%crsd, 25%fsd, 25%slt, 25%cly Sediment supply: 0.02 mm/yr Water velocity: 0.04 m/s Transport coefficient: 0.0001 Sea level: constant</p>
MODEL 2 (Case study)				<p>Sediment diffusion</p> $\frac{\partial h}{\partial t} = K \frac{\partial^2 h}{\partial x^2}$ <p>Diffusion coefficient (K): 10 m²/yr</p> <p>Steady flow</p> <p>Sediment source: 50%slt, 50%cly Sediment supply: 0.02 mm/yr Water velocity: 0.08 m/s Transport coefficient: 0.0001 Sea level: constant</p>

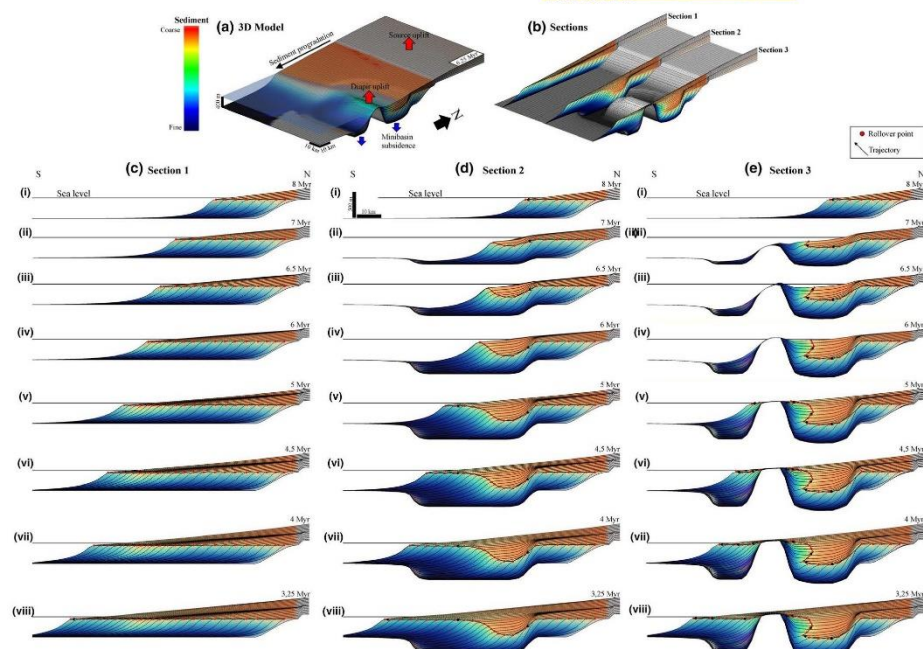


FIGURE 4 (a) Synthetic GPM model illustrating the possible effects of salt tectonics in prograding clinoforms based on diffusion-based sediment transport coupled with tectonics (salt withdrawal and diapir rise). (b) Location of the Sections 1, 2, 3. (c) Section 1 located in a stable platform without influence of salt tectonics. (d) Section 2 covering the edge of a salt withdrawal minibasin without salt diapirs. (e) Section 3 across the salt wall and two minibasins. Note that salt tectonics induce lateral variations in clinoform trajectories, geometries and sedimentary environments. Minibasin subsidence favours the preservation of coarse sediments, whereas these sediments are eroded in areas of diapir uplift and are probably transported to the slope or basin floor. Constant sediment input and eustatic sea level are assumed

0.25 Myr. An uplift area of 5,000 km² in the north acts as the main sediment source. The salt wall uplift rate is from 0.08 to 0.15 mm/yr, which is within the rising rates of buried salt diapirs (Jackson & Hudec, 2017). Salt withdrawal minibasins have a subsidence rate ranging between 0.07 and 0.13 mm/yr, whereas sea level remains constant during the simulation. It is important to notice that clinoforms are progressively rotated as they prograde through subsiding minibasins and rising diapirs (e.g. Figure 4d,e, steps III–VIII). Therefore, foreset angles and trajectories are measured before post-depositional rotation (Figure 5a,b).

Section 1 in the west is across the stable platform, which does not experience subsidence or uplift associated with salt tectonics (Figure 4b). This section shows the successive progradation of sigmoidal clinoforms with a general decrease in foreset angles as they become more fine-grained from the source (Figure 4c steps I–VIII, and Figure 5b). This part of the model is not affected by salt tectonics and the clinoforms

display a flat trajectory of the rollover point during the simulation (Figure 4c, step VIII, and Figure 5a, green line). Progradation rates decrease from 20 m/kyr close to the source to 13 m/kyr in the distal parts of the model (Figure 5c).

Middle Section 2 covers the edge of a subsiding minibasin surrounded by two stable platform areas (Figure 4b). The flat clinoforms trajectory of Section 1 (Figure 4c, step VIII and Figure 5a, green line) changes laterally into an ascending trajectory as it enters Section 2 where the rollover point moves upwards in response to basin subsidence and increase in relative sea level (Figure 4d, steps II–V and Figure 5a, blue line). It is important to note that this ascending trajectory within the minibasin allows the preservation of more coarse-grained sediments in the topsets in comparison with that in Section 1 (Figure 4c,d, step VIII). Similar to Section 1, sigmoidal clinoforms in Section 2 decrease in foreset angle as they become more distal from the source. However, clinoforms in Section 2 display relatively higher foreset angles (0.2–0.5° higher) due

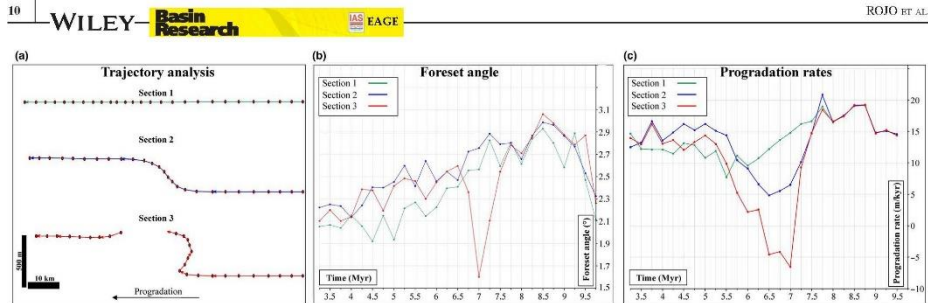


FIGURE 5 (a) Comparison between different clinoform trajectories observed in sections 1, 2, 3 of Figure 4. (b) Foreset angles along Sections 1, 2, 3. Note that Sections 2 and 3 display relatively higher foreset angles than Section 1 due to an increase in water depth induced by minibasin subsidence. The peak in Section 3 corresponds to a decrease in angle when the clinoforms approach the ascending diapir. (c) Measured progradation rates along Sections 1, 2 and 3. Note that Sections 2 and 3 show lower progradation rates than Section 1 due to the larger time required to fill the increasing accommodation space produced by minibasin subsidence. Negative values in Section 3 indicate retrogradation or landward movement of the rollover point

to minibasin subsidence and increase in water depth (Figure 5b, blue in comparison to green line). Minibasin subsidence also causes lateral variations in progradation rates, which are lower in areas with salt withdrawal due to the longer time required for the sediments to fill the increasing accommodation space (Figure 5c, blue in comparison to green line).

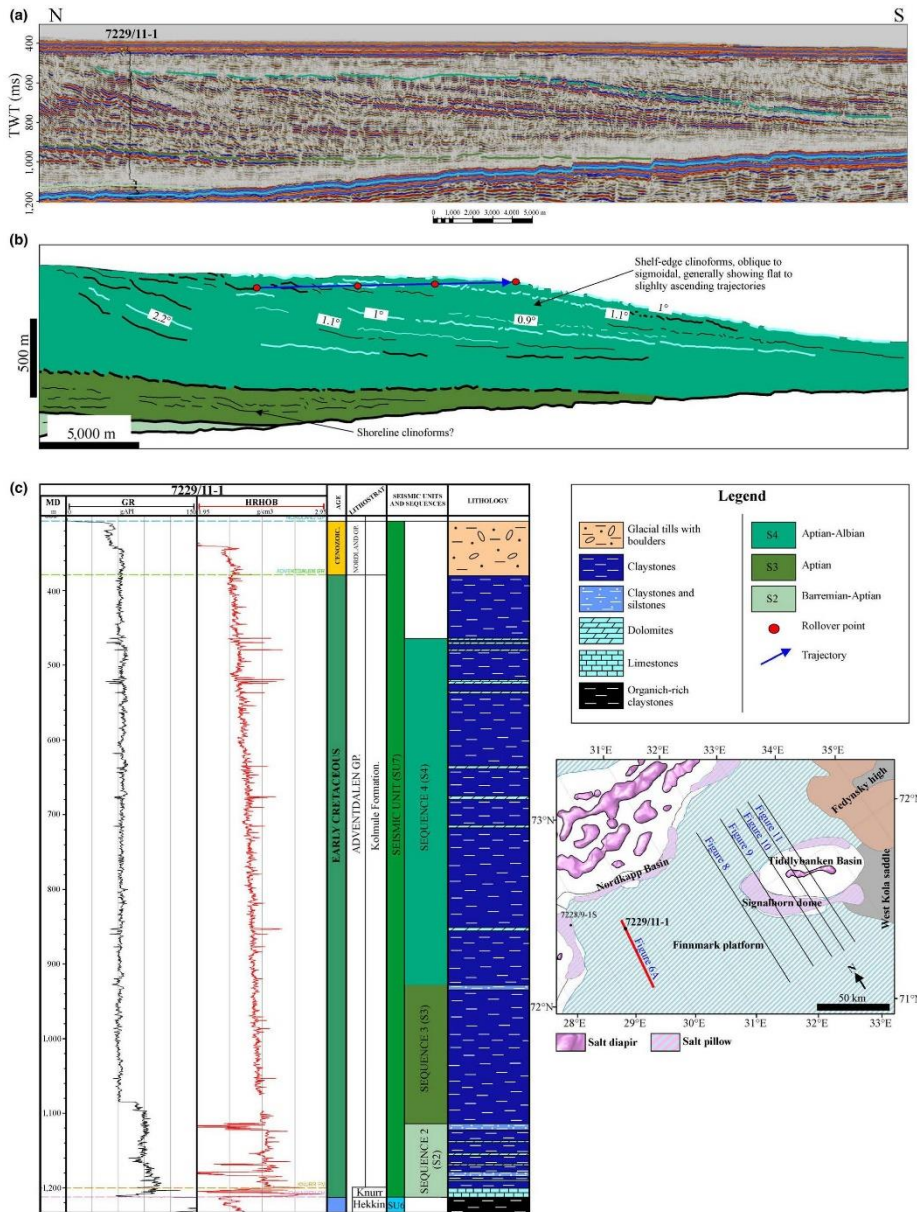
Section 3 in the east covers a rising salt wall flanked by two subsiding minibasins (Figure 4b). In this setting, relatively higher subsidence rates along the most proximal minibasin produce the retrogradation of the system and landward movement of the rollover point (Figure 4e, steps I–III, and Figure 5a, red line). Consequently, in this minibasin, distal and fine-grained sediments overlay proximal coarse grain sediments previously deposited on clinoform topsets (Figure 4e, steps I–III). As minibasin subsidence decreases with time, the system progrades again following an ascending trajectory (Figure 4e, steps III–V). Similar to Section 2, sigmoidal clinoforms prograding through the minibasin exhibit higher foreset angles than those in Section 1 due to increasing water depth by minibasin subsidence (Figure 5b, red line). As prograding clinoforms approach the rising diapir, water depth decreases and clinoforms reduce in foreset angle from 2.8 to 1.6° (Figure 5b, red low). Salt wall uplift causes a drop in relative sea level, forming a falling trajectory and producing the subaerial/marine erosion of bypassing clinoforms (Figure 4c, steps VI–V, and Figure 5a). Note that diapir-induced erosion does not allow the preservation of the topsets (Figure 4e, steps VI–VII). During steps VI–VIII, the clinoforms reach the second subsiding minibasin, resulting in a flat to

slightly ascending trajectory which finally becomes flat as the clinoforms prograde onto the stable platform (Figure 4c, steps VII–VIII and Figure 5a). In terms of progradation rates, Section 3 shows the lowest values of progradation among the three sections where negative values in the graph represent periods of retrogradation and landward movement of the rollover point (Figure 5c, red line). These differences in progradation rates in the three sections are the reason for spatial and temporal variations of the coastline and associated sedimentary environments (Figure 4a).

6 | CASE STUDY: LOWER CRETACEOUS CLINOFORMS IN THE BARENTS SEA

The case study consists of six N–S regional 2D seismic transects across the eastern part of the Norwegian Barents Sea (Figure 6, inset). The first regional transect is located in the Finnmark platform (Figure 6a), ca. at 100 km to the west of the Tiddlybanken Basin, and it intersects the well 7229/11-1. The other five regional transects cross the Finnmark platform, the Signalthorn dome and the Tiddlybanken Basin, which consists of a NW–SE salt wall surrounded by two salt withdrawal minibasins (Figure 7). In order to study the clinoforms, we have followed previous studies by Grundvåg et al., 2017; Marin et al., 2017, and as mentioned before, subdivided the Lower Cretaceous succession (SU6) into S2–S4 third-order sequences bounded by flooding surfaces (Vail,

FIGURE 6 (a) Seismic line through the Finnmark platform showing the location of the well 7229/11-1. Location of the line is shown in the inset map. (b) Depth-converted and decompacted interpretation of the Lower Cretaceous interval. Aptian clinoforms are low relief (<100 m). Aptian–Albian clinoforms are high relief (150–350 m), display low foreset angles (0.9–2.2°) and show a flat to slightly ascending trajectory (0.26°). (c) Wireline logs and cuttings from the well 7229/11-1 indicate that Lower Cretaceous clinoforms in S3 and S4 are mostly mud-prone with thin dolomite intervals



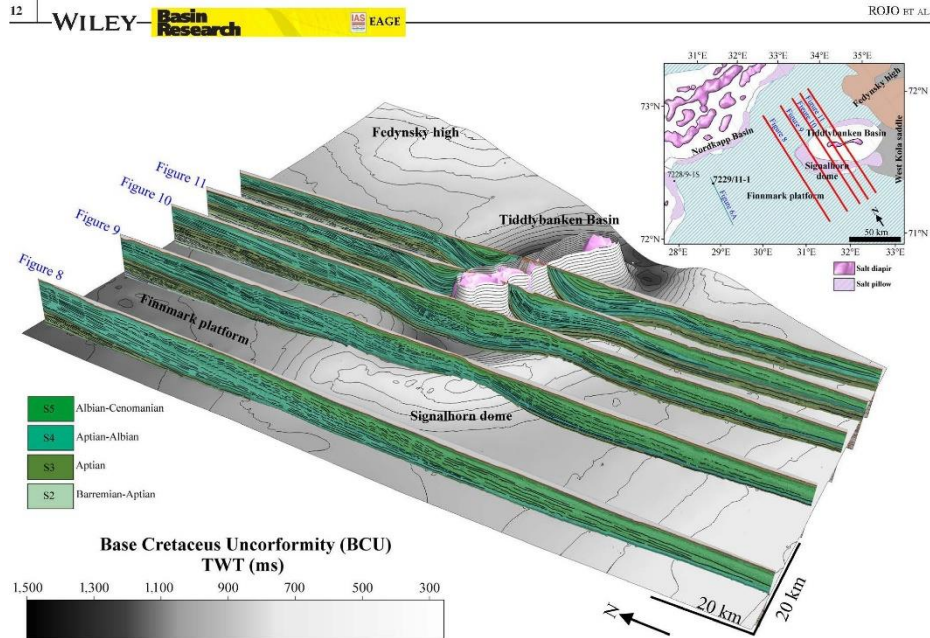


FIGURE 7 (a). Two-way travel time (TWT) surface map of the Base Cretaceous unconformity (BCU) including the location of the seismic sections analysed in this study through the Finnmark platform and Tiddlybanken Basin. Note how the clinoforms in S4 change their geometry laterally towards the Tiddlybanken Basin

Mitchum, & Thompson, 1977), which display a progradational pattern towards the SSW (Figure 7).

6.1 | Sequence 2 (S2), Barremian-Aptian and Sequence 3 (S3), Aptian

6.1.1 | Description

Based on well 7229/11-1 and previous studies by Marin et al. (2017), S2 includes part of the Kolje and Kolmule Formations of Barremian to Aptian age. S3 comprises the lower part of the Kolmule Formation of Aptian age (Figures 3b and 6c). The Gamma ray (GR) log through both sequences displays an erratic response, which is consistent with claystones, also observed in drilling cuttings (Figure 6c). In the seismic sections (Figures 8–11), S2 and S3 wedge out towards the west and south and are bounded by major flooding surfaces. In the Tiddlybanken Basin, S2 and S3 thin towards the central salt wall and onlap peridiapiric wedges (Figure 11). Internally, both sequences exhibit a progradational pattern towards the SSW consisting of low relief (<100m) and oblique clinoforms that show a descending trajectory (Figures 9–12, and Table 2).

6.1.2 | Interpretation

Based on previous studies by Marin et al. (2017), low relief and oblique clinoforms in S2 and S3 are interpreted as shoreline or deltaic clinoforms since they display a relief less than 100 m (Holland-Hansen & Hampson, 2009; Figures 9–11, and Table 2). Descending trajectories in the Finnmark platform indicate that clinoforms were deposited under decreasing relative sea level during a forced regression. Peridiapiric wedges and thinning of growth strata towards the salt wall provide evidence of salt growth during the deposition of both sequences (Figure 11).

6.2 | Sequence 4 (S4), Aptian–Albian

6.2.1 | Description

Sequence 4 consists of the Kolmule Formation of Aptian–Albian age (Marin et al., 2017). This sequence was drilled by well 7229/11-1 and is delimited at its base and top by major flooding surfaces (Figure 6). S4 thickens towards the NNW of the Finnmark platform and thins towards the SW (Figure 7). It shows large thickness variations in the Tiddlybanken Basin, increasing in thickness in salt minibasins and thinning

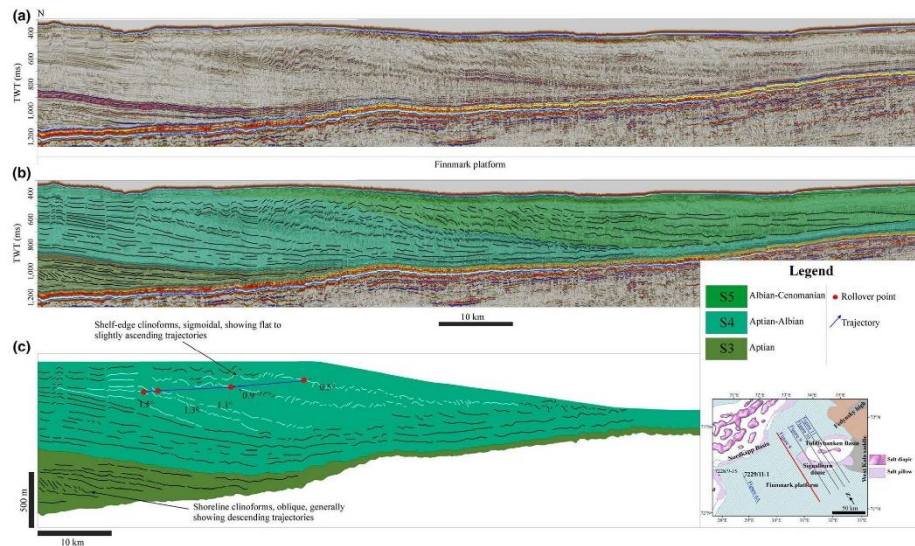


FIGURE 8 (a) Uninterpreted seismic line through the Finnmark platform. (b) Seismic interpretation of the Lower Cretaceous interval, including clinoforms. (c) Depth-conversion and decompaction of B. Clinoforms in S3 are low relief (<100 m) and display a descending trajectory. Clinoforms in S4 are high relief (150–350 m), have low foreset angles (0.5–1.5°) and display a flat to slightly ascending trajectory (0.24°). Red line in inset map shows the location of the profile

towards the salt wall (Figures 7–11). Internally, S4 consists of high relief clinoforms (>100 m). The GR log within the clinoforms displays an erratic response that corresponds to intervals of semi-continuous, low amplitude reflections in the seismic (Figure 6). Based on drilling cuttings, these intervals consist mostly of claystones. Spikes of high density and low GR are additionally encountered within this sequence and correlate with high amplitude foresets in the seismic (Figure 6). Drilling cuttings from these intervals indicate the presence of thin dolomite layers interbedded within thick packages of claystones (Figure 6). An important characteristic of the high relief clinoforms in S4 is their large variability in height (150 to 600 m), foreset angles (0.5–5.4°) and trajectories that change along the NW–SE axis of the Finnmark platform and Tiddlybanken Basin (Figures 7–11 and Table 2). In the Finnmark platform, high relief clinoforms display heights between 150 and 350 m, low foreset angles (0.5–1.5°) and a slightly ascending trajectory (0.24–0.26°; Figure 8 and Table 2). At the minibasin edge, high relief clinoforms show higher foreset angles (1.3–2.5°) and a flat to slightly descending trajectory (–0.06°; Figure 9 and Table 2). To the east, high relief clinoforms increase in height from 150 to 600 m and foreset angles vary from 0.7 to 5.4°, as they prograde from the Finnmark platform into the salt minibasins (Figures 10 and 11, and Table 2). High relief clinoforms (500–600 m) in

the minibasins are often overlapped by a wedge of low amplitude, semi-continuous to chaotic seismic reflectors (Figures 10 and 11). The clinoforms trajectory also changes, showing a flat to descending trajectory (–0.1°) at the Finnmark platform followed by a moderately ascending trajectory (0.6–1.2°) within the salt minibasins (Figures 10 and 11). It is also important to notice that the clinoforms decrease in foreset angle as they approach the central salt wall. However, their trajectories above the salt wall are not observed since S4 is eroded and truncated above this structure (Figure 11).

6.2.2 | Interpretation

High relief clinoforms in S4 are interpreted as shelf-edge clinoforms since they exhibit heights of hundreds of meters (Holland-Hansen & Hampson, 2009; Marin et al., 2017; Table 2). Ascending trajectories in the Finnmark platform were formed in response to increasing relative sea level (Figure 8). Local flat to descending trajectories followed by ascending trajectories in the Tiddlybanken Basin could be attributed to salt movement underneath, which may have induced local changes in relative sea level due to minibasin subsidence and salt growth (Figures 9–11). Thinning of growth strata towards the salt wall and thickening towards the minibasins support this hypothesis (Figures 10 and 11). Changes in foreset angle are more difficult to explain since the

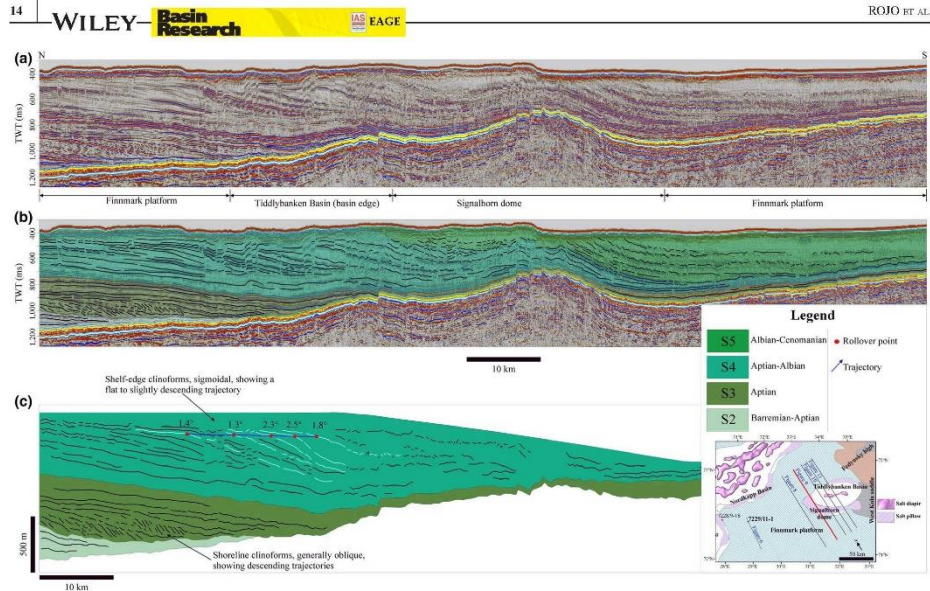


FIGURE 9 (a) Uninterpreted seismic line through the northern part of the Finnmark platform, edge of the Tiddlybanken minibasins and Signalhorn Dome. (b) Seismic interpretation of the Lower Cretaceous sequences and clinoforms. (c) Depth conversion, decompaction and unfolding of B. Clinoforms in S3 are low relief (<100 m) and display a descending trajectory. Clinoforms in S4 are high relief (150–350 m) and show foreset angles higher than in Figure 8 (1.3–2.5°). Also note that the clinoforms trajectory above the Finnmark platform is flat to slightly descending (−0.06°). Red line in inset map shows the location of the profile

variations between the Finnmark platform and the Tiddlybanken Basin can be attributed to several reasons: (a) local changes in sediment supply, (b) different grain size, (c) changes in water depth and (d) tectonic tilting caused by salt tectonics.

7 | CRETACEOUS SALT TECTONICS IN THE TIDDLYBANKEN BASIN

The interpreted seismic profiles show evidence of Lower Cretaceous deposition influenced by salt tectonics. Hence, the aim of this section was to illustrate the progressive evolution of salt structures and associated areas of uplift and subsidence during the Cretaceous based on 3D structural restoration of the study area (Figure 12).

7.1 | Barremian-Aptian (S2)

At the beginning of the Early Cretaceous, the study area consisted of a ramp-type, shallow shelf tilted towards the SSW (Grundvåg et al., 2017; Marin et al., 2017). The first arrival of prograding sediments from S2 triggered differential loading of

the salt in the Tiddlybanken Basin, causing the active growth of the salt wall and the formation of wide and shallow minibasins in the northern basin boundary (Figure 12a). During this time, the central salt wall formed a steep bathymetric high. Steep and unstable diapir flanks may have triggered the initiation of mass-transport complexes or debris flows, which explain the presence of peridiapiric wedges in S2 (Figure 11).

7.2 | Aptian (S3)

Progradational loading of Aptian sediments into the underlying salt contributed to further growth of salt structures and minibasins, creating a complex basin physiography characterized by drastic lateral variations in accommodation space (Figure 12b). On the one hand, the central salt wall continued growing, forming a smoother bathymetric high surrounded by minibasins. On the other hand, salt supply from beneath also caused the growth of a salt pillow to the west (Signalhorn dome).

7.3 | Aptian–Albian (S4)

Relatively higher sedimentation rates during the Aptian–Albian resulted in large salt withdrawal in the northern and southern

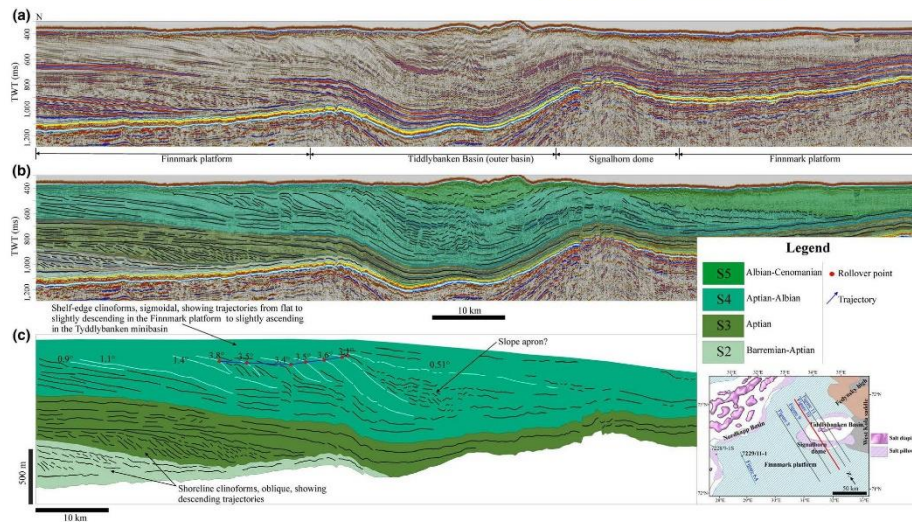


FIGURE 10 (a) Uninterpreted seismic line through the Finnmark platform and the Tiddlybanken Basin. (b) Seismic interpretation of the Lower Cretaceous sequences and clinoforms. (c) Depth conversion, decompaction and unfolding of B. Clinoforms in S3 are low relief (<100 m) and display a descending trajectory. Clinoforms in S4 are high relief (150–350 m) and show higher foreset angles as they approach the minibasin (0.9–3.6°). Note the change in clinoforms trajectory from flat to slightly descending (–0.11°) at the basin boundary, to slightly ascending (0.6°) in the minibasins. Marine onlaps may indicate the presence of slope aprons deposited in the minibasins. Red line in inset map shows the location of the profile

minibasins, which caused salt flow towards the central salt wall and southwestern salt pillow (Signalhorn dome; Figure 12c). These observations support the deposition of S4 controlled by salt tectonics, and explain the changes in geometry and trajectory of the shelf-edge clinoforms in this sequence (Figures 8–12).

7.4 | Cenozoic

Contraction and basin inversion rejuvenated the central salt wall and the Signalhorn dome. This event was followed by uplift and erosion of the Cenozoic and Upper Cretaceous strata. Today, the salt wall continues growing, forming a smooth bathymetric high at the sea floor (Figure 12d).

8 | SYN-TECTONIC DEPOSITION OF THE S4 ALBIAN CLINOFORMS: INSIGHTS FROM FORWARD STRATIGRAPHIC MODELLING

The forward stratigraphic model involves the reconstruction of the Albian sequence (S4) with the main purpose of understanding the syn-tectonic deposition of Albian clinoforms in the eastern part of the Norwegian Barents Sea (Figure 13 and Table 1, model 2). The model covers the Tiddlybanken

Basin and part of the Finnmark platform, and it is extrapolated towards the Fedinsky High and Bjarmeland platform to simulate a sediment source in the NE (Grundvåg et al., 2017; Marin et al., 2017). Based on well cuttings from well 7229/11-1 and the low foreset angles (from 0.5 to 1.5°) observed in the Finnmark platform, the model simulates mud-dominated shelf-edge clinoforms. The palaeo-seafloor and the uplift and subsidence rates are obtained from the 3D restoration (Figure 12 and Table 1, model 2). The model runs for 5 Myr (109 to 104 Ma) and each clinoform represents a time span of 0.5 Myr. Based on Grundvåg et al. (2017); Marin et al. (2017), and the observed thinning of S4 towards the SW, we assume a sediment progradation direction towards the SW. This progradation is modelled using the diffusion and steady flow equations with parameter values as described in Table 1, model 2. Progradation rates, slope angles and heights of shelf-edge clinoforms are measured in each step along the three sections (Figure 13c–e). They are all within realistic values for shelf-edge clinoforms, as discussed by Patruno and Helland-Hansen (2018).

8.1 | Finnmark platform

Similar to the seismic profiles (Figures 8–11), the model displays SW progradation of shelf-edge clinoforms in the northern

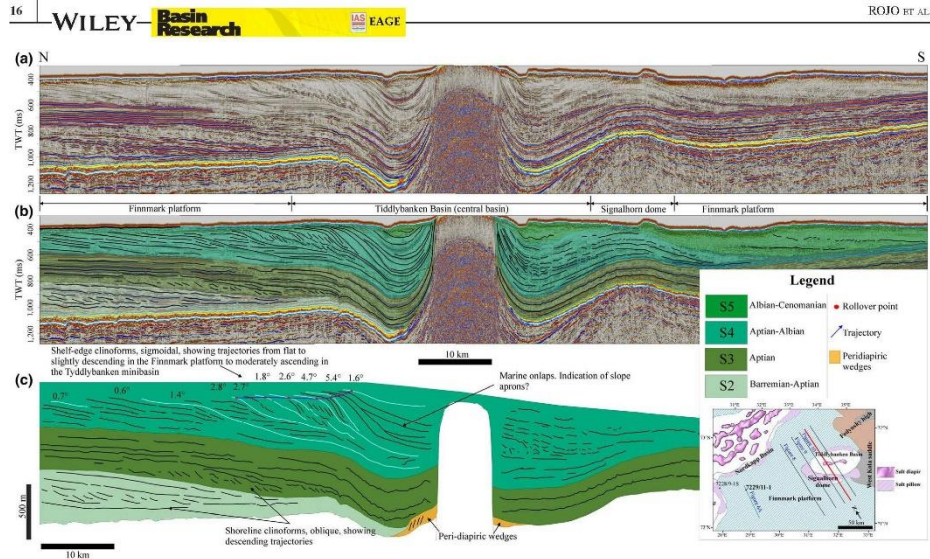


FIGURE 11 (a) Uninterpreted seismic line through the Finnmark platform and the Tiddybanken Basin. (b) Seismic interpretation of the Lower Cretaceous sequences and clinoforms. (c) Depth conversion, decompaction and unfolding of B. Clinoforms in S3 are low relief (<100m) and display a descending trajectory. Clinoforms in S4 are high relief (150-350m) and show higher foreset angles as they approach the minibasin (0.7–5.4°). Note the change in clinoforms trajectory from slightly ascending (0.11°) at the basin boundary to moderately ascending (1.15°) in the minibasins. Marine onlaps may indicate the presence of slope aprons deposited in minibasins. Red line in inset map shows the location of the profile

Finnmark platform, where clinoforms gradually increase in height ranging from 140 to 310 m, foreset angle from 0.92 to 1.6° and decrease progradation rates from 28 to 5 m/kyr (Figure 13c–e, steps I–II). These gradual changes are attributed to increasing subsidence rate from 0.01 to 0.03 mm/yr in the Finnmark platform and subsequent increment in palaeowater depth towards the SW (Table 1, model 2). An interesting feature in both the interpreted seismic (Figure 14a and d) and the model (Figure 14b and e) is the resulting flat to slightly falling clinoforms trajectory. Based on the model results (Figure 13c and d), this falling trajectory is due to the rotation of the clinoforms by the progressive subsidence and tilting of the Finnmark platform during deposition of S4. Removing this rotation results in a flat to slightly ascending clinoforms trajectory (Figure 14c and f), which is consistent with the increase in accommodation space caused by the progressive tilting of the Finnmark platform.

8.2 | Tiddybanken Basin

The model illustrates that the clinoforms prograding through the Tiddybanken minibasins experience changes in height,

foreset angle and trajectory (Figure 13c–d) with respect to the Finnmark platform (Figure 13c). This is consistent with the seismic sections (Figures 8–11). Uplift and subsidence maps indicate that the subsidence rates in the Tiddybanken minibasins range from 0.05 to 0.10 mm/yr, whereas the active growth and uplift of the diapir is approximately 0.1 mm/yr (Table 1, model 2). Higher subsidence rates by salt withdrawal, dramatically increase the water depth in the minibasins and generate steeper slopes from 1.6 to 2.8° (Figure 13c–d, steps II–V). The clinoform height is also affected by this process, increasing from 310 to 570 m in the minibasins. Increases in relative sea level associated with minibasin subsidence decreases the progradation rates from 19 to 5 m/kyr and results in moderately ascending trajectories at the edge of the minibasins (Figure 13c–d, VII), while during the same time areas in the Finnmark platform display flat trajectories and higher progradation rates (Figure 1, II–V). These lateral differences in clinoform progradation rates and trajectories among the three sections cause spatial and temporal variations of the coastline and shelf-edge (Figure 13a). Finally, as minibasins are filled with clinoform

FIGURE 12 3D structural restoration of the study area illustrating salt tectonics and associated changes in palaeobathymetry from the Cretaceous to the present. Note how prograding overburdens of S2, S3 and S4 cause the mobilization of the underlying salt which creates lateral variations in accommodation space. Red polygon in inset map shows the restored area

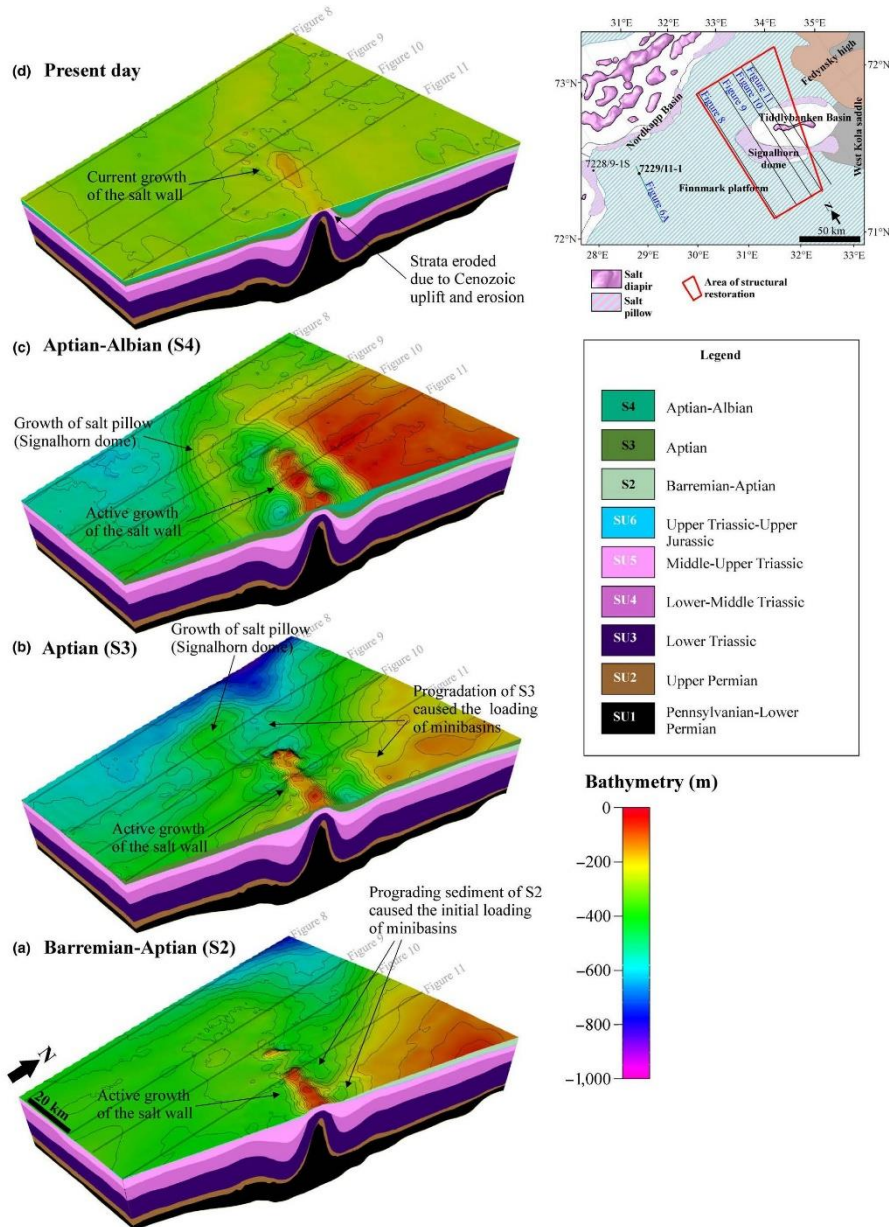
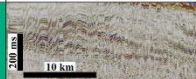
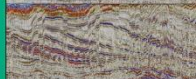
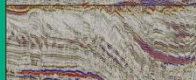
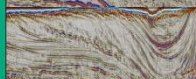
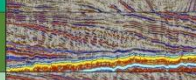



TABLE 2 Summary of the changes in height, foreset angle and trajectory of clinoforms in S2 to S4. Examples of clinoforms in S2 and S3 are in the Finnmark platform and those in S4 are in the Finnmark platform and different locations along the Tiddlybanken Basin.

	Seismic examples	Area of study	Scale	Foreset angle	Trajectory regimes	Geometry	Other observations
S4		Finnmark platform (Figs. 7 and 8)	Shelf-edge clinoforms 150-350 m	0.5-1.5°	Flat to slightly ascending (0.24- 0.26°)	High relief Low foreset angles Oblique to sigmoidal	Thin topsets and bottomsets
		Tiddlybanken Basin (basin edge) Finnmark platform and edge of the minibasin (Fig. 9)	Shelf-edge clinoforms 150-350 m	1.3-2.5°	Flat to slightly descending (-0.06°)	High relief Low to moderate foreset angles Oblique to sigmoidal	Thin topsets Thin bottomsets
		Tiddlybanken Basin (outer basin) Finnmark platform and minibasin without salt wall (Fig. 10)	Shelf-edge clinoforms 150-600 m	0.9-3.6°	First trajectory: flat to slightly descending trajectory (0.11°) Second trajectory: slightly ascending (0.6°)	High relief Low foreset angles in the Finnmark platform and high angles in the minibasin Sigmoidal	Thick topsets towards salt minibasins. Well developed bottomsets with possible presence of slope aprons
		Tiddlybanken Basin (central basin) Finnmark platform and minibasin with salt wall (Fig. 11)	Shelf-edge clinoforms 200-600 m	0.7-5.4°	First trajectory: flat to slightly descending (-0.08°) Second trajectory: moderately ascending (1.15°)	High relief Low foreset angles in the Finnmark platform and high angles in the minibasin Sigmoidal	Thick topsets towards salt minibasins. Well developed bottomset with possible presence of slope aprons
S3		Finnmark platform (Fig. 10)	Shoreline clinoforms <100 m	Not measured	Descending	Low relief High foreset angles Oblique	Topsets are not visible.
S2		Finnmark platform (Fig. 10)	Shoreline clinoforms <100 m	Not measured	Descending	Low relief High foreset angles Oblique	Topsets are not visible Presence of peridiapiric wedges adjacent to the salt wall

bottomsets, water depth and slope angle decreases (from 2.82 to 1.11°), and clinoforms bypass the salt minibasin and the diapir (Figure 13c–d, V–VII).

A comparison of the interpreted seismic and the model results shows that foreset angles in the Tiddlybanken minibasins measured in the seismic (2.6 to 5.4°, Figure 14a and d) are nearly similar to those in the model (1.70 to 4.27°, Figure 14b and e). However, modelling results illustrate that foreset angles are progressively rotated by minibasin subsidence (Figure 13c–d, steps I–VII), suggesting that the angles measured at the end of the simulation do not represent the depositional foreset angles. By removing the rotation of each clinoform in the model, foreset angles in the Tiddlybanken minibasins decrease from (1.70–4.27°) to (1.59 to 2.82°) (Figure 14b–c and 14e–f). The likely overestimation of foreset angles in seismic data is further addressed in the discussion section.

9 | DISCUSSION

9.1 | Impact of salt mobilization on prograding clinoforms and sediment partitioning

Clinoforms are often encountered in salt-related basins, acting in many cases as the main trigger of salt mobilization (Jackson & Hudec, 2017). Some examples where prograding overburdens

play an important role in salt mobilization are the Paradox Basin (e.g. Trudgill, 2011), Gulf of Mexico (e.g. Koyi, 1996), Precaspian Basin (Volozh, Talbot, & Ismail-Zadeh, 2003) and the Nordkapp Basin (Rojó et al., 2019; Rowan & Lindsø, 2017). Lack of well data, poor seismic resolution and post-depositional rotation and erosion during salt withdrawal and uplift are possibly the reasons why clinoforms within salt-bearing basins are poorly described in the literature. High seismic resolution and relatively low post-depositional deformation of the Lower Cretaceous strata in the Tiddlybanken Basin, however, allows study of the influence of halokinesis on prograding clinoforms. Based on a multidisciplinary approach including seismic interpretation, structural restoration and forward stratigraphic modelling, this work addresses the following effects of salt tectonics on prograding clinoforms and sediment partitioning:

1. **Enhancement of slope-readjustment processes.** Forward stratigraphic modelling shows that in the platform, foreset angles are constant, relatively low and are in equilibrium with sediment supply and water depth (Figures 4c, and 13c). In subsiding minibasins, progradation into increasing water depths enhances the deposition of clinoforms with relatively higher relief and foreset angle (Figures 4d–e, 4.5, 13b, and 4.5, 13c–d). Ross et al. (1994) suggest that tectonics (e.g. normal faulting) can considerably increase slope angles, affecting the equilibrium of the clinoform

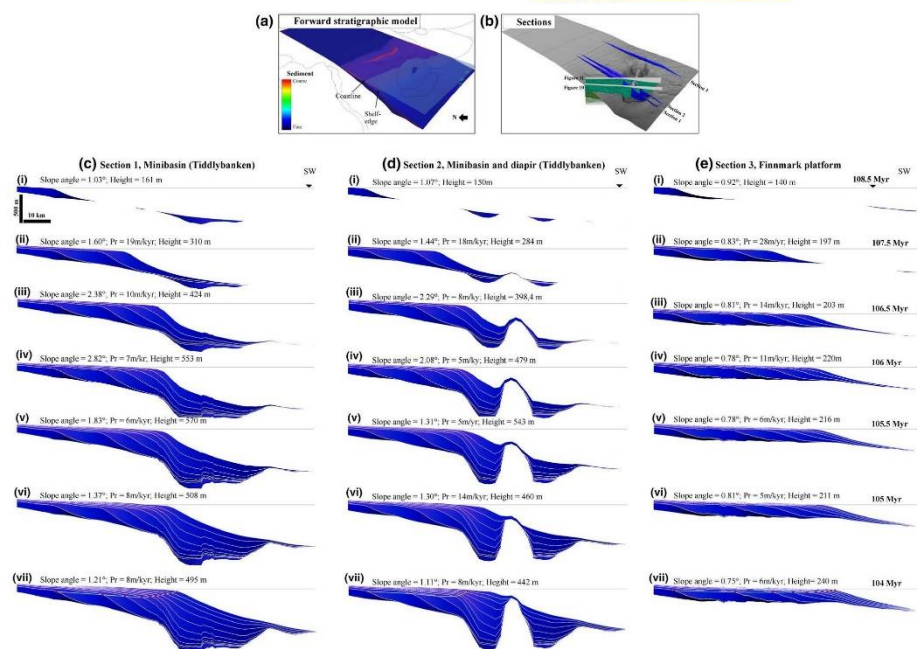


FIGURE 13 (a) Forward stratigraphic modelling of Albian clinoforms (S4), step 104 Myr. (b) Location of seismic sections and the selected model sections. The model sections are parallel to the progradation direction. (c–e) Progradation rates (Pr), heights, slope angles and clinoform trajectories in the three model sections. Differences of these parameters among the three sections are due to the local effect of salt tectonics. Constant sediment input and eustatic sea level are assumed

profile and triggering slope-readjustment processes such as slope erosion, sediment bypass by gravity flows and submarine fan-apron deposition. Evidence of these processes has been additionally documented by Kertznus and Kneller (2009) in the Ebro margin (offshore, western Mediterranean) and by Salazar et al. (2016) in the Tanaraki Basin (New Zealand). Following the same arguments, clinoforms prograding into a subsiding salt minibasin might experience slope-readjustment processes favouring the deposition of submarine fan-aprons. The occurrence of onlaps onto steep clinoforms in the Tiddlybanken minibasins most likely indicate the presence of muddy slope aprons due to the overstepping of the basinal profile by salt withdrawal (Figures 10 and 11). Additionally, the presence of smaller order clinoforms embedded in the shelf-edge clinoforms might indicate the presence of shelf-edge deltas, which could have been an additional mechanism for delivering sediments to the slope and basin floor during periods of relative sea level rise (Figures 10 and 11; Dixon et al., 2012; Jones et al., 2015; Muto & Steel, 2002; Porebski & Steel, 2006).

2. Creation of complex spatial and temporal variations in accommodation space. Lateral changes in accommodation can result in different progradation rates and shelf-edge trajectories, which will result in a complex spatial and temporal distribution of depositional environments (Jones et al., 2015). Forward modelling illustrates that subsidence in salt minibasins decreases the rates of seaward progradation, whereas other areas without salt withdrawal display higher progradation rates (Figures 4c–d, 4.5, 13c, and 4.5, 13c–e). These differences produce lateral variations in the coastline and shelf-edge along the basin (Figures 4a and 13a), resulting in a complex palaeogeography. Salt tectonics additionally contributes to the generation of different shelf-edge trajectories, which result in a wide variability of stacking patterns and depositional environments in the basin (Figures 4 and 13). Unfortunately, stacking patterns in the Tiddlybanken Basin are difficult to observe in both seismic and models due to the mud-prone character of Albian clinoforms and the lack of nearby exploration wells. Sandy clinoforms reproduced in the synthetic model (Figure 4c–e) show that moderately ascending

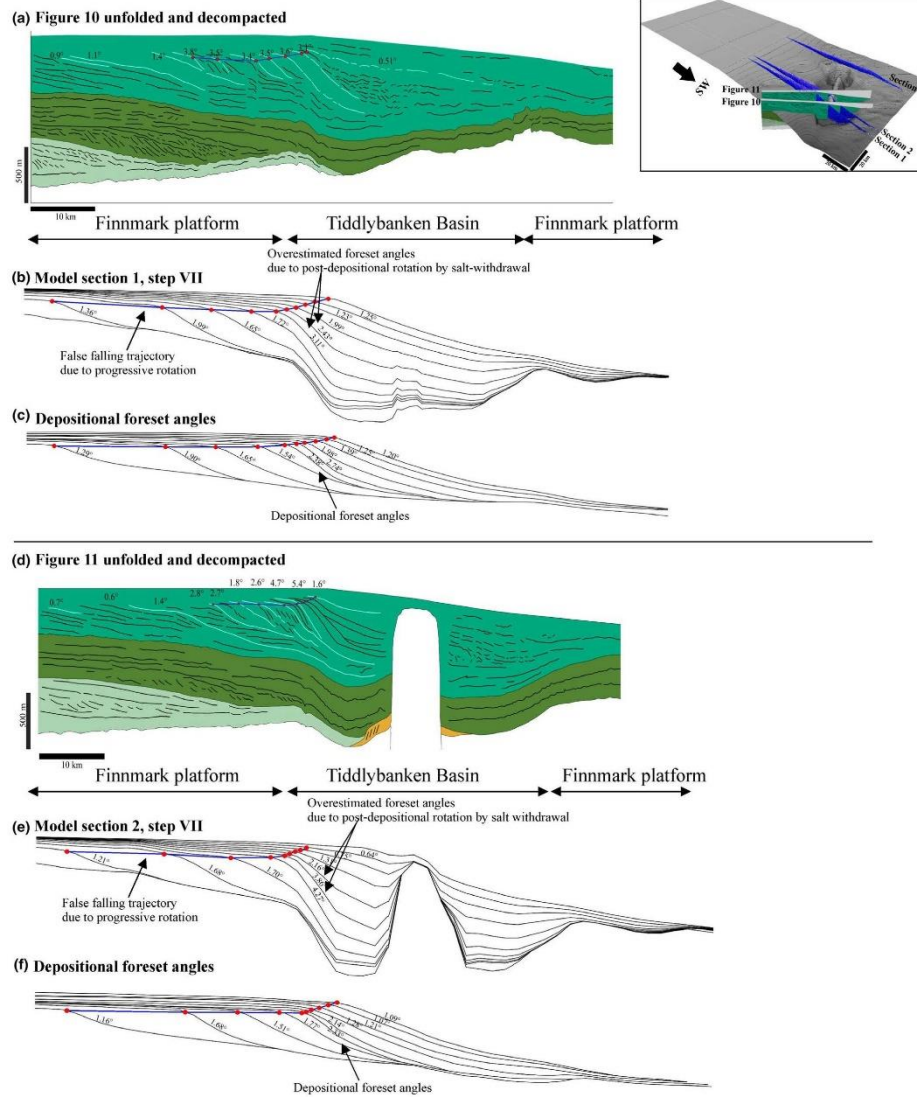


FIGURE 14 (a) Unfolded and decompacted seismic section from Figure 10 through the platform and minibasin. (b) Model Section 1 parallel to the progradation direction through the platform and minibasin. (c) Depositional palaeo-bathymetric profiles of each clinoform in model Section 2 before rotation. (d) Unfolded and decompacted seismic section from Figure 11 through the platform, salt wall and minibasins. (e) Model Section 2 parallel to the progradation direction through the platform, salt wall and minibasins. (f) Depositional palaeo-bathymetric profiles of each clinoform in model Section 3 before rotation

trajectories induced by salt withdrawal result in the vertical seaward stacking of fluviodeltaic/shelf deposits in the minibasin, which act as a temporary sediment trap of the prograding system. This agrees with analogue modelling results by Kopp and Kim (2015); Liang, Kim, and Passalacqua (2016) where tectonic tilting causes channel steering and produces stacked conformable sequences of delta lobes on the subsidence side. Nevertheless, relatively higher subsidence along the minibasin might also result in aggradational or even backstepped stacking of fluviodeltaic/shelf deposits (Figure 4e). Finally, flat to slightly ascending trajectories and poor vertical stacking of fluviodeltaic/shelf deposits characterize the surrounding platforms (Figure 4c). This lateral variability in trajectories and associated stacking patterns are consistent with the observations of Rojo and Escalona (2018) in the Nordkapp Basin, where shelf and fluviodeltaic depositional environments prograde and retrograde due to lateral variations in accommodation space during the Triassic. Diapir/pillow-induced falling trajectories were also observed in the forward models (Figures 4e, and 13d). However, its identification in salt-related basins might be an issue since clinoforms could be eroded by post-depositional diapir growth. Upper Jurassic deep-water sediments deposited during a possible diapir-induced force regression have been documented by Pena dos Reis, Pimentel, Fainstein, Reis, and Rasmussen (2017); Pimentel and Pena Dos Reis (2018) in the Lusitanian Basin (Portugal), where outcrops show spectacular incised turbiditic channels occurring at one side of a large salt wall. Based on the forward models (Figures 4e, and 13d), diapir-induced force regressions may be an important process of sediment delivery to the slope and basin floor in salt-bearing basins.

9.2 | The importance of forward models in the study of clinoforms in the areas of complex tectonics

Seismic studies of ancient clinoforms are well-documented in the literature (Klausen et al., 2018; Marin et al., 2017; Patruno et al., 2015; Patruno & Helland-Hansen, 2018), and are commonly used to identify the changes in relative sea level as well as depositional environments. The conventional methodology in clinoform analysis consists on flattening the sequence to a regional datum (e.g. topset or bottomset of maximum flooding surface), with the main purpose of making the clinoform topsets horizontal. Clinoforms are then backstripped or decompacted incorporating isostatic compensation. The resultant geometry is a good approximation of the clinoform palaeobathymetric profile at the time of deposition (Klausen & Helland-Hansen, 2018; Patruno et al., 2015). This methodology provides good results for clinoforms deposited in areas with low and

relatively constant subsidence rates such as epicontinental seas, which have later undergone post-depositional tilting or faulting (Klausen et al., 2018, 2015; Marin et al., 2017). However, in tectonically active areas (e.g. salt-related basins) where local bathymetry/topography may be modified during sedimentation, this methodology may lead to interpretation pitfalls in clinoform geometries and trajectories. One of these misinterpretations may arise when near-horizontal topsets progressively rotate to steeper angles after their deposition. For example, topsets are nearly horizontal at the top of S4 in the interpreted seismic (Figure 14a,d) and forward model (Figure 14b,e), whereas older topsets still preserve the rotation caused by the progressive tilting of the Finnmark platform. This progressive tilting may result in the wrong interpretation of forced regressions in actively subsiding basins (Fig 14b, e). A good indicator of this pitfall is the presence of well-preserved topsets, which contradict the interpreted falling trajectories (Figure 14a–e). Another misinterpretation may arise from post-depositional rotation of clinoforms by salt withdrawal, faulting or flexure, which might lead to the overestimation of foreset angles. In this study, foreset angles increase from 0.8° in the Finnmark platform to 5.4° in the Tiddlybanken minibasins (Figure 14a,d). These high foreset angles in salt minibasins could suggest the presence of sandy-prone clinoforms. However, well data from the Finnmark platform show that the clinoforms are mud-prone. Modelling results demonstrate that these measurements do not represent the depositional foreset angles and therefore are likely overestimated (Figures 13c–d, and 13,14a–f). The model also illustrates that part of this steepening, ca. 0.8 to 2.8° (Figure 13c,d, steps I–V), is due to the increasing water depth. The remaining dip change from ca. 2.8 to 5.4° (Figure 13c,d, steps V–VII) corresponds to post-depositional rotation due to withdrawal of the underlying salt. These arguments highlight the importance of using forward stratigraphic models coupled with tectonics to study clinoforms in salt-bearing basins and other tectonically active areas. The isolated use of conventional methodologies in clinoform analysis in these complex areas might lead to potential interpretation pitfalls such as wrong interpretation of trajectories and overestimation of foreset angles, which can have negative consequences for hydrocarbon exploration models.

9.3 | Model limitations and future work

Although the results clearly show the impact of salt tectonics on the geometry and trajectory of clinoforms, our simulations are based on the assumption of tectonically driven stratigraphic evolution, where uplift/subsidence rates from the structural restoration are given as input, and they do not change depending on how the sediment loading is distributed over the basin. Sediment loading is incorporated to

the restorations via decompaction and flexural deformation, but it does not dynamically reproduce the loading caused by each single clinoform. Analogue models by Piliouras et al. (2014); Kopriva and Kim (2015) and numerical models by Cohen and Hardy (1996) demonstrate that factors such as sedimentation rates, initial thickness of salt and salt viscosity strongly influence the width and subsidence rate of minibasins, which in turn affect the minibasin topography and bathymetry. Therefore, future work is oriented towards analysing bidirectional salt–sediment interaction via analogue modelling or numerical modelling, to further investigate salt-controlled sedimentary architectures in salt-bearing basins.

10 | CONCLUSIONS

High-resolution Albian clinoforms together with relatively simple salt-related deformation make the Tiddlybanker Basin an excellent analogue to study the impact of salt mobilization on prograding overburdens. Based on a multidisciplinary approach including seismic interpretation, 3D structural restoration and forward stratigraphic modelling, we conclude that salt mobilization affects prograding clinoforms in the following ways:

1. Salt withdrawal/uplift causes lateral variations in the coastline and shelf-break, resulting in a complex palaeogeography.
2. Salt evacuation increases slope angles, affecting the equilibrium of the clinoform profile and triggering slope-readjustment processes such as slope erosion, sediment bypass by gravity flows and submarine fan-apron deposition.
3. Lateral and temporal variations in accommodation space caused by salt tectonics may result in different clinoform trajectories and stacking patterns along the salt-bearing basin.
4. Post-depositional rotation of clinoforms in areas of salt tectonics and other tectonically active basins might lead to interpretation pitfalls such as the wrong interpretation of trajectories and overestimation of foreset angles. These pitfalls can negatively affect reservoir prediction in prograding clinoforms.

ACKNOWLEDGEMENTS

We acknowledge the Norwegian Petroleum Directorate for giving us access to the DISKOS database and for kindly providing the NPD-BA-11 2D seismic survey in the eastern Norwegian Barents Sea. Dora Marin thanks Locra and Julocra for supporting her research. We acknowledge Sergio Courtade, Per Salomonsen and Jan Tveiten at Schlumberger for their support and technical advice with GPM. We are

grateful to the reviewers William Helland-Hansen, Wonsuck Kim and Joshua F. Dixon, and the editor Ronald Steel, whose constructive comments and suggestions improved the manuscript. Thanks to Schlumberger and Midland Valley for providing academic licenses of their softwares Petrel-GPM and Move respectively.

DATA AVAILABILITY STATEMENT

Data sharing is not applicable to this article as no new data were created or analysed in this study.

ORCID

Luís Alberto Rojo  <https://orcid.org/0000-0002-7134-6071>

REFERENCES

- Adams, E. W., & Schlager, W. (2000). Basic Types of Submarine Slope Curvature. *Journal of Sedimentary Research*, 70, 814–828. <https://doi.org/10.1306/2dc4093a-0e47-11d7-8643000102c1865d>
- Albertz, M., & Ings, S. J. (2012). Some consequences of mechanical stratification in basin-scale numerical models of passive-margin salt tectonics: Geological Society, London, *Special Publications*, 363, 303–330. <https://doi.org/10.1144/sp363.14>
- Anderson, J. B. (2005). Diachronous development of late Quaternary shelf-margin deltas in the northwestern Gulf of Mexico: implications for sequence stratigraphy and deep-water reservoir occurrence. In L. Giosan, & J. P. Bhattacharya (eds.), *River Deltas—Concepts, Models, and Examples* (Vol. 83 pp. 257–276). SEPM Special Publication. <https://doi.org/10.2110/pec.05.83.0257>
- Anderson, J. B., Wallace, D. J., Simms, A. R., Rodriguez, A. B., Weight, R. W. R., & Taha, Z. P. (2016). Recycling sediments between source and sink during a eustatic cycle: Systems of late Quaternary northwestern Gulf of Mexico Basin. *Earth-Science Reviews*, 153, 111–138. <https://doi.org/10.1016/j.earscirev.2015.10.014>
- Anderson, P. B., Chidsey, J. T. C., Ryer, T. A., Adams, R. D., & McClure, K. (2004). Geologic Framework, Facies, Paleogeography, and Reservoir Analogs of the Ferron Sandstone in the Ivie Creek Area, East-Central Utah. In J. T. C. Chidsey, R. D. Adams, & T. H. Morris (Eds.), *Regional to Wellbore Analog for Fluvial-Deltaic Reservoir Modeling: The Ferron Sandstone of Utah*. American Association of Petroleum Geologists.
- Anell, I., Braathen, A., & Olaussen, S. (2014). The Triassic-Early Jurassic of the northern Barents Shelf: A regional understanding of the Longyearbyen CO 2 reservoir. *Norwegian Journal of Geology*, 94, 83–98.
- Baig, I., Faleide, J. L., Jahren, J., & Mondol, N. H. (2016). Cenozoic exhumation on the southwestern Barents Shelf: Estimates and uncertainties constrained from compaction and thermal maturity analyses. *Marine and Petroleum Geology*, 73, 105–130. <https://doi.org/10.1016/j.marpetgeo.2016.02.024>
- Banham, S. G., & Mountney, N. P. (2013). Controls on fluvial sedimentary architecture and sediment-fill state in salt-walled minibasins: Triassic Moenkopi Formation, Salt Anticline Region, SE Utah, USA. *Basin Research*, 25, 709–737. <https://doi.org/10.1111/bre.12022>

- Bugge, T., Mangerud, G., Elvebakk, G., Mork, A., Nilsson, I., Fanavoll, S., & Vigran, J. (1995). Upper Paleozoic succession on the Finnmark platform, Barents Sea. *Norwegian Journal of Geology*, *75*, 3–30.
- Bullimore, S., Henriksen, S., Liestøl, F. M., & Helland-Hansen, W. (2005). Clinoform stacking patterns, shelf-edge trajectories and facies associations in Tertiary coastal deltas, offshore Norway: Implications for the prediction of lithology in prograding systems. *Norwegian Journal of Geology/Norsk Geologisk Forening*, *85*, 169–187.
- Carvajal, C., Steel, R., & Petter, A. (2009). Sediment supply: The main driver of shelf-margin growth. *Earth-Science Reviews*, *96*, 221–248. <https://doi.org/10.1016/j.earscirev.2009.06.008>
- Carvajal, R. C., & Steel, R. J. (2006). Thick turbidite successions from supply-dominated shelves during sea-level highstand. *Geology*, *34*, 665–668. <https://doi.org/10.1130/G22505.1>
- Catneanu, O., Galloay, W. E., Kendall, C. G. S. C., Miall, A. D., Posamentier, H. W., Strasser, A., & Tucker, M. E. (2011). Sequence Stratigraphy: Methodology and Nomenclature. *Newsletters on Stratigraphy*, *44*, 173–245. <https://doi.org/10.1127/0078-0421/2011/0011>
- Clark, S. A., Gjørstad-Clark, E., Faleide, J. I., Schmid, D., Hartz, E. H., & Fjeldskaar, W. (2014). Southwest Barents Sea rift basin evolution: Comparing results from backstripping and time-forward modelling. *Basin Research*, *26*, 550–566. <https://doi.org/10.1111/bre.12039>
- Cohen, H. A., & Hardy, S. (1996). Numerical modelling of stratal architectures resulting from differential loading of a mobile substrate: Geological Society, London, *Special Publications*, *100*, 265–273. <https://doi.org/10.1144/gsl.sp.1996.100.01.17>
- Coleman, J. M., & Wright, L. (1975). In M. L. Broussard (Ed.), *Modern river deltas: variability and processes of sand bodies*, in (pp. 99–149). Deltas: Models for Exploration: Houston Geological Society.
- Dixon, J., Steel, R., & Olariu, C. (2012). Shelf-edge delta regime as a predictor of deep-water deposition. *Journal of Sedimentary Research*, *82*, 681–687. <https://doi.org/10.2110/jsr.2012.59>
- Dreyer, T., Whitaker, M., Dexter, J., Flesche, H., & Larsen, E. (2005). From spit system to tide-dominated delta: Integrated reservoir model of the Upper Jurassic Sognefjord Formation on the Troll West Field. *Geological Society, London, Petroleum Geology Conference, Series*, *6*, 423–448. <https://doi.org/10.1144/0060423>
- Eide, C. H., Klausen, T. G., Katkov, D., Suslova, A. A., & Helland-Hansen, W. (2017). Linking an Early Triassic delta to antecedent topography: Source-to-sink study of the southwestern Barents Sea margin. *GSA Bulletin*, *130*(1–2), 263–283. <https://doi.org/10.1130/B31639.1>
- Faleide, J. I., Tsikalas, F., Breivik, A. J., Mjelde, R., Ritzmann, O., Engen, O., ... Eldholm, O. (2008). Structure and evolution of the continental margin off Norway and the Barents Sea. *Episodes*, *31*, 82–91. <https://doi.org/10.18814/epiiugs/2008/v31i1/012>
- Faleide, J. I., Vågnes, E., & Gudlaugsson, S. T. (1993). Late Mesozoic–Cenozoic evolution of the south-western Barents Sea in a regional rift-shear tectonic setting. *Marine and Petroleum Geology*, *10*, 186–214. [https://doi.org/10.1016/0264-8172\(93\)90104-Z](https://doi.org/10.1016/0264-8172(93)90104-Z)
- Flemings, P. B., & Grotzinger, J. P. (1996). STRATA: Freeware for analyzing classic stratigraphic problems. *GSA Today*, *6*, 1–7.
- Gac, S., Klitzke, P., Minakov, A., Faleide, J. I., & Scheck-Wenderoth, M. (2016). Lithospheric strength and elastic thickness of the Barents Sea and Kara Sea region. *Tectonophysics*, *691*, 120–132. <https://doi.org/10.1016/j.tecto.2016.04.028>
- Ge, H., Jackson, M. P., & Vendeville, B. C. (1997). Kinematics and dynamics of salt tectonics driven by progradation. *AAPG Bulletin*, *81*, 398–423.
- Gernigon, L., Brønner, M., Dumais, M.-A., Grädmann, S., Grønlie, A., Nasuti, A., & Roberts, D. (2018). Basement inheritance and salt structures in the SE Barents Sea: Insights from new potential field data. *Journal of Geodynamics*, *119*, 82–106. <https://doi.org/10.1016/j.jog.2018.03.008>
- Gernigon, L., Brønner, M., Roberts, D., Olesen, O., Nasuti, A., & Yamasaki, T. (2014). Crustal and basin evolution of the southwestern Barents Sea: From Caledonian orogeny to continental breakup. *Tectonics*, *33*, 347–373. <https://doi.org/10.1002/2013TC003439>
- Gjørstad-Clark, E., Faleide, J. I., Lundschie, B. A., & Nystuen, J. P. (2010). Triassic seismic sequence stratigraphy and paleogeography of the western Barents Sea area. *Marine and Petroleum Geology*, *27*, 1448–1475. <https://doi.org/10.1016/j.marpetgeo.2010.02.008>
- Grundvåg, S. A., Marin, D., Kairanov, B., Śliwińska, K. K., Nøhr-Hansen, H., Jelby, M. E., ... Olausen, S. (2017). The Lower Cretaceous succession of the northwestern Barents Shelf: Onshore and offshore correlations. *Marine and Petroleum Geology*, *86*, 834–857. <https://doi.org/10.1016/j.marpetgeo.2017.06.036>
- Heiberg, V. (2018). The regional Cretaceous development of the southeastern part of the Norwegian Barents Sea: from seismic interpretation. Master thesis, University of Tromsø, 116 p.
- Helland-Hansen, W., & Gjelberg, J. G. (1994). Conceptual basis and variability in sequence stratigraphy: A different perspective. *Sedimentary Geology*, *92*, 31–52. [https://doi.org/10.1016/0037-0738\(94\)90053-1](https://doi.org/10.1016/0037-0738(94)90053-1)
- Helland-Hansen, W., & Hampson, G. J. (2009). Trajectory analysis: Concepts and applications. *Basin Research*, *21*, 454–483. <https://doi.org/10.1111/j.1365-2117.2009.00425.x>
- Henriksen, E., Bjørnseth, H., Hals, T., Heide, T., Kiryukhina, T., Kløvjan, O., ... Sollid, K. (2011a). Uplift and erosion of the greater Barents Sea: impact on prospectivity and petroleum systems. In A. M. Spencer, A. F. Embry, D. L. Gautier, A. V. Stoupakova, & K. Sørensen (Eds.), *Arctic Petroleum Geology* (Vol. 35 pp. 271–281). London, Memoirs: Geological Society. <https://doi.org/10.1144/M35.17>
- Henriksen, E., Ryseth, A., Larssen, G., Heide, T., Rønning, K., Sollid, K., & Stoupakova, A. (2011). Tectonostratigraphy of the greater Barents Sea: implications for petroleum systems. In A. M. Spencer, A. F. Embry, D. L. Gautier, A. V. Stoupakova, & K. Sørensen (Eds.), *Arctic Petroleum Geology* (pp. 163–195). London, Memoirs: Geological Society. <https://doi.org/10.1144/M35.10>
- Hernández-Molina, F. J., Fernández-Salas, L. M., Lobo, F., Somoza, L., Díaz-del-Río, V., & Alveirinho Dias, J. M. (2000). The infralittoral prograding wedge: A new large-scale progradational sedimentary body in shallow marine environments. *Geo-Marine Letters*, *20*, 109–117. <https://doi.org/10.1007/s003670000040>
- Houseknecht, D. W., Bird, K. J., & Schenk, C. J. (2009). Seismic analysis of clinoform depositional sequences and shelf-margin trajectories in Lower Cretaceous (Albian) strata, Alaska North Slope. *Basin Research*, *21*, 644–654. <https://doi.org/10.1111/j.1365-2117.2008.00392.x>
- Jackson, C. A. L., Jackson, M. P. A., & Hudec, M. R. (2015). Understanding the kinematics of salt-bearing passive margins: A critical test of competing hypotheses for the origin of the Albian Gap, Santos Basin, Offshore Brazil. *GSA Bulletin*, *127*, 1730–1751. <https://doi.org/10.1130/B31290.1>

- Jackson, M. P., & Hudec, M. R. (2017). *Salt Tectonics: Principles and Practice* (p. 498). Cambridge University Press.
- Johannessen, E. P., & Steel, R. J. (2005). Shelf-margin clinoforms and prediction of deepwater sands. *Basin Research*, 17, 521–550. <https://doi.org/10.1111/j.1365-2117.2005.00278.x>
- Jones, G. E. D., Hodgson, D. M., & Flint, S. S. (2015). Lateral variability in clinoform trajectory, process regime, and sediment dispersal patterns beyond the shelf-edge rollover in exhumed basin margin-scale clinoforms. *Basin Research*, 27, 657–680. <https://doi.org/10.1111/bre.12092>
- Kertzus, V., & Kneller, B. (2009). Clinoform quantification for assessing the effects of external forcing on continental margin development. *Basin Research*, 21, 738–758. <https://doi.org/10.1111/j.1365-2117.2009.00411.x>
- Klausen, T., Aas, T. J., Haug, E. C., Behzad, A., Snorre, O., & Domenico, C. (2018). Clinoform development and topset evolution in a mud-rich delta – the Middle Triassic Kobbe Formation, Norwegian Barents Sea. *Sedimentology*, 65, 1132–1169. <https://doi.org/10.1111/sed.12417>
- Klausen, T., & Helland-Hansen, W. (2018). Methods For Restoring and Describing Ancient Clinoform Surfaces. *Journal of Sedimentary Research*, 88(2), 241–259. <https://doi.org/10.2110/jsr.2018.8>
- Klausen, T. G., Ryseth, A. E., Helland-Hansen, W., Gawthorpe, R., & Laursen, I. (2015). Regional development and sequence stratigraphy of the Middle to Late Triassic Snadd Formation, Norwegian Barents Sea. *Marine and Petroleum Geology*, 62, 102–122. <https://doi.org/10.1016/j.marpetgeo.2015.02.004>
- Kopp, J., & Kim, W. (2015). The effect of lateral tectonic tilting on fluvio-deltaic surficial and stratal asymmetries: Experiment and theory. *Basin Research*, 27, 517–530. <https://doi.org/10.1111/bre.12086>
- Kopriva, B. T., & Kim, W. (2015). Coevolution of minibasin subsidence and sedimentation: Experiments. *Journal of Sedimentary Research*, 85, 254–264. <https://doi.org/10.2110/jsr.2015.24>
- Kostic, S., Parker, G., & Marr, J. G. (2002). Role of turbidity currents in setting the foreset slope of clinoforms prograding into standing fresh water. *Journal of Sedimentary Research*, 72, 353–362. <https://doi.org/10.1306/081501720353>
- Koyi, H. (1996). Salt flow by aggrading and prograding overburdens. *Geological Society, London, Special Publications*, 100(1), 243–258. <https://doi.org/10.1144/GSL.SP.1996.100.01.15>
- Koyi, H., Talbot, C. J., & Tørudbakken, B. O. (1995). Salt tectonics in the Northeastern Nordkapp basin, Southwestern Barents sea. In M. P. A. Jackson, D. G. Roberts, & S. Snelson (Eds.), *Salt Tectonics: A Global Perspective* (Vol. 65, pp. 437–447). AAPG Memoir.
- Larsen, G. B., Elvebakk, G., Henriksen, L. B., Kristensen, S. E., Nilsson, L., Samuelsen, T. J., ... Stemmerik, D. (2005). Worsley Upper Palaeozoic lithostratigraphy of the southern part of the Norwegian Barents Sea Norges geologiske undersøkelse Bulletin, pp. 3–45.
- Larsen, G. B., Elvebakk, G., Henriksen, L. B., Kristensen, S. E., Nilsson, L., Samuelsen, T. J., Svåná, L., ... Worsley, D. (2002). Worsley upper palaeozoic lithostratigraphy of the southern part of the norwegian barents sea. *Norges geologiske undersøkelse Bulletin*, 444, 3–45.
- Liang, M., Kim, W., & Passalacqua, P. (2016). How much subsidence is enough to change the morphology of river deltas? *Geophysical Research Letters*, 43, 10266–10276. <https://doi.org/10.1002/2016gl.1070519>
- LoCra, (2018). Lower Cretaceous clastic wedges, an under-explored play in the Arctic. A multi-university collaboration. University of Stavanger and University Centre in Svalbard (UNIS). Internal report.
- Lundschie, B. A., Høy, T., & Mørk, A. (2014). Triassic hydrocarbon potential in the Northern Barents Sea; integrating Svalbard and stratigraphic core data. *Norwegian Petroleum Directorate Bulletin*, 11, 3–20.
- Marin, D., Escalona, A., Nøhr-Hansen, H., Śliwińska Kasia, K., & Mordasova, A. (2017). Sequence stratigraphy and lateral variability of Lower Cretaceous clinoforms in the SW Barents Sea. *AAPG Bulletin*, 101, 1487–1517. <https://doi.org/10.1306/10241616010>
- Mattingsdal, R., Høy, T., Simonstad, E., & Brekke, H. (2015). An updated map of structural elements in the southern Barents Sea, 31st Geological Winter Meeting, 12–14 January 2015, Stavanger.
- Mitchum, R. M., Vail, P. R., & Sangree, J. B. (1977). Stratigraphic interpretation of seismic reflection patterns in depositional sequences. In C. E. Payton (Ed.), *Seismic Stratigraphy—Applications to Hydrocarbon Exploration* (pp. 117–123). AAPG Memoir.
- Muto, T., & Steel, R. J. (2002). In defense of shelf-edge delta development during falling and lowstand of relative sea level. *The Journal of Geology*, 110, 421–436. <https://doi.org/10.1086/340631>
- Nemec, W. (2009). Aspects of sediment movement on steep delta slopes. In A. Colella, & D. B. Prior (Eds.), *Coarse-grained deltas*, (Vol. 27, pp. 29). The International Association of Sedimentologists. <https://doi.org/10.1002/9781444303858.ch3>
- O'Grady, D. B., Syvitski, J. P., Pratson, L. F., & Sarg, J. (2000). Categorizing the morphologic variability of siliciclastic passive continental margins. *Geology*, 28, 207–210. [https://doi.org/10.1130/00091-7613\(2000\)028<0207:CTMVOS>2.3.CO;2](https://doi.org/10.1130/00091-7613(2000)028<0207:CTMVOS>2.3.CO;2)
- Ohm, S. E., Karlsen, D. A., & Austin, T. (2008). Geochemically driven exploration models in uplifted areas: Examples from the Norwegian Barents Sea. *AAPG Bulletin*, 92, 1191–1223. <https://doi.org/10.1306/06180808028>
- Orton, G. J., & Reading, H. G. (1993). Variability of deltaic processes in terms of sediment supply, with particular emphasis on grain size. *Sedimentology*, 40, 475–512. <https://doi.org/10.1111/j.1365-3091.1993.tb01347.x>
- Patruno, S., Hampson, G. J., Jackson, C. A. L., & Whipp, P. S. (2015). Quantitative progradation dynamics and stratigraphic architecture of ancient shallow-marine clinoform sets: A new method and its application to the Upper Jurassic Sognefjord Formation, Troll Field, Offshore. *Norway: Basin Research*, 27, 412–452. <https://doi.org/10.1111/bre.12081>
- Patruno, S., & Helland-Hansen, W. (2018). Clinoforms and clinoform systems: Review and dynamic classification scheme for shorelines, subaqueous deltas, shelf edges and continental margins. *Earth-Science Reviews*, 185, 202–233. <https://doi.org/10.1016/j.earscirev.2018.05.016>
- Pellegrini, C., Maselli, V., Gamberi, F., Asioli, A., Bohacs, K., Drexler, T. M., & Trincardi, F. (2017). How to make a 350-m-thick lowstand systems tract in 17,000 years: The Late Pleistocene Po River (Italy) lowstand wedge. *Geology*, 45, 327–330. <https://doi.org/10.1130/G38848.1>
- Pena dos Reis, R., Pimentel, N., Fainstein, R., Reis, M., & Rasmussen, B. (2017). Chapter 14 - Influence of Salt Diapirism on the Basin Architecture and Hydrocarbon Prospects of the Western Iberian Margin. In J. I. Soto, J. F. Finch, & G. Tari (Eds.), *Permo-Triassic Salt Provinces of Europe, North Africa and the Atlantic Margins* (pp. 313–329). Elsevier.
- Piliouras, A., Kim, W., Kocurek, G. A., Mohrig, D., & Kopp, J. (2014). Sand on salt: Controls on dune subsidence and determining salt substrate thickness. *Lithosphere*, 6(3), 195–199. <https://doi.org/10.1130/L323.1>

- Pimentel, N., & Pena Dos Reis, R. (2018). Salt tectonics at the Lusitanian Basin, Field-Trip Guide, Global Analogues for the Atlantic Margin, AAPG European Regional Conference, Lisbon (Portugal).
- Pirmez, C., Pratson, L. F., & Steckler, M. S. (1998). Clinoform development by advection-diffusion of suspended sediment: Modeling and comparison to natural systems. *Journal of Geophysical Research: Solid Earth*, *103*, 24141–24157. <https://doi.org/10.1029/98JB01516>
- Porębski, S. J., & Steel, R. J. (2003). Shelf-margin deltas: Their stratigraphic significance and relation to deepwater sands. *Earth-Science Reviews*, *62*, 283–326. [https://doi.org/10.1016/S0012-8252\(02\)00161-7](https://doi.org/10.1016/S0012-8252(02)00161-7)
- Porębski, S. J., & Steel, R. J. (2006). Deltas and sea-level change. *Journal of Sedimentary Research*, *76*, 390–403. <https://doi.org/10.2110/jsr.2006.034>
- Poyatos-Moré, M., Jones, G. D., Brunt, R. L., Hodgson, D. M., Wild, R. J., & Flint, S. S. (2016). Mud-dominated basin-margin progradation: processes and implications. *Journal of Sedimentary Research*, *86*, 863–878. <https://doi.org/10.2110/jsr.2016.57>
- Pratson, L. F., Nittrouer, C. A., Wiberg, P. L., Steckler, M. S., Swenson, J. B., Cacchione, D. A., ... Gerber, T. P. (2007). Seascape evolution on clastic continental shelves and slopes. In I. Jarvis, C. A. Nittrouer, J. A. Austin, M. E. Field, J. H. Kravitz, J. P. Syvitski, & P. L. Wiberg (eds.), *Continental margin sedimentation: from sediment transport to sequence stratigraphy* (pp. 339–380). International Association of Sedimentologists. <https://doi.org/10.1002/9781444304398.ch7>
- Riis, F., Lundschie, B. A., Høy, T., Mørk, A., & Mørk, M. B. E. (2008). Evolution of the Triassic shelf in the northern Barents Sea region. *Polar Research*, *27*, 318–338. <https://doi.org/10.1111/j.1751-8369.2008.00086.x>
- Royo, L. A., Cardozo, N., Escalona, A., & Koyi, H. (2019). Structural style and evolution of the Nordkapp Basin, Norwegian Barents Sea. *AAPG Bulletin*, *103*(9), 2177–2217. <https://doi.org/10.1306/01301918028>
- Royo, L. A., & Escalona, A. (2018). Controls on minibasin infill in the Nordkapp Basin: Evidence of complex Triassic synsedimentary deposition influenced by salt tectonics. *AAPG Bulletin*, *102*, 1239–1272. <https://doi.org/10.1306/0926171524316523>
- Royo, L. A., Escalona, A., & Schulte, L. (2016). The use of seismic attributes to enhance imaging of salt structures in the Barents Sea. *First Break*, *34*, 41–49. <https://doi.org/10.3997/1365-2397.2016014>
- Rønnevik, H., Beskow, B., & Jacobsen, H. P. (1982). Structural and stratigraphic evolution of the Barents Sea. In A. F. Embry, & H. R. Balkwill (Eds.), *Arctic Geology and Geophysics: Proceedings of the Third International Symposium on Arctic Geology Memoir* (Vol. 8, pp. 431–440). AAPG Memoir.
- Ross, R. C., Halliwell, B. A., May, J. A., Watts, D. E., & Syvitski, J. P. M. (1994). Slope readjustment: A new model for the development of submarine fans and aprons. *Geology*, *22*, 511–514. [https://doi.org/10.1130/0091-7613\(1994\)022<0511:SRANMF>2.3.CO;2](https://doi.org/10.1130/0091-7613(1994)022<0511:SRANMF>2.3.CO;2)
- Rowan, M. G. (1996). Benefits and limitations of section restoration in areas of extensional salt tectonics: An example from offshore Louisiana. *Geological Society, London, Special Publications*, *99*, 147–161. <https://doi.org/10.1144/GSL.SP.1996.099.01.12>
- Rowan, M. G., & Lindso, S. (2017). Chapter 12 - Salt Tectonics of the Norwegian Barents Sea and Northeast Greenland Shelf A2 - Soto, Juan I. In J. I. Soto, J. F. Flinch, & G. Tari (Eds.), *Permo-Triassic Salt Provinces of Europe, North Africa and the Atlantic Margins* (pp. 265–286). Elsevier. <https://doi.org/10.1016/B978-0-12-809417-4.00013-6>
- Rowan, M. G., & Ratliff, R. A. (2012). Cross-section restoration of salt-related deformation: Best practices and potential pitfalls. *Journal of Structural Geology*, *41*, 24–37. <https://doi.org/10.1016/j.jsg.2011.12.012>
- Salazar, M., Moscardelli, L., & Wood, L. (2016). Utilising clinoform architecture to understand the drivers of basin margin evolution: A case study in the Taranaki Basin, New Zealand. *Basin Research*, *28*, 840–865. <https://doi.org/10.1111/bre.12138>
- Salazar, M., Moscardelli, L., & Wood, L. (2018). Two-dimensional stratigraphic forward modeling, reconstructing high-relief clinoforms in the northern Taranaki Basin. *AAPG Bulletin*, *102*, 2409–2446. <https://doi.org/10.1306/04241817235>
- Sangree, J., & Widmier, J. (1978). Seismic stratigraphy and global changes of sea level, part 9: Seismic interpretation of clastic depositional facies. *AAPG Bulletin*, *62*, 752–771. <https://doi.org/10.1306/C1EA4E46-16C9-11D7-8645000102C1865D>
- Sclater, J. G., & Christie, P. A. F. (1980). Continental stretching: An explanation of the Post-Mid-Cretaceous subsidence of the central North Sea Basin. *Journal of Geophysical Research: Solid Earth*, *85*, 3711–3739. <https://doi.org/10.1029/JB085iB07p03711>
- Steckler, M. S., Mountain, G. S., Miller, K. G., & Christie-Blick, N. (1999). Reconstruction of Tertiary progradation and clinoform development on the New Jersey passive margin by 2-D backstripping. *Marine Geology*, *154*, 399–420. [https://doi.org/10.1016/S0025-3227\(98\)00126-1](https://doi.org/10.1016/S0025-3227(98)00126-1)
- Steel, R. J., Carvajal, C., Petter, A. L., Uroza, C., Hampson, G., Burgess, P., & Dalrymple, R. (2008). Shelf and shelf-margin Growth in Scenarios of Rising and Falling Sea Level. *Recent Advances in Models of Siliciclastic shallow-marine Stratigraphy*, *90*, 47–71.
- Steel, R., Olsen, T., Armentrout, J., & Rosen, N. (2002). *Clinoforms, clinoform trajectories and deepwater sands: Sequence-stratigraphic models for exploration and production: Evolving methodology, emerging models and application histories*. Gulf Coast Section SEPMP 22nd Research Conference (pp. 367–381). Houston Texas.
- Stemmerik, L., Elvebakk, G., & Worsley, D. (1999). Upper Palaeozoic carbonate reservoirs on the Norwegian arctic shelf; delineation of reservoir models with application to the Loppa High. *Petroleum Geoscience*, *5*, 173–187. <https://doi.org/10.1144/ptgeo.5.2.173>
- Stemmerik, L., & Worsley, D. (2005). 30 years on-Arctic Upper Palaeozoic stratigraphy, depositional evolution and hydrocarbon prospectivity. *Norwegian Journal of Geology*, *85*, 151–168.
- Tetzlaff, D. M., & Harbaugh, J. W. (1989). *Simulating clastic sedimentation*. New York: Van Nostrand Reinhold Series on Computer Methods in Geosciences. 202 p. <https://doi.org/10.1007/978-1-4757-0692-5>
- Tetzlaff, D. M., & Schafmeister, M.-T. (2007). Interaction among sedimentation, compaction, and groundwater flow in coastal settings, in J. Harff, W. W. Hay, and D. M. Tetzlaff (Eds.), *Coastline Changes: Interrelation of Climate and Geological Processes* (Vol. 426), Geological Society of America. [https://doi.org/10.1130/2007.2426\(05\)](https://doi.org/10.1130/2007.2426(05)).
- Tetzlaff, D. M., & Schafmeister, M.-T. (2007). Interaction among sedimentation, compaction, and groundwater flow in coastal settings. In J. Harff, W. W. Hay, & D. M. Tetzlaff (Eds.), *Coastline Changes: Interrelation of Climate and Geological Processes* (Vol. 426). Boulder, Colorado: Geological Society of America.
- Trudgill, B. (2011). Evolution of salt structures in the northern Paradox Basin: Controls on evaporite deposition, salt wall growth and supra-salt stratigraphic architecture. *Basin Research*, *23*, 208–238. <https://doi.org/10.1111/j.1365-2117.2010.00478.x>

- Ulmishek, G. F. (2003). *Petroleum geology and resources of the West Siberian Basin, Russi*. Virginia: US Department of the Interior, US Geological Survey Reston.
- Vail, P. R., Mitchum, R. Jr, & Thompson, S. III (1977). Seismic Stratigraphy and Global Changes of Sea Level: Part 4. Global Cycles of Relative Changes of Sea Level: Section 2. Application of Seismic Reflection Configuration to Stratigraphic Interpretation, In C. E. Payton (Ed.), *Seismic Stratigraphy - Applications to Hydrocarbon Exploration* (Vol. 26, pp. 83–97). AAPG Memoir.
- Volozh, Y., Talbot, C., & Ismail-Zadeh, A. (2003). Salt structures and hydrocarbons in the Pricaspian basin. *AAPG Bulletin*, 87, 313–334. <https://doi.org/10.1306/09060200896>
- Warsitzka, M., Kley, J., & Kukowski, N. (2013). Salt diapirism driven by differential loading—Some insights from analogue modelling. *Tectonophysics*, 591, 83–97. <https://doi.org/10.1016/j.tecto.2011.11.018>
- Worsley, D. (2008). The post-Caledonian development of Svalbard and the western Barents Sea. *Polar Research*, 27, 298–317. <https://doi.org/10.1111/j.1751-8369.2008.00085.x>

How to cite this article: Rojo LA, Marín D, Cardozo N, Escalona A, Koyi H. The influence of halokinesis on prograding clinoforms: Insights from the Tiddlybanken Basin, Norwegian Barents Sea. *Basin Res.* 2019;00:1–26. <https://doi.org/10.1111/bre.12411>

Intentionally left blank

Paper IV

Controls on minibasin infill in the Nordkapp Basin: Evidence of complex Triassic synsedimentary deposition influenced by salt tectonics

Luis Alberto Rojo¹ and Alejandro Escalona¹

¹Department of Energy Resources, University of Stavanger, 4036
Stavanger, Norway

2018, AAPG Bulletin, v. 102, no. 7, pp. 1239-1272
DOI: 10.1111/bre.12411

This paper is not in Brage due to copyright

Intentionally left blank

Paper V

The impact of salt tectonics on the thermal evolution and petroleum systems of confined rift basins: Insights from basin modelling of the Nordkapp Basin, Norwegian Barents Sea

Andrés Cedeño¹, Luis Alberto Rojo¹, Nestor Cardozo¹,
Luis Centeno¹, and Alejandro Escalona¹

¹Department of Energy Resources, University of Stavanger, 4036
Stavanger, Norway

2019, Geosciences, v. 9
DOI: 10.3390/geosciences9070316

Article

The Impact of Salt Tectonics on the Thermal Evolution and the Petroleum System of Confined Rift Basins: Insights from Basin Modeling of the Nordkapp Basin, Norwegian Barents Sea

Andrés Cedeño *, Luis Alberto Rojo, Néstor Cardozo, Luis Centeno and Alejandro Escalona

Department of Energy Resources, University of Stavanger, 4036 Stavanger, Norway

* Correspondence: andres.f.cedenomotta@uis.no

Received: 27 May 2019; Accepted: 15 July 2019; Published: 17 July 2019



Abstract: Although the thermal effect of large salt tongues and allochthonous salt sheets in passive margins is described in the literature, little is known about the thermal effect of salt structures in confined rift basins where sub-vertical, closely spaced salt diapirs may affect the thermal evolution and petroleum system of the basin. In this study, we combine 2D structural restorations with thermal modeling to investigate the dynamic history of salt movement and its thermal effect in the Nordkapp Basin, a confined salt-bearing basin in the Norwegian Barents Sea. Two sections, one across the central sub-basin and another across the eastern sub-basin, are modeled. The central sub-basin shows deeply rooted, narrow and closely spaced diapirs, while the eastern sub-basin contains a shallower rooted, wide, isolated diapir. Variations through time in stratigraphy (source rocks), structures (salt diapirs and minibasins), and thermal boundary conditions (basal heat flow and sediment-water interface temperatures) are considered in the model. Present-day bottom hole temperatures and vitrinite data provide validation of the model. The modeling results in the eastern sub-basin show a strong but laterally limited thermal anomaly associated with the massive diapir, where temperatures in the diapir are 70 °C cooler than in the adjacent minibasins. In the central sub-basin, the thermal anomalies of closely-spaced diapirs mutually interfere and induce a combined anomaly that reduces the temperature in the minibasins by up to 50 °C with respect to the platform areas. Consequently, source rock maturation in the areas thermally affected by the diapirs is retarded, and the hydrocarbon generation window is expanded. Although subject to uncertainties in the model input parameters, these results demonstrate new exploration concepts (e.g., deep hydrocarbon kitchens) that are important for evaluating the prospectivity of the Nordkapp Basin and similar basins around the world.

Keywords: salt; thermal modeling; basin modeling; source rock maturation; petroleum system

1. Introduction

The occurrence of evaporitic intervals in sedimentary basins and their subsequent mobilization play an important role in the evolution of the petroleum system [1,2]. Salt mobilization and diapirism control the spatial and temporal distribution of suprasalt reservoirs and source rocks [3–5], and they influence the style and timing of stratigraphic and structural traps. Salt's low permeability also inhibits the vertical migration of hydrocarbons, deflecting migration pathways [6]. Likewise, local salt depletion by salt withdrawal may lead to the formation of welds, which can provide migration pathways between subsalt source rocks and suprasalt reservoirs [7].

Salt has a thermal conductivity that is 2 to 3 times higher than sedimentary formations [6,8,9]. Accordingly, salt structures can modify the spatial and temporal thermal regime of the basin through

focusing and defocusing of heat [8,10]. Salt domes create a dipole-shaped thermal anomaly with a negative thermal anomaly towards their base and a positive thermal anomaly in the suprasalt strata [9]. When salt bodies reach the surface, the dipole-shaped anomaly becomes a negative monopole, creating a conduit of low thermal resistance for heat conduction out of the basin [10]. Due to the difference in thermal conductivity between the salt and the surrounding sedimentary formations, thermal anomalies are also induced in the vicinity of salt bodies. The size and shape of these anomalies is controlled by the size of the salt bodies [8,10]. Maturation of kerogen within source rocks and reservoir diagenesis are temperature-controlled processes; therefore, any salt-related temperature deviation from the regional trend may have a significant impact on these processes.

The Nordkapp basin is a NE-SW trending rift basin of Late Paleozoic age located in the Norwegian Barents Sea (Figure 1A,B). Thick Pennsylvanian-Lower Permian layered evaporite sequences (LES) and their subsequent Mesozoic and Cenozoic mobilization generated numerous and closely spaced salt diapirs along the basin axis, and salt pillows generated along the basin margins [11–14]. Hydrocarbon exploration in the basin dates back to the 1980s. However, exploration has exclusively focused on the western sub-basin, while the central and eastern sub-basins remain underexplored (Rojo and Escalona, 2018). Only one non-commercial discovery in the western sub-basin, the Pandora discovery (well 7228/7-1A, Figure 1B), has been made in Triassic sediments which flank a salt diapir [15].

The Norwegian Barents Sea is known to host various petroleum systems sourced by Upper Paleozoic and Mesozoic organic rich intervals [16,17]. In the Nordkapp Basin, however, Paleozoic and Mesozoic strata are deeply buried due to Triassic halokinesis [18]. Therefore, it is tempting to assume that these source rocks became overmature for hydrocarbon generation in the Mesozoic. Interestingly, 2D structural restorations by [18,19] show that diapirs reached the seafloor since the Triassic, which may have cooled the basin and delayed maturation of the source rocks, as documented in offshore Mexico and Brazil [6,9]. Hence, this can open the possibility for a deeper prospectivity of the Nordkapp Basin and other salt-bearing basins in the Barents Sea.

Although there is potential for commercial discoveries in the Nordkapp Basin, there is an imperative need for understanding the impact of halokinesis on the thermal history of the basin and source rock maturation. In particular, the effect of closely spaced diapirs on the thermal evolution of this confined basin must be addressed. Therefore, in this study we explore the dynamic history of salt movement and its thermal effect by integrating 2D structural restorations with thermal modeling in order to: (1) evaluate how halokinesis impacted the thermal distribution of the basin through time, and (2) explore the implications of the modeled thermal history on the petroleum system and prospectivity of the basin. We use the structural restorations and selected model parameter values as a reasonable scenario to accomplish these objectives. Testing the sensitivity of different restoration or thermal parameters is beyond the scope of this work.

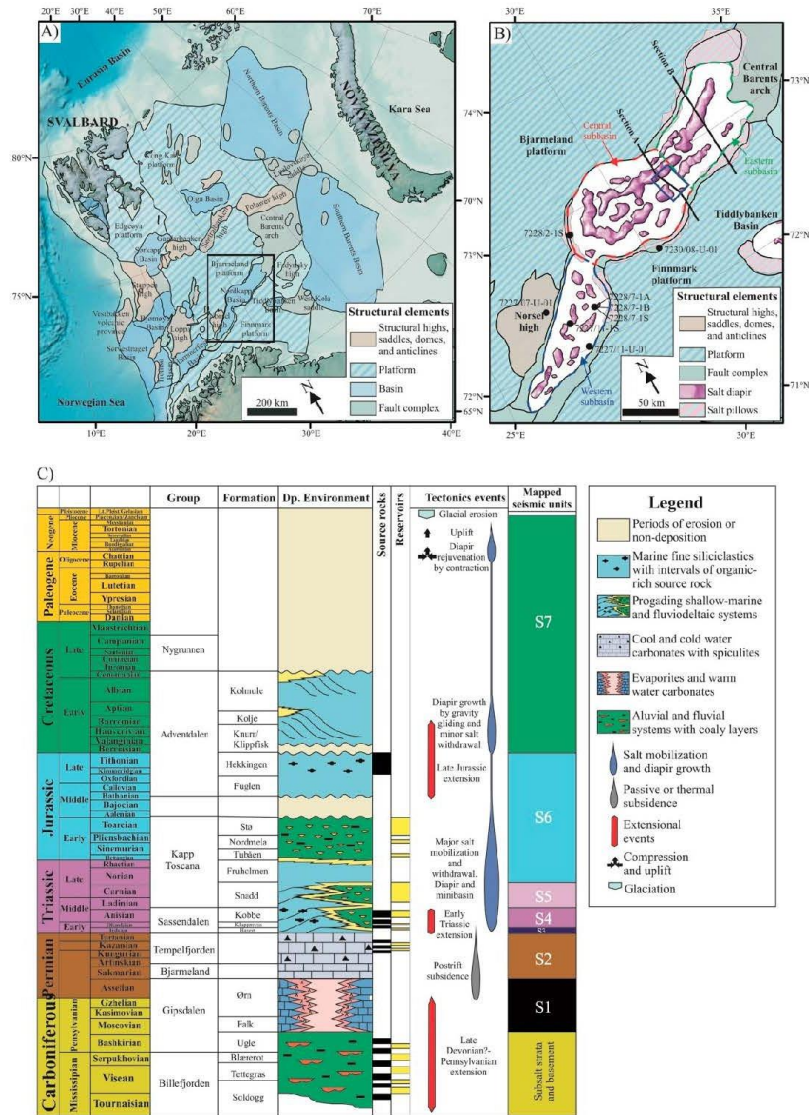


Figure 1. (A) Main structural elements of the Barents Sea. The Nordkapp Basin is indicated by the black rectangle. (B) Main structural elements of the Nordkapp Basin (modified from Rojo et al. [18]). The basin is divided in three sub-basins: western, central and eastern sub-basins. Black dots are exploration and shallow stratigraphic wells, whereas black lines show the location of the studied sections through the central (section A) and eastern (section B) sub-basins. (C). A chronostratigraphic chart illustrating the main stratigraphic units, depositional environments, tectonic events, and mapped seismic units of the Barents Sea and Nordkapp Basin (based on [17,18]).

2. Geologic Evolution of the Nordkapp Basin

2.1. Late Paleozoic

The Nordkapp Basin formed as the result of two extensional events of different orientation [19–23] (Figure 1B): (1) pre-Mississippian NE-SW extension, which reactivated previous NW-SE Caledonian structures and formed the central sub-basin; and (2) Pennsylvanian NW-SE extension which reactivated NE-SW Caledonian structures, forming the western and eastern sub-basins. Based on outcrops in Svalbard [24,25] and wells in the Finnmark platform [26], the syn-rift section of the Nordkapp basin is expected to contain siliciclastics interbedded with coal of the Mississippian Billefjorden Group (Figure 1C). Potential Mississippian reservoirs include sandstones deposited within meandering and braided fluvial systems, and interlayered coals are potential gas-prone source rocks.

Basin extension continued from the Pennsylvanian to the Early Permian, and it was followed by a period of thermal subsidence until the end of the Paleozoic [17,27]. Basin restriction favored the precipitation of syn-rift to early post-rift evaporites along the basin axis, whereas deposition of warm water carbonate buildups and gypsum occurred at the basin boundaries (Gipsdalen Group) [28–30] (Figure 1C). These deposits were overlain by cool-water carbonates of the Bjarmeland Group and cold water carbonates and spiculites of the Tempelfjorden Group [17,27] (Figure 1C). Based on the Alta and Ghota discoveries in the Loppa High, Upper Permian carbonaceous mudstones and limestones of the Tempelfjorden Group are expected to contain intervals of oil-prone source rocks, and possible reservoirs associated with karstified carbonates in the Nordkapp Basin [17].

2.2. Mesozoic

The onset of salt mobilization and diapirism occurred during the earliest Triassic, and it was triggered by basement-involved extension and differential loading induced by prograding siliciclastic sediments sourced from the Uralides [14,18,19,31]. Minibasin growth and diapir uplift ceased by the end of the Middle Triassic due to welding of the underlying salt [14,18]. Diapir growth after the Middle Triassic is attributed to evacuation of remaining salt adjacent to diapirs and basinward suprasalt gliding and contraction [14]. The Triassic minibasins of the Nordkapp Basin record the NW-SE transgressive-regressive fluviodeltaic systems of the Sassendalen and Kapp Toscana groups, which progressively prograded towards the NW of the Barents Shelf (Figure 1C) [32–35]. Based on the Goliat discovery in the Hammerfest Basin, oil and gas-prone source rocks may be present in the Sassendalen Group, whereas shallow marine and fluviodeltaic reservoirs can be present in the Sassendalen and Kapp Toscana groups [5,17].

The Late Triassic-Early Jurassic was marked by a regional decrease in accommodation in the Barents Shelf, including the Nordkapp Basin [36]. This resulted in a complex drainage system characterized by erosion and reworking of previous Triassic deposits, which favored the deposition of shallow marine and fluviodeltaic Lower Jurassic reservoirs of good quality (e.g., Stø Formation in the Kapp Toscana Group) [17]. A new episode of extension associated with the initial opening of the North Atlantic to the west of the Barents Shelf [21], partially affected the Nordkapp Basin during the Late Jurassic-Early Cretaceous [12] (Figure 1C). Normal fault systems at basin boundaries caused basinward gravity gliding of suprasalt strata and subsequent thin-skinned contraction and growth of pre-existing diapirs [14]. Lower Jurassic deposits were flooded and overlain by the Upper Jurassic marine black shales of the Hekkingen Formation, which is considered to be a potential source rock in the Barents Sea [16,17]. These marine shales were in turn covered by Lower Cretaceous, SSW prograding sediments sourced from the northern Barents Shelf [37,38].

2.3. Late Cretaceous-Cenozoic

During the Late Cretaceous-Cenozoic, the Nordkapp Basin underwent several contractional events, which are attributed to plate tectonic reorganizations related to the opening of the North Atlantic (Figure 1C; [21]). Consequently, pre-existing diapirs in the Nordkapp Basin were rejuvenated

by contractional diapirism [13,14]. Finally, successive events of uplift and erosion, including the Pleistocene glacial erosion, removed about 1.5 km of Cretaceous and Cenozoic strata in the basin [39,40].

3. Methodology

In order to model the thermal evolution of the Nordkapp Basin, we considered two processes: (1) the evolving basin geometry, and (2) the evolution of thermal boundary conditions, i.e., basal heat flow and sediment-water interface temperatures. The evolving basin geometry was reconstructed from structural restoration of two sections, one across the central sub-basin (section A) and another across the eastern sub-basin (section B) (Figure 2). Section A has deeply rooted, narrow and closely spaced diapirs (Figure 2A), whereas section B contains a shallower rooted, wider, isolated diapir (Figure 2B). Before the restoration process, the sections were depth-converted using the velocity model from Rojo et al. [18], which uses interval velocities and k factors (change in interval velocities vs depth) from wells 7228/9-1, 7228/7-1, 7125/1-1, 7124/3-1, and 7229/11-1 (Figure 3).

Details of the restoration are described in Rojo et al. [18]. In short, kinematic restorations were performed using the *Move* software (Midland Valley). These restorations account for uplift and erosion in the Late Cenozoic, restore the Cenozoic and pre-diapir units using flexural slip, restore the syn-diapir units using vertical shear, and assume flexural isostasy with a lithospheric elastic thickness of 20 km [41].

Thermal modeling of selected restoration stages (paleo-geometries) was performed using the *PetroMod* software (Schlumberger). Each stage was imported into the software, and polygons representing each seismic unit (Figure 2B,D) were digitized. At each stage, the lower boundary condition of the thermal model is the heat flow at the basement-sediment interface. The evolution of this basal heat flow through time was reconstructed from the present thermal gradient of the basin from nearby wells, the history of rifting and evolution of the stretching (β) factor [42], and inverse modeling using a modified McKenzie model [43]. The upper boundary condition of the thermal model is the sediment-water interface temperature (SWIT). This surface temperature was reconstructed from the paleo-latitude of the basin and water depths over time. The following section describes the input paleo-geometries, thermal boundary conditions, and model parameters in detail.

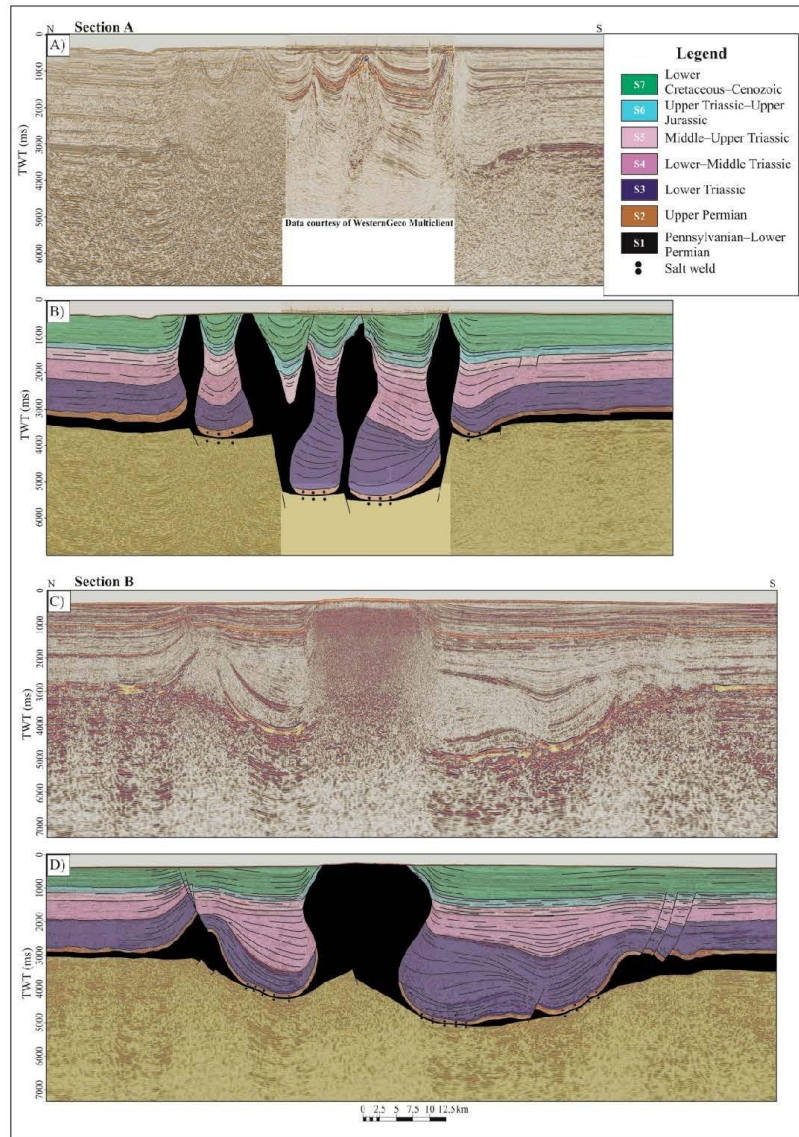


Figure 2. (A) Uninterpreted seismic section A across the central sub-basin. The central seismic panel is from a higher-resolution, full azimuth seismic data provided by WesternGeco Multiclient. (B) Interpreted section A. The base salt was estimated based on parallel seismic sections that extend to 7000 ms. (C) Uninterpreted seismic section B across the eastern sub-basin. (D) Interpreted section B. Legend shows the interpreted seismic units (Figure 1C). See Figure 1B for location of these sections. Figures modified from Rojo et al. [18].

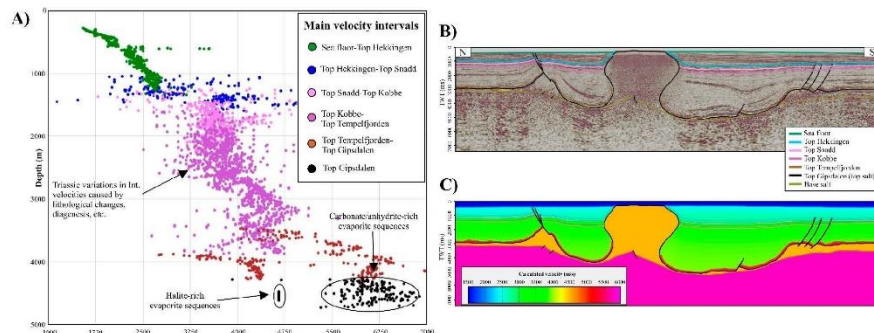


Figure 3. (A) Plot showing calculated interval velocities vs depth from wells 7228/9-1, 7228/7-1A, 7125/1-1, 7124/3-1, 7229/11-1. (B) Seismic section B showing the location of the main velocity transitions. (C) Seismic section B displaying the interval velocities used to depth convert the seismic profile (modified from Rojo et al. [18]).

4. Paleo-Geometries, Boundary Conditions, and Model Parameters

4.1. Paleogeometries

Figure 4 displays the restoration of the two cross sections in the central (section A, Figure 4A) and eastern (section B, Figure 4B) sub-basins. The restoration stages are the paleo-geometries input to the thermal model. It should be noted that in Figure 4 and later figures (Figures 7 and 9), for the purpose of display and comparison between sections, section A is not vertically exaggerated while section B has a vertical exaggeration of 2. Below we present a short description of the geologic evolution portrayed by the restorations.

4.1.1. Section A, Central Sub-basin

Syn-rift to early post-rift layered evaporate sequences (LES) precipitated in a symmetric graben and were overlain by pre-kinematic Upper Permian carbonates (Figure 4A, VIII). During the earliest Triassic, thick-skinned extension accompanied by differential loading of Triassic sediments sourced from the Urals, created a structural style consisting of NW shifting patterns in salt withdrawal and ENE-WSW-trending passive diapirs (Figure 4A, V–VII). Passive diapirism and welding occurred diachronously across the section, and first occurred in the northern part of the graben due to the preferential loading of salt in this region (Figure 4A, V). In the southern part, minor loading caused the formation of a salt pillow. During the Early-Middle Triassic, differential loading focused on the southern part of the graben, which caused a shift in salt withdrawal and subsequent salt expulsion towards the south (Figure 4A, IV). This favored the formation of a half turtle structure and a passive diapir above the southern boundary fault. By the end of this period, the minibasins grounded the base salt forming salt welds (Figure 4A, IV). During the Late Triassic to Late Jurassic, thick-skinned extension induced diapir collapse of the northern diapir since the underlying salt was almost totally evacuated (Figure 4A, III). This formed a minibasin above the diapir crest, filled by Upper Triassic and Jurassic strata. Minor differential loading of the remaining salt in the south favored the continued growth of the southern and central salt diapirs (Figure 4A, III). During the Cretaceous and Cenozoic, higher sedimentation rates than diapir growth rates led to burial of the salt diapirs (Figure 4A, II). This episode was then followed by Late Cenozoic contraction, diapirism and uplift, which eroded approximately 1.5 km of Cretaceous and Cenozoic strata (Figure 4A, I).

4.1.2. Section B, Eastern Sub-basin

LES in this section precipitated in a more sag-type basin, which was later covered by Upper Permian carbonates (Figure 4B, VIII). Earliest Triassic sediment loading accompanied by thick-skinned extension generated expulsion rollovers towards the north and a central passive diapir (Figure 4B, V–VII). Differential loading occurred preferentially at the basin axis forming the first salt weld by the earliest Triassic, whereas a significant amount of salt remained on the northern and southern basin boundaries (Figure 4B, V–VI). During the Middle Triassic, differential loading focused mostly on the north, forming the northern minibasin and favoring the growth of the northern salt pillow and the central passive diapir (Figure 4B, IV). To the south, differential loading caused a shift in salt withdrawal, which resulted in the welding of the southern minibasin and the formation of a half-turtle structure. Continuous basin subsidence by thick-skinned extension and salt withdrawal produced the flexure and extension of suprasalt strata at basin boundaries, resulting in the generation of suprasalt fault complexes (Figure 4B, IV). By the end of the Middle Triassic, the northern and southern minibasins grounded the base salt (Figure 4B, IV). Even though most of the underlying salt was evacuated, the central salt diapir continued to grow during the rest of the Mesozoic by gliding of suprasalt strata towards the basin axis and thin-skinned contraction (Figure 4B, II–IV). Higher sedimentation rates than diapir growth rates caused the burial of salt structures during the Cretaceous and Cenozoic (Figure 4B, II). During the Cenozoic, salt structures were rejuvenated by contraction. This episode was followed by Late Cenozoic uplift and erosion, which removed approximately 1.5 km of Cretaceous and Cenozoic strata (Figure 4B, I).

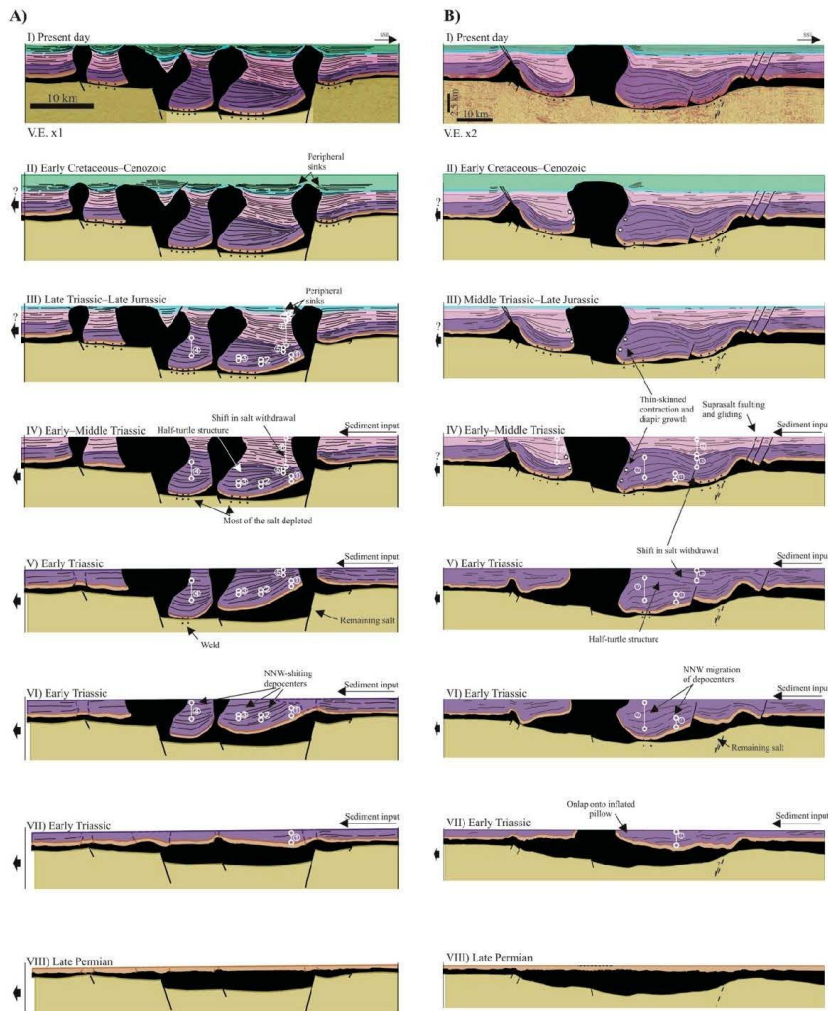


Figure 4. (A) Structural restoration of section A (Figure 2B) in the central sub-basin. (B) Structural restoration of section B (Figure 2D) in the eastern sub-basin. The different restoration stages are the paleo-geometries input to the thermal model. Colored rock units correspond to the interpreted seismic units in Figure 2 (and Figure 1C). See Figure 1B for location of the sections. Restorations modified from Rojo et al. [18].

4.2. Thermal Boundary Conditions

Thermal boundary conditions determine the primary energetic inputs to reproduce the temperature history of the basin and, consequently, for the maturation of source rocks. As mentioned above, the sediment-water interface temperature (SWIT) represents the upper boundary condition whereas the basal heat flow represents the lower boundary condition. These parameters were constrained to ensure that the modeled thermal field best-fits temperature data in the basin.

For the SWIT, we used the automatic SWIT tool in PetroMod, which extracts a standard temperature at sea level over geological time based on the basin's present-day geographic location and paleo-latitude (Figure 5A). A transformation that corrects the surface temperature against the paleo-water depth was applied and the SWIT estimated. The latitudinal position assigned to the Nordkapp basin was 72°N, and paleo-water depths (Figure 4B) were taken from [18].

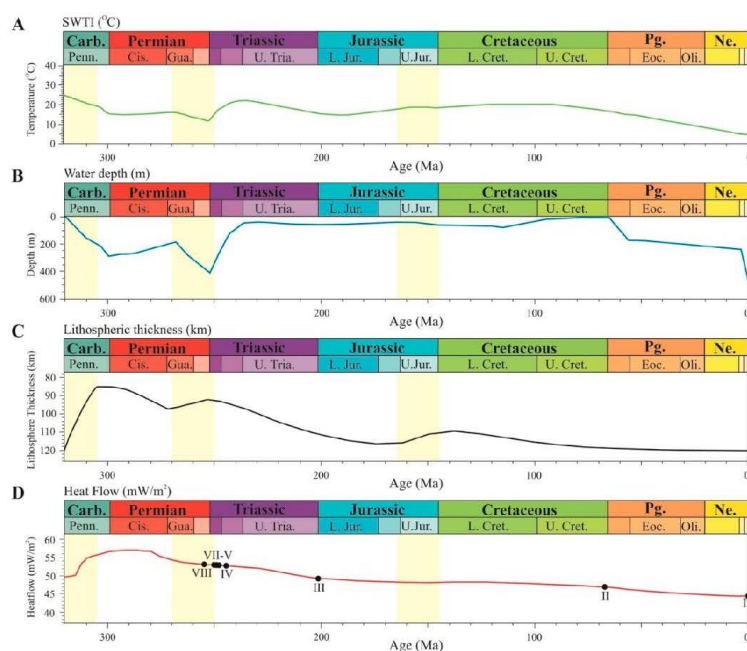


Figure 5. Modeled (A) sediment-water interface temperature (SWIT), (B) water depth, (C) lithospheric thickness, and (D) basal heat flow through time in the Nordkapp Basin. Yellow rectangles show the three rifting periods. Dots in D are the selected restoration stages in Figure 4.

The basal heat flow was calculated by reconstructing the lithospheric thickness from the Late Carboniferous to the present (Figure 5C). In order to do this, we adopted mean values for the stretching factor (β) of each rift phase (Figure 5, yellow rectangles): Late Carboniferous (320–305 Ma, $\beta = 1.6$), Late Permian (270–250 Ma, $\beta = 1.25$), and Late Jurassic–Early Cretaceous (165–145 Ma, $\beta = 1.15$), as proposed by [42]. The Post-Caledonian lithosphere and crustal thicknesses were defined at the rift initiation. An initial lithospheric thickness of 120 km and an initial crustal thickness of 35 km (17.5 km upper crust, 17.5 km lower crust) were adopted from Clark et al. (2014). The present-day crustal thickness is 18 km (16 km upper crust, 2 km lower crust) as documented by [41,42,44]. The temperature at the lithosphere-asthenosphere boundary was set to 1300 °C and the mantle heat flow to 30 mW/m². Figure 5C,D depict the modeled lithospheric thickness and basal heat flow through time, respectively.

A good fit between measured and calculated temperature values of five exploration wells (7228/7-1B, 7228/7-1S, 7228/2-1S, 7228/7-1A, 7228/2-1S) and three shallow wells in the Nordkapp Basin (7227/11-U-02, 7227/07-U-01, 7230/08-U-01) was achieved using estimated basal heat flow values of ~45 mW/m² (Figure 6A). Extrapolating the thermal model calculated in the western sub-basin to the entire Nordkapp Basin is unrealistic due to possible variations in the initial thickness of the Post-Caledonian crust and lithosphere [42], and the magnitude of rifting across the basin. Nevertheless,

we chose to do so in order keep the model as simple as possible and to avoid biasing the model with poorly-constrained inputs. In addition, the effects of episodic glacial loading-unloading and erosion during the Late Cenozoic documented by several authors [45–49] are not considered in the model.

Unlike temperature, vitrinite reflectance data display higher maturities than the calculated trend (Figure 6B). Vitrinite measurements from wells 7228/7-1A and 7228/7-1S in the central part of the basin plot closer to the calculated trend than corresponding values from well 7228/2-1S in the northern rim of the basin (Figure 6B, see Figure 1B for well locations). This most likely reflects different amounts of erosion at different locations in the basin. Well 7228/2-1 S shows a characteristic pattern of increasing thermal maturity with stratigraphic age from Cenozoic to Middle Triassic (Figure 6B). However, at ~3600 m depth, a sudden increase in vitrinite values is observed near the top of the Lower Triassic Havert Formation. Here, the well values define a steeper vitrinite trend, implying higher temperature gradient. Igneous activity could explain this higher thermal gradient, but there is no evidence of such activity. The modeled paleo-heat flow (Figure 5D) depicts higher flow rates (~54 mW/m²) during and immediately after the Late Permian rifting, which seem to be a plausible explanation to the higher thermal gradient. Thus, the modeled heat flow (Figure 5D) is a reasonable scenario for the Nordkapp Basin, and together with the SWIT (Figure 5A), it defines the boundary conditions for the thermal model. Transient heat-flow conditions were assumed at all times.

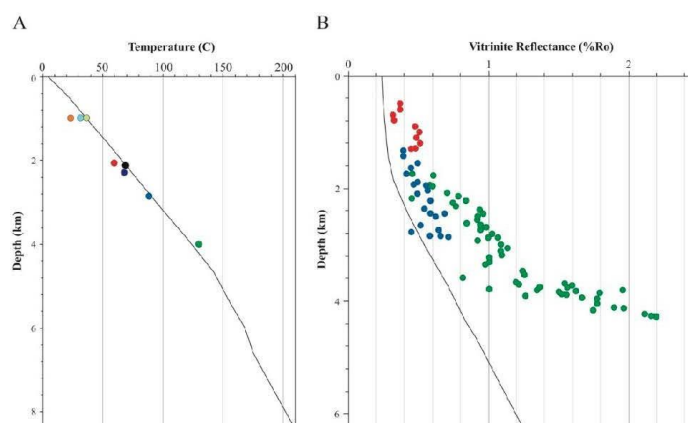


Figure 6. (A) Bottom hole temperature measurements of wells 7228/7-1B (black), 7227/11-U-02 (orange), 7227/07-U-01 (light blue), 7230/08-U-01 (light green), 7228/7-1S (red), 7228/2-1S (purple), 7228/7-1A (dark blue), and 7228/2-1S (dark green). Line shows the modeled, present temperature versus depth trend. (B) Vitrinite reflectance data from wells 7228/7-1S (red), 7228/7-1A (blue), and 7228/2-1S (green). Line shows the modeled vitrinite reflectance. Figure 1B shows the location of the wells.

4.3. Model Parameters

The restoration stages in Figure 4 were imported and digitized in Petromod for thermal modeling. Sediment types and ages were defined based on the seismic units in Figure 1C. Rock properties were assigned to each unit (Table 1). Lithologies were user-defined considering the proportion of different sediments, i.e., sandstone, siltstone, shale, limestone, coal, and salt. Each defined lithology was assigned an initial porosity value and a porosity versus depth trend (factor *c* in Table 1) that decreases exponentially with the greatest porosity loss happening at shallow depths [50,51]. The thermal conductivity of the various units was set to vary linearly as a function of porosity. The model also accounts for variations in the thermal conductivity with increasing temperature following the model described by [52], i.e., the conductivity of salt drops from 6.5 (W/mk) at 20 °C to 4.14 (W/mk) at 220 °C.

Finally, the thermal model was computed numerically using finite elements on a regular grid with $300(x) \times 150(y)$ cells.

Five source rock intervals were modeled: The Upper Jurassic Hekkingen Formation (S6), the Upper Triassic Snadd Formation (S5), the Lower to Middle Triassic Kobbe Formation (S4), the Permian Tempelfjorden Group (S2), and a Carboniferous pre-salt coaly source rock (Figure 1C, green rows in Table 1). Since S4 is remarkably thick (Figure 2), we considered the source rock interval, presumably correlatable with the Botneheia Formation in the western Barents Sea [33,35,53], to be only in the uppermost 300 m of this unit. The large stratigraphic interval encompassed by the modeled source rocks reflects the uncertainty in source rock distribution and thickness in the basin.

Table 1. Rock units and their parameter values for thermal modeling. For lithology definition, the percentage of sandstone (ss), siltstone (slt), shale (sh), limestone (ls), coal (co) and salt (sl) is defined. Source rock intervals are colored green. Values of thermal conductivity and heat capacity are given for each unit at 20 °C.

Unit	Lithology	Density (kg/m ³)	Surface Porosity (%)	Factor c (1/km)	Thermal Conductivity (W/mK)	Radiogenic Heat (microW/m ³)	Specific Heat Capacity (Kcal/K/Kg)
S7	ss20, sh80	2730	53.5	0.57	2.01	1.31	0.21
S6	ss10, shs20,sh70	2721	59.5	0.65	2.11	1.37	0.21
S5	ss70, sh30	2714	49.7	0.47	3.03	0.88	0.2
S4	ss30, sh70	2566	61.3	0.67	2.13	1.31	0.21
S3	ss30, sh70	2706	61.3	0.67	2.13	1.31	0.21
S2	sh10, ls90	2709	52.9	0.55	2.51	0.73	0.2
S1	sl100				6.5	0.01	0.21
Pre-salt	ss25, sh50, co25	2540	63.65	0.64	1.34	0.97	0.23
Basement	Gneiss				2.7	2	0.19

5. Results

5.1. Thermal Evolution

Figure 7 depicts the modeled evolution of temperature through time in the central sub-basin (Figure 7A) and eastern sub-basin (Figure 7B). During the initial Late Permian stage prior to salt mobilization, in the central part of the basin the thermal gradient is reduced within the salt (up to 3 km thick) as depicted by widely spaced isotherms (Figure 7A,B, VIII). Temperatures are elevated above the salt, implying enhanced heat flow. Towards the shoulders of the basin, the regional thermal gradient is reestablished.

In the Early to Middle Triassic stages, when salt was mobilized and reached the surface (Figure 7, IV to VII), the temperature distribution was altered as salt diapirs provided vertical conduits for conducting heat out of the basin, inducing a negative thermal anomaly in the interior of the diapirs. This thermal anomaly is highest at the center of the diapirs and gradually decreases outwards. Isotherms within the diapirs are widely spaced and, as a consequence, isotherms are deeper below salt than in the adjacent minibasins. Around the salt diapirs, the temperature is also affected by the reduced geothermal gradient inside the diapir. The wide, isolated diapir in the eastern sub-basin shows this effect more clearly (Figure 7B, IV). In this diapir, the temperature contrast between the salt interior and surrounding minibasins at ~3 km is as much as 30 °C. In the central sub-basin (section A), the negative thermal anomaly of a single diapir cannot be seen as the diapirs are narrower and closer together (Figure 7A, IV). In this section, the thermal effect of each diapir mutually interferes, resulting

in a combined effect that lowers the isotherms below the regional trend. In the center of the basin, temperatures are as much as 60 °C lower than those in the platform areas far from the salt effect.

After deposition of the Upper Jurassic and Cretaceous-Cenozoic sediments, the salt diapirs are no longer connected to the surface (Figure 7, stages II and III). A positive thermal anomaly developed above the closely spaced diapirs in section A and above the single diapir in section B owing to the focusing of heat by the underlying salt. In section A, the temperature rises ~10 °C above the largest diapir compared to the surrounding sediments (Figure 7A, II) while in section B the temperature rises ~15 °C above the massive diapir (Figure 7B, II). The negative thermal anomaly within the salt diapirs is still present, but at a lower intensity than in previous stages.

Several pseudo-wells along the sections demonstrate the thermal effect of the salt at present day. In the central sub-basin (section A), we extracted temperatures in pseudo-wells through a small diapir at 9 km from the northern edge of the cross-section, and through a wider diapir at 17 km. Temperatures were also extracted in pseudo-wells at 27 km and at 56 km in a minibasin and a platform area, respectively (Figure 7A, I). Figure 8A depicts the distribution of temperature in these wells. The thermal gradient in the small diapir (9 km well) is greater than in the large diapir (17 km well). The temperature difference between these wells is ~15 °C at a depth of 5 km. In both diapirs, the thermal gradient beneath the salt increases and depicts a similar trend to the one observed at the well in the platform area (56 km well). The temperature beneath the small diapir (9 km well) is still ~25 °C higher than below the large diapir (17 km well) (Figure 8A). These differences are most likely related to the size of the diapirs, with the wider diapir conducting heat more efficiently. Significant thermal differences exist between the two wells outside salt structures (27 and 56 km wells). The maximum temperature difference between these two wells is ~35 °C at a depth of 5 km (Figure 8A). Although both wells are outside the salt diapirs, the well in the minibasin (27 km) is between closely spaced diapirs whose mutually interfering effect induces a broad negative thermal anomaly in the central part of the basin. Therefore, temperatures in the minibasin resemble those in the salt diapirs rather than those in the platform areas.

In the eastern sub-basin (section B), we extracted temperatures in pseudo-wells at 29 km from the northern edge of the cross-section in a minibasin, at 45 km through the massive diapir, and at 100 km in the platform area (Figure 7B, I). Figure 8B displays the distribution of temperature in these wells. The temperature gradient in the salt diapir (45 km well) is considerably lower than in the minibasin and platform area (29 and 100 km wells). The greatest temperature difference is ~110 °C at a depth of 7 km between the wells in the diapir (45 km) and the platform area (100 km). The well in the minibasin (29 km) shows intermediate temperatures, although still it is ~70 °C warmer than the diapir at a depth of 7 km (Figure 8B). These significant thermal differences are most likely related to the large size (width) of the salt diapir.

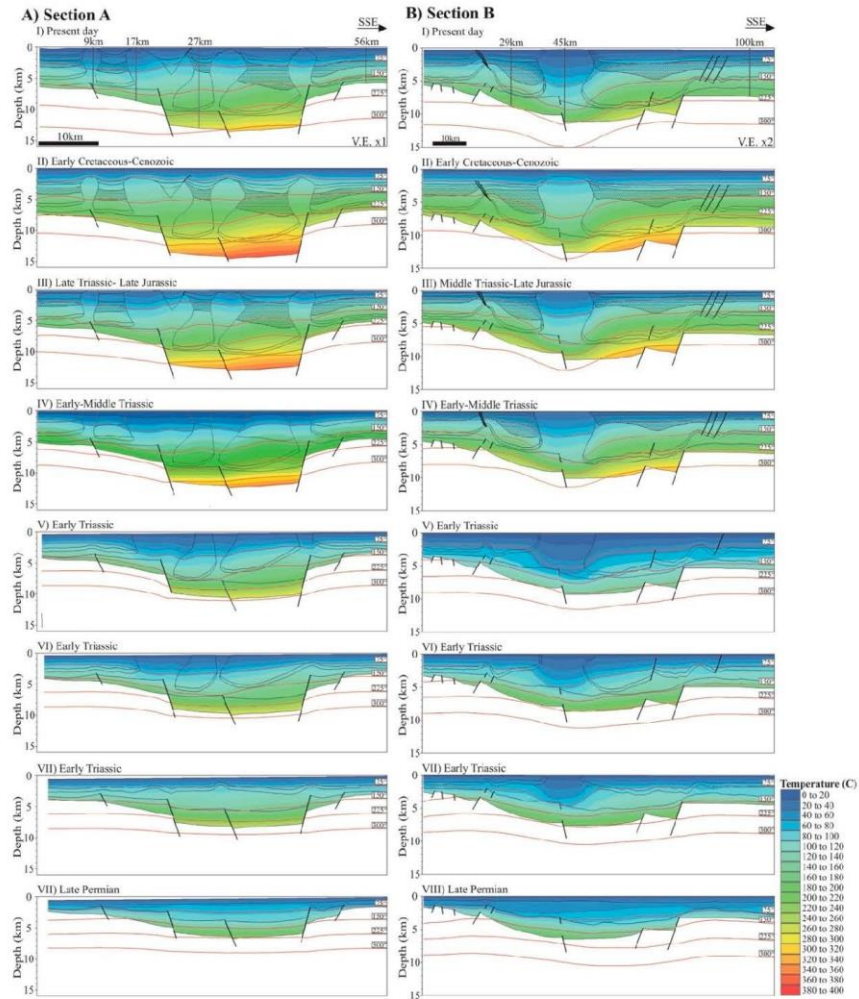


Figure 7. Evolution of temperature through time in (A) section A in the central sub-basin, and (B) section B in the eastern sub-basin. Black lines are unit contacts and red lines are isotherms. For guidance, stippled unit is the Lower to Middle Triassic Kobbe Formation (S4). Figure 1B shows the location of the sections.

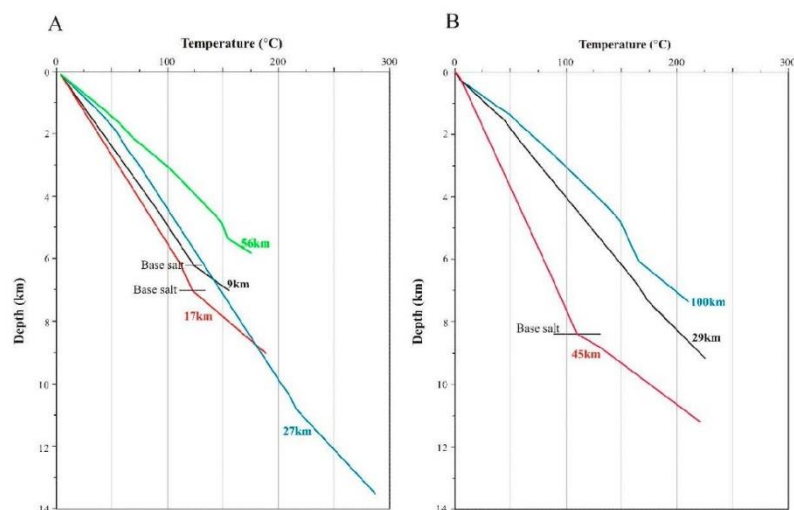


Figure 8. Modeled, present temperature distribution in pseudo-wells along (A) section A in the central sub-basin, and (B) section B in the eastern sub-basin. Thick lines in the minibasins and platforms wells show the temperature distribution in potential reservoirs. Figure 6 (I) shows the location of the pseudo-wells.

5.2. Source Rock Maturation

Figure 9 depicts the evolution in thermal maturity that each of the modeled source rock units experienced through time. The vitrinite reflectance model developed by Sweeney and Burnham [54] was implemented for maturation modeling of the source rocks. It simulates the onset of the oil window at 0.55%Ro, and the upper limit of thermogenic gas (dry) generation at 4%Ro.

In the Late Permian, pre-salt source rocks in the central part of the basin were buried at depths of more than 4 km, and maturities of 0.7–1.0%Ro were attained (Figure 9, VIII). In the basin's margins, the same rocks were shallower at ~2 km and accordingly, they were immature (<0.5%Ro). Upper Permian (S2) source rocks were shallowest and immature.

From the Early Triassic until the Late Jurassic, salt mobilization was confined to the central part of the basin (Figure 9, III–VII). Salt evacuation resulted in minibasin subsidence and infill, causing progressive maturation along the axes of the rapidly subsiding minibasins. Pre-salt and Upper Permian (S2) source rock units were deeply buried in the central part of the basin where their maturities were highest. Maturity in these units systematically decreases updip away from the salt bodies. In the central sub-basin, source rock maturity exceeded 2.0%Ro and reached maturities beyond any hydrocarbon generation (>4%Ro, Figure 9A, III). In the eastern sub-basin, the thermal maturities generally were lower and ranged from 0.55 to 4.0%Ro, although locally these source rocks exceeded values of 4.0%Ro (Figure 9B, III). The base of the source rocks modeled at the top of the Lower to Middle Triassic (S4) unit locally attained maturity values higher than 0.55%Ro in the central sub-basin (Figure 9A, III).

From the Early Cretaceous through the Cenozoic, widespread sedimentation increased the burial of source rocks to their maximum maturity. In the central sub-basin, Paleozoic (pre-salt and S2) source rocks mostly became overmature (>4%Ro) in the central part of the basin, whereas over the platforms they lied within the gas window (1.3–4%Ro, Figure 9A, II). In the eastern sub-basin, the Paleozoic source rocks lied within the gas window, except in the southern mini-basin where they were overmature (Figure 9B, II). The maturity of the Triassic (S4 to S5) and Jurassic (S6) source rocks generally exceeded 0.55%Ro, and locally reached a maximum of 1.0–1.3%Ro in the central sub-basin (Figure 9A, II). In the

eastern sub-basin, Upper Triassic to Jurassic source rocks (S5 and S6) were immature near the diapir, while Upper Permian source rocks (S2) were still in the late oil to wet gas window adjacent to this diapir (Figure 9B, II). A similar although less pronounced effect is observed along the flanks of the northern, widest diapir of the central sub-basin (Figure 9A, II).

In the Late Cenozoic, compression caused widespread uplift and exhumation, and subsequently the Mesozoic-Cenozoic section underwent erosion, freezing maturation. At present-day, exceptionally low maturity in the Upper Permian to Jurassic source rocks exists along the flanks of the salt diapirs (Figure 9, I). This reduction in thermal maturation in the vicinity of salt diapirs is ubiquitous, indicating that source rock maturation was not only controlled by burial, but also by the thermal anomalies induced by the salt structures. In the central part of the basin, pre-salt and Upper Permian (S2) source rocks are deeper and mostly overmature in the central sub-basin, while in the eastern sub-basin they are in the late oil to dry gas window (Figure 9, I).

In order to better visualize the effect of salt on source rock maturation, we generate vitrinite reflectance versus depth trends in two pseudo-wells through minibasin locations, at 27 km in section A and at 29 km in section B (Figure 9, I). 1D modeling was performed both with the presence of the salt diapirs (continuous lines, Figure 10) and with the salt diapirs substituted by sediments (dashed lines, Figure 10). It should be noted that maturation freezes at ~23 Ma when regional uplift of the basin is simulated.

At the 27 km location in the central sub-basin, pre-salt and Upper Permian (S2) source rocks experienced a rapid maturation that drove them into the dry (pre-salt) and wet gas (S2) window at ~240 Ma (Figure 10A). Thermal maturation continued, and both intervals became overmature (>4%Ro) at around 150 Ma (pre-salt) and 50 Ma (S2). Without the negative thermal effect of salt structures, these source rocks would have entered the oil window as early as 315 Ma (pre-salt) and 255 Ma (S2), and they would have become overmature at ~255 Ma. The Lower-Middle Triassic (S4) source rocks entered the oil window at ~220 Ma, and gradually matured to present values of ~1%Ro (Figure 10A). In the absence of salt structures, these rocks would have reached the oil window at ~250 Ma, and they would presently be in the wet gas window (~1.7%Ro). The Middle-Upper Triassic (S5) source rocks entered the oil window at ~85 Ma and reached a maximum vitrinite reflectance of ~0.8%Ro. On the other hand, The Upper Triassic-Upper Jurassic (S6) source rocks barely reached the oil window at ~30 Ma (Figure 10A). These two organic rich intervals would have been oil mature at ~135 Ma and 75 Ma, and they would presently be in the late (1.15%Ro) and main (0.75%Ro) oil window, respectively, if no salt structures existed in the basin.

In the eastern sub-basin at the 29 km location, the pre-salt and Upper Permian (S2) source rocks experienced a rapid transition from immature to the wet gas window in the Early Triassic (~250 Ma, Figure 10B). Maturation continued without interruption and these units reached the dry gas window (pre-salt = 3.7 and S2 = 3.35%Ro) before the Oligocene uplift (~23 Ma). In the absence of salt structures, these potential source rocks would have been overmature at ~170 Ma and 85 Ma, respectively. Mesozoic source rocks (S4, S5, and S6) are overall marginally to mid-mature (Figure 10B). The Lower-Middle Triassic (S4) source rocks entered the oil window at ~105 Ma, and reached a maximum maturity of ~0.7%Ro. The Middle-Upper Triassic (S5) interval entered the oil window at ~60 Ma and attained a maturity of ~0.65%Ro. The youngest Triassic-Upper Jurassic (S6) source rocks are marginally mature with vitrinite values of ~0.53%Ro. Without the massive salt diapir, the maturity of these three organic rich intervals would be 0.9, 0.75, and 0.65%Ro, respectively.

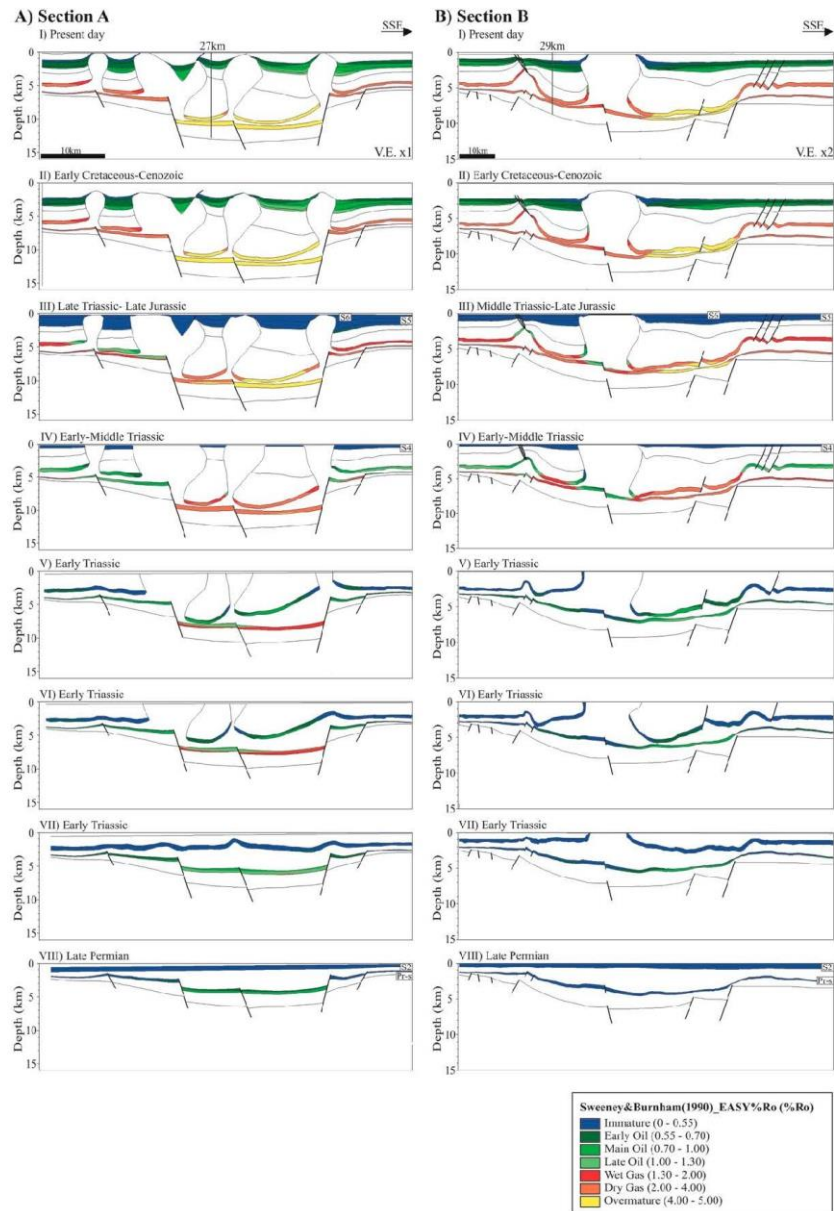


Figure 9. Source rock maturation through time in (A) section A in the central sub-basin, and (B) section B in the eastern sub-basin. Figure 1B shows the location of the sections.

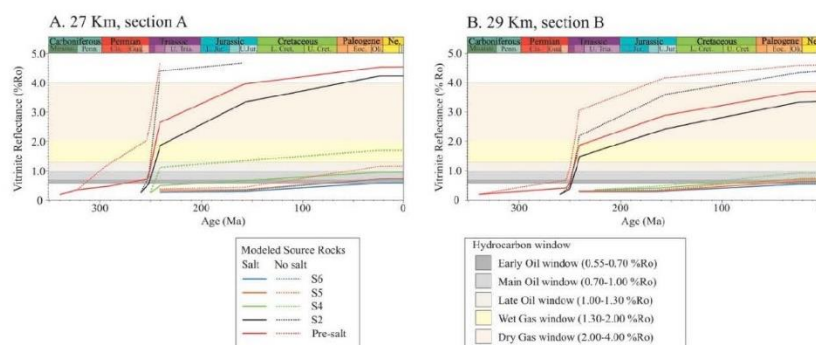


Figure 10. Source rock maturation through time in a pseudo-well perforating a minibasin in (A) section A in the central sub-basin, and (B) section B in the eastern sub-basin. Two scenarios are compared: One with salt structures as observed today (continuous lines), and another without salt structures (dashed lines). Figure 9 (I) shows the location of the pseudo-wells.

6. Discussion

6.1. Uncertainties

In confined salt-bearing basins, such as the Nordkapp Basin, seismic imaging and interpretation of salt bodies are certainly challenging due to the steeply dipping diapir flanks and complex ray paths of the seismic waves travelling through the salt [55,56]. Consequently, poor seismic imaging of salt structures can lead to incorrect interpretation of their shapes, which undoubtedly has negative consequences for determining the progressive evolution and thermal effect of salt structures through time. Uncertainty also arises from depth conversion of the seismic profiles. Figure 3A displays a wide range of interval velocities due to lateral variations in lithology and different degrees of compaction and diagenesis. In addition, the velocities of deep sediments within the Nordkapp minibasins are unknown because there are no exploration wells through the entire minibasins stratigraphy. Despite these uncertainties, the velocity model used in this study provides similar results (depths) to previous magnetic and gravity studies by Gemigon et al. [23] in the Eastern Barents Sea.

2D structural reconstructions involve several uncertainties associated with the type of unfolding method (flexural slip vs simple shear), decompaction curves, water depth, and elastic thickness. Testing different restoration parameters will indeed result in different paleogeometries. However, the objective of this paper is not to test the sensitivity of model parameters but rather use reasonable parameter values. For example, we use simple shear to remove the deformation caused by passive diapirism because the length loss adjacent to salt diapirs is negligible compared to the length of the section. On the other hand, we use flexural slip in sequences SU2 and SU3 because it preserves length in these parallel-folded units [57]. Based on studies by Klausen and Helland-Hansen [58], we use the Sclater and Christie [51] decompaction curve because it fits well the porosity versus depth trends observed on borehole data in the Barents Sea. Finally, an elastic thickness of 20 km was chosen based on Gac et al. [41].

In terms of thermal modeling, most of the crucial stages (IV to VIII) for the formation of the Nordkapp Basin encompass a relatively short (~20 Ma) and old (Permian-Early Triassic) time interval (Figure 5D). Therefore, restoring sensible boundary conditions (basal heat flow and SWTI) for this period is crucial. Inevitably, assumptions are intrinsic to the model due to the general lack of calibration data, with the exception of a few bottom well temperatures and vitrinite data (Figure 6). Extrapolating boundary conditions calculated in the western sub-basin to the central and eastern sub-basins can be unrealistic, since the initial thickness of the Post-Caledonian crust and lithosphere,

and the amount of rifting defined by β most likely varied along the basin [42]. Additional uncertainty arises from the need to simplify lithologies, particularly for the deepest units, given the importance of their thermal conductivities and heat capacities in the simulations.

On the other hand, the model, as designed, would greatly benefit from assessing the distribution and thickness of the source rocks in each of the minibasins. For the petroleum system, the evaluation of the actual presence of good reservoir levels in the basin is a must. Despite these limitations, the modeling results represent the Nordkapp Basin geology and tectonic evolution, and they can be used to develop further exploration concepts in this basin and other basins alike.

6.2. The Importance of Thermal Modeling in Confined Salt-bearing Basins

The thermal effect of salt structures has been documented by previous studies in passive margins such as the Gulf of Mexico [6,9]. In this tectonic setting, salt deposition occurs in unconfined large areas where accommodation is controlled by thermal subsidence [59]. This also produces tilting of the margin, which in turn triggers downslope salt gliding and structures such as salt stocks, salt tongues, and allochthonous salt sheets [2]. These structures have received special attention due to their sealing capacity and their impact on maturation of underlying source rocks [6,8–10].

In the case of salt-bearing rift basins, syn-rift salt deposition is really limited by the rift geometry [59]. Salt mobilization by either extension and/or differential loading results in a structural style consisting of sub-vertical and closely spaced salt structures, which commonly coincide with the presence of subsalt faults [60–62]. Factors such as diapir shape and spacing play an important role in the thermal evolution of these basins [9].

Combined structural restorations and thermal modeling from the Nordkapp Basin indicate that the shape of salt diapirs and their inherent thermal anomalies vary through time and display a characteristic negative thermal effect (i.e., downward shift of isotherms), which is directly proportional to the width of the salt diapir (Figure 7). This is clearly observed in the eastern sub-basin (section B), where the presence of a wider and isolated salt diapir induces a strong, but laterally limited, negative anomaly. Temperatures along the diapir flanks could be up to 70 °C cooler and exceptionally low (~150 °C) at depths of ~9 km beneath the diapir. This integrated approach also highlights that closely-spaced diapirs in the central sub-basin mutually interfere and produce a combined negative thermal anomaly, which lowers the temperature in the minibasins by up to 50 °C with respect to the adjacent platform areas. Thus, although large salt tongues and allochthonous salt sheets are absent in confined basins, sub-vertical and closely spaced salt structures still generate a combined thermal anomaly that extends over large areas of the basin.

6.3. Implications for the Petroleum System

Salt diapirs in confined basins impact the petroleum system by retarding maturation of organic rich sediments, expanding the hydrocarbon generation window, and hindering diagenetic processes in reservoir levels. Figure 11 summarizes the implications of our results for the petroleum system of the Nordkapp Basin.

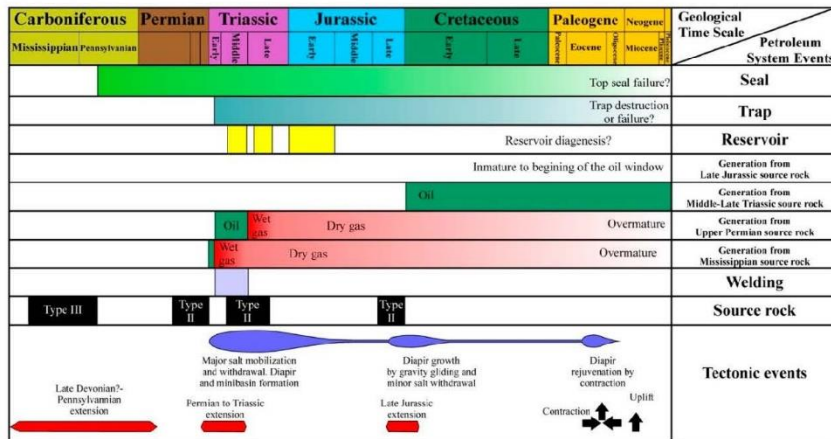


Figure 11. Petroleum systems chart for the Nordkapp Basin. Insights from the modeling results are incorporated in the chart.

6.3.1. Source rocks

Present day vitrinite reflectance values in the Nordkapp Basin indicate that when maturation ceased upon uplift in the Oligocene, Mississippian (gas-prone) and Permian (oil-prone) source rock units were mostly overmatured (Figure 9A, I, and Figure 11). In areas where pre-salt source rocks lied at shallower depths (e.g., eastern sub-basin and basin shoulders), Paleozoic source rocks were still within the gas window (Figure 9B, I, and Figure 11). The modeled Permian source rocks show exceptional low maturity at the flanks of the massive salt diapir in the eastern sub-basin. The Middle-Upper Triassic oil and gas prone source rocks were most probably able to generate hydrocarbons as they entered well into the oil window (Figures 10 and 11). Hydrocarbon generation from the Upper Jurassic oil-prone source rocks, however, is limited since these rocks were marginally to early mature. It is noteworthy that in the vicinity of salt structures, i.e., minibasins, thermal maturation rates are diminished (Figure 10). In the absence of such structures, the timing of maturation and generation of the different hydrocarbon phases is much earlier than what is implied in Figure 11, substantially affecting the petroleum system evolution.

6.3.2. Reservoirs

The negative thermal anomaly caused by salt diapirs may have prevented temperature-driven diagenetic processes (e.g., quartz cementation) in potential reservoirs of Triassic and Jurassic age (Figure 7, II). Nevertheless, diapir widening must also be considered when assessing the impact of diagenesis in flanking reservoirs. This process can naturally enhance the stress at diapir flanks, causing quartz pressure dissolution, and subsequent decrease of reservoir quality [2]. This needs to be given attention in the Nordkapp Basin since structural restorations suggest significant diapir widening from the Middle Triassic to the Late Jurassic (Figure 4, III–IV).

6.3.3. Traps

Based on the structural restorations, near-diapir structural and stratigraphic traps were present since the end of the Early Triassic (Figures 4 and 11). Megaflaps [5,63] and halokinetic sequences [5,64,65], which formed in response to the active and passive stages of diapirism from the Early Triassic to Cretaceous (Figure 4, IV–VII, and Figure 11), are present at different stratigraphic levels. Potential traps

also include Early–Middle Triassic half turtle structures (Figure 4, IV) and suprasalt fault complexes at the basin boundaries (Figure 4B, I).

6.3.4. Seal and migration

Impermeable salt can act as a seal rock for vertical and lateral migration of hydrocarbons in the Nordkapp Basin. The structural restorations illustrate that salt welds were present since the end of the Early Triassic (Figure 4, V). This welding may have allowed gas migration from Mississippian gas-prone source rocks into suprasalt Mesozoic reservoirs, which in turn may have favored reservoir porosity preservation at high depths, as documented by McBride et al. [6] for the Gulf of Mexico. Additionally, closely spaced diapirs in the central sub-basin can generate laterally sealed minibasins, which if capped by fine-grained rocks could create favorable scenarios for hydrocarbon entrapment.

Continuous diapir growth and successive reactivation of suprasalt fault complexes during the Mesozoic and Cenozoic could have also modified and/or destroyed structural traps and breached seals, causing migration of hydrocarbons to shallower traps or escape from the system (Rojo et al. [18]; their Figure 20). Late Cenozoic regional uplift and erosion [39] may have led to hydrocarbon phase separation, top seal failure, and remigration. The modification and destruction of traps, together with deep hydrocarbon kitchens, could have resulted in a complex petroleum system, where migration of petroleum, flushing of older traps, and mixing of hydrocarbons of different maturity and ages are dominant features. These observations are consistent with the current understanding of the petroleum system and geochemical data by Ohm et al. [16] and Lerch et al. [66] for the Norwegian Barents Sea.

7. Conclusions

In this study, we have integrated 2D structural restorations with thermal modeling to investigate how halokinesis impacted the thermal evolution of the basin through time and to explore the implications of the modeled thermal history on the petroleum system of the Nordkapp Basin, a confined, salt-bearing rift basin.

Combined structural restorations and thermal modeling show that the shape of salt diapirs and their negative thermal effect change through time. In the case of an isolated salt diapir, it induces a strong, but laterally limited, negative anomaly, which is directly proportional to its width. Temperatures along the diapir flanks are 70 °C cooler and are exceptionally low (~150 °C) at depths of ~9 km beneath the salt. On the other hand, the thermal anomalies of closely-spaced diapirs mutually interfere and generate a combined negative thermal anomaly that reduces the temperature in the minibasins by up to 50 °C with respect to the adjacent platform areas.

Although large salt tongues and allochthonous salt sheets are generally absent in confined rift basins, sub-vertical and closely spaced salt structures still generate a combined anomaly that extends over large areas of the basin. As a result, thermal maturation of the source rocks in the minibasins is retarded, and the hydrocarbon generation window is expanded. Thus, laterally-sealed minibasins offer favorable scenarios for deeper than normal hydrocarbons kitchens and entrapment in various near-diapir structural and stratigraphic traps.

Author Contributions: Conceptualization, A.C., L.A.R., N.C. and L.C.; methodology, A.C., L.A.R., L.C. and N.C.; software, A.C., L.A.R., L.C. and N.C.; validation, A.C., L.A.R., L.C. and N.C.; formal analysis, A.C., L.A.R., N.C. and L.C.; investigation, A.C., L.A.R., N.C. and L.C.; resources, A.C., L.A.R., L.C. and N.C.; writing—original draft preparation, A.C., L.A.R., N.C. and L.C.; writing—review and editing, A.C., L.A.R., N.C., L.C. and A.E.; visualization, A.C., L.A.R., N.C. and L.C.; supervision, A.C., L.A.R. and N.C.; project administration, A.C., L.A.R. and N.C.

Funding: This research received no direct funding. However, Andrés Cedeño was supported by the JuLoCrA project.

Acknowledgments: This work evolved from a Master thesis by Luis Centeno at the University of Stavanger. We are grateful to WesternGeco Multiclient for providing full azimuth 3D seismic data from the Nordkapp Basin, and the Norwegian Petroleum Directorate for kindly providing the NPD-BA-11 2D seismic survey in the eastern Norwegian Barents Sea. Thanks to Schlumberger and Midland Valley for providing academic licenses of their

softwares PetroMod and Move, respectively. The authors are grateful to two anonymous reviewers and to the guest editor Willy Fjeldskaar for their valuable contributions. Andres Cedeno thanks the JuLoCrA project for economic support.

Conflicts of Interest: The authors declare no conflict of interest.

References

- Hudec, M.R.; Jackson, M.P. Terra infirma: Understanding salt tectonics. *Earth-Sci. Rev.* **2007**, *82*, 1–28. [[CrossRef](#)]
- Jackson, M.P.; Hudec, M.R. *Salt Tectonics: Principles and Practice*; Cambridge University Press: Cambridge, UK, 2017; 498p.
- Matthews, W.J.; Hampson, G.J.; Trudgill, B.D.; Underhill, J.R. Controls on fluvio-lacustrine reservoir distribution and architecture in passive salt-diapir provinces: Insights from outcrop analogs. *AAPG Bull.* **2007**, *91*, 1367–1403. [[CrossRef](#)]
- Banham, S.G.; Mountney, N.P. Controls on fluvial sedimentary architecture and sediment-fill state in salt-walled mini-basins: Triassic Moenkopi Formation, Salt Anticline Region, SE Utah, USA. *Basin Res.* **2013**, *25*, 709–737. [[CrossRef](#)]
- Rojo, L.A.; Escalona, A. Controls on minibasin infill in the Nordkapp Basin: Evidence of complex Triassic syndimentary deposition influenced by salt tectonics. *AAPG Bull.* **2018**, *102*, 1239–1272. [[CrossRef](#)]
- McBride, B.C.; Weimer, P.; Rowan, M.G. The effect of allochthonous salt on the petroleum systems of northern Green Canyon and Ewing Bank (offshore Louisiana), northern Gulf of Mexico. *AAPG Bull.* **1998**, *82*, 1083–1112.
- Rowan, M.G.; Lawton, T.F.; Giles, K.A. Anatomy of an exposed vertical salt weld and flanking strata, La Popa Basin, Mexico. In *Salt Tectonics, Sediments and Prospectivity*; Alsop, G.I., Archer, S.G., Hartley, A.J., Grant, N.T., Hodgkinson, R., Eds.; Geological Society: London, UK, 2012; Volume 363, pp. 33–57.
- Lerche, I.; O'Brien, J.J. *Dynamical Geology of Salt and Related Structures*; Academic Press: San Diego, CA, USA, 1987; p. 832.
- Mello, U.T.; Kamer, G.D.; Anderson, R.N. Role of salt in restraining the maturation of subsalt source rocks. *Mar. Pet. Geol.* **1995**, *12*, 697–716. [[CrossRef](#)]
- Yu, A.; Lerche, I. Thermal impact of salt: Simulation of thermal anomaly in the Gulf of Mexico. *Pure Appl. Geophys.* **1992**, *2*, 180–192. [[CrossRef](#)]
- Gabrielsen, R.; Kløvjan, O.; Rasmussen, A.; Stølan, T. Interaction between halokinesis and faulting: Structuring of the margins of the Nordkapp Basin, Barents Sea region. In *Structural and Tectonic Modeling and Its Implication to Petroleum Geology*; Larsen, B., Brekke, H., Larsen, B., Talleraas, E., Eds.; Norwegian Petroleum Society (NPF): Oslo, Norway, 1992; Volume 1, pp. 121–131.
- Jensen, L.N.; Sørensen, K. Tectonic framework and halokinesis of the Nordkapp Basin, Barents Sea. In *Structural and Tectonic Modeling and Its Application to Petroleum Geology*; Larsen, R.M., Brekke, H., Larsen, B.T., Talleraas, E., Eds.; Norwegian Petroleum Society (NPF), Special Publications: Oslo, Norway, 1992; Volume 1, pp. 109–120.
- Koyi, H.; Talbot, C.J.; Tørudbakken, B.O. Salt tectonics in the Northeastern Nordkapp basin, Southwestern Barents Sea. In *Salt Tectonics: A Global Perspective*; Jackson, M.P.A., Roberts, D.G., Snelson, S., Eds.; American Association of Petroleum Geologists: Tulsa, OK, USA, 1995; AAPG Memoir 65; pp. 437–447.
- Nilsen, K.T.; Vendeville, B.C.; Johansen, J.-T. Influence of regional tectonics on halokinesis in the Nordkapp Basin, Barents Sea. In *Salt Tectonics: A Global Perspective*; Jackson, M.P.A., Roberts, D.G., Snelson, S., Eds.; American Association of Petroleum Geologists: Tulsa, OK, USA, 1995; AAPG Memoir 65; pp. 413–436.
- Stadtler, C.; Fichler, C.; Hokstad, K.; Myrland, E.A.; Wienecke, S.; Fotland, B. Improved salt imaging in a basin context by high resolution potential field data: Nordkapp Basin, Barents Sea. *Geophys. Prospect.* **2014**, *62*, 615–630. [[CrossRef](#)]
- Ohm, S.E.; Karlsen, D.A.; Austin, T. Geochemically driven exploration models in uplifted areas: Examples from the Norwegian Barents Sea. *AAPG Bull.* **2008**, *92*, 1191–1223. [[CrossRef](#)]
- Henriksen, E.; Bjørnseth, H.; Hals, T.; Heide, T.; Kiryukhina, T.; Kløvjan, O.; Larssen, G.; Ryseth, A.; Rønning, K.; Sollid, K. Uplift and erosion of the greater Barents Sea: Impact on prospectivity and petroleum

- systems. In *Arctic Petroleum Geology*; Spencer, A.M., Embry, A.F., Gautier, D.L., Stoupakova, A.V., Sørensen, K., Eds.; Geological Society, London, Memoirs: London, UK, 2011; Volume 35, pp. 271–281.
18. Rojo, L.A.; Cardozo, N.; Escalona, A.; Koyi, H. Structural style and evolution of the Nordkapp Basin, Norwegian Barents Sea. *AAPG Bull.* **2019**, in press. [[CrossRef](#)]
 19. Rowan, M.G.; Lindso, S. Chapter 12—Salt Tectonics of the Norwegian Barents Sea and Northeast Greenland Shelf A2. In *Permo-Triassic Salt Provinces of Europe, North Africa and the Atlantic Margins*; Soto, J.L., Flinch, J.F., Tari, G., Eds.; Elsevier: Amsterdam, The Netherlands, 2017; pp. 265–286.
 20. Dengo, C.; Røssland, K. Extensional tectonic history of the western Barents Sea. In *Structural and Tectonic Modeling and Its Application to Petroleum Geology*; Larsen, R.M., Brekke, H., Larsen, B.T., Talleraas, E., Eds.; Norwegian Petroleum Society (NPF): Oslo, Norway, 1992; Volume 1, pp. 91–108.
 21. Faleide, J.I.; Tsikalas, F.; Breivik, A.J.; Mjelde, R.; Ritzmann, O.; Engen, O.; Wilson, J.; Eldholm, O. Structure and evolution of the continental margin off Norway and the Barents Sea. *Episodes* **2008**, *31*, 82–91.
 22. Gemigon, L.; Brønner, M.; Roberts, D.; Olesen, O.; Nasuti, A.; Yamasaki, T. Crustal and basin evolution of the southwestern Barents Sea: From Caledonian orogeny to continental breakup. *Tectonics* **2014**, *33*, 347–373. [[CrossRef](#)]
 23. Gemigon, L.; Brønner, M.; Dumais, M.-A.; Gradmann, S.; Grønlie, A.; Nasuti, A.; Roberts, D. Basement inheritance and salt structures in the SE Barents Sea: Insights from new potential field data. *J. Geodyn.* **2018**, *119*, 82–106. [[CrossRef](#)]
 24. Worsley, D. The post-Caledonian development of Svalbard and the western Barents Sea. *Polar Res.* **2008**, *27*, 298–317. [[CrossRef](#)]
 25. Smyrak-Sikora, A.; Johannessen, E.P.; Olaussen, S.; Sandal, G.; Braathen, A. Sedimentary architecture during Carboniferous rift initiation—The arid Billefjorden Trough, Svalbard. *J. Geol. Soc.* **2018**, *176*, 225–252. [[CrossRef](#)]
 26. Bugge, T.; Mangerud, G.; Elvebakk, G.; Mork, A.; Nilsson, I.; Fanavoll, S.; Vigran, J. Upper Paleozoic succession on the Finnmark platform, Barents Sea. *Nor. J. Geol.* **1995**, *75*, 3–30.
 27. Gudlaugsson, S.; Faleide, J.; Johansen, S.; Breivik, A. Late Palaeozoic structural development of the south-western Barents Sea. *Mar. Pet. Geol.* **1998**, *15*, 73–102. [[CrossRef](#)]
 28. Stemmerik, L.; Elvebakk, G.; Worsley, D. Upper Palaeozoic carbonate reservoirs on the Norwegian arctic shelf; delineation of reservoir models with application to the Loppa High. *Pet. Geosci.* **1999**, *5*, 173–187. [[CrossRef](#)]
 29. Stemmerik, L. Late Palaeozoic evolution of the North Atlantic margin of Pangea. *Palaeogeogr. Palaeoclimatol. Palaeoecol.* **2000**, *161*, 95–126. [[CrossRef](#)]
 30. Stemmerik, L.; Worsley, D. 30 years on-Arctic Upper Palaeozoic stratigraphy, depositional evolution and hydrocarbon prospectivity. *Nor. J. Geol.* **2005**, *85*, 151–168.
 31. Koyi, H.; Talbot, C.J.; Torudbakken, B. Analogue models of salt diapirs and seismic interpretation in the Nordkapp Basin, Norway. *Pet. Geosci.* **1995**, *1*, 185–192. [[CrossRef](#)]
 32. Glørstad-Clark, E.; Faleide, J.I.; Lundschiøn, B.A.; Nystuen, J.P. Triassic seismic sequence stratigraphy and paleogeography of the western Barents Sea area. *Mar. Pet. Geol.* **2010**, *27*, 1448–1475. [[CrossRef](#)]
 33. Klausen, T.G.; Ryseth, A.E.; Helland-Hansen, W.; Gawthorpe, R.; Laursen, I. Regional development and sequence stratigraphy of the Middle to Late Triassic Snadd Formation, Norwegian Barents Sea. *Mar. Pet. Geol.* **2015**, *62*, 102–122. [[CrossRef](#)]
 34. Eide, C.H.; Klausen, T.G.; Katkov, D.; Suslova, A.A.; Helland-Hansen, W. Linking an Early Triassic delta to antecedent topography: Source-to-sink study of the southwestern Barents Sea margin. *GSA Bull.* **2017**, *130*, 263–283. [[CrossRef](#)]
 35. Klausen, T.; Aas, T.J.; Haug, E.C.; Behzad, A.; Snorre, O.; Domenico, C. Clinofold development and topset evolution in a mud-rich delta—The Middle Triassic Kobbe Formation, Norwegian Barents Sea. *Sedimentology* **2018**, *65*, 1132–1169. [[CrossRef](#)]
 36. Anell, I.; Braathen, A.; Olaussen, S. The Triassic—Early Jurassic of the northern Barents Shelf: A regional understanding of the Longyearbyen CO₂ reservoir. *Nor. J. Geol.* **2014**, *94*, 83–98.
 37. Grundtvåg, S.A.; Marin, D.; Kairanov, B.; Śliwińska, K.K.; Nøhr-Hansen, H.; Jelby, M.E.; Escalona, A.; Olaussen, S. The Lower Cretaceous succession of the northwestern Barents Shelf: Onshore and offshore correlations. *Mar. Pet. Geol.* **2017**, *86*, 834–857. [[CrossRef](#)]

38. Marin, D.; Escalona, A.; Nøhr-Hansen, H.; Kasia, K.Ś.; Mordasova, A. Sequence stratigraphy and lateral variability of Lower Cretaceous clinofolds in the SW Barents Sea. *AAPG Bull.* **2017**, *101*, 1487–1517. [[CrossRef](#)]
39. Henriksen, E.; Ryseth, A.; Larssen, G.; Heide, T.; Rønning, K.; Sollid, K.; Stoupakova, A. Tectonostratigraphy of the greater Barents Sea: Implications for petroleum systems. In *Arctic Petroleum Geology*; Spencer, A.M., Embry, A.F., Gautier, D.L., Stoupakova, A.V., Sørensen, K., Eds.; Geological Society, London, Memoirs: London, UK, 2011; Volume 35, pp. 163–195.
40. Baig, I.; Faleide, J.I.; Jahren, J.; Mondol, N.H. Cenozoic exhumation on the southwestern Barents Shelf: Estimates and uncertainties constrained from compaction and thermal maturity analyses. *Mar. Pet. Geol.* **2016**, *73*, 105–130. [[CrossRef](#)]
41. Gac, S.; Klitzke, P.; Minakov, A.; Faleide, J.I.; Scheck-Wenderoth, M. Lithospheric strength and elastic thickness of the Barents Sea and Kara Sea region. *Tectonophysics* **2016**, *691*, 120–132. [[CrossRef](#)]
42. Clark, S.A.; Glerstad-Clark, E.; Faleide, J.I.; Schmid, D.; Hartz, E.H.; Fjeldskaar, W. Southwest Barents Sea rift basin evolution: Comparing results from backstripping and time-forward modeling. *Basin Res.* **2014**, *26*, 550–566. [[CrossRef](#)]
43. He, Z.; Crews, S.G.; Corrigan, J. Rifting and Heat Flow: Why the Mckenzie model is only part of the story: AAPG Hedberg Conference. In Proceedings of the Basin Modeling Perspectives: Innovative Developments and Novel Applications, The Hague, The Netherlands, 6–9 May 2007.
44. Klitzke, P.; Faleide, J.I.; Scheck-Wenderoth, M.; Sippel, J. A lithosphere-scale Structural model of the Barents Sea and Kara Sea region. *Solid Earth* **2015**, *6*, 153–172. [[CrossRef](#)]
45. Gac, S.; Hansford, P.A.; Faleide, J.I. Basin modeling of the SW Barents Sea. *Mar. Pet. Geol.* **2018**, *95*, 167–187. [[CrossRef](#)]
46. Riis, F. Dating and measuring of erosion, uplift and subsidence in Norway and the norwegian shelf in glacial periods. *Norsk Geologisk Tidsskrift* **1992**, *72*, 325–331.
47. Fjeldskaar, W.; Lindholm, C.; Dehls, J.F.; Fjeldskaar, I. Postglacial uplift, neo- tectonics and seismicity in Fennoscandia. *Quat. Sci. Rev.* **2000**, *19*, 413–1422. [[CrossRef](#)]
48. Cavanagh, A.J.; di Primio, R.; Scheck-Wenderoth, M.; Horsfield, B. Severity and timing of Cenozoic exhumation in the Southwestern Barents Sea. *J. Geol. Soc.* **2006**, *163*, 761–774. [[CrossRef](#)]
49. Fjeldskaar, W.; Amantov, A. Effects of glaciations on sedimentary basins. *J. Geodyn.* **2018**, *118*, 66–81. [[CrossRef](#)]
50. Athy, L.F. Density, porosity and compaction of sedimentary rocks. *AAPG Bull.* **1930**, *14*, 1–24.
51. Sclater, J.G.; Christie, P.A.F. Continental stretching: An explanation of the post-mid Cretaceous subsidence of the Central North Sea Basin. *J. Geophys. Res.* **1980**, *85*, 3711–3739. [[CrossRef](#)]
52. Sekiguchi, K. A method for determining terrestrial heat flow in oil basin areas. In *Terrestrial Heat Flow Studies and Structure of the Lithosphere*; Rybach, C.L., Chapman, D.S., Eds.; Tectonophysics, Science Direct: Liblice, Czechoslovakia, 1984; Volume 103, pp. 67–79.
53. Mørk, A.; Dallmann, W.K.; Dypvik, H.; Johannessen, E.P.; Larssen, G.B.; Nagy, J.; Nøttvedt, A.; Olaussen, S.; Pchelina, T.M.; Worsley, D. Mesozoic lithostratigraphy. In *Lithostratigraphic Lexicon of Svalbard. Review and Recommendations for Nomenclature Use. Upper Palaeozoic to Quaternary Bedrock*; Dallmann, W.K., Ed.; Norsk Polarinstittutt: Tromsø, Norway, 1999; pp. 127–214.
54. Sweeney, J.J.; Burnham, A.K. Evaluation of a simple model of vitrinite reflectance based on chemical kinetics (1). *AAPG Bull.* **1990**, *74*, 1559–1570.
55. Jones, I.F.; Davison, I. Seismic imaging in and around salt bodies. *Interpretation* **2014**, *2*, 1–20. [[CrossRef](#)]
56. Rojo, L.A.; Escalona, A.; Schulte, L. The use of seismic attributes to enhance imaging of salt structures in the Barents Sea. *First Break* **2016**, *34*, 41–49. [[CrossRef](#)]
57. Rowan, M.G.; Ratliff, R.A. Cross-section restoration of salt-related deformation: Best practices and potential pitfalls. *J. Struct. Geol.* **2012**, *41*, 24–37. [[CrossRef](#)]
58. Klausen, T.; Helland-Hansen, W. Methods for Restoring and Describing Ancient Clinofold Surfaces. *J. Sediment. Res.* **2018**, *88*, 241–259. [[CrossRef](#)]
59. Warren, J.K. Evaporites through time: Tectonic, climatic and eustatic controls in marine and nonmarine deposits. *Earth-Sci. Rev.* **2010**, *98*, 217–268. [[CrossRef](#)]
60. Koyi, H.; Petersen, K. Influence of basement faults on the development of salt structures in the Danish Basin. *Mar. Pet. Geol.* **1993**, *10*, 82–94. [[CrossRef](#)]

61. Stewart, S.; Ruffell, A.; Harvey, M. Relationship between basement-linked and gravity-driven fault systems in the UKCS salt basins. *Mar. Pet. Geol.* **1997**, *14*, 581–604. [[CrossRef](#)]
62. Withjack, M.O.; Callaway, S. Active normal faulting beneath a salt layer: An experimental study of deformation patterns in the cover sequence. *AAPG Bull.* **2000**, *84*, 627–651.
63. Rowan, M.G.; Giles, K.A.; Hearon, T.E., IV; Fiduk, J.C. Megaflaps adjacent to salt diapirs. *AAPG Bull.* **2016**, *100*, 1723–1747. [[CrossRef](#)]
64. Giles, K.A.; Rowan, M.G. Concepts in halokinetic-sequence deformation and stratigraphy. In *Salt Tectonics, Sediments and Prospectivity*; Alsop, G.I., Archer, S.G., Hartley, A.J., Grant, N.T., Hodgkinson, R., Eds.; Geological Society: London, UK, 2012; Volume 363, pp. 7–31.
65. Hearon, T.E., IV; Rowan, M.G.; Giles, K.A.; Hart, W.H. Halokinetic deformation adjacent to the deepwater Auger diapir, Garden Banks 470, northern Gulf of Mexico: Testing the applicability of an outcrop-based model using subsurface data. *Interpretation* **2014**, *2*, SM57–SM76. [[CrossRef](#)]
66. Lerch, B.; Karlsen, D.A.; Matapour, Z.; Seland, R.; Backer-Owe, K. Organic geochemistry of Barents Sea petroleum: Thermal maturity and alteration and mixing processes in oils and condensates. *J. Pet. Geol.* **2016**, *39*, 125–148. [[CrossRef](#)]



© 2019 by the authors. Licensee MDPI, Basel, Switzerland. This article is an open access article distributed under the terms and conditions of the Creative Commons Attribution (CC BY) license (<http://creativecommons.org/licenses/by/4.0/>).

APPENDIX

Conference abstracts

Peri-diapiric sedimentary wedges in the Nordkapp Basin.

Luis Alberto Rojo, Nestor Cardozo, and Alejandro Escalona

2016, Norsk Petroleumsforening (NPF) Conference, Tromsø, Norway

Controls on suprasalt deformation in the Nordkapp Basin, Norwegian Barents Sea.

Luis Alberto Rojo, Nestor Cardozo, and Alejandro Escalona

2017, EAGE Conference and Exhibition, Paris, France.

The influence of halokinesis in the trajectory and geometry of prograding clinoforms: insights from the Tiddlybanken Basin, Norwegian Barents Sea

Luis Alberto Rojo, Dora Marin, Nestor Cardozo, Alejandro Escalona, and Hemin Koyi

2018, AAPG Europe Regional Conference, Global Analogues of the Atlantic Margin, Lisbon, Portugal

The impact of basement configuration on the development of salt structures in confined salt-related basins: insights from analogue modelling

Luis Alberto Rojo, Nestor Cardozo, Hemin Koyi, and Alejandro Escalona

2019, TSG AGM, Bergen, Norway.